Doctoral Dissertation

Development of Chemical Tactics to Study Fundamental Aspects of Pathogenic Factors Found in Neurodegenerative Diseases

Juhye Kang

Department of Chemistry

Graduate School of UNIST

2019

Development of Chemical Tactics to Study Fundamental Aspects of Pathogenic Factors Found in Neurodegenerative Diseases

Juhye Kang

Department of Chemistry

Graduate School of UNIST

Development of Chemical Tactics to Study Fundamental Aspects of Pathogenic Factors Found in Neurodegenerative Diseases

A dissertation submitted to the Graduate School of UNIST
in partial fulfillment of the requirements
for the degree of Doctor of Philosophy of Science

Juhye Kang

March 29, 2019

Approved by

Advisor
Associate Professor Tae-Hyuk Kwon

Development of Chemical Tactics to Study Fundamental Aspects of Pathogenic Factors Found in Neurodegenerative Diseases

Juhye Kang

This certifies that the dissertation of Juhye Kang is approved.

March 29, 2019

Advisor: Associate Professor Tae-Hyuk Kwon

Associate Professor Mi Hee Lim

Associate Professor Hyun-Woo Rhee

Assistant Professor Jung-Min Kee

Assistant Professor Young S. Park

Abstract

Amyloidogenic peptides are considered central pathological factors in neurodegenerative diseases; however, their roles in the pathologies of the diseases have not been fully understood. Amyloidogenic peptides have indicated their multiple faces on formation, aggregation, and accumulation that portray the complexity of the intrinsically disordered protein stemming from their convoluted structure and heterogeneous nature. Although the latest research suggests oligomeric forms of amyloidogenic peptides as toxic species towards neurodegeneration, their direct involvements in the pathologies and the corresponding mechanistic details remain rudimentary. Therefore, novel chemical approaches to modify amyloidogenic peptides at the molecular level would be useful in advancing our comprehension of those aspects and the subject.

In Chapter 1, we briefly introduce outline and discuss possible therapeutic targets in Alzheimer's disease. In Chapter 2, the design of an Ir(III) complex, **Ir-1**, is described as a chemical tool for oxidizing amyloidogenic peptides upon photoactivation and subsequently modulating their aggregation pathways. Biochemical and biophysical investigations illuminate that the oxidation of representative amyloidogenic peptides [i.e., amyloid-β (Aβ), α-synuclein, and human islet amyloid polypeptide] is promoted by light-activated **Ir-1**, which can alter the conformations and aggregation pathways of the peptides. In Chapter 3, effective chemical strategies for modifications of Aβ peptides implemented by a single Ir(III) complex are illustrated. Such peptide variations can be achieved by our rationally designed Ir(III) complexes leading to the significant modulation of the aggregation pathways of $A\beta_{40}$ and $A\beta_{42}$ as well as the production of toxic Aβ species.

Amyloidogenic peptides can coordinate to metal ions, including Zn(II), which can subsequently affect the peptides' aggregation and toxicity, leading to neurodegeneration. Unfortunately, the detection of metal–amyloidogenic peptide complexation has been very challenging. In Chapter 4, we report the development and utilization of a probe (**A-1**) capable of monitoring metal–Aβ complexation based on Förster resonance energy transfer (FRET). Moreover, as the FRET signal of Zn(II)-added **A-1** is drastically changed when the interaction between Zn(II) and **A-1** is disrupted, the Zn(II)-treated probe can be used for screening a chemical library to determine effective inhibitors against metal–Aβ interaction.

Overall, we demonstrate chemical tactics for modifications of amyloidogenic peptides in an effective and manageable manner utilizing the coordination capacities and/or photophysical properties of chemical reagents. Our approaches will provide the foundation for developing effective and efficient methods for elucidating fundamental properties of pathological factors at the molecular level and assisting in identifying therapeutic candidates against neurodegenerative disorders.

Table of Contents

List of Figures

List of Tables

List of Schemes

List of Abbreviations

5Y	SH-SY5Y
Aβ	Amyloid-β
ABDA	9,10-Anthracenediyl-bis(methylene)dimalonic acid
Acetyl-CoA	Acetyl coenzyme A
ACh	Acetylcholine
AChE	Acetylcholinesterase
AChEIs	Acetylcholinesterase inhibitors
AD	Alzheimer's disease
AFM	Atomic force microscopy
ALS	Amyotrophic lateral sclerosis
ApoE	Apolipoprotein E
APP	Amyloid precursor protein
α-Syn	α-Synuclein
ATDs	Arrival time distributions
BACE1	β-Site APP cleaving enzyme
BAX	Bcl-2 associated X
BBB	Blood-brain barrier
Bcl-2	B-cell lymphoma 2
BuChE	Butyrylcholinesterase
cAMP	Cyclic adenosine monophosphate
CcO	Cytochrome c oxidase
CD	Circular dichroism spectroscopy
cdk5	Cyclin-dependent kinase-5
cGMP	Cyclic guanosine monophosphate
ChAT	Choline acetyltransferase
ChEIs	Cholinesterases inhibitors
ChEs	Cholinesterases
CNS	Central nervous system
COMMD1	COMM domain-containing protein 1
CP-MD simulation	Car–Parrinello molecular dynamics simulation
CREB	cAMP (cyclic adenosine monophosphate) response element binding
CSPs	Chemical shift perturbations
CTFα	C-terminal fragment α

CypD	Cyclophilin D
DβM	Dopamine β monooxygenase
DCM	Dichloromethane
DIPEA	*N*,*N*-Diisopropylethylenediamine
DKK1	Dickkopf1
DMEM	Dulbecco modified eagle medium
DMF	*N*,*N*-Dimethylformamide
DMSO	Dimethyl sulfoxide
DMT1	Divalent metal-ion transporter-1
Dnap	1-Naphthylethylenediamine
DPBS	Dulbecco's phosphate-buffered saline
ECL	Enhanced chemiluminescence
EDTA	Ethylenediamine tetraacetic acid
EPR	Electron paramagnetic resonance spectroscopy
ER	Endoplasmic reticulum
ESI	Electrospray ionization
ESI-IM-MS	Electrospray ionization ion mobility mass spectrometry
ESI-MS	Electrospray ionization-mass spectrometry
Et_2O	Diethyl ether
EtOAc	Ethyl acetate
EXAFS	Extended X-ray absorption fine structure
FBS	Fetal bovine serum
FDA	Food and Drug Administration
FRET	Förster resonance energy transfer
FTD	Frontotemporal dementia
FTIR	Fourier-transform infrared spectroscopy
GABA	Aminobutyric acid
Gel/Western blot	Gel electrophoresis with Western blotting
GSK3	Glycogen synthase kinase 3
hAChE	Human acetylcholinesterase
HBTU	2-(1*H*-Benzotriazol-1-yl)-1,1,3,3-tetramethyluronium hexafluorophosphate
HDACs	Histone deacetylases
HEPES	4-(2-Hydroxyethyl)-1-piperazineethanesulfonic acid
HFIP	1,1,1,3,3,3-Hexafluoro-2-propanol
hIAPP	Human islet amyloid polypeptide
HOAt	1-Hydroxy-7-azabenzotriazole

HOBt	1-Hydroxy-benzotriazole
HPLC	High-performance liquid chromatography
HRMS	High-resolution mass spectrometry
ICT	Isothermal titration calorimetry
IM-MS	Ion mobility mass spectrometry
IRF	Instrument response function
JNK	c-Jun N-terminal kinase
K_d	Binding affinities
LTP	Long-term potentiation
MALDI-TOF	Matrix-assisted laser desorption/ionization time-of-flight
MAO	Monoamine oxidase
MAPs	Microtubule-associated proteins
MCI	Mild cognitive impairment
MEM	Minimum essential medium
MS	Mass spectrometry
MS^2	Tandem mass spectrometry
MTs	Metallothioneins
MTT	3-(4,5-Dimethyl-2-thiazolyl)-2,5-diphenyl-2*H*-tetrazolium bromide
MWs	Molecular weights
N2a	Neuro-2a
NADPH oxidase	Nicotinamide adenine dinucleotide phosphate oxidase
Nap	*N*-Naphthylethylenediamine
NFTs	Neurofibrillary tangles
NMDA	*N*-Methyl-D-aspartate
NMDAR	N-Methyl-D-aspartate receptor
NMR	Nuclear magnetic resonance
PAS	Peripheral anionic site
PBS	Phosphate-buffered saline
PD	Parkinson's disease
PDB	Protein data bank
PDEIs	Phosphodiesterases inhibitors
PDEs	Phosphodiesterases
pGlu-Aβ	Pyroglutamate Aβ
PHFs	Paired helical filaments
PIPES	Piperazine-*N*,*N*'-bis(2-ethanesulfonic acid)
PLA2s	Phospholipase A2

PPARγ	Peroxisome proliferator activator receptor γ
ptau	Hyperphosphorylated tau
ROS	Reactive oxygen species
S.E.M.	Standard errors of mean
sAPPα	Soluble amyloid precursor protein α
SAXS	Small-angle X-ray scattering
SDS	Sodium dodecyl sulfate
SFs	Straight filaments
SHG	Second harmonic generation
SOD	Superoxide dismutase
SOFAST-HMQC	2D band-selective optimized flip-angle short transient heteronuclear multiple quantum correlation
SPPS	Solid phase peptide synthesis
SPR	Surface plasmon resonance
SPs	Senile plaques
TBS	Tris-buffered saline
TCSPC	Timecorrelated single-photon counting
TEM	Transmission electron microscopy
TFA	Trifluoroacetic acid
ThT	Thioflavin-T
TLC	Thin layer chromatography
TNF	Tumor necrosis factor
TNFα	Tumor necrosis factor α
TRAIL	Tumor necrosis factor-related apoptosis-inducing ligand
TRAIL-R1	Tumor necrosis factor-related apoptosis-inducing ligand receptor 1
TRAIL-R2	Tumor necrosis factor-related apoptosis-inducing ligand receptor 2
Tris	Tris(hydroxymethyl)aminomethane
UV-vis	Ultraviolet-visible spectroscopy
XANES	X-ray absorption near edge structure
XAS	X-ray absorption spectroscopy
ZIPs	Zinc-regulated transporters, iron-regulated transporter-like proteins
ZnT	Zinc transporter
ZnT-3	Zinc transporter 3

Chapter 1.

Potential Pathological Factors in Alcheimer's Disease

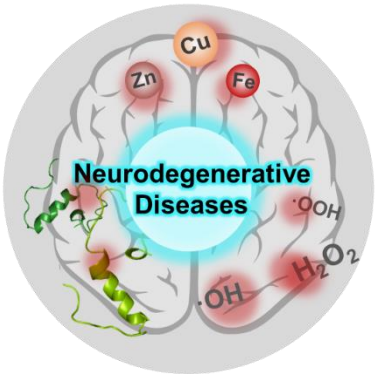

This chapter was adapted from the publication [Savelieff M. G.;† Nam, G.;† Kang, J.;† Lee, H. J.; Lee, M.; Lim, M. H. *Chem. Rev.* **2019**, *119*, 1221–1322 (†equal contribution)]. I thank Professor Mi Hee Lim for her assistance and guidance throughout the writing of this manuscript.

1.1. Introduction

1.1.1. Neurodegenerative Diseases

Neurodegenerative diseases are characterized by the progressive loss of neuronal function. Despite a herculean effort, neurodegenerative diseases remain incurable. Research is revealing parallels between Alzheimer's disease (AD), the most prevalent form of dementia which accounts for ca. 60−80% of cases,[1] and other neurodegenerative diseases, including Parkinson's disease (PD)[2] and amyotrophic lateral sclerosis (ALS).[3] As the global population ages and the number of individuals expected to develop neurodegenerative conditions increases, the search for an effective cure is becoming progressively more urgent.

An obstacle to drug discovery can in part be attributed to the multifactorial nature of most neurodegenerative illnesses. Although the specifics vary, several unifying threads that run through multiple neurodegenerative diseases have been identified. Proteopathy is one recurrent aspect, generally in the form of misfolded and aggregation-prone proteins and peptides, which may occur concurrently with defects in their clearance (Figure 1.1).[4–6] AD is characterized by the deposition of senile plaques (SPs) and neurofibrillary tangles (NFTs), composed of the aggregates of amyloid-β (Aβ) and hyperphosphorylated tau (ptau), respectively.[7,8]

Another prominent theme is metal ion dyshomeostasis in the brains of patients suffering from neurodegeneration.[8–12] Under normal conditions, metal ions play several critical roles in the brain. They are cofactors for numerous enzymes with important catalytic activities (e.g., energy production) and serve as active participants in metal-dependent neurotransmission. Therefore, the proper regulation of metal ions is necessary for normal neuronal function. In neurodegenerative diseases, elevated or lowered levels as well as miscompartmentalization of metal ions are observed, leading to dysregulation of various downstream processes (Figure 1.1). One important consequence of metal ion dyshomeostasis [especially, redox-active Cu(I/II) and Fe(II/III)] is oxidative stress caused by reactive oxygen species (ROS) overproduced from Fenton-like reactions.[10,13] In addition, metal ions are coordinated to amyloidogenic peptides (e.g., Aβ) and consequently modify their aggregation pathways.[14–16] Other pathological features common to several neurodegenerative diseases include mitochondrial dysfunction,[17–19] elevated oxidative stress,[20] defects in energy metabolism,[21,22] aberrant axonal transport,[23–25] and pervasive, sustained chronic inflammation (Figure 1.1).[7,26] Thus, these pathological elements could trigger neuronal loss, alter neurotransmitter levels, and lower the capacity for signal transduction precipitating the progressive decline of cognitive and/or motor function and eventual death. Based on their inter-related roles in the pathogenesis of AD, metal ions and other inter-related pathological factors are implicated as important therapeutic targets in these diseases.

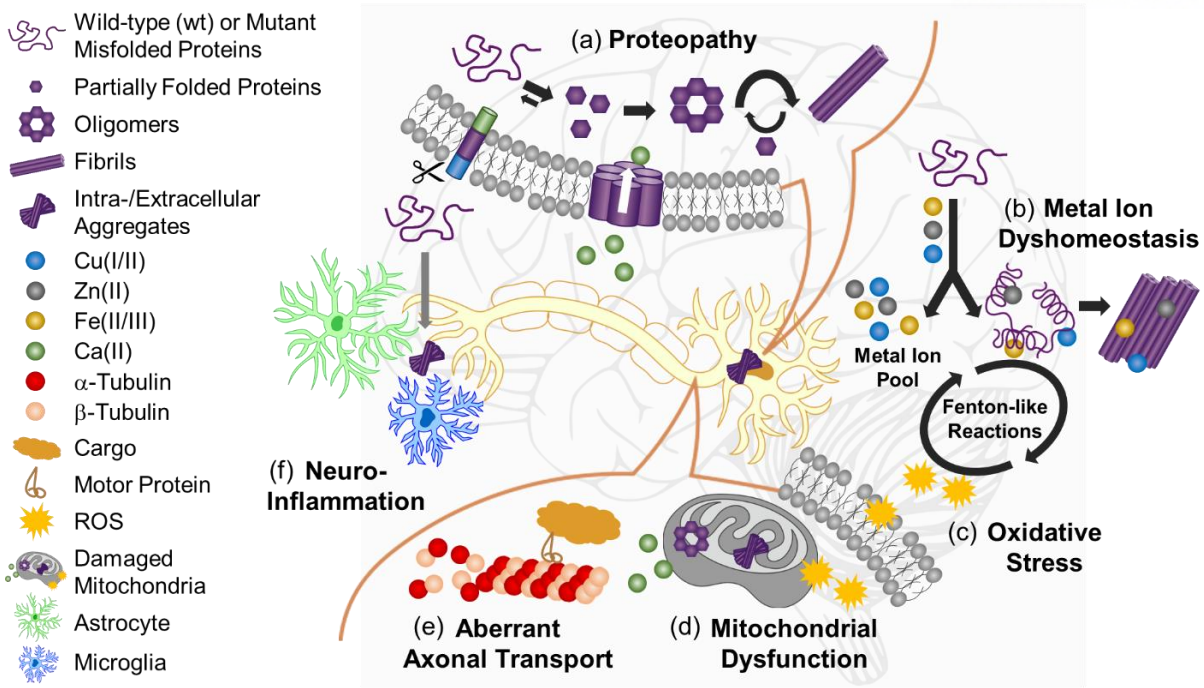

Figure 1.1. Multifactorial nature of neurodegenerative diseases. (a) Proteopathy of wild-type (wt) or mutant intra- or extracellular unfolded proteins/peptides. Unfolded monomers partially fold and aggregate into oligomers and fibrils. Oligomers may interact with various organelles (e.g., mitochondria) or cell membrane disrupting Ca(II) homeostasis and signaling. (b) Dyshomeostasis of metal ions that, depending on the disease, can bind to misfolded proteins/peptides affecting their aggregation or accumulate in the brain or spinal cord. (c) Elevated oxidative stress resulting from redox-active metal ions (i.e., Cu and Fe) via Fenton-like reactions or ROS escaping from damaged mitochondria. ROS can attack cellular proteins, nucleic acids, and lipids causing oxidative damage. (d) Mitochondrial dysfunction and defects in energy metabolism that can occur as a consequence of protein/peptide aggregates. (e) Aberrant axonal transport from hyperphosphorylated microtubule binding proteins, mutant tubulin proteins, or mutant motor proteins. (f) Pervasive, sustained chronic inflammation with reactive microglia and astrocytes as well as altered inflammatory signaling pathways.

Current therapeutic strategies are palliative and only manage symptoms for a short duration of time before cognitive abilities or motor function continue to degenerate. At present, for instance, widely administered treatments for AD are acetylcholinesterase inhibitors (AChEIs) which curb acetylcholine (ACh) degradation and thus maintain levels of neurotransmission.[27] This approach, however, invariably fails, and patients eventually succumb to deteriorating cognitive health. Development of efficacious drugs for neurodegenerative illnesses has been challenging because their precise etiology is not completely identified. A thorough comprehension of disease etiology would be beneficial to aid the discovery of effective therapeutics capable of targeting the root cause of neurodegenerative conditions in a disease-modifying manner. For example, the amyloid cascade hypothesis, the most widely held AD hypothesis, posits that the aggregates of Aβ peptides, produced in the brain, are the primary cause of neurodegeneration.[28] Drugs altering the production, clearance, and aggregation of Aβ have been developed and many have entered clinical trials. None, however, has successfully yielded significant

benefits, although some improvements were observed.[29] These failures have prompted a reexamination of the hypothesis suggesting that other factors, in addition to Aβ, may be mutually operating in neurodegeneration.[30] Another hurdle is timely treatment because neurodegeneration begins prior to disease onset and diagnosis. Intervening at this stage could halt further damage, but it may not be able to reverse the deterioration, which has already occurred. Compounded with these problems are challenges that come from treating a condition in the brain, which is generally nonregenerative, highly heterogeneous, and insulated by the blood-brain barrier (BBB).

Taken together, the multifaceted nature of neurodegenerative diseases suggests that an effective treatment might require a multipronged approach to simultaneously combat several pathological features. Towards this aim, numerous chemical tools capable of targeting and regulating pathological aspects of neurodegenerative disorders have been rationally designed, and studies have been conducted to assess their efficacies. This chapter describes possible therapeutic targets in AD-affected brains to advance our understanding of the etiology fo the disease.

1.2. Alzheimer's Disease (AD)

In 1906, Alois Alzheimer introduced the world to a devastating disease widely known today as AD.[31] AD is a progressive neurodegenerative disease responsible for 60 to 80% of dementia cases.[1,32] According to the World Alzheimer Report, 47 million people worldwide were affected by AD in 2015 and this number is projected to increase to 75 million by 2030.[1] With the aging world population, the social and economic impact of AD is expected to rise significantly.[33] Since the discovery of AD, a great deal of progress has been made towards understanding its pathogenesis; however, we have yet to pinpoint its causative factors or fully elucidate its pathology. More importantly, there are no treatments for AD that can cure or halt its progression. Current AD therapies either temporarily relieve symptoms by inhibiting acetylcholinesterase (AChE) to maintain the levels of ACh and cholinergic transmission or regulating the activation of *N*-methyl-D-aspartate (NMDA) receptors. Five AD treatments approved by the Food and Drug Administration (FDA) are available to relieve the symptoms of AD (Table 1.1): (i) three AChE inhibitors (i.e., **donepezil**, **galantamine**, and **rivastigmine**); (ii) an NMDA receptor (NMDAR) antagonist (i.e., **memantine**); (iii) a mixture of **donepezil** and **memantine**. The imminent amplification of the socioeconomic impact of AD and the lack of an effective treatment illustrate the urgent necessity to identify the underlying AD pathogenesis.

Loss of short-term and long-term memory is the most widely recognized AD symptom. Throughout the progression of AD, patients manifest a general decline in mental ability: language and motor skills, sensory information processing, and memory formation and retrieval.[34] The anatomical hallmarks of AD include the shrinkage of the hippocampus and cortex.[35] Histopathologically, AD compromises SPs and NFTs composed primarily of Aβ and tau, respectively.[28,36,37] Along with its proteopathy, metal ion dyshomeostasis, imbalance between the production and removal of ROS, and

loss of cholinergic transmission are also implicated in AD pathology. Several hypotheses have arisen in an attempt to identify the principal pathological factors in AD: (i) amyloid cascade hypothesis; (ii) tau hypothesis; (iii) metal ion hypothesis; (iv) oxidative stress hypothesis; (v) cholinergic hypothesis. Thus, therapeutics targeting singular pathological factors presented in these hypotheses have proven ineffective, inferring the intricate nature of AD pathogenesis. Consequently, the contemporary direction concerning AD etiopathology increasingly appreciates its complexity and has transitioned from focusing on individual pathological components to illuminating the interrelations among multiple pathological factors.

Table 1.1. Currently available AD treatments.

Generic Name[a]	Structure	Approved for	FDA Approved	Therapeutic Target[b]
Donepezil	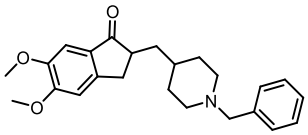	All Stages	1996	AChE
Galantamine	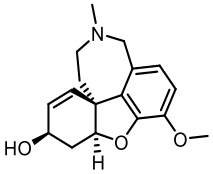	Mild to Moderate	2001	AChE
Memantine	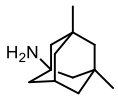	Moderate to Severe	2003	NMDAR
Rivastigmine	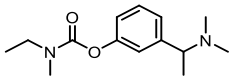	Mild to Moderate	2000	AChE and BuChE
Donepezil + **Memantine**		Moderate to Severe		

[a]**Donepezil**, 2-[(1-benzylpiperidin-4-yl)methyl]-5,6-dimethoxy-2,3-dihydro-1*H*-inden-1-one; **galantamine**, (4a*S*,6*R*,8a*S*)-5,6,9,10,11,12-hexahydro-3-methoxy-11-methyl-4a*H*-[1]benzofuro[3a,3,2-*ef*][2]-benzazepin-6-ol; **memantine**, 3,5-dimethyl-tricyclo[3.3.1.13,7]decan-1-amine; **rivastigmine**, (*S*)-3-[1-(dimethylamino)ethyl]phenyl-*N*-ethyl-*N*-methylcarbamate. [b]AChE, acetylcholinesterase; BuChE, butyrylcholinesterase; NMDAR, *N*-methyl-D-aspartate receptor.

1.2.1. Amyloid-β (Aβ) and Tau

AD proteopathy is portrayed by two highly recognized AD hypotheses: the amyloid cascade and tau hypotheses. The amyloid cascade hypothesis posits that Aβ, a proteolytic product of amyloid precursor protein (APP), is the causative factor in the course of AD pathology.[36] Genetic studies support the pertinence of Aβ in the pathogenesis of AD. Numerous AD genes are shown to influence Aβ pathology (e.g. *APOE*, *APP*, *PSEN1*, and *PSEN2*).[38] A common polymorphism, *ε*4, within *APOE* is reportedly associated with the late onset of AD. This mutation is characterized by elevated Aβ aggregation and

reduced Aβ clearance.[39,40] Genetic variants in APP are connected with early onset familial AD.[41] According to an AD mutation database, 51 APP gene mutations are believed to be linked to the increased $A\beta_{42}$:$A\beta_{40}$ ratio as well as the production and aggregation of Aβ leading to AD.[38,41] *PSEN1* and *PSEN2* mutations are indicated to be involved in the pathology of AD with 219 and 16 variants identified, respectively.[41] Genetic mutations to *PSEN1* and *PSEN2* are shown to enhance the $A\beta_{42}$:$A\beta_{40}$ ratio.[38]

Responsible for the production of Aβ, APP processing can be categorized into nonamyloidogenic and amyloidogenic pathways.[42–44] In nonamyloidogenic APP processing, the soluble APPα (sAPPα) and the C-terminal fragment α (CTFα) are formed by α-secretase cleavage.[42–44] Subsequent cleavage of CTFα by γ-secretase results in the generation of p3, a nonamyloidogenic peptide. Amyloidogenic APP processing is initiated by β-secretase cleavage [e.g., β-site APP cleaving enzyme (BACE1)] producing sAPPβ and CTFβ.[42–44] The generated CTFβ is then cleaved by γ-secretase at multiple sites within the transmembrane domain, producing a range of Aβ monomers with 38 to 43 amino acid residues.[42–45]

Aβ peptides possess a propensity to aggregate, which is a subject of intensive research. As an intrinsically disordered protein, Aβ lacks stabilized secondary or tertiary structures; however, it can exist in partially folded states depending on genetic mutations and external factors (e.g., pH, temperature, peptide concentration, and intermolecular interactions).[46] During on-pathway aggregation, composed of a nucleation phase followed by an elongation phase, monomeric Aβ species oligomerize through interactions between their self-recognition sites and hydrophobic C-terminal regions (Figure 1.2).[43] These metastable Aβ oligomers can further aggregate into protofibrils and fibrils which exhibit a β-sheet conformation.[46] Fibrils have been reported to contribute to the accumulation of Aβ oligomers through fragmentation and secondary nucleation.[47,48] Due to their prominent presence in extracellular SPs, fibrils were initially thought to be responsible for the neurotoxicity found in AD.[49,50] A lack of the correlation between SP load and the extent of neurodegeneration, however, led to the reevaluation of this notion.[36] Recent studies have supported an alternative concept of structured Aβ oligomers as potential toxic species.[51–54] The toxic mechanisms of structured Aβ oligomers have been proposed to arise from their interactions with membranes and membrane receptors and the disruption of intracellular processes [e.g., induction of endoplasmic reticulum (ER) stress, lysosomal leakage, mitochondrial dysfunction, and signal interruption].[46,55] Furthermore, Aβ transmissibility through a seeding effect has been suggested as a means to spread its toxicity, possibly to remote areas, through cell-to-cell transmission mechanisms.[56,57] Overall, the amyloid cascade hypothesis presents potential therapeutic candidates that can directly influence the production, clearance, and aggregation of Aβ.

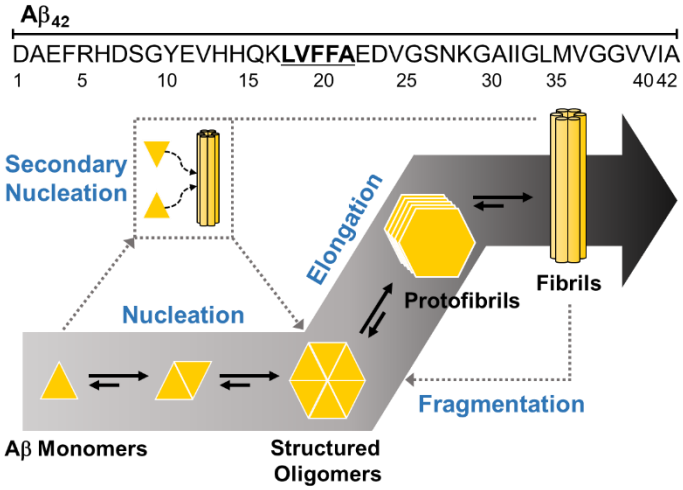

Figure 1.2. Schematic representation of the on-pathway aggregation of Aβ. During the nucleation phase, Aβ monomers aggregate to oligomers through interactions between their self-recognition sites (LVFFA; highlighted in bold and underlined in the amino acid sequence of Aβ). Structured Aβ oligomers are implicated as potential toxic species. Oligomeric Aβ species are further transformed into protofibrils and fibrils. Fragmentation of preformed fibrils, along with secondary nucleation, also contributes to the formation of Aβ oligomers.

NFTs, the second prominent histopathological feature of AD, are mainly found within neurons and predominantly contain aggregates of the tau protein.[123,144] Proponents of the tau hypothesis links the toxicity in AD to the pathogenicity of tau, whose NFT burden correlates more accurately with neurodegeneration than Aβ plaque load.[37,60] Tau, a phosphoprotein, belongs to the family of microtubule-associated proteins (MAPs) that stabilize microtubules, promote, among other functions, anterograde (nucleus to periphery) and retrograde (periphery to nucleus) axonal transport, and sustain dendrite structure.[61] Thus, properly functioning tau is essential to neuronal trafficking and synapse architecture.

Tau is encoded by a single gene on chromosome 17 that gives rise to six isoforms varying in length from 352 to 441 amino acids, which are all found aggregated and hyperphosphorylated in NFTs.[37,58] Tau hyperphosphorylation causes a loss-of-function, which hinders its ability to bind to microtubules, inducing the deterioration of axonal trafficking and dendrite structure leading to microtubule depolymerization.[37,58,62] pTau aggregation occurs in stages, as for Aβ, first into oligomers and amorphous tangles that mature into paired helical filaments (PHFs) and straight filaments (SFs). Similar to Aβ fibrils, PHFs and SFs also contain a cross-β structural feature but additionally include a β-helix motif.[63] Other proteins [e.g., normal tau and alternative MAPs (MAP1/2)] and post-translationally modified and truncated tau/ptau are coaggregated with PHFs and SFs.[64] A greater understanding of tau's aggregation pathway may prove useful in the development of tau-targeting therapeutics. Noble et al. linked the initiation of tau aggregation to cyclin-dependent kinase-5 (cdk5) in

a transgenic (Tg) mouse model.[65] Further research regarding tau phosphorylation and aggregation in AD is necessary to determine their cause-and-effect relationship leading to neuronal degradation and suggest prospective therapeutic approaches.

Gain-of-toxic function from tau is suspected to arise from ptau oligomers rather than from NFTs or SFs. Recent studies on the tau oligomers have increasingly supported their role in the early pathology of AD since they could disrupt anterograde axonal transport and impair long-term potentiation (LTP) in Tg mice.[66,67] For the above-mentioned reasons, the modulation of abnormal hyperphosphorylation and aggregation of tau presents a potential approach for drug discovery. Aside from AD, the diseases, known as tauopathies [e.g., sporadic corticobasal degeneration, progressive supranuclear palsy, and frontotemporal dementia (FTD)], have been linked to tau, suggesting a mutual connection among multiple neurodegenerative diseases.[68]

Increasing evidence indicates a link between the amyloidogenic proteopathy and tauopathy in AD.[69] Tau and ptau have been reported to directly and indirectly interact with Aβ. In a perspective article introducing the amyloid cascade hypothesis, Aβ was accountable for the formation of NFTs.[36] The parallel between Aβ and tau with respect to the toxicity of oligomeric forms has led to the suggestion that the oligomeric species of Aβ and tau may synergistically act to induce neurotoxicity and synaptic dysfunction.[69−72] Moreover, the disruption of calcium homeostasis, glycogen synthase kinase 3 (GSK3), cdk5, and free fatty acids have been implicated as bridging factors between Aβ and tau.[36,62,65,73,74] The interrelationship of Aβ and tau appears to be complex, and further clarification would benefit from agents capable of interacting with both of them.

1.2.2. Metal Ions

Metal ions are involved in biologically vital processes, such as signal transmission, catalysis, stabilization of proteins' structures, and metabolism.[10,75] The functions of the essential first-row transitions metals (e.g., Fe, Cu, and Zn) have been widely studied. These metal ions are strongly regulated across the BBB due to their pertinent role in biologically essential processes.[76] Therefore, the dysregulation of these regulatory mechanisms could lead to disease. In fact, previous studies have demonstrated the colocalization of the above-mentioned metal ions in SPs from AD patients' brain tissue.[8,10] The metal ion hypothesis posits that the dyshomeostasis and miscompartmentalization of metal ions contribute to AD pathology.[77] In this section, we discuss metals' functionality, toxicity, homeostasis, and binding to Aβ, as well as the pathological implications of metal−Aβ.

Among essential transition metals, Zn is the second-most abundant in biological systems.[78] Available in both protein-bound and labile forms in the body, Zn(II) is a d^{10} metal ion that does not possess a biologically relevant redox activity.[78] Zn(II) sites in proteins are tetrahedral or distorted tetrahedral, and as a transition metal ion with borderline hardness, Zn(II) binds to nitrogen (N), oxygen

(O), and sulfur (S) donor atoms of amino acid residues.[79,80] Zn(II) is heterogeneously distributed throughout the brain with relatively high concentrations observed in the hippocampus, amygdala, neocortex, and olfactory bulb areas.[81] Protein-bound Zn(II) [e.g., zinc finger proteins and Cu/Zn superoxide dismutase1 (SOD1)] accounts for over 90% of the total Zn(II) content of the brain. The remaining labile pools of Zn(II), primarily localized within synaptic vesicles of glutaminergic neurons, have been indicated in LTP.[78,82] The interactions of Zn(II) with γ-aminobutyric acid (GABA) receptors and NMDARs and its extracellular release following neuronal stimulation have led researchers to propose its involvement as a neurotransmitter and secondary messenger.[83−85]

Cu, the third-most abundant transition metal in the human body, is found in protein-bound [e.g., cytochrome c oxidase (CcO), Cu/Zn SOD1, ceruloplasmin, and dopamine β monooxygenase (DβM)] and labile forms.[78,86] As a redoxactive metal, Cu acts as a critical cofactor involved in enzymatic functions, including the biochemistry of dioxygen (O_2).[78,87] The two major oxidation states of Cu are +1 and +2. Cu(I) exists under intracellular reducing conditions, while Cu(II) is likely to be present under oxidizing conditions. Cu(I) and Cu(II) are considered soft and borderline acids, respectively, and bind to N, O, and S donor atoms. Cu(I), like Zn(II), is a d^{10} metal ion with preferred coordination numbers 2, 3, or 4, indicating linear, trigonal planar, or (distorted) tetrahedral geometries, respectively. As a d^9 metal ion, Cu(II) can be coordinated to 4, 5, or 6 ligands, with square planar, square pyramidal, or (axially distorted) octahedral geometries, respectively.[88]

Cu(I)-/Cu(II)-coordinated proteins can be categorized into two groups based on their relation to metal ions: (i) proteins utilizing the redox chemistry of Cu(I)/Cu(II) to carry out specific functions (e.g., SOD1 and CcO) and (ii) proteins involved in the Cu transport [e.g., CTR1, ATP7, and CCS].[9,89] Cu adopts important roles in the brain. In order to compensate for the high level of O_2 metabolism in the brain and the potential accidental release of ROS, neurons and glia require Cu for antioxidant enzymes (e.g., SOD1). Cu is also associated with the homeostasis of neurotransmitters, neuropeptides, and dietary amines by acting as a cofactor for DβM, peptidylglycine α-hydroxylating monooxygenase, tyrosinase, and amine oxidases.[78] Micromolar Cu is released into the extracellular space upon neuronal depolorization.[90] Although the role of Cu in signal transmission is not fully understood, previous reports suggest that micromolar Cu is capable of antagonizing NMDA, GABA, and glycine receptors.[91] In addition, exogenous Cu is reported to affect K(I) and Ca(II) channels.[78] Further research regarding the link of labile Cu(II) to neurotransmission is necessary to gain a better understanding of its neurophysiological role.

Fe, known for its role in O_2 transport and metabolism, is the most abundant transition metal in the human body.[92,93] Like Cu, the utility of Fe as a redox-active component manifests the basis of its enzymatic involvement. Fe is an essential element of enzymes (e.g., heme proteins, nonheme proteins, and Fe SOD1) responsible for a spectrum of biological functions, such as electron transfer, O_2 chemistry, gene regulation, and regulation of cell growth and differentiation.[94] The resting state of Fe in enzymes

is mainly found as Fe(II) and Fe(III), while higher oxidation states can be observed as intermediatesin catalytic cycles.[78] Labile Fe(II) and Fe(III) are reported to exist in pools at intracellular concentrations of up to 100 μM,[78] but the nonenzymatic role of Fe in neurobiology has not been clearly identified.

Metal ion homeostasis, balancing functionality against toxicity, is a critical aspect in the proper functioning of biological systems.[78,95] Zn(II) homeostasis is managed by proteins, such as SLC30A (zinc transporter 3; ZnT-3), Zinc-regulated transporters, iron-regulated transporter-like proteins (ZIPs), and metallothioneins (MTs).[78,96–98] ZIP transporters bring Zn(II) into the cytoplasm, while zinc transporter (ZnT), voltage-gated calcium channels, and NMDARs are shown to mediate the extracellular release of Zn(II).[9] Greenough and co-workers implicated the expression of presenilins, a component of γ-secretase, as a major contributor toward the control of Zn(II) and Cu(I)/Cu(II) in the brain.[99] The dysregulation of Zn(II) can lead to excitotoxicity that may induce cell death via the upregulated activity of glutamate receptors, ROS generation, and overactivation of nitric oxide (NO) signaling.[98,100,101] Cu(I)/Cu(II) homeostasis is regulated by proteins, such as CCS, CTR1, ATP7A, COX17, and Cu metabolism COMM domaincontaining protein 1 (COMMD1) domain.[9,89] On the basis of its redox activity, the dysregulation of Cu(I) and Cu(II) can cause the overproduction of ROS leading to oxidative stress. In addition, due to its imperative roles in enzymes, such as SOD1, CcO, and DβM, the colocalization of Cu in amyloid plaques may result in Cu-deficient proteins, causing irregularity in biological functions. Similar to Cu, the notable redox reactivity of Fe makes it a double-edged sword, enabling a wide range of biological functions but generating ROS, whose release can induce toxicity if unregulated and left unchecked. Fe homeostasis is controlled by different types of proteins, including Fe transporters [e.g., divalent metal-ion transporter-1 (DMT1), ferroportin-1, mitoferrin-1, and ZIP14],[102] heme transporters (e.g., HRG1 and FLVCR1),[103,104] Fe chaperones (e.g., PCBPs), ferrireductases, hepcidin, ferritin, and transferrin.[105]

The essential function of metals in the brain coupled with the detrimental effects of their dysregulation suggests that metal ion dyshomeostasis could lead to disease.[8,9,10,86,106–111] In 1994, Bush et al. discovered the relevance of metal ions in AD pathogenesis.[112] They reported the induction of $A\beta_{40}$ fibrillization in the presence of Zn(II),[112] launching intense research into the binding of transition metal ions to Aβ.[15] Moreover, highly concentrated Cu(I/II), Zn(II), and Fe(II/III) (ca. 400, 1000, and 900 μM, respectively) were found within SPs compared to healthy age-matched controls, reinforcing their interaction with Aβ in vivo and possible involvement in AD pathogenesis.[113] Since binding of Zn(II), Cu(I/II), and Fe(II) to Aβ modifies its aggregation, the investigations of molecular-level interactions between metal ions and Aβ can be challenging. Researchers circumvented this issue by employing $A\beta_{16}$ or $A\beta_{28}$ that bind Cu(II) and Zn(II) without significant aggregation.[114–131] The proposed coordination of Zn(II), Cu(I/II), and Fe(II) to Aβ is summarized in Table 1.2 and Figure 1.3.

Table 1.2. Proposed amino acid residues of Aβ for metal coordination.

Metal Ions	Peptides	Amino Acid Residues for Metal Coordination	Technique	Reference
Fe(II)	$A\beta_{16}$ and $A\beta_{40}$	N-terminal NH_2, (D1 or E3), (D1-A2 or H6-D7; Carbonyl from the Amide Group), H6, and (H13 or H14)	NMR	129
Fe(III)	$A\beta_{28}$	n.d.[a]	NMR, ESI-MS	130
Cu(I)	$A\beta_{6-14}$	H13 and H14	EXAFS	123
	$A\beta_{10-14}$	H13 and H14	EXAFS	123
	$A\beta_{16}$	H13 and H14	EXAFS, EPR	124
	$A\beta_{16}$	H13 and H14	NMR, XANES	125
	$A\beta_{16}$	H13 and H14	CP-MD Simulation	126
	$A\beta_{40}$	H13 and H14	EXAFS, EPR	124
Cu(II)	$A\beta_{16}$	pH 6.5: H6, (H13 or 14), N-terminal NH_2, (D1; Side-chain Carboxylate Group), and (D1-A2; Carbonyl from the Amide Group) pH 9.0: N-terminal NH_2, (D1-A2; N from the Amide Group), (A2-E3; Carbonyl from the Amide Group), and (H6, H13, and H14)	EPR	134
	$A\beta_{16}$	pH 6.3: N-terminal NH_2, (D1-A2; Carbonyl from the Amide Group), H6, and (H13 or H14); pH 8.0: (A2-E3; Carbonyl from the Amide Group), H6, H13, and H14	EPR	127
	$A\beta_{16}$	pH 6.3: D1, (D1-A2; Carbonyl from the Amide Group), H6, and (H13 or H14); pH 8.0: (A2-E3; Carbonyl from the Amide Group), H6, H13, and H14	EPR	128
	$A\beta_{28}$	pH 5.5: H6, Y10, H13, and H14	NMR, EPR	119
	$A\beta_{28}$	pH 7.4: N-terminal NH_2, H6, H13, and H14	EPR	138
Zn(II)	$A\beta_{16}$	R5, H6, H13, and H14	ESI-MS	114
	$A\beta_{16}$	D1, H6, H13, and H14	NMR	115

$A\beta_{16}$	H6, H13, H14, and (E11; Side-chain Carboxylate Group)	NMR	116
$A\beta_{16}$	$A\beta_{11\text{-}14}$ Residues (E11 and H14)	SPR, ESI-MS	117
$pA\beta_{16}$ (S8)	H6, D7, Phosphorylated S8, E11, H13, and H14	ITC, ESI-MS, NMR	118
N-terminal acetylated $A\beta_{16}$	H6, E11, (H13 or H14), (D1, E3, or D7), and N-terminal NH_2	NMR, XAS	131
D7H-$A\beta_{10}$	(D1-A2; Carbonyl from the Amide Group), E3, H6, and H7	NMR, EXAFS, MS, ITC	122
$A\beta_{28}$	H6, H13, and H14	NMR, EPR	119
$A\beta_{28}$	H6, H13, and H14	NMR, CD	120
$A\beta_{28}$	N-terminal NH_2, H6, H13, (H14, and/or E11), and (Y10 for Conformational Rearrangement)	NMR	121
$A\beta_{40}$	N-terminal NH_2, H6, H13, and H14	NMR	132

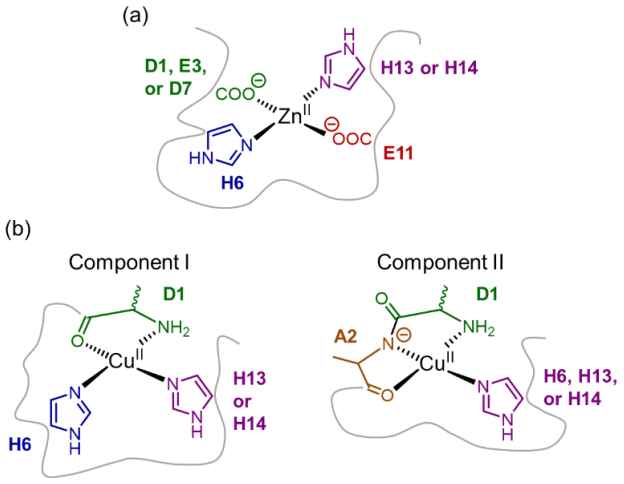

Figure 1.3. Examples of metal coordination to Aβ. Each metal [Zn(II) and Cu(II)] coordination is published in refs 131 and 134, respectively. Possible fifth ligands on the metal centers are not indicated in this figure.

Numerous studies have focused on possible binding modes of Zn(II) and Aβ.[114−122,131,132] On the basis of previous findings, the feasible Zn(II) binding sites in Aβ are primarily composed of 4−6 ligands: H6, H13, and/or H14 with additional candidates that include D1 (N-terminal NH_2 or side chain carboxylate), E3, R5 (backbone amide), D7, Y10, E11, or water molecules.[8,106,108,114−116,119,120,132,133] In

addition, Y10 is implicated in a Zn(II)-dependent conformational rearrangement under membrane-mimicking environments.[121] Kulikova et al. reported that phosphorylated residues may be involved in Zn(II) binding based on studies with Aβ containing phosphorylated S8 (pAβ). Proposed binding residues are the phosphate group, the imidazole ring of H6, and a backbone carbonyl group of either H6 or D7.[118] This binding mode stimulates peptide dimerization with an additional Zn(II) coordinated to two pairs of E11 and H14 from two separate peptide subunits.[118] This observation of Zn(II)-induced dimerization provides insight into the initiation of metal-induced Aβ aggregation.

Recently, an unprecedented coordination of Zn(II)−$A\beta_{10}$ was presented with the Taiwanese mutation D7H using a suite of structural characterization methods.[122] The 1:1 stoichiometry was confirmed via nuclear magnetic resonance (NMR) and isothermal titration calorimetry (ITC). Additionally, the formation of the proposed complex [Zn_2(D7H-$A\beta_{10}$)$_2$], which consisted of a binuclear Zn(II) core where both ions were bound to two D7H-$A\beta_{10}$ peptides, was validated by mass spectrometry (MS) and isotope-edited NMR.[122] The NMR investigations revealed that the carbonyl group (D1-A2), carboxyl group (E3), H6 (from one polypeptide chain), and H7 (from the second polypeptide) were bound to Zn(II).[122] These observations were theoretically refined and supported by extended X-ray absorption fine structure (EXAFS) spectroscopy.[122]

The Cu(II)−Aβ binding mode occurs in two forms, components I and II (Figure 1.3), depending on the pH (i.e., pH 6.5 and pH ≥ 8, respectively).[8,106,119,127,128,133−137] At pH ≥ 8, component II is predominant with three main potential binding configurations of Cu(II)−Aβ: (i) 3N1O coordination {e.g., for 3N, [H6, D1 (N-terminal NH_2), and D1-A2 (deprotonated backbone amide)] or (H6, H13, and H14); for 1O, carbonyl backbone oxygen (A2-E3)},[127,128,134] (ii) 4N coordination with three histidines (H6, H13, and H14) and either N-terminal amino group or deprotonated backbone amide,[138,139] or (iii) 5N1O coordination with potential binding sites: N-terminal NH_2, the N donor atom from the D1-A2 backbone, carbonyl backbone from A2-E3, H6, H13, and H14.[134]

Component I is the prevalent Cu(II) binding mode with Aβ under physiological conditions. Several reports have proposed 3N1O coordination involving: (i) the N-terminal primary amino group of D1, an O donor atom from a carbonyl backbone between D1 and A2, H6, and either H13 or H14 or (ii) D1 (N-terminal amine), D1-A2 (a carbonyl backbone), and two histidines among H6, H13, and H14, with the possibility of an additional coordination with D1 (carboxylate).[8,106,108,127,128,133−136] Dorlet et al. reported the observation of a 5-coordination mode using electron paramagnetic resonance spectroscopy (EPR) in conjunction with specific isotopic labeling.[134] They detected and identified a 3N2O coordination site in Aβ consisted of two histidines (H6 and either H13 or H14), the N-terminal NH_2, the carbonyl group between D1 and A2, and the carboxylate group of D1. The carbonyl and carboxylate groups from D1 were reported in the equatorial and axial positions, respectively. The exact binding atoms of D1 in Aβ is controversial. The N-terminal NH_2, the carboxylate, and the amide backbone have

all been suggested to be possible binding atoms from D1.[127,128,134] Moreover, the involvement of Y10 via conformational rearrangement of Cu(II)−Aβ at pH 6.9 has been suggested.[119] Previous studies demonstrated that the pH-dependent oxidation state of the Aβ-bound Cu dictates the coordination geometry of the complex.[124,140] When Cu K-edge X-ray absorption spectroscopy (XAS) was applied to Cu(II)−Aβ, a square-planar Cu(II) center with mixed N/O ligation, including imidazole groups of histidine ligands, was indicated.[124,141] After reduction of Cu(II)−Aβ, the EXAFS data fit best a linear two-coordinate geometry with two imidazole ligands, possibly H13 and H14, coordinated to Cu(I)−Aβ.[123−126,141] Studies of the Fe(II)−Aβ binding via NMR demonstrated a coordination composed of the N-terminal NH_2 (D1), a carboxylate from either D1 or E3, a carbonyl group from D1-A2 or H6-D7, and two N donor atoms from H6 and either H13 or H14.[129] There is limited information regarding the binding of Fe(III)−Aβ.[129,130]

Determination of binding affinities of metal−Aβ complexes at different conditions can be valuable, especially towards the development of therapeutics with metal chelating capabilities. Comparative studies regarding binding affinities of metal−Aβ to novel metal chelators may allow researchers to estimate their ability to target labile metal ions and metal−Aβ versus metal ions from metalloproteins essential for biological functions. The reported range of K_d for Zn(II) and Aβ is 10^{-9}–10^{-6} M.[8,108,132,135,142−148] The presented K_d values for metal−Aβ are dependent on the experimental conditions and techniques, such as ITC, fluorescence spectroscopy, and potentiometry.[108,110,132,143−146] For Cu(II)−Aβ, the K_d value was calculated to be 10^{-11}–10^{-7} M, while Cu(I)−Aβ showed 10^{-15}–10^{-8} M in K_d.[8,107,132,135,138,142,144−146,149−160] Cu(II) seems to exhibit stronger binding to Aβ than Zn(II). Fe(II) forms less stable complexes (K_d = ca. 10^{-5} M), compared to those of Cu(II) or Zn(II).[145] The reported K_d values of Zn(II)−Aβ, Cu(I/II)−Aβ, and Fe(II)−Aβ are summarized in Table 1.3. The propensity of Aβ to aggregate poses a challenge in studying its metal binding properties. As a solution, researchers have been utilizing various Aβ fragments with slower aggregation kinetics. Although soluble Aβ fragments enable the study of metal binding and coordination, various conformations of the full-length Aβ (e.g., monomers, oligomers, and fibrils) are expected to exhibit different metal coordination environments.[146,159] On the basis of currently available literature, a wide range of binding affinities is reported because metal binding to Aβ is dependent on Aβ species, techniques, and experimental conditions (e.g., buffer composition, temperature, concentrations, and peptide purity).

Table 1.3. Binding affinities of metal ions to Aβ.

Metal Ions	Peptides	K_d (x 10^{-6} M)	Conditions[a]	Technique	Reference
Fe(II)	$A\beta_{40}$	76 (± 20)	10 mM Tris, pH 7.4, 100 mM NaCl	Fluorescence	145
Cu(I)	$A\beta_{16}$	2.7 (± 2.1) x 10^{-9}	20 mM *N*-Ethylmorpholine, pH 7.0	UV-Vis	154
	H6A-$A\beta_{16}$	8.9 (± 3.7) x 10^{-9}	20 mM *N*-Ethylmorpholine, pH 7.0	UV-Vis	154
	H13A-$A\beta_{16}$	1.1 (± 0.7) x 10^{-8}	20 mM *N*-Ethylmorpholine, pH 7.0	UV-Vis	154
	H14A-$A\beta_{16}$	1.0 (± 0.8) x 10^{-8}	20 mM *N*-Ethylmorpholine, pH 7.0	UV-Vis	154
	$A\beta_{42}$	5.4 (± 0.9) x 10^{-2}	100 mM HEPES, pH 7.4	UV-Vis	154
Cu(II)	$A\beta_{16}$	47 (± 5)	100 mM Tris, pH 7.4, 150 mM NaCl	Fluorescence	149
	$A\beta_{16}$	0.1	H_2O, pH 7.8	Fluorescence	150
	$A\beta_{16}$	0.09	50 mM HEPES, pH 7.4, 100 mM NaCl	ITC	151
	$A\beta_{16}$	0.7 x 10^{-3}	20 mM HEPES, pH 7.2, 150 mM NaCl	ITC	158
	$A\beta_{16}$	0.3 x 10^{-3}	20 mM PIPES, pH 7.4, 160 mM NaCl	ITC	160
	$A\beta_{4\text{-}16}$	8 (± 2)	100 mM Tris, pH 7.4, 150 mM NaCl	Fluorescence	149
	$A\beta_{28}$	0.1	H_2O, pH 7.8	Fluorescence	138
	$A\beta_{28}$	28 (± 5)	100 mM Tris, pH 7.4, 150 mM NaCl	Fluorescence	149
	$A\beta_{28}$	0.07	50 mM HEPES, pH 7.4, 100 mM NaCl	ITC	151
	$A\beta_{28}$	0.4 (± 0.1)	10 mM Phosphate, pH 7.2	Fluorescence	156
	$A\beta_{28}$	2.5 (± 0.2)	10 mM HEPES, pH 7.2	Fluorescence	156
	$A\beta_{28}$	1.2 (± 0.1)	10 mM Phosphate, pH 6.5	Fluorescence	156

	$A\beta_{40}$	1.6 (± 0.9)	10 mM Tris, pH 7.4, 100 mM NaCl	Fluorescence	145
	$A\beta_{40}$	11 (± 1)	100 mM Tris, pH 7.4, 150 mM NaCl	Fluorescence	149
	$A\beta_{40}$	ca. 8	50 mM Phosphate, pH 7.4, 100 mM NaCl	Fluorescence	152
	$A\beta_{40}$	0.5 (± 0.2)	10 mM Tris, pH 7.4, 100 mM NaCl	Fluorescence	144
	$A\beta_{40}$	1.2 (± 0.4)	20 mM Tris, pH 7.4, 100 mM NaCl	Fluorescence	144
	$A\beta_{40}$	3.8 (± 0.9)	50 mM Tris, pH 7.4, 100 mM NaCl	Fluorescence	144
	$A\beta_{40}$	30 (± 6)	100 mM Tris, pH 7.4, 100 mM NaCl	Fluorescence	144
	$A\beta_{40}$	0.6 (± 0.2)	20 mM HEPES, pH 7.4, 100 mM NaCl	Fluorescence	144
	$A\beta_{40}$	2.5 (± 0.6)	100 mM HEPES, pH 7.4, 100 mM NaCl	Fluorescence	144
	$A\beta_{40}$	0.9×10^{-3}	20 mM HEPES, pH 7.2, 160 mM NaCl	ITC	155
	$A\beta_{40}$	0.4×10^{-3}	20 mM HEPES, pH 7.4, 160 mM NaCl	ITC	155
	$A\beta_{40}$	1.6	5 mM Phosphate, pH 7.3	NMR	157
	$A\beta_{40}$	5.2×10^{-4}	20 mM PIPES, pH 7.4, 160 mM NaCl	ITC	160
	F4W-$A\beta_{40}$	0.6 (± 0.2)	10 mM Tris, pH 7.4, 100 mM NaCl	Fluorescence	155
	$A\beta_{42}$	2.0 (± 0.8)	10 mM Tris, pH 7.4, 100 mM NaCl	Fluorescence	155
	$A\beta_{42}$	0.8 (± 1.0)	20 mM HEPES, pH 7.4, 100 mM NaCl	Fluorescence	154
Zn(II)	$A\beta_{16}$	22 (± 15)	20 mM Tris, pH 7.4, 100 mM NaCl	ITC	153
	$A\beta_{16}$	14 (± 5)	20 mM HEPES, pH 7.4, 100 mM NaCl	UV-Vis	153
	$A\beta_{16}$	9	50 mM HEPES, pH 7.1	UV-Vis	148

$A\beta_{28}$	6.6 (± 0.2)	10 mM HEPES, pH 7.2	Fluorescence	132
$A\beta_{28}$	1.1 (± 0.1)	10 mM Phosphate, pH 7.2	Fluorescence	132
$A\beta_{28}$	3.2 (± 0.1)	10 mM Phosphate, pH 6.5	Fluorescence	132
$A\beta_{28}$	12 (± 5)	20 mM HEPES, pH 7.4, 100 mM NaCl	UV-Vis	143
$A\beta_{28}$	10 (± 8)	20 mM Tris, pH 7.4, 100 mM NaCl	ITC	143
$A\beta_{40}$	1.2 (± 0.03)	10 mM Phosphate, pH 7.2	NMR	132
$A\beta_{40}$	300 (± 100)	10 mM Tris, pH 7.4, 100 mM NaCl	Fluorescence	145
$A\beta_{40}$	7 (± 3)	20 mM Tris, pH 7.4, 100 mM NaCl	ITC	143
$A\beta_{40}$	7 (± 3)	20 mM HEPES, pH 7.4, 100 mM NaCl	UV-Vis	143
$A\beta_{40}$	65 (± 3)	20 mM HEPES, pH 7.4, 100 mM NaCl	Fluorescence	144
$A\beta_{40}$	124 (± 32)	20 mM HEPES, pH 7.4, 100 mM NaCl	UV-Vis	144
$A\beta_{40}$	60 (± 14)	10 mM Tris, pH 7.4, 100 mM NaCl	Fluorescence	144
$A\beta_{40}$	184 (± 30)	100 mM Tris, pH 7.4, 100 mM NaCl	Fluorescence	144
$A\beta_{40}$ fibrils	9 (± 6)	20 mM HEPES, pH 7.4, 100 mM NaCl	UV-Vis	143
F4W-$A\beta_{40}$	90 (± 30)	10 mM Tris, pH 7.4, 100 mM NaCl	Fluorescence	145
$A\beta_{42}$	57 (± 28)	10 mM Tris, pH 7.4, 100 mM NaCl	Fluorescence	145
$A\beta_{42}$	7 (± 3)	20 mM HEPES, pH 7.4, 100 mM NaCl	UV-Vis	143
$A\beta_{42}$	91 (± 16)	20 mM HEPES, pH 7.4, 100 mM NaCl	Fluorescence	144
$A\beta_{42}$	6.2 (± 0.9)	20 mM HEPES, pH 7.4	ITC	147

[a]Tris, tris(hydroxymethyl)aminomethane; HEPES, 4-(2-hydroxyethyl)-1-piperazineethanesulfonic acid; PIPES, piperazine-*N*,*N*′-bis(2-ethanesulfonic acid); PBS, phosphate-buffered saline.

The influence of transition metal ions on Aβ aggregation has also been examined in depth since the first description of Zn(II)-dependent $Aβ_{40}$ aggregation.[11,112,161] At physiological pH, Cu(II) and Fe(II/III) also promote $Aβ_{40}$ aggregation,[161,162] although induction by Cu(II) requires a slightly acidic condition (e.g., pH 6.8).[163] Even trace metal ions (< 0.8 μM) are sufficient to stimulate $Aβ_{40}$ aggregation, resulting in less structured aggregates.[164,165] Metal-induced Aβ aggregation is shown to be rapid, and it could result in the production of nonfibrillar, amorphous aggregates depending on the ratio of metal to Aβ (vide infra). A mixture of $Aβ_{42}$:Cu(II) in a 1:5 ratio resulted in a diminished fluorescence intensity of thioflavin-T (ThT), and smaller-sized aggregates as determined by atomic force microscopy (AFM), relative to $Aβ_{42}$ only.[166] This observation was extended to other metal ions, including Zn(II) and Fe(II).[167] Ultrafast spectroscopic techniques demonstrated an immediate interaction within milliseconds between micromolar Zn(II) and $Aβ_{40}$ showing resultant nonfibrillar peptide aggregates that were possibly toxic.[168] A detailed study suggested that Zn(II)−$Aβ_{40}$ species might inhibit fibril formation by disrupting fibril elongation.[169] Interaction of Cu(II) with $Aβ_{40}$ (pH 6.7) was also observed on a time scale of subseconds with the formation of amorphous Cu(II)−Aβ species.[170] Likewise, Fe(III) was observed to retard $Aβ_{42}$ fibrillization by redirecting the aggregation pathways towards unstructured, less toxic Fe(III)−Aβ aggregates.[171] Although the precise nature of metal−Aβ conformations is uncertain, the measurements by circular dichroism spectroscopy (CD) propose that their transition may involve the generation of β-enriched structures, distinct from the fibrillar β-sheet conformation.[172]

Metal ions appear to increase the proportion of soluble oligomers compared to fibrils.[173−175] Since structured soluble oligomers are associated with toxicity,[176,177] this may constitute a potential mechanism of toxicity that arises from metal−Aβ species. Addition of Cu(II) to Aβ yielded soluble toxic oligomers enriched in a β-sheet configuration.[174] In another report, Cu(II) and Zn(II) triggered the production of transient Aβ oligomers.[175] While Zn(II) developed annular Aβ protofibrils without undergoing a nucleation process, Cu(II) and Fe(III) prevented the formation of fibrils by lengthening the nucleation phase.[175]

The relative ratio of metal ions to Aβ also impacts the aggregation pathways of Aβ.[178,179] Increasing the relative amount of Cu(II) to $Aβ_{40}$ from 0.1 to 0.6 causes a shift from fibrillar structures to amorphous granular aggregates.[178] Another study examined a wider Cu(II):$Aβ_{40}$ range from sub- to supra-stoichiometric amounts.[179] The Cu(II):Aβ ratio was found to affect the aggregation kinetics and aggregate morphology, deviating from fibrillar to nonfibrillar with increasing Cu(II):Aβ proportions. Structures of Cu(II)−Aβ aggregates were dynamic. The transient and impermanent nature of metal−Aβ species has made their structural characterization difficult. Still, progress towards an understanding of their general characteristics has been made. A small-angle X-ray scattering (SAXS) study examined the generation of Aβ oligomers at extremely short time scales by combining the technique with in-line rapid

mixing.[180] Modeling of the scattering data can approximate oligomers' size (i.e., diameter), molecular weight, and polydispersity.

Although the aggregation kinetics, species distribution, and toxicity of metal−Aβ species have been extensively studied, their precise mechanism of toxicity has been still uncertain. Recently, Matheou et al. illustrated the distinct influence of substoichiometric Cu(II) on the aggregation pathways of $A\beta_{40}$ and $A\beta_{42}$.[181] While fibrillization was favored for $A\beta_{40}$, oligomeric and protofibrillar forms of $A\beta_{42}$ were observed in the presence of Cu(II). These species could cause leakage from lipid vesicles in a manner reminiscent of metal-free Aβ oligomers.[182] Mutations of Aβ may also impact its aggregation properties in the presence of metal ions and may be one mechanism linking familial forms of AD to pathogenesis. The Taiwanese mutation (D7H) led Zn(II)- and Cu(II)-induced aggregates of both $A\beta_{40}$ and $A\beta_{42}$ from fibrillar forms to smaller-sized oligomers.[183] The pathogenic A2V mutation imparted different Aβ aggregation kinetics and metal binding properties in response to addition of Cu(II).[184] The Cu(II)−$A\beta^{A2V}$ complex showed a preference for the component I configuration of the Cu(II) center.

On the basis of cumulative experimental and theoretical evidence, metal ions have been considered potential therapeutic targets in AD. The utilization of metal chelators has demonstrated their potential as AD treatments, but further optimization of metal chelators is necessary to develop effective therapeutics.[185,186] Moreover, fine-tuning metal binding affinities (K_d) of compounds to specifically target metal ions bound to Aβ without disrupting vital enzymatic activities is an important parameter for rational design.

1.2.3. Oxidative Stress

O_2 is indispensable to aerobic organisms. In metabolic systems, ROS are generated from endogenous processes, such as O_2 metabolism and cellular signaling, while exogenous ROS can be produced from environmental stress (e.g., ionizing radiation and heat exposure).[187−189] Biologically relevant ROS include superoxide anion radical ($O_2^{\bullet-}$), hydroxyl radical (•OH), hydrogen peroxide (H_2O_2), hydroperoxyl radical ($\bullet O_2H$), singlet oxygen ($^1O_2$), peroxide (O_2^{2-}), and hydroxide ion (OH^-). A membrane-bound enzyme, nicotinamide adenine dinucleotide phosphate oxidase (NADPH oxidase), found in cell membranes, mitochondria, and ER, is responsible for substantial intracellular ROS production.[190,191] NADPH oxidase generates superoxide anion radicals ($O_2^{\bullet-}$) by transferring electrons from NADPH within the cell across the membrane.[190,192] ROS are necessary for a variety of cellular functions, including receptor-mediated signaling pathways and transcriptional activation.[193−199] In addition, ROS plays a critical role in cellular homeostasis through regulation of apoptosis. ROS control apoptotic signaling initiated via two pathways:[198,200] (i) ROS-triggered death receptors [e.g., Fas (CD95 or APO-1), tumor necrosis factor (TNF) receptor 1, TNF-related apoptosis-inducing ligand (TRAIL) receptor 1 (TRAIL-R1 or DR4), and TRAIL receptor 2 (TRAIL-R2 or DR5)] can mediate the extrinsic

pathway of apoptosis by clustering and forming lipid-raft-derived signaling platforms, suggested as a major mechanism of apoptotic signaling,[200,201] and (ii) ROS are associated with mitochondrial permeabilization by generating pores in the mitochondrial outer membrane, which stimulates the release of proapoptotic proteins [e.g., members of the B-cell lymphoma 2 (Bcl-2) gene family and BAX (Bcl-2 associated X)] that are essential for the activation of apoptosis.[198,200,202−204]

Various types of ROS can be found in cellular environments.[193,194] Prominent biological ROS are hydroxyl radical (•OH), $O_2^{\bullet-}$, and H_2O_2. Hydroxyl radicals are produced by Fenton-like reactions.[8,142] Due to its relatively short half-life (10^{-9} s), •OH is known to be involved in "site-specific" reactions in the vicinity of its formation site.[205,206] $O_2^{\bullet-}$, the product of the one-electron reduction of O_2, is generated by multiple systems in organisms of animals and plants (e.g., xanthine oxidase and NADPH oxidase).[188,192,194,207] $O_2^{\bullet-}$ can react with many substrates by converting into other species.[111,194,195] $O_2^{\bullet-}$ is capable of transforming into •OH by the Haber-Weiss reaction, which generates •OH from H_2O_2 and $O_2^{\bullet-}$.[207] Both •OH and $O_2^{\bullet-}$ can initiate lipid peroxidation that can lead to apoptosis.[8,107,188,195,207,208] H_2O_2 is a common byproduct of diverse enzymatic reactions, including those involving SOD.[107,111,188,194,195,209] H_2O_2 is related to a broad range of biological processes: (i) immune response; (ii) oxidative biosynthesis, such as tyrosine crosslinking mediated by peroxidases; (iii) cellular signaling in mediating mitogenic signaling pathways.[195,209,210]

Under normal conditions, the levels of the above-mentioned ROS are regulated by innate antioxidant defenses.[10,111,190,211−213] Pathological conditions, however, can elicit an imbalance between the production and removal of ROS, resulting in elevated ROS levels.[9,111,195] Oxidative stress is characterized by dysregulation of ROS and the resultant cellular damage through the oxidation of lipids, proteins, and DNA.[86,111,189,193−195] Oxidative stress in biological systems has been strongly implicated as a causative factor for a wide spectrum of diseases and aging.[9,111,195] Thus, maintaining proper ROS load is important to the preservation of biological homeostasis.

Oxidative stress is believed to be involved in neurodegenerative diseases, including AD.[9,10,86,110,111,142,187−189,208,211,213,214] Oxidative stress is a prevailing component in the manifestation of multiple pathological factors (e.g., Aβ, metal ions, and metal−Aβ) as well as toxic mechanisms of these factors.[142,107,215] Three major aspects are connected with oxidative stress to AD pathology: (i) Aβ production and accumulation;[211,215−218] (ii) metal ion dyshomeostasis;[219] (iii) mitochondrial dysfunction.[111,187,189,193,194,214,215] Researchers have suggested that oxidative stress enhances Aβ production by decreasing the activity of α-secretase while increasing the activity of β- and γ-secretases.[211,215] In addition, oxidative stress could activate the pathway of c-Jun N-terminal kinase (JNK), which could modulate the expression of β-secretase.[211,215] The generated Aβ accumulates in the brain and forms SPs, a hallmark of AD.[86,109]

Pathological factors of AD (e.g., metal ions, Aβ, and tau) are suggested to be involved in redox-active processes capable of inducing oxidative stress via ROS generation.[10,106,220] Multiple in vitro and in vivo studies report that Aβ peptides trigger oxidative stress.[221−236] A Tg *C. elegans* worm model expressing human $A\beta_{42}$ exhibited enhanced oxidative stress as evidenced by elevated carbonyl levels associated with the oxidation of proteins.[233,237] I31 and M35 in Aβ are proposed to be potentially responsible for oxidative damage (vide infra).[228,229,231,237] Especially, M35 is reported as a critical amino acid residue for ROS production.[221,223,230] The α-helical conformation in the C-terminal region of Aβ allows the S atom of M35 to interact with the O atom from the carbonyl of I31,[229,231,236] which could result in the formation of the methionine sulfuranyl radical (MetS•).[228,236,238] Aβ can also act as a source of ROS and initiate lipid peroxidation by producing carbon-centered radicals.[231,236] Moreover, oligomeric Aβ has been observed to increase the generation of ROS directly by activating NADPH oxidase and indirectly through NMDARs by stimulating the release of arachidonic acid, a retrograde messenger involved in modulating synaptic plasticity.[232,239]

The dysregulation of redox-active metal ions, including Cu(I/II) and Fe(II/III), in the central nervous system (CNS) is observed in the AD-affected brain.[240−243] Furthermore, these metal ions are able to produce ROS through Fenton-like reactions.[244,245] Overproduction of ROS by metal ions can result in oxidative stress that causes neuronal death in the brain.[10,213,214] Moreover, Zn(II), a redox-inert metal ion, indirectly increases ROS levels.[246−250] Mitochondrial uptake of labile Zn(II) from the cytoplasm through the calcium uniporter can alter mitochondrial polarization and disrupt the electron transport chain leading to the formation of ROS, such as $O_2^{\bullet-}$.[246−250]

Along with the individual impact of metal ions and Aβ on ROS production, metal−Aβ species have been observed to generate ROS. Redox-active metal ions associated with Aβ [i.e., Cu(I/II)−Aβ and Fe(II/III)−Aβ] can generate ROS via Fenton-like reactions, similar to redox-active metal ions.[10,251,252] In vitro studies demonstrate that Cu(I/II)−Aβ or Fe(II/III)−Aβ can overproduce ROS leading to oxidative stress.[8,10,213,251,253,254] ROS generation mediated by Cu(I/II)−Aβ has been widely studied.[86,129,136,255,256] Cu(I/II)−Aβ is indicated to catalytically form ROS. In the presence of a reductant (e.g., ascorbate), Cu(II)−Aβ could be reduced to Cu(I)−Aβ and transfer an electron to O_2 to yield $O_2^{\bullet-}$.[86,255,257] Then, a hydroperoxyl radical ($\bullet O_2H$) can be formed via electron/proton transfer, finally resulting in the production of H_2O_2 (vide supra).[8,10,259] The generated H_2O_2 can then react with either Cu(I)−Aβ or Cu(II)−Aβ affording $\bullet O_2H$ or •OH through Fenton-like reactions.[8,86,258] Spectroscopic and spectrometric studies presented that the D1, H13/H14, and M35 residues in Aβ may be involved in the electron transfer between Cu(I/II) and Aβ responsible for ROS generation.[221,230,255,259−263]

Oxidative stress can damage cells by disrupting cell signaling and causing mitochondrial dysfunction.[111,181,189,193,215] Mitochondrial function is vulnerable to oxidative stress; however, paradoxically, the mitochondrial respiratory chain is a major source of intracellular ROS.[193,215,264]

Mitochondrial respiratory complexes could generate ROS, such as $O_2^{\bullet-}$ and H_2O_2, and the increased concentrations of these ROS could produce •OH and react with biomolecules, including lipids and proteins.[8,188,195,207,265] Biological systems are observed to protect themselves from oxidative stress by maintaining appropriate levels of ROS with endogenous defensive systems.[107,111,187,193–195] For example, (i) Cu/Zn SOD1 binds to Cu and Zn to catalyze the dismutation of $O_2^{\bullet-}$ into either O_2 and H_2O_2;[9,86,111,188,208] (ii) another important antioxidant is glutathione that is converted to its oxidized form (i.e., glutathione disulfide) upon interaction with ROS;[188,194] (iii) catalases catalyze the decomposition of H_2O_2 to H_2O and O_2.[209,210] Thus, the imbalance between ROS production and removal could occur by deficient antioxidant defense, inhibition of electron flow, or exposure to xenobiotics.[265]

Oxidative stress is indicated to play an underlying role in the pathology of AD based upon the impact of ROS on the production and aggregation of Aβ, metal ion homeostasis, and mitochondrial dysfunction. These pathological features could contribute back to oxidative stress through ROS generation in direct and indirect manners. Thus, the utilization of antioxidants to reduce the level of ROS offers a potential approach for drug discovery in AD. The strategy of regulating ROS only with antioxidants, however, has not been successful in clinical trials, possibly due to the multifaceted nature of AD pathology.[266]

1.2.4. Cholinesterases (ChEs)

The cholinergic hypothesis proposes that the degeneration of cholinergic neurons and the associated loss of cholinergic neurotransmission in the cerebral cortex are contributors to the deterioration of cognitive function observed in the brain of AD patients.[267,268] ACh, the neurotransmitter in cholinergic transmission responsible for learning and memory in the CNS, is a cationic agonist of muscarinic and nicotinic receptors.[269,270] ACh production from choline and acetyl coenzyme A (acetyl-CoA) is catalyzed by choline acetyltransferase (ChAT) in neurons.[271] Cholinergic transmission is initiated by the ACh release from the presynapse into the synaptic cleft, where ACh diffuses and binds to postsynaptic receptors. Subsequently, ChEs, serine hydrolases abundant in the synaptic cleft, rapidly terminate signal transmission by converting ACh into acetate and choline. To complete the cycle of cholinergic transmission, the presynaptic neuronal reuptake of catabolic products occurs to produce ACh. Cholinergic deficits from decreased ACh levels are a characteristic of the brain affected by AD.[272] As the main culprit of this phenomenon, ChEs have been widely studied as a therapeutic target for AD leading to the development of AChEIs for AD treatment (Table 1.1). There are two main types of ChEs: (i) AChE and (ii) butyrylcholinesterase (BuChE). AChE is responsible for the majority of the ChE activity in healthy human brains, while the remaining is accounted for by BuChE.[273,274] AChE has been a therapeutic target in AD based on its role in hydrolyzing the majority of ACh in the brain.[275,276]

The active site of AChE is located at the bottom of a gorge, a narrow cavity lined with 14 highly conserved aromatic residues.[277] The active site of human AChE (hAChE) is composed of an esteratic

site containing the catalytic triad (i.e., S200, H440, and E327), and an anionic site, where the quaternary ammonium of ACh binds through cation−π interactions. Analysis of the crystal structure of AChE revealed that the anionic site, which binds the quaternary trimethylammonium choline moiety of the substrate via cation−π interactions, is in fact uncharged and hydrophobic due to the presence of numerous aromatic residues.[278–280] The cumulative system of intermolecular interactions and geometric constraints of the active site gorge may contribute to the substrate specificity and rapid enzyme kinetics of AChE through mechanisms, such as aromatic guidance.[280,281] In addition, the peripheral anionic site (PAS), located near the rim of the gorge, has been reported to transiently bind to substrates as an initiating step of the catalytic process.[282,283] Szegletes et al. reported that binding of ACh to the PAS of AChE led to accelerated hydrolysis.[283]

BuChE can also hydrolyze ACh.[284,285] BuChE also possesses the overall structure, the amino acid sequence, and the catalytic mechanism similar to AChE.[286] While AChE is specific for ACh, BuChE can hydrolyze a range of esters and amides, in addition to ACh. One explanation for this disparity in substrate specificity is the size difference of their active-site gorges. The reported active-site gorge of BuChE (ca. 500 Å) is much larger than that of AChE (ca. 300 Å).[287] Furthermore, BuChE lacks the PAS that contributes towards AChE's activity.[288] The distinct structural characteristics of the two ChEs present a parameter to consider when compounds capable of inhibiting the activity of either AChE, BuChE, or both are rationally designed.[289] The physiological and pathological roles of BuChE remain unclear. Specific inhibitors for AChE and BuChE may help determine their impact on cholinergic transmission and AD pathogenesis. Thus, the potential therapeutic benefits of targeting BuChE, explored less than AChE, could provide a valuable direction for AD research.

In recent years, the lack of success in halting AD progression with ChE inhibitors (ChEIs) has led researchers to reevaluate the cholinergic hypothesis. A comparative study monitoring the levels of cholinergic markers in human subjects with mild cognitive impairment (MCI) and severe late stage of AD suggested that cholinergic dysfunction may be influential during the later stages of the disease.[290] Compensatory responses, such as upregulation of ChAT in the frontal cortex and hippocampus, have been proposed as resistance mechanisms working against the transition from MCI to AD.[291] Based on the current direction in understanding AD pathology, reassessment of the cholinergic hypothesis focuses on the interrelationships between ChEs and other pathological factors, including Aβ, tau, metal ions, and ROS.[292–298] Both AChE and BuChE have been found to be colocalized with Aβ aggregates in SPs.[299] Moreover, evidence has indicated that AChEs could affect Aβ aggregation[299–302] and toxicity via interactions between the PAS and Aβ.[292,299] For example, the complexation of AChE and Aβ, at the hydrophobic PAS of AChE could accelerate Aβ aggregation.[299,301] Further research is needed to fully elucidate the pathological relationships between ChEs and other pathological elements.

1.2.5. Additional Targets

In this section, we briefly introduce additional pathological factors in AD that may serve as therapeutic targets in the design of multifunctional molecules. Glutamate is a central excitatory neurotransmitter in the mammalian cortex.[303] Glutamate receptors, primarily located in the CNS, are involved in synaptic plasticity, learning, and memory.[304,305] There are two types of glutamate receptors: metabotropic and ionotropic. Ionotropic glutamate receptors form ion channel pores that allow the nonselective flux of cations upon activation by binding of glutamate.[306] Among the ionotropic glutamate receptors, NMDARs, named according to its selective binding of NMDA, have been researched for their role in a range of CNS disorders.[307] A majority of NMDARs are tetramers composed of two NR1 subunits, forming the channel, and two NR2A, NR2B, NR2C, or NR2D subunits.[308] The physiological and pharmacological properties of NMDARs vary depending on the combination of NR1 and NR2 subunits.[309] Under normal conditions, the NMDAR channel is blocked by Mg(II) in a voltage-dependent manner, which can be activated to control the influx of cations [e.g., Na(I), K(I), and Ca(II)].[310] The depolarization of NMDARs under pathological conditions is proposed to lead to the loss of Mg(II) from the channel, resulting in its overactivation.[311] Dysregulation of NMDAR activation contributes towards the pathology of the disease via cellular Ca(II) dyshomeostasis.[312,313] Therefore, the modulation of NMDARs has been suggested as a strategy to develop potential therapeutics for CNS-related disorders. Memantine, an uncompetitive NMDAR antagonist for AD treatment approved by the U.S. FDA (Table 1.1), has exhibited its effectiveness in attenuating cognitive decline in moderate to severe AD cases.[314] The utilization of NMDARs as a target in the past has been challenging due to adverse side effects, a consequence of nonspecific NMDAR recognition.[315] Nonetheless, the success of memantine has proven its therapeutic potential, and a more specific approach to antagonize NMDARs targeting the neurons affected by AD could be advantageous.[314] Furthermore, fine-tuning various parameters to inhibit NMDARs through the derivatization of uncompetitive NMDAR antagonists could provide insight into the invention of multifunctional molecules as potential drugs for AD.

Monoamine oxidase (MAOs), a family of enzymes that oxidatively deaminates monoamines, are linked to the pathogenesis of PD since they regulate dopaminergic and serotonergic neurotransmission.[316–319] The commonalities and correlated onsets between AD and PD have led researchers to investigate the role of MAOs in the pathology of AD. MAOs, found on the outer mitochondrial membrane, are divided into two isoforms, MAO-A and MAO-B, which exhibit overlapping substrate specificities against dopamine, tyramine, and tryptamine.[320] MAO-A, however, is capable of deaminating serotonin, melatonin, norepinephrine, and epinephrine, whereas MAO-B is mainly responsible for breaking down phenethylamine. MAO-catalyzed reactions produce H_2O_2 and ammonia as byproducts.[316] Thus, the overactivity of MAOs enhances the generation of H_2O_2 possibly leading to oxidative stress.[316] Inhibition of MAOs has been studied as a promising approach to treat AD.[321]

Phosphodiesterases (PDEs), composed of 12 families of enzymes responsible for the hydrolysis of cyclic adenosine monophosphate (cAMP) and cyclic guanosine monophosphate (cGMP), play a role in the regulation of intracellular signaling cascades, LTP, and synaptic plasticity.[322–324] Various members of PDEs have been implicated in a wide range of disorders, including AD and PD.[322] Specifically, the change in the expression of PDE4, PDE7, and PDE8 has been indicated in the AD-affected brain.[322–324] PDE inhibitors (PDEIs) have been shown to control signaling pathways by elevating the levels of cAMP and cGMP with subsequent activation of the cAMP response element binding (CREB) protein.[325,326] Such activation of the CREB protein is involved in LTP and synaptic plasticity.[327,328] Incorporation of the inhibitory activity against specific PDEs in the rational design of multifunctional molecules could be an effective means to construct them into potential drugs for AD. Furthermore, a link between PDEs and tau has been suggested through the direct relation between cAMP and protein kinase A associated with the phosphorylation of tau.[329,330]

Apolipoprotein E (ApoE) is recognized as a major determinant in lipoprotein metabolism, cholesterol homeostasis, and cardiovascular disease.[331] Research regarding the connection between ApoE polymorphisms and AD led to the discovery of ApoE4 as a strong genetic factor.[332–334] ApoE isoforms (i.e., ApoE2, ApoE3, and ApoE4) have only one or two different amino acid residues; however, they exhibit distinct biological functions.[335] For example, the ApoE4 allele is strongly implicated in sporadic AD, while ApoE2 is observed to be linked to neuroprotection.[334,336,337]

The direct and indirect relationships between ApoE4 and Aβ are controversial with research supporting both ApoE's pathological (for ApoE4) and remedial roles (possibly, for ApoE2) in AD. ApoE's effect on Aβ deposition and neuritic degradation was shown to be specific for the isoform. For example, an increase in the Aβ burden, fibrillogenesis, and neuritic plaque formation through binding to ApoE4 was greater than that of ApoE3 binding.[338] Hashimoto et al. presented that ApoE increased the levels of Aβ oligomers in an isoform-dependent manner (ApoE2 < ApoE3 < ApoE4).[339] In addition, ApoE4-expressing astrocytes were indicated to enhance amyloidogenic processing of APP in neurons, and the lack of ApoE4 reduced Aβ deposition in Tg mice overexpressing human APP^{V717F}.[340] On the other hand, Jiang et al. reported the capability of ApoE to promote the proteolytic degradation of Aβ in an isoformdependent manner, where ApoE4 impaired Aβ proteolysis, relative to ApoE2 and ApoE3.[341] Upregulated at the sites of elevated inflammation, ApoE3 and ApoE4 were reported to block glial secretion of TNFα, implying its connection to inflammatory processes.[342] Further research to identify ApoE's multifactorial role in AD would be valuable to gain a better understanding to find a direction for developing effective therapeutics. One approach is to inhibit the interactions between ApoE4 and AD pathological factors (e.g., Aβ) using small molecules. Chen et al. indicated that small molecules able to control the intramolecular interactions between the amino- and carboxyl-terminal domains of ApoE4 could eliminate its detrimental effects in vitro.[343] A recent study displayed a link between ApoE4

and tau pathology, further cementing the involvement of ApoE4 in AD pathogenesis.[344] Knock-in of human ApoE4 into a mouse model of tauopathy (1N4R P301S tau) resulted in exacerbated ptau pathology compared to that of ApoE2 and ApoE3, while knockout of ApoE had a protective effect.[344] ApoE4/P301S mice further displayed more neurodegeneration and neuroinflammation than ApoE2/P301S and ApoE3/P301S mice, and ApoE knockout mice were once more protected from these pathological changes.[344] The isoform-dependent genetic implications of ApoE indicate an aspect of AD in connection to Aβ and tau, suggesting its therapeutic potential to be considered for the design of multifunctional compounds as possible drug candidates.

Pyroglutamate Aβ (pGlu-Aβ) is a variation of Aβ with an N-terminal pyroglutamate residue implicated for its toxicity.[345–348] Glutaminyl cyclase is a catalytic enzyme responsible for the pGlu modification of Aβ.[349] Glutaminyl cyclase has been gaining the attention of researchers as a potential therapeutic target for AD due to its upregulation in the areas of the brain affected by AD and its potential contribution toward Aβ-mediated toxicity.[346,348–350] Overexpression of glutaminyl cyclase has been shown to induce behavioral deficits in Tg mice, whereas glutaminyl cyclase knockout improved the behavioral phenotype in 5xFAD mice.[346] Increasing evidence supporting the effectiveness of inhibiting glutaminyl cyclase implies a tactic that could be valuable to consider in the design of multifunctional molecules as potential therapeutics.[348,350,351]

Neuroinflammation is a biological response of the nervous tissue initiated in reaction to detriments (e.g., infection and traumatic brain injury).[352] Pathological events of AD, including Aβ accumulation and tau hyperphosphorylation, are reported to invoke inflammatory responses in vulnerable regions of the AD-affected brain.[353] Gliosis and activated glial cells are two major histopathological signs of neuroinflammation in AD.[353] Previous studies suggest that the direct and indirect damage from inflammation may exacerbate the pathological processes through a positive feedback loop.[353] The interconnected inflammation pathways can be activated by Aβ aggregates[354] and NFTs[355] through classical and alternative complement pathways.[353]

1.3. Conclusions

Multiple aspects of AD presented thus far represent a large portion of the research effort devoted toward determining the factors responsible for neurodegeneration observed in AD. Although a great deal of work has been dedicated to the cause, it is still unclear if the pathological elements mainly indicated in the AD-affected brain serve as causative factors of the disease or are the products of unidentified upstream events. The number of potential pathological components [e.g., peroxisome proliferator activator receptor γ (PPARγ),[356,357] phospholipase A2 (PLA2s),[358,359] cyclophilin D (CypD),[360,361] GD3 synthase,[362] plasminogen activator,[363,364] dickkopf1 (DKK1),[365] calpain,[366,367] and histone deacetylases (HDACs)[368]], speculated to play a role in AD pathology, represent the gap between our understanding

of the disease and its complexity. On the basis of diverse potential pathological targets and their suggested interconnections towards the pathogenesis of AD, the development of chemical tools would be valuable for understanding and modifying pathogenic factors in neurodegenerative diseases.

1.4. Acknowledgments

This research is supported by the Korea Advanced Institute of Science and Technology (KAIST) and the National Research Foundation of Korea (NRF) grant funded by the Korean government (NRF-2016R1A5A1009405 and NRF-2017R1A2B3002585). J.K. thanks the Global Ph.D. fellowship program for support through the National Research Foundation of Korea (NRF) funded by the Ministry of Education (NRF-2015HIA2A1030823).

1.5. References

(1) Alzheimer's Association. *Alzheimers Dement.* **2017**, *13*, 325–373.
(2) Kalia, L. V.; Lang, A. E. *Lancet* **2015**, *386*, 896–912.
(3) Al-Chalabi, A.; Hardiman, O. *Nat. Rev. Neurol.* **2013**, *9*, 617–628.
(4) Chiti, F.; Dobson, C. M. *Annu. Rev. Biochem.* **2017**, *86*, 27–68.
(5) Sweeney, P.; Park, H.; Baumann, M.; Dunlop, J.; Frydman, J.; Kopito, R.; McCampbell, A.; Leblanc, G.; Venkateswaran, A.; Nurmi, A.; et al. *Transl. Neurodegener.* **2017**, *6*, 6.
(6) Ross, C. A.; Poirier, M. A. *Nat. Med.* **2004**, *10*, S10–S17.
(7) Jakob-Roetne, R.; Jacobsen, H. *Angew. Chem. Int. Ed.* **2009**, *48*, 3030–3059.
(8) Savelieff, M. G.; Lee, S.; Liu, Y.; Lim, M. H. *ACS Chem. Biol.* **2013**, *8*, 856–865.
(9) Barnham, K. J.; Bush, A. I. *Chem. Soc. Rev.* **2014**, *43*, 6727–6749.
(10) Kepp, K. P. *Chem. Rev.* **2012**, *112*, 5193–5239.
(11) Bonda, D. J.; Lee, H.-g.; Blair, J. A.; Zhu, X.; Perry, G.; Smith, M. A. *Metallomics* **2011**, *3*, 267–270.
(12) Bolognin, S.; Messori, L.; Zatta, P. *Neuromolecular Med.* **2009**, *11*, 223–238.
(13) Greenough, M. A.; Camakaris, J.; Bush, A. I. *Neurochem. Int.* **2013**, *62*, 540–555.
(14) De Ricco, R.; Valensin, D.; Dell'Acqua, S.; Casella, L.; Hureau, C.; Faller, P. *ChemBioChem* **2015**, *16*, 2319–2328.
(15) Faller, P.; Hureau, C.; Berthoumieu, O. *Inorg. Chem.* **2013**, *52*, 12193–12206.
(16) Hamley, I. W. *Chem. Rev.* **2012**, *112*, 5147–5192.
(17) Grimm, A.; Eckert, A. *J. Neurochem.* **2017**, *143*, 418–431.
(18) Gao, J.; Wang, L.; Liu, J.; Xie, F.; Su, B.; Wang, X. *Antioxidants* **2017**, *6*, 25.
(19) Charles, F.; Pierre, J. M.; Sylvain, L. *Curr. Pharm. Des.* **2015**, *21*, 3570–3581.
(20) Radi, E.; Formichi, P.; Battisti, C.; Federico, A. *J. Alzheimers Dis.* **2014**, *42*, S125–S152.
(21) Verdin, E. *Science* **2015**, *350*, 1208–1213.
(22) Yin, F.; Boveris, A.; Cadenas, E. *Antioxid. Redox Signal.* **2014**, *20*, 353–371.
(23) Millecamps, S.; Julien, J.-P. *Nat. Rev. Neurosci.* **2013**, *14*, 161–176.
(24) Maday, S.; Twelvetrees, A. E.; Moughamian, A. J.; Holzbaur, E. L. F. *Neuron* **2014**, *84*, 292–309.
(25) Vicario-Orri, E.; Opazo, C. M.; Munoz, F. J. *J. Alzheimers Dis.* **2015**, *43*, 1097–1113.
(26) Heneka, M. T.; Kummer, M. P.; Latz, E. *Nat. Rev. Immunol.* **2014**, *14*, 463–477.
(27) Allgaier, M.; Allgaier, C. *Front. Biosci.* **2014**, *19*, 1345–1354.

(28) Hardy, J. A.; Higgins, G. A. *Science* **1992**, *256*, 184–185.
(29) Karran, E.; Mercken, M.; Strooper, B. D. *Nat. Rev. Drug Discov.* **2011**, *10*, 698–712.
(30) Herrup, K. *Nat. Neurosci.* **2015**, *18*, 794–799.
(31) Alzheimer, A.; Stelzmann, R. A.; Schnitzlein, H. N.; Murtagh, F. R. *Clin. Anat.* **1995**, 8, 429–431.
(32) Bunch, T. J.; Weiss, J. P.; Crandall, B. G.; May, H. T.; Bair, T. L.; Osborn, J. S.; Anderson, J. L.; Muhlestein, J. B.; Horne, B. D.; Lappe, D. L.; et al. *Heart Rhythm* **2010**, *7*, 433–437.
(33) Wimo, A.; Jönsson, L.; Bond, J.; Prince, M.; Winblad, B. *Alzheimers Dement.* **2013**, *9*, 1–11.
(34) Buckner, R. L. *Neuron* **2004**, *44*, 195–208.
(35) Frisoni, G. B.; Laakso, M. P.; Beltramello, A.; Geroldi, C.; Bianchetti, A.; Soininen, H.; Trabucchi, M. *Neurology* **1999**, *52*, 91–100.
(36) Hardy, J.; Selkoe, D. J. *Science* **2002**, *297*, 353–356.
(37) Grundke-Iqbal, I.; Iqbal, K.; Tung, Y. C.; Quinlan, M.; Wisniewski, H. M.; Binder, L. I. *Proc. Natl. Acad. Sci. U. S. A.* **1986**, *83*, 4913–4917.
(38) Tanzi, R. E.; Bertram, L. *Cell* **2005**, *120*, 545–555.
(39) Schmechel, D. E.; Saunders, A. M.; Strittmatter, W. J.; Crain, B. J.; Hulette, C. M.; Joo, S. H.; Pericak-Vance, M. A.; Goldgaber, D.; Roses, A. D. *Proc. Natl. Acad. Sci. U. S. A.* **1993**, *90*, 9649–9653.
(40) Farrer, L. A.; Cupples, L. A.; Haines, J. L.; Hyman, B.; Kukull, W. A.; Mayeux, R.; Myers, R. H.; Pericak-Vance, M. A.; Risch, N.; van Duijn, C. M. *JAMA* **1997**, *278*, 1349–1356.
(41) Cruts, M.; Theuns, J.; Broeckhoven, C. V. *Hum. Mutat.* **2012**, *33*, 1340–1344.
(42) Esch, F. S.; Keim, P. S.; Beattie, E. C.; Blacher, R. W.; Culwell, A. R.; Oltersdorf, T.; McClure, D.; Ward, P. J. *Science* **1990**, *248*, 1122–1124.
(43) DeToma, A. S.; Salamekh, S.; Ramamoorthy, A.; Lim, M. H. *Chem. Soc. Rev.* **2012**, *41*, 608–621.
(44) Zhang, Y.-W.; Thompson, R.; Zhang, H.; Xu, H. *Mol. Brain* **2011**, *4*, 3.
(45) Selkoe, D. J.; Wolfe, M. S. *Cell* **2007**, *131*, 215–221.
(46) Lee, S. J. C.; Nam, E.; Lee, H. J.; Savelieff, M. G.; Lim, M. H. *Chem. Soc. Rev.* **2017**, *46*, 310–323.
(47) Cohen, S. I. A.; Linse, S.; Luheshi, L. M.; Hellstrand, E.; White, D. A.; Rajah, L.; Otzen, D. E.; Vendruscolo, M.; Dobson, C. M.; Knowles, T. P. J. *Proc. Natl. Acad. Sci. U. S. A.* **2013**, *110*, 9758–9763.
(48) Xue, W.-F.; Hellewell, A. L.; Hewitt, E. W.; Radford, S. E. *Prion* **2010**, *4*, 20–25.
(49) Finder, V. H.; Glockshuber, R. *Neurodegener. Dis.* **2007**, *4*, 13–27.
(50) Lorenzo, A.; Yankner, B. A. *Proc. Natl. Acad. Sci. U. S. A.* **1994**, *91*, 12243–12247.
(51) Ahmed, M.; Davis, J.; Aucoin, D.; Sato, T.; Ahuja, S.; Aimoto, S.; Elliott, J. I.; Van Nostrand, W. E.; Smith, S. O. *Nat. Struct. Mol. Biol.* **2010**, *17*, 561–567.
(52) Cleary, J. P.; Walsh, D. M.; Hofmeister, J. J.; Shankar, G. M.; Kuskowski, M. A.; Selkoe, D. J.; Ashe, K. H. *Nat. Neurosci.* **2005**, *8*, 79–84.
(53) Esparza, T. J.; Zhao, H.; Cirrito, J. R.; Cairns, N. J.; Bateman, R. J.; Holtzman, D. M.; Brody, D. L. *Ann. Neurol.* **2013**, *73*, 104–119.
(54) Haass, C.; Selkoe, D. J. *Nat. Rev. Mol. Cell Biol.* **2007**, *8*, 101–112.
(55) Benilova, I.; Karran, E.; Strooper, B. D. *Nat. Neurosci.* **2012**, *15*, 349−357.
(56) Guo, J. L.; Lee, V. M. Y. *Nat. Med.* **2014**, *20*, 130–138.
(57) Lee, S.-J.; Desplats, P.; Sigurdson, C.; Tsigelny, I.; Masliah, E. *Nat. Rev. Neurol.* **2010**, *6*, 702–706.
(58) Goedert, M.; Spillantini, M.; Jakes, R.; Rutherford, D.; Crowther, R. *Neuron* **1989**, *3*, 519–

526.
(59) Jack, C. R. Jr.; Knopman, D. S.; Jagust, W. J.; Shaw, L. M.; Aisen, P. S.; Weiner, M. W.; Petersen, R. C.; Trojanowski, J. Q. *Lancet Neurol.* **2010**, *9*, 119–128.
(60) Josephs, K. A.; Whitwell, J. L.; Ahmed, Z.; Shiung, M. M.; Weigand, S. D.; Knopman, D. S.; Boeve, B. F.; Parisi, J. E.; Petersen, R. C.; Dickson, D. W.; et al. *Ann. Neurol.* **2008**, *63*, 204–212.
(61) Ballatore, C.; Lee, V. M.-Y.; Trojanowski, J. Q. *Nat. Rev. Neurosci.* **2007**, *8*, 663–672.
(62) Baudier, J.; Cole, R. D. *J. Biol. Chem.* **1987**, *262*, 17577–17583.
(63) Daebel, V.; Chinnathambi, S.; Biernat, J.; Schwalbe, M.; Habenstein, B.; Loquet, A.; Akoury, E.; Tepper, K.; Müller, H.; Baldus, M.; et al. *J. Am. Chem. Soc.* **2012**, *134*, 13982–13989.
(64) Hall, G. F.; Chu, B.; Lee, G.; Yao, J. *J. Cell. Sci.* **2000**, *113*, 1373–1387.
(65) Noble, W.; Olm, V.; Takata, K.; Casey, E.; Mary, O.; Meyerson, J.; Gaynor, K.; LaFrancois, J.; Wang, L.; Kondo, T.; et al. *Neuron* **2003**, *38*, 555–565.
(66) Fá, M.; Puzzo, D.; Piacentini, R.; Staniszewski, A.; Zhang, H.; Baltrons, M. A.; Puma, D. D. L.; Chatterjee, I.; Li, J.; Saeed, F.; et al. *Sci. Rep.* **2016**, *6*, 19393.
(67) Ward, S. M.; Himmelstein, D. S.; Lancia, J. K.; Binder, L. I. *Biochem. Soc. Trans.* **2012**, *40*, 667–671.
(68) Lee, V. M.-Y.; Goedert, M.; Trojanowski, J. Q. *Annu. Rev. Neurosci.* **2001**, *24*, 1121–1159.
(69) Ittner, L. M.; Götz, J. *Nat. Rev. Neurosci.* **2011**, *12*, 67–72.
(70) Guerrero-Muñoz, M. J.; Gerson, J.; Castillo-Carranza, D. L. *Front. Cell. Neurosci.* **2015**, *9*, 464.
(71) Roberson, E. D.; Scearce-Levie, K.; Palop, J. J.; Yan, F.; Cheng, I. H.; Wu, T.; Gerstein, H.; Yu, G.-Q.; Mucke, L. *Science* **2007**, *316*, 750–754.
(72) Takashima, A.; Noguchi, K.; Sato, K.; Hoshino, T.; Imahori, K. *Proc. Natl. Acad. Sci. U. S. A.* **1993**, *90*, 7789–7793.
(73) Wilson, D. M.; Binder, L. I. *Am. J. Pathol.* **1997**, *150*, 2181–2195.
(74) Phiel, C. J.; Wilson, C. A.; Lee, V. M.-Y.; Klein, P. S. *Nature* **2003**, *423*, 435–439.
(75) Gschwind, A.; Zwick, E.; Prenzel, N.; Leserer, M.; Ullrich, A. *Oncogene* **2001**, *20*, 1594–1600.
(76) Zheng, W.; Monnot, A. D. *Pharmacol. Ther.* **2012**, *133*, 177–188.
(77) Bush, A. I.; Tanzi, R. E. *Neurotherapeutics* **2008**, *5*, 421–432.
(78) Que, E. L.; Domaille, D. W.; Chang, C. J. *Chem. Rev.* **2008**, *108*, 1517–1549.
(79) Vallee, B. L.; Auld, D. S. *Biochemistry* **1990**, *29*, 5647–5659.
(80) Berg, J. M.; Shi, Y. *Science* **1996**, *271*, 1081–1085.
(81) Frederickson, C. J. *Int. Rev. Neurobiol.* **1989**, *31*, 145–238.
(82) Frederickson, C. J.; Suh, S. W.; Silva, D.; Frederickson, C. J.; Thompson, R. B. *J. Nutr.* **2000**, *130*, 1471S–1483S.
(83) Kay, A. R. *Trends Neurosci.* **2006**, *29*, 200–206.
(84) Paoletti, P.; Ascher, P.; Neyton, J. *J. Neurosci.* **1997**, *17*, 5711–5725.
(85) Hollmann, M.; Boulter, J.; Maron, C.; Beasley, L.; Sullivan, J.; Pecht, G.; Heinemann, S. *Neuron* **1993**, *10*, 943–954.
(86) Lee, H. J.; Korshavn, K. J.; Kochi, A.; Derrick, J. S.; Lim, M. H. *Chem. Soc. Rev.* **2014**, *43*, 6672–6682.
(87) Boal, A. K.; Rosenzweig, A. C. *Chem. Rev.* **2009**, *109*, 4760–4779.
(88) Rubino, J. T.; Franz, K. J. *J. Inorg. Biochem.* **2012**, *107*, 129–143.
(89) Prohaska, J. R. *Am. J. Clin. Nutr.* **2008**, *88*, 826S–829S.
(90) Bush, A. I. *Trends Neurosci.* **2003**, *26*, 207–214.
(91) Trombley, P. Q.; Shepherd, G. M. *J. Neurophysiol.* **1996**, *76*, 2536–2546.

(92) Mason, H. S. *Science* **1957**, *125*, 1185–1188.
(93) Lieu, P. T.; Heiskala, M.; Peterson, P. A.; Yang, Y. *Mol. Aspects Med.* **2001**, *22*, 1–87.
(94) Beard, J. L. *J. Nutr.* **2001**, *131*, 568S–580S.
(95) Kepp, K. P. *Coord. Chem. Rev.* **2017**, *351*, 127–159.
(96) Sensi, S. L.; Canzoniero, L. M. T.; Yu, S. P.; Ying, H. S.; Koh, J.-Y.; Kerchner, G. A.; Choi, D. W. *J. Neurosci.* **1997**, *17*, 9554–9564.
(97) Kambe, T.; Yamaguchi-Iwai, Y.; Sasaki, R.; Nagao, M. *Cell Mol. Life Sci.* **2004**, *61*, 49–68.
(98) Maret, W. *Biochemistry* **2004**, *43*, 3301–3309.
(99) Greenough, M. A.; Volitakis, I.; Li, Q.-X.; Laughton, K.; Evin, G.; Ho, M.; Dalziel, A. H.; Camakaris, J.; Bush, A. I. *J. Biol. Chem.* **2011**, *286*, 9776–9786.
(100) Weiss, J. H.; Sensi, S. L. *Trends Neurosci.* **2000**, *23*, 365–371.
(101) Kim, Y.-H.; Kim, E. Y.; Gwag, B. J.; Sohn, S.; Koh, J.-Y. *Neuroscience* **1999**, *89*, 175–182.
(102) Liuzzi, J. P.; Aydemir, F.; Nam, H.; Knutson, M. D.; Cousins, R. J. *Proc. Natl. Acad. Sci. U. S. A.* **2006**, *103*, 13612–13617.
(103) White, C.; Yuan, X.; Schmidt, P. J.; Bresciani, E.; Samuel, T. K.; Campagna, D.; Hall, C.; Bishop, K.; Calicchio, M. L.; Lapierre, A.; et al. *Cell Metab.* **2013**, *17*, 261–270.
(104) Rajadhyaksha, A. M.; Elemento, O.; Puffenberger, E. G.; Schierberl, K. C.; Xiang, J. Z.; Putorti, M. L.; Berciano, J.; Poulin, C.; Brais, B.; Michaelides, M.; et al. *Am. J. Hum. Genet.* **2010**, *87*, 643–654.
(105) Knutson, M. D. *J. Biol. Chem.* **2017**, *292*, 12735–12743.
(106) Atrian-Blasco, E.; Conte-Daban, A.; Hureau, C. *Dalton Trans.* **2017**, *46*, 12750–12759.
(107) Gamez, P.; Caballero, A. B. *AIP Adv.* **2015**, *5*, 092503.
(108) Tõugu, V.; Palumaa, P. *Coord. Chem. Rev.* **2012**, *256*, 2219–2224.
(109) Pithadia, A. S.; Lim, M. H. *Curr. Opin. Chem. Biol.* **2012**, *16*, 67–73.
(110) Faller, P.; Hureau, C. *Dalton Trans.* **2009**, *7*, 1080–1094.
(111) Sayre, L. M.; Perry, G.; Smith, M. A. *Chem. Res. Toxicol.* **2008**, *21*, 172–188.
(112) Bush, A. I; Pettingell, W. H.; Multhaup, G.; Paradis, M. D.; Vonsattel, J.-P.; Gusella, J. F.; Beyreuther, K.; Masters, C. L.; Tanzi, R. E. *Science* **1994**, *265*, 1464–1467.
(113) Lovell, M. A.; Robertson, J. D.; Teesdale, W. J.; Campbell, J. L.; Markesbery, W. R. *J. Neurol. Sci.* **1998**, *158*, 47–52.
(114) Zirah, S.; Rebuffat, S.; Kozin, S. A.; Debey, P.; Fournier, F.; Lesage, D.; Tabet, J.-C. *Int. J. Mass. Spectrom.* **2003**, *228*, 999–1016.
(115) Mekmouche, Y.; Coppel, Y.; Hochgräfe, K.; Guilloreau, L.; Talmard, C.; Mazarguil, H.; Faller, P. *ChemBioChem* **2005**, *6*, 1663–1671.
(116) Zirah, S.; Kozin, S. A.; Mazur, A. K.; Blond, A.; Cheminant, M.; Ségalas-Milazzo, I.; Debey, P.; Rebuffat, S. *J. Biol. Chem.* **2006**, *281*, 2151–2161.
(117) Kozin, S. A.; Mezentsev, Y. V.; Kulikova, A. A.; Indeykina, M. I.; Golovin, A. V.; Ivanov, A. S.; Tsvetkov, P. O.; Makarov, A. A. *Mol. BioSyst.* **2011**, *7*, 1053–1055.
(118) Kulikova, A. A.; Tsvetkov, P. O.; Indeykina, M. I.; Popov, I. A.; Zhokhov, S. S.; Golovin, A. V.; Polshakov, V. I.; Kozin, S. A.; Nudler, E.; Makarov, A. A. *Mol. BioSyst.* **2014**, *10*, 2590–2596.
(119) Curtain, C. C.; Ali, F.; Volitakis, I.; Cherny, R. A.; Norton, R. S.; Beyreuther, K.; Barrow, C. J.; Masters, C. L.; Bush, A. I.; Barnham, K. J. *J. Biol. Chem.* **2001**, *276*, 20466–20473.
(120) Syme, C. D.; Viles, J. H. *Biochim. Biophys. Acta* **2006**, *1764*, 246–256.
(121) Gaggelli, E.; Janicka-Klos, A.; Jankowska, E.; Kozlowski, H.; Migliorini, C.; Molteni, E.; Valensin, D.; Valensin, G.; Wieczerzak, E. *J. Phys. Chem. B* **2008**, *112*, 100–109.
(122) Polshakov, V. I.; Mantsyzov, A. B.; Kozin, S. A.; Adzhubei, A. A.; Zhokhov, S. S.; van Beek,

W.; Kulikova, A. A.; Indeykina, M. I.; Mitkevich, V. A.; Makarov, A. A. *Angew. Chem. Int. Ed.* **2017**, *56*, 11734–11739.
(123) Himes, R. A.; Park, G. Y.; Siluvai, G. S.; Blackburn, N. J.; Karlin, K. D. *Angew. Chem. Int. Ed.* **2008**, *47*, 9084–9087.
(124) Shearer, J.; Szalai, V. A. *J. Am. Chem. Soc.* **2008**, *130*, 17826–17835.
(125) Hureau, C.; Balland, V.; Coppel, Y.; Solari, P. L.; Fonda, E.; Faller, P. *J. Biol. Inorg. Chem.* **2009**, *14*, 995–1000.
(126) Furlan, S.; Hureau, C.; Faller, P.; La Penna, G. *J. Phys. Chem. B* **2010**, *114*, 15119–15133.
(127) Drew, S. C.; Masters, C. L.; Barnham, K. J. *J. Am. Chem. Soc.* **2009**, *131*, 8760–8761.
(128) Drew, S. C.; Noble, C. J.; Masters, C. L.; Hanson, G. R.; Barnham, K. J. *J. Am. Chem. Soc.* **2009**, *131*, 1195–1207.
(129) Bousejra-ElGarah, F.; Bijani, C.; Coppel, Y.; Faller, P.; Hureau, C. *Inorg. Chem.* **2011**, *50*, 9024–9030.
(130) Valensin, D.; Migliorini, C.; Valensin, G.; Gaggelli, E.; La Penna, G.; Kozlowski, H.; Gabbiani, C.; Messori, L. *Inorg. Chem.* **2011**, *50*, 6865–6867.
(131) Alies, B.; Conte-Daban, A.; Sayen, S.; Collin, F.; Kieffer, I.; Guillon, E.; Faller, P.; Hureau, C. *Inorg. Chem.* **2016**, *55*, 10499–10509.
(132) Danielsson, J.; Pierattelli, R.; Banci, L.; Gräslund, A. *FEBS J.* **2007**, *274*, 46–59.
(133) Telpoukhovskaia, M. A.; Orvig, C. *Chem. Soc. Rev.* **2013**, *42*, 1836–1846.
(134) Dorlet, P.; Gambarelli, S.; Faller, P.; Hureau, C. *Angew. Chem. Int. Ed.* **2009**, *48*, 9273–9276.
(135) Faller, P.; Hureau, C.; La Penna, G. *Acc. Chem. Res.* **2014**, *47*, 2252–2259.
(136) Hureau, C. *Coord. Chem. Rev.* **2012**, *256*, 2164–2174.
(137) Alies, B.; Eury, H.; Bijani, C.; Rechignat, L.; Faller, P.; Hureau, C. *Inorg. Chem.* **2011**, *50*, 11192–11201.
(138) Syme, C. D.; Nadal, R. C.; Rigby, S. E. J.; Viles, J. H. *J. Biol. Chem.* **2004**, *279*, 18169–18177.
(139) Karr, J. W.; Szalai, V. A. *J. Am. Chem. Soc.* **2007**, *129*, 3796–3797.
(140) Trujano-Ortiz, L. G.; González, F. J.; Quintanar, L. *Inorg. Chem.* **2015**, *54*, 4–6.
(141) Shearer, J.; Callan, P. E.; Tran, T.; Szalai, V. A. *Chem. Commun.* **2010**, *46*, 9137–9139.
(142) Savelieff, M. G.; DeToma, A. S.; Derrick, J. S.; Lim, M. H. The Ongoing Search for Small Molecules to Study Metal-Associated Amyloid- Species in Alzheimer's Disease. *Acc. Chem. Res.* **2014**, *47*, 2475–2482.
(143) Talmard, C.; Bouzan, A.; Faller, P. *Biochemistry* **2007**, *46*, 13658–13666.
(144) Tõugu, V.; Karafin, A.; Palumaa, P. *J. Neurochem.* **2008**, *104*, 1249–1259.
(145) Garzon-Rodriguez, W.; Yatsimirsky, A. K.; Glabe, C. G. *Bioorg. Med. Chem. Lett.* **1999**, *9*, 2243–2248.
(146) Zawisza, I.; Rózga, M.; Bal, W. *Coord. Chem. Rev.* **2012**, *256*, 2297–2307.
(147) Guo, J.; Sun, W.; Liu, F. *J. Inorg. Biochem.* **2017**, *177*, 183–189.
(148) Noël, S.; Bustos Rodriguez, S.; Sayen, S.; Guillon, E.; Faller, P.; Hureau, C. *Metallomics* **2014**, *6*, 1220–1222.
(149) Karr, J. W.; Akintoye, H.; Kaupp, L. J.; Szalai, V. A. *Biochemistry* **2005**, *44*, 5478–5487.
(150) Ma, Q.-F.; Hu, J.; Wu, W.-H.; Liu, H.-D.; Du, J.-T.; Fu, Y.; Wu, Y.-W.; Lei, P.; Zhao, Y.-F.; Li, Y.-M. *Biopolymers* **2006**, *83*, 20–31.
(151) Guilloreau, L.; Damian, L.; Coppel, Y.; Mazarguil, H.; Winterhalter, M.; Faller, P. *J. Biol. Inorg. Chem.* **2006**, *11*, 1024–1038.
(152) Raman, B.; Ban, T.; Yamaguchi, K.-i.; Sakai, M.; Kawai, T.; Naiki, H.; Goto, Y. *J. Biol. Chem.* **2005**, *280*, 16157–16162.
(153) Alies, B.; Badei, B.; Faller, P.; Hureau, C. *Chem. Eur. J.* **2012**, *18*, 1161–1167.

(154) Feaga, H. A.; Maduka, R. C.; Foster, M. N.; Szalai, V. A. *Inorg. Chem.* **2011**, *50*, 1614–1618.
(155) Hatcher, L. Q.; Hong, L.; Bush, W. D.; Carducci, T.; Simon, J. D. *J. Phys. Chem. B* **2008**, *112*, 8160–8164.
(156) Atwood, C. S.; Scarpa, R. C.; Huang, X.; Moir, R. D.; Jones, W. D.; Fairlie, D. P.; Tanzi, R. E.; Bush, A. I. *J. Neurochem.* **2000**, *75*, 1219–1233.
(157) Hou, L.; Zagorski, M. G. *J. Am. Chem. Soc.* **2006**, *128*, 9260–9261.
(158) Hong, L.; Bush, W. D.; Hatcher, L. Q.; Simon, J. *J. Phys. Chem. B* **2008**, *112*, 604–611.
(159) Arena, G.; Pappalardo, G.; Sovago, I.; Rizzarelli, E. *Coord. Chem. Rev.* **2012**, *256*, 3–12.
(160) Hong, L.; Carducci, T. M.; Bush, W. D.; Dudzik, C. G.; Millhauser, G. L.; Simon, J. D. *J. Phys. Chem. B* **2010**, *114*, 11261–11271.
(161) Tõugu, V.; Tiiman, A.; Palumaa, P. *Metallomics* **2011**, *3*, 250–261.
(162) Mantyh, P. W.; Ghilardi, J. R.; Rogers, S.; DeMaster, E.; Allen, C. J.; Stimson, E. R.; Maggio, J. E. *J. Neurochem.* **1993**, *61*, 1171–1174.
(163) Atwood, C. S.; Moir, R. D.; Huang, X.; Scarpa, R. C.; Bacarra, N. M. E.; Romano, D. M.; Hartshorn, M. A.; Tanzi, R. E.; Bush, A. I. *J. Biol. Chem.* **1998**, *273*, 12817–12826.
(164) Huang, X.; Atwood, C. S.; Moir, R. D.; Hartshorn, M. A.; Tanzi, R. E.; Bush, A. I. *J. Biol. Inorg. Chem.* **2004**, *9*, 954–960.
(165) Innocenti, M.; Salvietti, E.; Guidotti, M.; Casini, A.; Bellandi, S.; Foresti, M. L.; Gabbiani, C.; Pozzi, A.; Zatta, P.; Messori, L. *J. Alzheimers Dis.* **2010**, *19*, 1323–1329.
(166) Zou, J.; Kajita, K.; Sugimoto, N. *Angew. Chem. Int. Ed.* **2001**, *40*, 2274–2277.
(167) Yoshiike, Y.; Tanemura, K.; Murayama, O.; Akagi, T.; Murayama, M.; Sato, S.; Sun, X.; Tanaka, N.; Takashima, A. *J. Biol. Chem.* **2001**, *276*, 32293–32299.
(168) Noy, D.; Solomonov, I.; Sinkevich, O.; Arad, T.; Kjaer, K.; Sagi, I. *J. Am. Chem. Soc.* **2008**, *130*, 1376–1383.
(169) Abelein, A.; Gräslund, A.; Danielsson, J. *Proc. Natl. Acad. Sci. U. S. A.* **2015**, *112*, 5407–5412.
(170) Pedersen, J. T.; Borg, C. B.; Michaels, T. C. T.; Knowles, T. P. J.; Faller, P.; Teilum, K.; Hemmingsen, L. *ChemBioChem* **2015**, *16*, 1293–1297.
(171) Liu, B.; Moloney, A.; Meehan, S.; Morris, K.; Thomas, S. E.; Serpell, L. C.; Hider, R.; Marciniak, S. J.; Lomas, D. A.; Crowther, D. C. *J. Biol. Chem.* **2011**, *286*, 4248–4256.
(172) Chen, Y. R.; Huang, H. B.; Chyan, C. L.; Shiao, M. S.; Lin, T. H.; Chen, Y. C. *J. Biochem.* **2006**, *139*, 733–740.
(173) Klug, G. M. J. A.; Losic, D.; Supundi; Subasinghe, S. S.; Aguilar, M.-I.; Martin, L. L.; Small, D. H. *Eur. J. Biochem.* **2003**, *270*, 4282–4293.
(174) Tew, D. J.; Bottomley, S. P.; Smith, D. P.; Ciccotosto, G. D.; Babon, J.; Hinds, M. G.; Masters, C. L.; Cappai, R.; Barnham, K. J. *Biophys. J.* **2008**, *94*, 2752–2766.
(175) Chen, W.-T.; Liao, Y.-H.; Yu, H.-M.; Cheng, I. H.; Chen, Y.-R. *J. Biol. Chem.* **2011**, *286*, 9646–9656.
(176) Bernstein, S. L.; Dupuis, N. F.; Lazo, N. D.; Wyttenbach, T.; Condron, M. M.; Bitan, G.; Teplow, D. B.; Shea, J.-E.; Ruotolo, B. T.; Robinson, C. V.; et al. Amyloid- Protein Oligomerization and the Importance of Tetramers and Dodecamers in the Aetiology of Alzheimer's Disease. *Nat. Chem.* **2009**, *1*, 326 –331.
(177) Quist, A.; Doudevski, I.; Lin, H.; Azimova, R.; Ng, D.; Frangione, B.; Kagan, B.; Ghiso, J.; Lal, R. *Proc. Natl. Acad. Sci. U. S. A.* **2005**, *102*, 10427–10432.
(178) Jun, S.; Saxena, S. *Angew. Chem. Int. Ed.* **2007**, *46*, 3959–3961.
(179) Pedersen, J. T.; Østergaard, J.; Rozlosnik, N.; Gammelgaard, B.; Heegaard, N. H. H. *J. Biol. Chem.* **2011**, *286*, 26952–26963.
(180) Ryan, T. M.; Kirby, N.; Mertens, H. D. T.; Roberts, B.; Barnham, K. J.; Cappai, R.; Pham, C.

L. L.; Masters, C. L.; Curtain, C. C. *Metallomics* **2015**, *7*, 536–543.
(181) Matheou, C. J.; Younan, N. D.; Viles, J. H. *Biochem. J.* **2015**, *466*, 233–242.
(182) Sciacca, M. F. M.; Kotler, S. A.; Brender, J. R.; Chen, J.; Lee, D.-k.; Ramamoorthy, A. *Biophys. J.* **2012**, *103*, 702–710.
(183) Chen, W.-T.; Hong, C.-J.; Lin, Y.-T.; Chang, W.-H.; Huang, H.-T.; Liao, J.-Y.; Chang, Y.-J.; Hsieh, Y.-F.; Cheng, C.-Y.; Liu, H.-C.; et al. *PLoS One* **2012**, *7*, e35807.
(184) Somavarapu, A. K.; Shen, F.; Teilum, K.; Zhang, J.; Mossin, S.; Thulstrup, P. W.; Bjerrum, M. J.; Tiwari, M. K.; Szunyogh, D.; Søtofte, P. M.; et al. *Chem. Eur. J.* **2017**, *23*, 13591–13595.
(185) Ritchie, C. W.; Bush, A. I.; Mackinnon, A.; Macfarlane, S.; Mastwyk, M.; MacGregor, L.; Kiers, L.; Cherny, R.; Li, Q.-X.; Tammer, A.; et al. *Arch. Neurol.* **2003**, *60*, 1685–1691.
(186) Adlard, P. A.; Cherny, R. A.; Finkelstein, D. I.; Gautier, E.; Robb, E.; Cortes, M.; Volitakis, I.; Liu, X.; Smith, J. P.; Perez, K.; et al. *Neuron* **2008**, *59*, 43–55.
(187) Chen, Z.; Zhong, C. *Neurosci. Bull.* **2014**, *30*, 271–281.
(188) Bhattacharyya, A.; Chattopadhyay, R.; Mitra, S.; Crowe, S. E. *Physiol. Rev.* **2014**, *94*, 329–354.
(189) Poljsak, B.; Šuput, D.; Milisav, I. *Oxid. Med. Cell Longev.* **2013**, *2013*, 956792.
(190) Finkel, T.; Holbrook, N. J. *Nature* **2000**, *408*, 239–247.
(191) Muller, F. *J. Amer. Aging Assoc.* **2000**, *23*, 227–253.
(192) Panday, A.; Sahoo, M. K.; Osorio, D.; Batra, S. *Cell. Mol. Immunol.* **2015**, *12*, 5–23.
(193) Bhat, A. H.; Dar, K. B.; Anees, S.; Zargar, M. A.; Masood, A.; Sofi, M. A.; Ganie, S. A. *Biomed. Pharmacother.* **2015**, *74*, 101–110.
(194) Apel, K.; Hirt, H. *Annu. Rev. Plant Biol.* **2004**, *55*, 373–399.
(195) Schieber, M.; Chandel, N. S. *Curr. Biol.* **2014**, *24*, R453–R462.
(196) Martindale, J. L.; Holbrook, N. J. *J. Cell. Physiol.* **2002**, *192*, 1–15.
(197) Huang, R.-P.; Wu, J.-X.; Fan, Y.; Adamson, E. D. *J. Cell Biol.* **1996**, *133*, 211–220.
(198) Simon, H.-U.; Haj-Yehia, A.; Levi-Schaffer, F. *Apoptosis* **2000**, *5*, 415–418.
(199) Schreck, R.; Rieber, P.; Baeuerle, P. A. *EMBO J.* **1991**, *10*, 2247–2258.
(200) Circu, M. L.; Aw, T. Y. *Free Radic. Biol. Med.* **2010**, *48*, 749–762.
(201) Ashkenazi, A.; Dixit, V. M. *Curr. Opin. Cell Biol.* **1999**, *11*, 255–260.
(202) Zamzami, N.; Marchetti, P.; Castedo, M.; Decaudin, D.; Macho, A.; Hirsch, T.; Susin, S. A.; Petit, P. X.; Mignotte, B.; Kroemer, G. *J. Exp. Med.* **1995**, *182*, 367–377.
(203) Jiang, X.; Wang, X. *Annu. Rev. Biochem.* **2004**, *73*, 87–106.
(204) Murphy, K. M.; Ranganathan, V.; Farnsworth, M. L.; Kavallaris, M.; Lock, R. B. *Cell Death Differ.* **2000**, *7*, 102–111.
(205) Sies, H. *Eur. J. Biochem.* **1993**, *215*, 213–219.
(206) Pryor, W. A. *Annu. Rev. Physiol.* **1986**, *48*, 657–667.
(207) Benov, L. *Protoplasma* **2001**, *217*, 33–36.
(208) Scheiber, I. F.; Mercer, J. F. B.; Dringen, R. *Prog. Neurobiol.* **2014**, *116*, 33–57.
(209) Halliwell, B.; Clement, M. V.; Long, L. H. *FEBS Lett.* **2000**, *486*, 10–13.
(210) Stone, J. R.; Yang, S. *Antioxid. Redox Signal.* **2006**, *8*, 243–270.
(211) Zhao, Y.; Zhao, B. *Oxid. Med. Cell Longev.* **2013**, *2013*, 316523.
(212) Ray, P. D.; Huang, B.-W.; Tsuji, Y. *Cell. Signal.* **2012**, *24*, 981–990.
(213) Faller, P.; Hureau, C. *Chem. Eur. J.* **2012**, *18*, 15910–15920.
(214) Maynard, C. J.; Bush, A. I.; Masters, C. L.; Cappai, R.; Li, Q.-X. *Int. J. Exp. Pathol.* **2005**, *86*, 147–159.
(215) Ganguly, G.; Chakrabarti, S.; Chatterjee, U.; Saso, L. *Drug Des. Devel. Ther.* **2017**, *11*, 797–810.

(216) Duce, J. A.; Bush, A. I. *Prog. Neurobiol.* **2010**, *92*, 1–18.
(217) White, A. R.; Du, T.; Laughton, K. M.; Volitakis, I.; Sharples, R. A.; Xilinas, M. E.; Hoke, D. E.; Holsinger, R. M. D.; Evin, G.; Cherny, R. A.; et al. *J. Biol. Chem.* **2006**, *281*, 17670–17680.
(218) Misonou, H.; Morishima-Kawashima, M.; Ihara, Y. *Biochemistry* **2000**, *39*, 6951–6959.
(219) Nam, E.; Han, J.; Suh, J.-M.; Yi, Y.; Lim, M. H. *Curr. Opin. Chem. Biol*. **2018**, *43*, 8–14.
(220) Coyle, J. T.; Puttfarcken, P. *Science* **1993**, *262*, 689–695.
(221) Ali, F. E.; Separovic, F.; Barrow, C. J.; Cherny, R. A.; Fraser, F.; Bush, A. I.; Masters, C. L.; Barnham, K. J. *J. Peptide Sci.* **2005**, *11*, 353–360.
(222) Boyd-Kimball, D.; Poon, H. F.; Lynn, B. C.; Cai, J.; Pierce Jr., W. M.; Klein, J. B.; Ferguson, J.; Link, C. D.; Butterfield, D. A. *Neurobiol. Aging* **2006**, *27*, 1239–1249.
(223) Butterfield, D. A.; Boyd-Kimball, D. *Brain Pathol.* **2004**, *14*, 426–432.
(224) Butterfield, D. A.; Galvan, V.; Lange, M. B.; Tang, H.; Sowell, R. A.; Spilman, P.; Fombonne, J.; Gorostiza, O.; Zhang, J.; Sultana, R.; et al. *Free Radic. Biol. Med.* **2010**, *48*, 136–144.
(225) Butterfield, D. A.; Reed, T.; Newman, S. F.; Sultana, R. *Free Radic. Biol. Med.* **2007**, *43*, 658–677.
(226) Cai, Z.; Zhao, B.; Ratka, A. *Neuromol. Med.* **2011**, *13*, 223–250.
(227) Ill-Raga, G.; Ramos-Fernández, E.; Guix, F. X.; Tajes, M.; Bosch-Morató, M.; Palomer, E.; Godoy, J.; Belmar, S.; Cerpa, W.; Simpkins, J. W.; et al. *J. Alzheimers Dis.* **2010**, *22*, 641–652.
(228) Kanski, J.; Aksenova, M.; Butterfield, D. A. *Neurotox. Res.* **2002**, *4*, 219–223.
(229) Kanski, J.; Aksenova, M.; Schöneich, C.; Butterfield, D. A. *Free Radic. Biol. Med.* **2002**, *32*, 1205–1211.
(230) Pogocki, D.; Schöneich, C. *Chem. Res. Toxicol.* **2002**, *15*, 408–418.
(231) Schöneich, C.; Pogocki, D.; Hug, G. L.; Bobrowski, K. *J. Am. Chem. Soc.* **2003**, *125*, 13700–13713.
(232) Shelat, P. B.; Chalimoniuk, M.; Wang, J.-H.; Strosznajder, J. B.; Lee, J. C.; Sun, A. Y.; Simonyi, A.; Sun, G. Y. *J. Neurochem.* **2008**, *106*, 45–55.
(233) Drake, J.; Link, C. D.; Butterfield, D. A. *Neurobiol. Aging* **2003**, *24*, 415–420.
(234) Wan, L.; Nie, G.; Zhang, J.; Luo, Y.; Zhang, P.; Zhang, Z.; Zhao, B. *Free Radic. Biol. Med.* **2011**, *50*, 122–129.
(235) Butterfield, D. A.; Hardas, S. S.; Lange, M. L. B. *J. Alzheimers Dis.* **2010**, *20*, 369–393.
(236) Schöneich, C. *Biochim. Biophys. Acta* **2005**, *1703*, 111–119.
(237) Yatin, S. M.; Varadarajan, S.; Link, C. D.; Butterfield, D. A. *Neurobiol. Aging* **1999**, *20*, 325–330.
(238) Varadarajan, S.; Kanski, J.; Aksenova, M.; Lauderback, C.; Butterfield, D. A. *J. Am. Chem. Soc.* **2001**, *123*, 5625–5631.
(239) Cipak Gasparovic, A.; Zarkovic, N.; Zarkovic, K.; Semen, K.; Kaminskyy, D.; Yelisyeyeva, O.; Bottari, S. P. *Br. J. Pharmacol.* **2017**, *174*, 1771–1783.
(240) Aquino, D.; Bizzi, A.; Grisoli, M.; Garavaglia, B.; Bruzzone, M. G.; Nardocci, N.; Savoiardo, M.; Chiapparini, L. *Radiology* **2009**, *252*, 165–172.
(241) Cobine, P. A.; Pierrel, F.; Winge, D. R. *Biochim. Biophys. Acta* **2006**, *1763*, 759–772.
(242) Roberts, B. R.; Ryan, T. M.; Bush, A. I.; Masters, C. L.; Duce, J. A. *J. Neurochem.* **2012**, *120*, 149–166.
(243) von Bernhardi, R.; Eugenín, J. *Antioxid. Redox Signal.* **2012**, *16*, 974–1031.
(244) Imlay, J. A.; Chin, S. M.; Linn, S. *Science* **1988**, *240*, 640–642.
(245) Lloyd, D. R.; Phillips, D. H. *Mutat. Res.* **1999**, *424*, 23–36.
(246) Sensi, S. L.; Ton-That, D.; Sullivan, P. G.; Jonas, E. A.; Gee, K. R.; Kaczmarek, L. K.; Weiss, J. H. *Proc. Natl. Acad. Sci. U. S. A.* **2003**, *100*, 6157–6162.

(247) McCord, M. C.; Aizenman, E. *Front. Aging Neurosci.* **2014**, *6*, 77.
(248) Sensi, S. L.; Yin, H. Z.; Carriedo, S. G.; Rao, S. S.; Weiss, J. H. *Proc. Natl. Acad. Sci. U. S. A.* **1999**, *96*, 2414–2419.
(249) Dineley, K. E.; Richards, L. L.; Votyakova, T. V.; Reynolds, I. J. *Mitochondrion* **2005**, *5*, 55–65.
(250) Medvedeva, Y. V.; Lin, B.; Shuttleworth, C. W.; Weiss, J. H. *J. Neurosci.* **2009**, *29*, 1105–1114.
(251) Cheignon, C.; Jones, M.; Atrián-Blasco, E.; Kieffer, I.; Faller, P.; Collin, F.; Hureau, C. *Chem. Sci.* **2017**, *8*, 5107–5118.
(252) Eskici, G.; Axelsen, P. H. *Biochemistry* **2012**, *51*, 6289–6311.
(253) Mayes, J.; Tinker-Mill, C.; Kolosov, O.; Zhang, H.; Tabner, B. J.; Allsop, D. *J. Biol. Chem.* **2014**, *289*, 12052–12062.
(254) Nadal, R. C.; Rigby, S. E. J.; Viles, J. H. *Biochemistry* **2008**, *47*, 11653–11664.
(255) Cheignon, C.; Tomas, M.; Bonnefont-Rousselot, D.; Faller, P.; Hureau, C.; Collin, F. *Redox Biol.* **2018**, *14*, 450–464.
(256) Nakamura, M.; Shishido, N.; Nunomura, A.; Smith, M. A.; Perry, G.; Hayashi, Y.; Nakayama, K.; Hayashi, T. *Biochemistry* **2007**, *46*, 12737–12743.
(257) Dikalov, S. I.; Vitek, M. P.; Mason, R. P. *Free Radic. Biol. Med.* **2004**, *36*, 340–347.
(258) Jomova, K.; Vondrakova, D.; Lawson, M.; Valko, M. *Mol. Cell Biochem.* **2010**, *345*, 91–104.
(259) Cassagnes, L.-E.; Hervé, V.; Nepveu, F.; Hureau, C.; Faller, P.; Collin, F. *Angew. Chem. Int. Ed.* **2013**, *52*, 11110–11113.
(260) Clementi, M. E.; Marini, S.; Coletta, M.; Orsini, F.; Giardina, B.; Misiti, F. *FEBS Lett.* **2005**, *579*, 2913–2918.
(261) Smith, D. G.; Cappai, R.; Barnham, K. J. *Biochim. Biophys. Acta* **2007**, *1768*, 1976–1990.
(262) Schiewe, A. J.; Margol, L.; Soreghan, B. A.; Thomas, S. N.; Yang, A. J. *Pharm. Res.* **2004**, *21*, 1094–1102.
(263) Kanski, J.; Varadarajan, S.; Aksenova, M.; Butterfield, D. A. *Biochim. Biophys. Acta* **2001**, *1586*, 190–198.
(264) Cadenas, E.; Davies, K. J. A. *Free Radic. Biol. Med.* **2000**, *29*, 222–230.
(265) Turrens, J. F. *J. Physiol.* **2003**, *552*, 335–344.
(266) Polidori, M. C.; Nelles, G. *Curr. Pharm. Des.* **2014**, *20*, 3083–3092.
(267) Francis, P. T.; Palmer, A. M.; Snape, M.; Wilcock, G. K. *J. Neurol. Neurosurg. Psychiatry* **1999**, *66*, 137–147.
(268) Hardy, J. A.; Mann, D. M. A.; Wester, P.; Winblad, B. *Neurobiol. Aging* **1986**, *7*, 489–502.
(269) Hasselmo, M. E.; Bower, J. M. *Trends Neurosci.* **1993**, *16*, 218–222.
(270) Hasselmo, M. E. *Trends Cogn. Sci.* **1999**, *3*, 351–359.
(271) Fonnum, F. *Biochem. J.* **1969**, *115*, 465–472.
(272) Richter, J. A.; Perry, E. K.; Tomlinson, B. E. *Life Sci.* **1980**, *26*, 1683–1689.
(273) Perry, E. K.; Perry, R. H.; Blessed, G.; Tomlinson, B. E. *Neuropathol. Appl. Neurobiol.* **1978**, *4*, 273–277.
(274) Arendt, T.; Bigl, V.; Walther, F.; Sonntag, M. *Lancet* **1984**, *323*, 173.
(275) Kaduszkiewicz, H.; Zimmermann, T.; Beck-Bornholdt, H.-P.; van den Bussche, H. *BMJ.* **2005**, *331*, 321–327.
(276) Raina, P.; Santaguida, P.; Ismaila, A.; Patterson, C.; Cowan, D.; Levine, M.; Booker, L.; Oremus, M. *Ann. Intern. Med.* **2008**, *148*, 379–397.
(277) Ordentlich, A.; Barak, D.; Kronman, C.; Ariel, N.; Segall, Y.; Velan, B.; Shafferman, A. *J. Biol. Chem.* **1995**, *270*, 2082–2091.
(278) Nolte, H.-J.; Rosenberry, T. L.; Neumann, E. *Biochemistry* **1980**, *19*, 3705–3711.

(279) Harel, M.; Schalk, I.; Ehret-Sabatier, L.; Bouet, F.; Goeldner, M.; Hirth, C.; Axelsen, P. H.; Silman, I.; Sussman, J. L. *Proc. Natl. Acad. Sci. U. S. A.* **1993**, *90*, 9031–9035.

(280) Sussman, J. L.; Harel, M.; Frolow, F.; Oefner, C.; Goldman, A.; Toker, L.; Silman, I. *Science* **1991**, *253*, 872–879.

(281) Harel, M.; Quinn, D. M.; Nair, H. K.; Silman, I.; Sussman, J. L. *J. Am. Chem. Soc.* **1996**, *118*, 2340–2346.

(282) Dvir, H.; Silman, I.; Harel, M.; Rosenberry, T. L.; Sussman, J. L. *Chem. Biol. Interact.* **2010**, *187*, 10–22.

(283) Szegletes, T.; Mallender, W. D.; Thomas, P. J.; Rosenberry, T. L. *Biochemistry* **1999**, *38*, 122–133.

(284) Darvesh, K. V.; Pottie, I. R.; McDonald, R. S.; Martin, E.; Darvesh, S. in *Quantum Biochemistry*, ed. Matta, C. F. Wiley-VCH Verlag GmbH & Co. KGaA: Weinheim, **2010**, ch. Targeting Butyrylcholinesterase for Alzheimer's Disease Therapy, pp. 757–780.

(285) Greig, N. H.; Lahiri, D. K.; Sambamurti, K. *Int. Psychogeriatr.* **2002**, *14*, 77–91.

(286) Brus, B.; Kosak, U.; Turk, S.; Pišlar, A.; Coquelle, N.; Kos, J.; Stojan, J.; Colletier, J.-P.; Gobec, S. *J. Med. Chem.* **2014**, *57*, 8167–8179.

(287) Saxena, A.; Redman, A. M. G.; Jiang, X.; Lockridge, O.; Doctor, B. P. *Biochemistry* **1997**, *36*, 14642–14651.

(288) Savini, L.; Gaeta, A.; Fattorusso, C.; Catalanotti, B.; Campiani, G.; Chiasserini, L.; Pellerano, C.; Novellino, E.; McKissic, D.; Saxena, A. *J. Med. Chem.* **2003**, *46*, 1–4.

(289) Radić, Z.; Pickering, N. A.; Vellom, D. C.; Camp, S.; Taylor, P. *Biochemistry* **1993**, *32*, 12074–12084.

(290) Davis, K. L.; Mohs, R. C.; Marin, D.; Purohit, D. P.; Perl, D. P.; Lantz, M.; Austin, G.; Haroutunian, V. *JAMA.* **1999**, *281*, 1401–1406.

(291) DeKosky, S. T.; Ikonomovic, M. D.; Styren, S. D.; Beckett, L.; Wisniewski, S.; Bennett, D. A.; Cochran, E. J.; Kordower, J. H.; Mufson, E. J. *Ann. Neurol.* **2002**, *51*, 145–155.

(292) Alvarez, A.; Alarcón, R.; Opazo, C.; Campos, E. O.; Muñoz, F. J.; Calderón, F. H.; Dajas, F.; Gentry, M. K.; Doctor, B. P.; De Mello, F. G.; et al. *J. Neurosci*. **1998**, *18*, 3213–3223.

(293) Ramsay, R. R.; Majekova, M.; Medina, M.; Valoti, M. *Front. Neurosci.* **2016**, *10*, 375.

(294) Melo, J. B.; Agostinho, P.; Oliveira, C. R. *Neurosci. Res.* **2003**, *45*, 117–127.

(295) Rees, T.; Hammond, P. I.; Soreq, H.; Younkin, S.; Brimijoin, S. *Neurobiol. Aging* **2003**, *24*, 777–787.

(296) García-Ayllón, M.-S.; Small, D. H.; Avila, J.; Sáez-Valero, J. *Front. Mol. Neurosci.* **2011**, *4*, 22.

(297) Frasco, M. F.; Fournier, D.; Carvalho, F.; Guilhermino, L. *Biomarkers* **2005**, *10*, 360-375.

(298) Kale, M.; Rathore, N.; John, S.; Bhatnagar, D. *Toxicol. Lett.* **1999**, *105*, 197–205.

(299) Inestrosa, N. C.; Alvarez, A.; Pérez, C. A.; Moreno, R. D.; Vicente, M.; Linker, C.; Casanueva, O. I.; Soto, C.; Garrido, J. *Neuron* **1996**, *16*, 881–891.

(300) Bartolini, M.; Bertucci, C.; Cavrini, V.; Andrisano, V. *Biochem. Pharmacol.* **2003**, *65*, 407–416.

(301) De Ferrari, G. V.; Canales, M. A.; Shin, I.; Weiner, L. M.; Silman, I.; Inestrosa, N. C. *Biochemistry* **2001**, *40*, 10447–10457.

(302) Greig, N. H.; Utsuki, T.; Ingram, D. K.; Wang, Y.; Pepeu, G.; Scali, C.; Yu, Q.-S.; Mamczarz, J.; Holloway, H. W.; Giordano, T.; et al. *Proc. Natl. Acad. Sci. U. S. A.* **2005**, *102*, 17213–17218.

(303) Petroff, O. A. C. *Neuroscientist* **2002**, *8*, 562–573.

(304) Debanne, D.; Daoudal, G.; Sourdet, V.; Russier, M. Brain Plasticity and Ion Channels. *J. Physiol.* **2003**, *97*, 403–414. Levitt, P.; Pintar, J. E.; Breakefield, X. O. *Proc. Natl. Acad. Sci. U. S. A.* **1982**, *79*, 6385–6389.
(305) Ikonomidou, C.; Bosch, F.; Miksa, M.; Bittigau, P.; Vockler, J.; Dikranian, K.; Tenkova, T. I.; Stefovska, V.; Turski, L.; Olney, J. W. *Science* **1999**, *283*, 70–74.
(306) Asztély, F.; Gustafsson, B. *Molecular neurobiology* **1996,** *12*, 1.
(307) Parsons, M. P.; Raymond, L. A. *Neuron* **2014**, *82*, 279–293.
(308) Monyer, H.; Burnashev, N.; Laurie, D. J.; Sakmann, B.; Seeburg, P. H. *Neuron* **1994**, *12*, 529–540.
(309) Dingledine, R.; Borges, K.; Bowie, D.; Traynelis, S. F. *Pharmacol. Rev.* **1999**, *51*, 7–62.
(310) Mayer, M. L.; Westbrook, G. L.; Guthrie, P. B. *Nature* **1984**, *309*, 261–263.
(311) Zeevalk, G. D.; Nicklas, W. J. *J. Neurochem.* **1992**, 59, 1211–1220.
(312) Choi, D. W. *J. Neurobiol.* **1992**, *23*, 1261–1276.
(313) Hartley, D. M.; Kurth, M. C.; Bjerkness, L.; Weiss, J. H.; Choi, D. W. *J. Neurosci.* **1993**, *13*, 1993–2000.
(314) Reisberg, B.; Doody, R.; Stöffler, A.; Schmitt, F.; Ferris, S.; Möbius, H. J. *N. Engl. J. Med.* **2003**, *348*, 1333–1341.
(315) Lipton, S. A. *NeuroRx* **2004**, *1*, 101–110.
(316) Bortolato, M.; Chen, K.; Shih, J. C. *Adv. Drug Deliv. Rev.* **2008**, *60*, 1527–1533.
(317) Pisani, L.; Catto, M.; Leonetti, F.; Nicolotti, O.; Stefanachi, A.; Campagna, F.; Carotti, A. *Curr. Med. Chem.* **2011**, *18*, 4568–4587.
(318) Heikkila, R. E.; Manzino, L.; Cabbat, F. S.; Duvoisin, R. C. *Nature* **1984**, *311*, 467–469.
(319) Levitt, P.; Pintar, J. E.; Breakefield, X. O. *Proc. Natl. Acad. Sci. U. S. A.* **1982,** *79*, 6385-6389.
(320) Nagatsu, T. *Neurotoxicology* **2004,** *25*, 11-20.
(321) Sterling, J.; Herzig, Y.; Goren, T.; Finkelstein, N.; Lerner, D.; Goldenberg, W.; Miskolczi, I.; Molnar, S.; Rantal, F.; Tamas, T. *J. Med. Chem.* **2002**, *45*, 5260–5279.
(322) Bollen, E.; Prickaerts, J. *IUBMB Life* **2012**, *64*, 965–970.
(323) Pérez-Torres, S.; Mengod, G. *Int. Congr. Ser.* **2003**, *1251*,127–138.
(324) Rabal, O.; Sánchez-Arias, J. A.; Cuadrado-Tejedor, M.; de Miguel, I.; Pérez-González, M.; García-Barroso, C.; Ugarte, A.; Estella-Hermoso de Mendoza, A.; Sáez, E.; Espelosin, M.; et al. *J. Med. Chem.* **2016**, *59*, 8967–9004.
(325) Impey, S.; Mark, M.; Villacres, E. C.; Poser, S.; Chavkin, C.; Storm, D. R. *Neuron* **1996**, *16*, 973–982.
(326) Lu, Y.-F.; Kandel, E. R.; Hawkins, R. D. *J. Neurosci.* **1999**, *19*, 10250–10261.
(327) Tully, T. *Proc. Natl. Acad. Sci. U. S. A.* **1997**, *94*, 4239–4241.
(328) Yin, J.; Del Vecchio, M.; Zhou, H.; Tully, T. *Cell* **1995**, *81*, 107–115.
(329) Shi, J.; Qian, W.; Yin, X.; Iqbal, K.; Grundke-Iqbal, I.; Gu, X.; Ding, F.; Gong, C.-X.; Liu, F. *J. Biol. Chem.* **2011**, *286*, 14639–14648.
(330) Hanger, D. P.; Anderton, B. H.; Noble, W. *Trends Mol. Med.* **2009**, *15*, 112–119.
(331) Mahley, R. W.; Rall, S. C. Jr. *Annu. Rev. Genomics Hum. Genet.* **2000**, *1*, 507–537.
(332) Corder, E. H.; Saunders, A. M.; Strittmatter, W. J.; Schmechel, D. E.; Gaskell, P. C.; Small, G. W.; Roses, A. D.; Haines, J. L.; Pericak-Vance, M. A. *Science* **1993**, *261*, 921–923.
(333) Strittmatter, W. J.; Saunders, A. M.; Schmechel, D.; Pericak-Vance, M.; Enghild, J.; Salvesen, G. S.; Roses, A. D. *Proc. Natl. Acad. Sci. U. S. A.* **1993**, *90*, 1977–1981.
(334) Saunders, A. M.; Strittmatter, W. J.; Schmechel, D.; George-Hyslop, P. H. St.; Pericak-Vance, M. A.; Joo, S. H.; Rosi, B. L.; Gusella, J. F.; Crapper-MacLachlan, D. R.; Alberts, M. J.; et al. *Neurology* **1993**, *43*, 1467–1472.

(335) Mahley, R. W.; Weisgraber, K. H.; Huang, Y. *J. Lipid Res.* **2009**, *50*, S183–S188.
(336) Corder, E. H.; Saunders, A. M.; Risch, N. J.; Strittmatter, W. J.; Schmechel, D. E.; Gaskell, P. C.; Rimmler, J. B.; Locke, P. A.; Conneally, P. M.; Schmader, K. E.; et al. *Nat. Genet.* **1994**, *7*, 180–184.
(337) Rebeck, G. W.; Reiter, J. S.; Strickland, D. K.; Hyman, B. T. *Neuron* **1993**, *11*, 575–580.
(338) Holtzman, D. M.; Bales, K. R.; Tenkova, T.; Fagan, A. M.; Parsadanian, M.; Sartorius, L. J.; Mackey, B.; Olney, J.; McKeel, D.; Wozniak, D.; *et al. Proc. Natl. Acad. Sci. U. S. A.* **2000**, *97*, 2892–2897.
(339) Hashimoto, T.; Serrano-Pozo, A.; Hori, Y.; Adams, K. W.; Takeda, S.; Banerji, A. O.; Mitani, A.; Joyner, D.; Thyssen, D. H.; Bacskai, B. J.; et al. *J. Neurosci*. **2012**, *32*, 15181–15192.
(340) Bales, K. R.; Verina, T.; Cummins, D. J.; Du, Y.; Dodel, R. C.; Saura, J.; Fishman, C. E.; DeLong, C. A.; Piccardo, P.; Petegnief, V.; et al. *Proc. Natl. Acad. Sci. U. S. A.* **1999**, *96*, 15233–15238.
(341) Jiang, Q.; Lee, C. Y. D.; Mandrekar, S.; Wilkinson, B.; Cramer, P.; Zelcer, N.; Mann, K.; Lamb, B.; Willson, T. M.; Collins, J. L.; et al. *Neuron* **2008**, *58*, 681–693.
(342) Laskowitz, D. T.; Goel, S.; Bennett, E. R.; Matthew, W. D. *J. Neuroimmunol*. **1997**, *76*, 70–74.
(343) Chen, H. K.; Liu, Z.; Meyer-Franke, A.; Brodbeck, J.; Miranda, R. D.; McGuire, J. G.; Pleiss, M. A.; Ji, Z.-S.; Balestra, M. E.; Walker, D. W.; et al. *J. Biol. Chem*. **2012**, *287*, 5253–5266.
(344) Shi, Y.; Yamada, K.; Liddelow, S. A.; Smith, S. T.; Zhao, L.; Luo, W.; Tsai, R. M.; Spina, S.; Grinberg, L. T.; Rojas, J. C.; et al. *Nature* **2017**, *549*, 523–527.
(345) Jawhar, S.; Wirths, O.; Bayer, T. A. *J. Biol. Chem*. **2011**, *286*, 38825–38832.
(346) Jawhar, S.; Wirths, O.; Schilling, S.; Graubner, S.; Demuth, H.-U.; Bayer, T. A. *J. Biol. Chem.* **2011**, *286*, 4454–4460.
(347) Saido, T. C.; Iwatsubo, T.; Mann, D. M. A.; Shimada, H.; Ihara, Y.; Kawashima, S. *Neuron* **1995**, *14*, 457–466.
(348) Schilling, S.; Zeitschel, U.; Hoffmann, T.; Heiser, U.; Francke, M.; Kehlen, A.; Holzer, M.; Hutter-Paier, B.; Prokesch, M.; Windisch, M.; et al. *Nat. Med*. **2008**, *14*, 1106–1111.
(349) Morawski, M.; Schilling, S.; Kreuzberger, M.; Waniek, A.; Jäger, C.; Koch, B.; Cynis, H.; Kehlen, A.; Arendt, T.; Hartlage-Rübsamen, M.; et al. *J. Alzheimers Dis*. **2014**, *39*, 385–400.
(350) Schilling, S.; Appl, T.; Hoffmann, T.; Cynis, H.; Schulz, K.; Jagla, W.; Friedrich, D.; Wermann, M.; Buchholz, M.; Heiser, U. *J. Neurochem*. **2008**, *106*, 1225–1236.
(351) Buchholz, M.; Heiser, U.; Schilling, S.; Niestroj, A. J.; Zunkel, K.; Demuth, H.-U. *J. Med. Chem*. **2006**, *49*, 664–677.
(352) Gendelman, H. E. *J. Neurovirol.* **2002**, *8*, 474–479.
(353) Akiyama, H.; Barger, S.; Barnum, S.; Bradt, B.; Bauer, J.; Cole, G. M.; Cooper, N. R.; Eikelenboom, P.; Emmerling, M.; Fiebich, B. L.; et al. *Neurobiol. Aging.* **2000**, *21*, 383–421.
(354) Afagh, A.; Cummings, B. J.; Cribbs, D. H.; Cotman, C. W.; Tenner, A. J. *Brain. Exp. Neurol.* **1996**, *138*, 22–32.
(355) Shen, Y.; Lue, L.-F.; Yang, L.-B.; Roher, A.; Kuo, Y.-M.; Strohmeyer, R.; Goux, W. J.; Lee, V.; Johnson, G. V. W.; Webster, S. D.; et al. *Neurosci. Lett.* **2001**, *305*, 165–168.
(356) Kitamura, Y.; Shimohama, S.; Koike, H.; Kakimura, J.; Matsuoka, Y.; Nomura, Y.; Gebicke-Haerter, P. J.; Taniguchi, T. *Biochem. Biophys. Res. Commun*. **1999**, *254*, 582–586.
(357) Landreth, G. E.; Heneka, M. T. *Neurobiol. Aging*. **2001**, *22*, 937–944.
(358) Sanchez-Mejia, R. O.; Newman, J. W.; Toh, S.; Yu, G.-Q.; Zhou, Y.; Halabisky, B.; Cissé, M.; Scearce-Levie, K.; Cheng, I. H.; Gan, L.; et al. *Nat. Neurosci.* **2008**, *11*, 1311–1318.
(359) Sun, G. Y.; Xu, J.; Jensen, M. D.; Simonyi, A. *J. Lipid Res*. **2004**, *45*, 205–213.
(360) Du, H.; Guo, L.; Fang, F.; Chen, D.; Sosunov, A. A.; McKhann, G. M.; Yan, Y.; Wang, C.;

Zhang, H.; Molkentin, J. D.; et al. *Nat. Med*. **2008**, *14*, 1097–1105.
(361) Du, H.; Yan, S. S. *Biochim. Biophys. Acta* **2010**, *1802*, 198–204.
(362) Bernardo, A.; Harrison, F. E.; McCord, M.; Zhao, J.; Bruchey, A.; Davies, S. S.; Jackson Roberts II, L.; Mathews, P. M.; Matsuoka, Y.; Ariga, T.; et al. *Neurobiol. Aging* **2009**, *30*, 1777–1791.
(363) Asahina, M.; Yoshiyama, Y.; Hattori, T. *Clin. Neuropathol.* **2001**, *20*, 60–63.
(364) Melchor, J. P.; Pawlak, R.; Strickland, S. *J. Neurosci*. **2003**, *23*, 8867–8871.
(365) Caricasole, A.; Copani, A.; Caraci, F.; Aronica, E.; Rozemuller, A. J.; Caruso, A.; Storto, M.; Gaviraghi, G.; Terstappen, G. C.; Nicoletti, F. *J. Neurosci*. **2004**, *24*, 6021–6027.
(366) Saito, K.-I.; Elce, J. S.; Hamos, J. E.; Nixon, R. A. *Proc. Natl. Acad. Sci. U. S. A.* **1993**, *90*, 2628–2632.
(367) Nixon, R. A.; Saito, K.-I.; Grynspan, F.; Griffin, W. R.; Katayama, S.; Honda, T.; Mohan, P. S.; Shea, T. B.; Beermann, M. *Ann. N. Y. Acad. Sci*. **1994**, *747*, 77–91.
(368) Kilgore, M.; Miller, C. A.; Fass, D. M.; Hennig, K. M.; Haggarty, S. J.; Sweatt, J. D.; Rumbaugh, G. *Neuropsychopharmacology* **2010**, *35*, 870−880.

Chapter 2.

An Iridium(III) Complex as a Photoactivatable Tool for Oxidation of Amyloidogenic Peptides with Subsequent Modulation of Peptide Aggregation

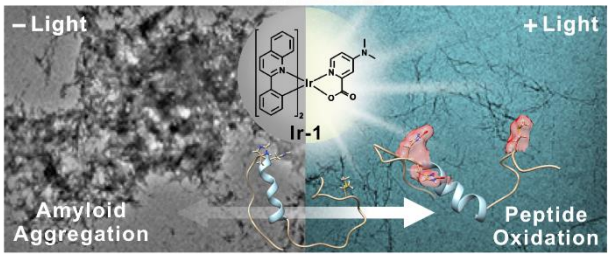

The results and discussion presented in this chapter were reported in the publication [Kang, J.;† Lee, S. J. C.;† Nam, J. S.;† Lee, H. J.; Kang, M.-G.; Korshavn, K. J.; Kim, H.-T.; Cho, J.; Ramamoorthy, A.; Rhee, H.-W.; Kwon, T.-H.; Lim, M. H. *Chem. Eur. J.* **2017**, *23*, 1645–1653 (†equal contribution)]. Professor Tae-Hyuk Kwon, Jung Seung Nam, and Hyun-Tak Kim prepared **Ir-1** and measured its photophysical properties with data analysis. Professor Ayyalusamy Ramamoorthy and Dr. Kyle J. Korshavn carried out the studies of 2D HMQC NMR. Dr. Shin Jung C. Lee and I performed the mass spectrometric investigations with data analysis, and Professor Hyun-Woo Rhee and Myeong-Gyun Kang conducted in-gel digestion studies. I conducted gel/Western blot and TEM with data analysis. I, Dr. Shin Jung C. Lee, and Dr. Hyuck Jin Lee wrote the manuscript under the assistance of Professor Mi Hee Lim.

2.1. Introduction

Amyloidogenic peptides are found in human degenerative diseases [e.g., amyloid-β (Aβ) for Alzheimer's disease (AD), α-synuclein (α-Syn) for Parkinson's disease (PD), and human islet amyloid polypeptide (hIAPP) for type II diabetes].[1–6] Amyloidogenic peptides have aggregate-prone properties to form β-strand fibrils through oligomeric conformations, and their aggregation has been suggested to be linked to the pathogenesis of degenerative disorders.[1–6] Thus, a variety of approaches have been developed to regulate or suppress the aggregation pathways of amyloidogenic peptides.[2,7–12] Among such methods, peptide modifications, including peptide oxidation, have been recently implicated as a strategy suitable for modulation of amyloidogenic peptide aggregation (Figure 2.1a).[13–23]

To trigger the oxidation of peptides, some chemical reagents, such as metal ions, have been utilized.[14,24–27] Metal ions are frequently used for peptide oxidation; however, they require harsh additional oxidants.[14,24–27] In addition, chemical reagents capable of generating oxidants from O_2 upon photoactivation have been developed for use as photosensitizers in various fields because light is a readily accessible resource.[13,28–40] A series of organic molecules, such as riboflavin, rose bengal, methylene blue, and porphyrins, have been used as photoinduced reagents;[13,29–35] however, (i) many of them have relatively lower quantum yields than those of photoactivatable transition-metal complexes;[41–44] and (ii) some organic agents are less stable, which potentially indicates their degradation upon irradiation.[28,36] Photoactivatable metal complexes present relatively high quantum yields, structural stability, and tunable geometries and properties upon ligand substitution.[28,36] Due to these beneficial aspects, multiple metal complexes have been designed and mediated for photoinduced oxidation of peptides.[37–40] One inorganic complex, $[Ru(bpy)_3]^{2+}$ (bpy = 2,2'-bipyridine), has been frequently employed for oxidative modifications of peptides through light exposure.[38–40] To achieve peptide oxidation, this ruthenium(II) complex still needs an additional electron acceptor (e.g., ammonium persulfate), however, which could lead to cytotoxicity and limit its applications.[38–40,45] Thus, robust inorganic complexes able to efficiently oxidize peptides simply by light introduction without the assistance of harsh additives would be of significant value for gaining a greater understanding of peptide-related chemistry and biology.

Herein, we report an iridium(III) complex, **Ir-1** (Figure 2.1b), as a chemical tool for the oxidation of amyloidogenic peptides with the subsequent control of their aggregation under mild conditions that only include readily available O_2 and visible light. **Ir-1** was rationally designed as such a tool through incorporating the general properties of Ir(III) complexes previously reported for various applications, including photoactivation, formation of reactive oxygen species (ROS) upon light exposure, and relatively stable octahedral geometry, as well as relatively easy introduction of a ligand containing a structural moiety, suggested to be important for interactions with amyloidogenic peptides, on the Ir(III)

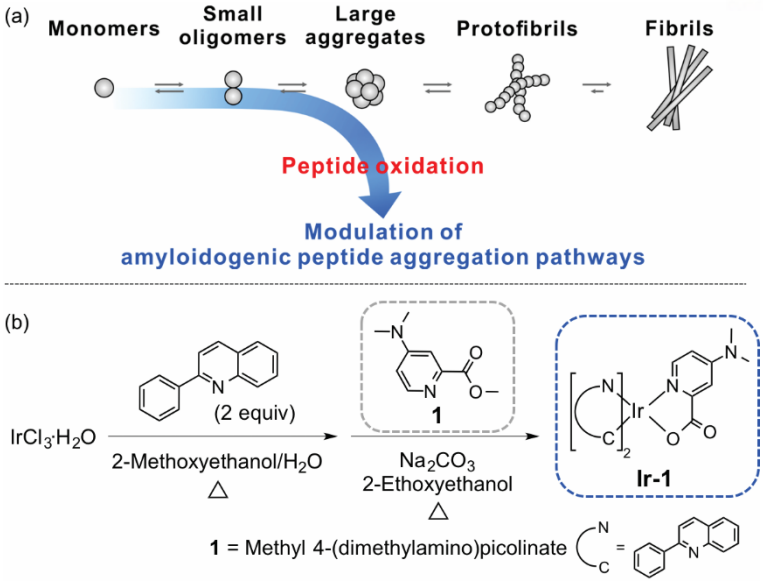

Figure 2.1. Schematic description of amyloidogenic peptide aggregation and chemical structures of **Ir-1** and **1**. As shown in (a), oxidation of amyloidogenic peptides could control their aggregation pathways. (b) Synthetic routes to **Ir-1**.

center.[28,46–53] Representative amyloidogenic peptides (i.e., Aβ, α-Syn, and hIAPP) were indicated to be noticeably oxidized upon treatment of **Ir-1** with photoactivation under aerobic conditions, as monitored by electrospray ionization mass spectrometry (ESI-MS), and their oxidation sites (as potential sites, methionine, histidine, and tyrosine residues) were identified by tandem MS (ESI-MS^2). Even with oxidative modifications of a few residues in these amyloidogenic peptides, the aggregation pathways were noticeably modulated, resulting in distinct morphological features (e.g., smaller-sized or amorphous peptide species, instead of fibrils). Taken together, our rational design and investigations into **Ir-1** illustrate the potential of transition metal complexes as chemical tools for the oxidative modification of amyloidogenic peptides simply by employing light and O_2. In addition, our studies corroborate that small changes in amyloidogenic peptides, such as oxidation at a few specific residues, are able to transform overall peptide aggregation pathways; this suggests novel and viable directions for amyloid management (Figure 2.1a).

2.2. Results and Discussion

2.2.1. Rational Design of Ir-1 for Oxidation of Amyloidogenic Peptides

For the oxidation of amyloidogenic peptides simply upon photoactivation under mild conditions, **Ir-1** (Figure 2.1b) was rationally designed as a chemical tool by taking into account the characteristics found in previously reported photoactivatable Ir(III) complexes, as well as specificity for amyloidogenic peptides: (i) photoproperties with relatively low-energy radiation (i.e., visible light) ;[49,50] (ii) the ability to produce ROS [e.g., singlet oxygen ($^1O_2$)] from redundant O_2, which is responsible for peptide oxidation, upon photoactivation;[28,48] (iii) robust octahedral coordination, which can provide relative

structural stability without any structural modifications when light is introduced;[48] (iv) strong spin-orbit coupling of the Ir(III) center, which could facilitate electronic transitions without the assistance of additional electron acceptors;[49,50] and (v) incorporation of a ligand (**1**) containing a dimethylamino group, suggested to be crucial for interactions with amyloidogenic peptides,[46,47] onto the Ir(III) center (Figure 2.1b).

Ir-1 was obtained in relatively high yield (ca. 80%) through previously known two-step procedures with slight modifications, as depicted in Figure 2.1b.[54] Moreover, **Ir-1** is easily photoactivatable under mild conditions [e.g., excitation with visible light {ε (463 nm) = 5.78 (± 0.12) × 10^3 M^{-1} cm^{-1}; Table 2.1} and aerobic conditions] as shown by its quantum yield for phosphorescence [Φ_p = 0.41 (± 0.02); Table 2.1]. The ability of **Ir-1** to generate singlet oxygen ($^1O_2$) from triplet dioxygen ($^3O_2$) was also confirmed by determining the quantum yield of $^1O_2$ [Φ_s = 0.25 (± 0.03); Table 2.1]. Overall, an octahedral Ir(III) complex, **Ir-1**, was constructed as a photoactivatable tool to oxidize amyloidogenic peptides without the need for harsh conditions through relatively easy synthetic routes with a high yield, and demonstrated to generate oxidants (i.e., $^1O_2$) from readily accessible O_2.

Table 2.1. Photophysical properties of **Ir-1**.

	Ir-1
$\lambda_{ex,\ max}$ (nm)	463
$\lambda_{em,\ max}$ (nm)	600
ε [$M^{-1}cm^{-1}$; 463 nm; in H_2O (1% v/v DMSO)]	5.78 (± 0.12) x 10^3
Lifetime (ns)	238
Φ_p	0.41 (± 0.02)
Φ_s	0.25 (± 0.03)

2.2.2. Oxidative Modifications of Amyloidogenic Peptides by Ir-1

To investigate whether the oxidation of amyloidogenic peptides by **Ir-1** under aerobic conditions would occur with light activation, three amyloidogenic peptides (i.e., Aβ, α-Syn, and hIAPP found in AD, PD, and type II diabetes, respectively) were chosen as representative amyloidogenic peptides, and the resultant monomeric peptide species upon treatment with **Ir-1** were first monitored by means of ESI-MS (Figure 2.2). These three amyloidogenic peptides were observed to be oxidized with the addition of lightactivated **Ir-1** under aerobic conditions. Without light, even in the presence of **Ir-1**, all amyloidogenic peptides were in nonoxidized forms (Figure 2.2, middle, gray). In the case of $A\beta_{40}$, the oxidized Aβ monomers had a 16 Da increase in mass from nonoxidized peptides; this implied the

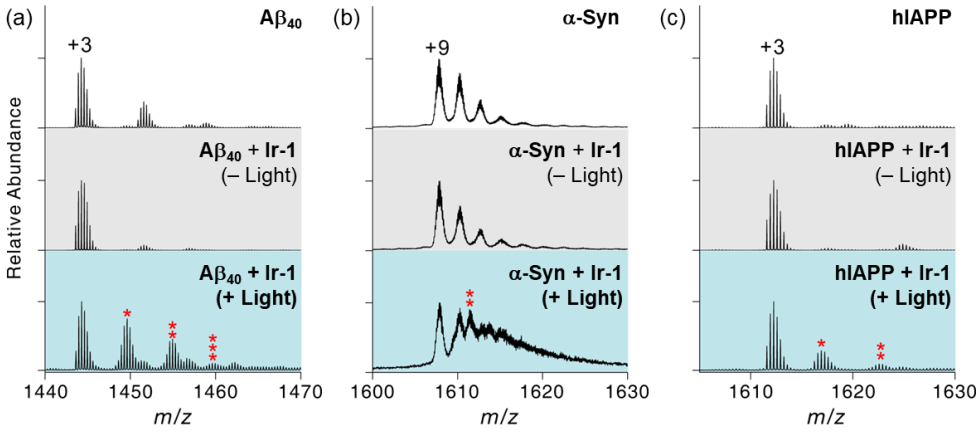

Figure 2.2. Oxidation of amyloidogenic peptides by **Ir-1** upon light activation. Mass spectrometric analyses of amyloidogenic peptides [(a) $A\beta_{40}$, (b) α-Syn, and (c) hIAPP] upon treatment with **Ir-1** in the presence of light. Oxidized peptide ions are indicated with red asterisks, and the number of asterisks indicates the number of oxygen atoms incorporated into the peptides. Conditions: [peptide] = 100 μM; [**Ir-1**] = 500 μM; pH 7.4; 37 °C; 1 h; no agitation; 1 sun light for 10 min (for samples treated with light); aerobic conditions. Details for the assignment of oxidized peaks are included in the Experimental Section.

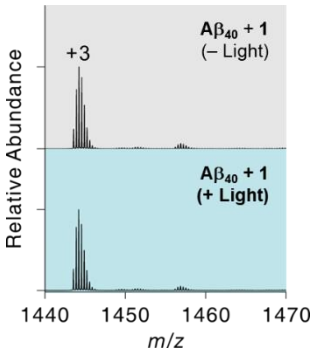

Figure 2.3. ESI-MS spectra for $A\beta_{40}$ with **1** in the absence (top) and presence (bottom) of light. Conditions: [$A\beta_{40}$] = 100 μM; [**1**] = 500 μM; pH 7.4; 37 °C; 1 h; no agitation; 1 sun light for 10 min (for the samples treated with light); aerobic conditions.

incorporation of one oxygen atom into the peptide (Figure 2.2a, bottom, blue). Notably, ligand **1** alone was not able to oxidize $A\beta_{40}$ (Figure 2.3). Similar to $A\beta_{40}$, doubly oxidized α-Syn with a 32 Da increase in mass, relative to that of the native peptide, was indicated; this suggested the introduction of two oxygen atoms into the peptide (Figure 2.2b, bottom, blue). Slightly different from both Aβ and α-Syn, singly oxidized monomeric hIAPP presented a 14 Da difference in mass from nonoxidized peptides (Figure 2.2c, bottom, blue). A 14 Da increase in mass could result from the addition of one oxygen atom to hIAPP, along with deprotonation.[13,33,55]

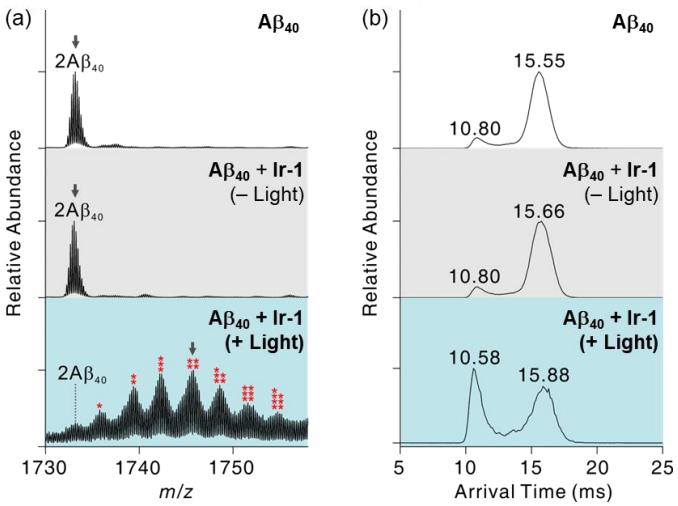

Figure 2.4. Oxidation of Aβ$_{40}$ dimers by **Ir-1** upon photoactivation. (a) ESI-MS spectra for +5-charged dimers with **Ir-1** in the absence and presence of light. The oxidized dimers are only detected by **Ir-1** with light exposure (bottom, blue). The number of red asterisks indicates the number of oxygen atoms incorporated into Aβ$_{40}$ dimers. (b) ATDs for nonoxidized (top and middle) and tetraoxidized dimers (bottom). Each ion selected for IM-MS analysis is indicated with gray arrows in (a). The oxidized dimer incorporated with four oxygen atoms presents the higher abundance in the distribution with short drift time (bottom) than that of nonoxidized Aβ$_{40}$ (top and middle), which implies that structural compaction can be induced by oxidation. Conditions: [Aβ$_{40}$] = 100 μM; [**Ir-1**] = 500 μM; pH 7.4; 37 °C; 1 h; no agitation; 1 sun light for 10 min (for samples treated with light); aerobic conditions.

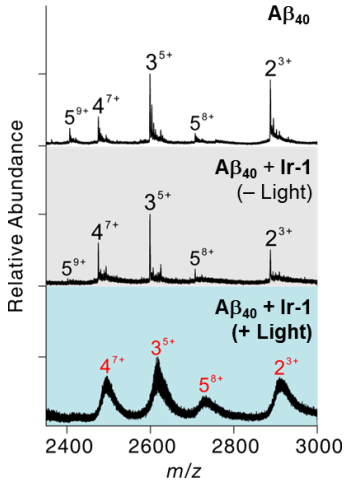

Figure 2.5. ESI-MS spectra for oligomeric Aβ$_{40}$ with **Ir-1** in the absence and presence of light. The +*z*-charged *n*-mer is denoted as n^{z+}. Peak annotations for oxidized oligomers are highlighted in red. Conditions: [Aβ$_{40}$] = 100 μM; [**Ir-1**] = 500 μM; pH 7.4; 37 °C; 1 h; no agitation; 1 sun light for 10 min (for the samples treated with light); aerobic conditions.

Second, we examined whether amyloidogenic peptide oligomers (focusing on Aβ oligomers) by **Ir-1** could be oxidized with light activation under aerobic conditions. From the samples containing Aβ

and **Ir-1** upon exposure to light and O_2, the oxidation of both dimers and larger oligomers was revealed (Figures 2.4a and 2.5). As demonstrated in Figure 2.4a, multiple oxygen atoms (e.g., for dimers, up to seven oxygen atoms) were indicated to be incorporated into the oxidized oligomers.

Moreover, structural changes to monomeric and oligomeric peptide species accompanied by oxidation were probed by means of ion mobility mass spectrometry (IM-MS), which enabled to characterize conformations based on the mobility of ions passing through a cell filled with neutral gas.[56] In the case of Aβ monomers, there was no remarkable difference in arrival time distributions (ATDs) between singly oxidized and nonoxidized $A\beta_{40}$ monomers (Figure 2.6). Distinguishable from Aβ monomers, a change in the IM-MS data of $A\beta_{40}$ dimers upon oxidation was presented at two dominant ATDs, centered at 10.80 and 15.55 ms, respectively (Figure 2.4b). Nonoxidized $A\beta_{40}$ dimers exhibited greater dominance in the larger ATD, whereas the oxidized dimers had the opposite tendency, which suggested that peptide oxidation could lead to structural compaction in the dimers. Although structural details of oxidized dimers have not been elucidated, their structural compaction might assist in modulating peptide aggregation because previous studies indicated that conformationally compact Aβ species could alter peptide aggregation pathways to form amorphous aggregates.[8–11]

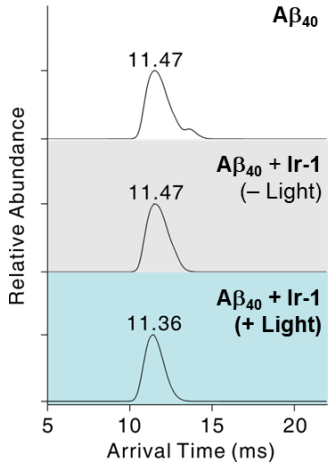

Figure 2.6. IM-MS spectra for +3-charged $A\beta_{40}$ monomers. ATD for nonoxidized (top and middle) and singly oxidized monomeric $A\beta_{40}$ (bottom). There is no significant difference between ATD of nonoxidized $A\beta_{40}$ (top and middle) and that of singly oxidized $A\beta_{40}$ upon addition of **Ir-1** in the presence of light (bottom).

Furthermore, the oxidation of a nonamyloidogenic structured protein, ubiquitin, was also investigated when **Ir-1** was added with light under aerobic conditions. Ubiquitin was selected as an archetypal structured protein because all secondary structures (e.g., α-helix, β-strand, and random coil) could be found in ubiquitin.[57] Ubiquitin treated with **Ir-1** was shown to be oxidized with light exposure under aerobic conditions (Figure 2.7, bottom, blue); however, oxidized ubiquitin was significantly less abundant than the oxidized forms of intrinsically disordered amyloidogenic peptides (i.e., $A\beta_{40}$, α-Syn,

and hIAPP). Overall, oxidative modifications of amyloidogenic peptides, lacking ordered structures, are more readily achieved over structured peptides by **Ir-1** under mild conditions, including light and O_2, which could direct structural compaction; this supports the utilization of **Ir-1** as a photoactivatable tool for the oxidation of amyloidogenic peptides.

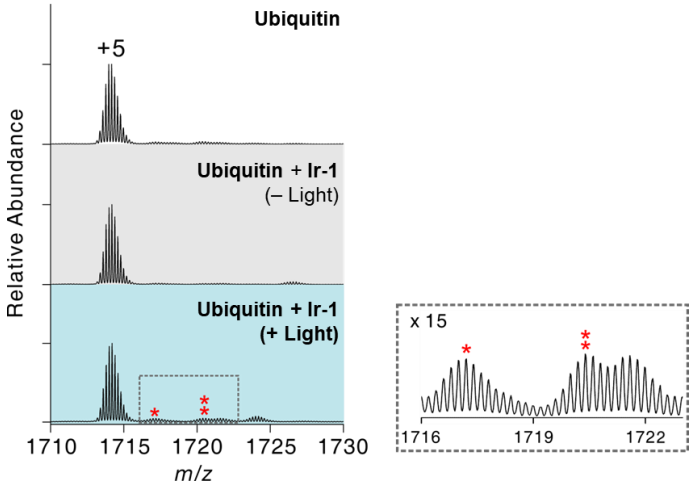

Figure 2.7. ESI-MS spectra for ubiquitin with **Ir-1** in the absence and presence of light. The number of red asterisks indicates the number of the oxygen atoms incorporated into the peptide. The oxidized ubiquitin peaks are magnified and indicated in the dotted box. Conditions: [ubiquitin] = 100 μM; [**Ir-1**] = 500 μM; pH 7.4; 37 ℃; 1 h; no agitation; 1 sun light for 10 min (for the samples treated with light); aerobic conditions.

2.2.3. Identification of Oxidation Sites in Amyloidogenic Peptides

The resultant oxidized amyloidogenic peptides, produced by the addition of **Ir-1** with light exposure under aerobic conditions, were further studied by ESI-MS^2 to determine the oxidation sites in the peptides.[10,11] The fragment ions generated by selectively applying collisional energy to the singly and doubly oxidized amyloidogenic peptides were analyzed (Figure 2.8). First, the oxidation sites in $A\beta_{40}$ were identified. The singly oxidized fragments, highlighted in red, were observed in *b* fragments, which were cleaved from the N-terminus (Figure 2.8b). All *b* fragments smaller than b_{13} existed as nonoxidized forms, whereas those larger than b_{34} represented only oxidized fragments. Methionine 35 (M35) is known to be the most readily oxidizable amino acid in Aβ.[22] If oxidation occurred only at M35, all fragments smaller than b_{35} would not be oxidized (Figure 2.8a); however, oxidized b fragments were indicated to be smaller than b_{35}, which implied the existence of other oxidation sites (Figure 2.8b). Based on previously reported studies, other possible oxidation sites could be histidine residues (i.e., H13, H14).[26,59] In the ESI-MS^2 spectrum for doubly oxidized $A\beta_{40}$, there was no oxidized fragment smaller than b_{13} (Figure 2.8d). Because fragments from b_{13} to b_{34} only existed in singly oxidized forms (highlighted in red in Figure 2.8), this region would include one oxidation site, possibly H13 or H14.

All fragments larger than b_{34} were doubly oxidized (denoted in green), which implied the incorporation of one oxygen atom into M35 to generate a sulfoxide form (Figure 2.8c and d).

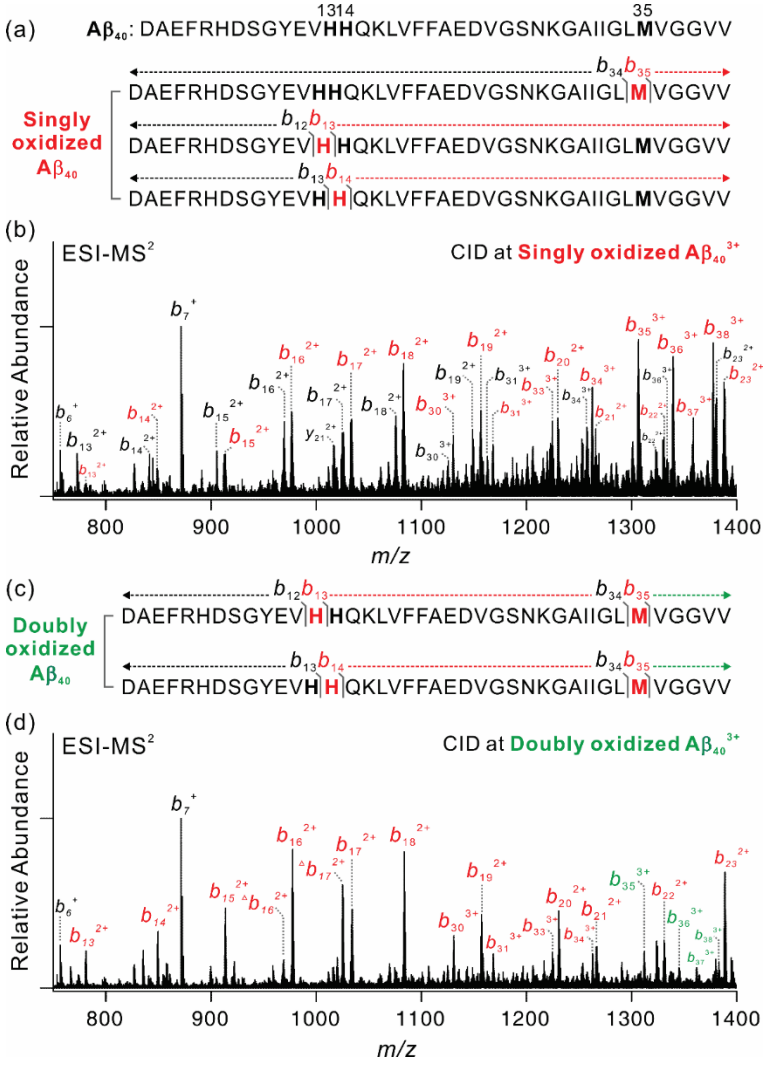

Figure 2.8. Identification of the oxidation sites in Aβ$_{40}$. (a and c) The peptide sequence and annotation for ESI-MS^2 and (b and d) ESI-MS^2 spectra for singly and doubly oxidized Aβ$_{40}$. Singly and doubly oxidized *b* fragments (N-terminal fragment ions) or *y* fragments (C-terminal fragment ions) are denoted in red and green, respectively. The peaks assigned as triangles (b_{16} and b_{17}) indicate that the loss of a water molecule occurs at serine, threonine, glutamate, or aspartate residues in these fragment ions.[58]

For further analysis of the oxidation sites in Aβ, Aβ$_{40}$ treated with **Ir-1** in the absence and presence of light was evaluated by 2D band-selective optimized flip-angle short transient heteronuclear multiple quantum correlation (SOFAST-HMQC) NMR spectroscopy (Figures 2.9). In the absence of light, minimal chemical shift perturbations (CSPs) of uniformly ^{15}N-labeled Aβ$_{40}$ appeared upon incubation with **Ir-1** (Figure 2.9c), which implied no significant interaction of **Ir-1** with the peptide. Following exposure of the Aβ samples containing **Ir-1** to light, a dramatic increase in the CSPs at V12, D23, and M35 was observed (Figure 2.9d). A noticeable change in the CSP of M35 suggests that there

are interactions near M35, which is consistent with observation monitored by ESI-MS^2. In the case of histidine residues, although they were not well resolved within the spectra due to peak overlap, the enhanced CSP of V12, proximately located to H13 or H14, could be expected, which proposed oxidative modifications at H13 or H14, as shown in our ESI-MS^2 studies. Notably, in the NMR spectra, D23 was adjacent to M35 with some overlap, so the shift of M35 might affect its CSP. Thus, our NMR data support that Aβ_{40} is oxidized at specific sites (potentially, M35, H13, and H14) by **Ir-1** upon light stimulation under aerobic conditions.

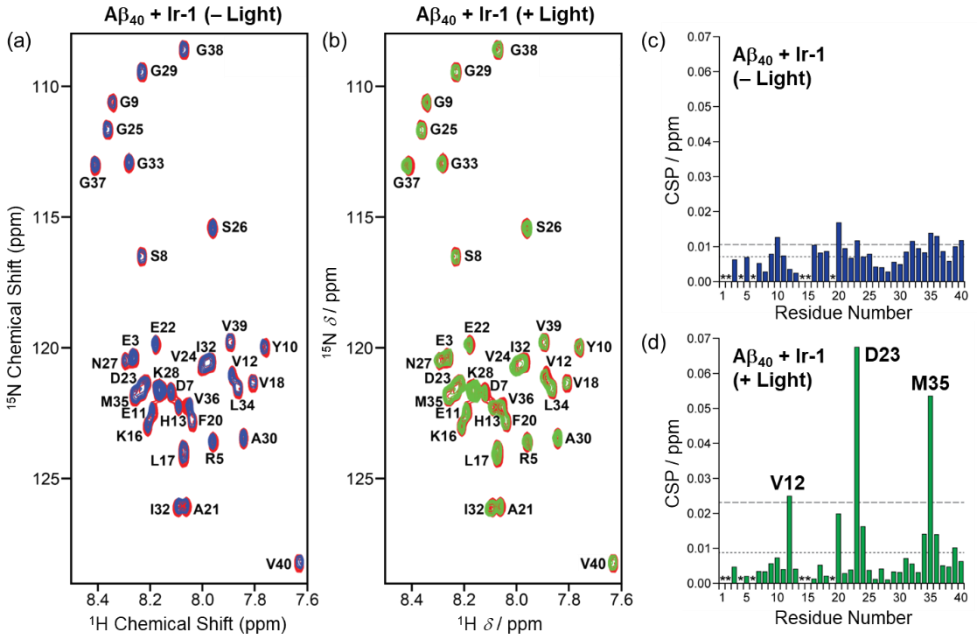

Figure 2.9. SOFAST-HMQC NMR studies of uniformly ^{15}N-labeled Aβ_{40} monomer upon treatment with **Ir-1** with and without light. (c and d) The chemical shift perturbations (CSPs) for each spectrum [in the (a) absence or (b) presence of light], relative to the spectrum of Aβ_{40} without **Ir-1**, were calculated. Conditions: [^{15}N-labeled Aβ_{40}] = 80 μM; [**Ir-1**] = 160 μM; pH 7.4; 37 °C; ambient light for 1 h (for samples treated with light); aerobic conditions. *Residues could not be resolved for analysis.

Potential oxidation sites in the other amyloidogenic peptides (i.e., α-Syn and hIAPP), when treated with **Ir-1** in the presence of light under aerobic conditions, were also investigated by means of ESI-MS^2 (Figure 2.10). When the collisional energy was applied at doubly oxidized α-Syn (Figure 2.10a and b), no oxidation was found in small N-terminal fragments; this reflects that oxidation at M1 and M5 rarely occurs. The C-terminal fragment y_{13} was detected in a nonoxidized form, but b_{119} was present in both oxidized and nonoxidized forms. One oxidation site existed between P120 and M127, and the most plausible location was M127. Since singly oxidized b_{116} and b_{119} ions were relatively abundant, M116 was also estimated to be possibly oxidized. There were oxidized fragments smaller than b_{116}, such as b_{63}, b_{65}, and b_{66}, which implied that there were oxidation sites other than M116 and

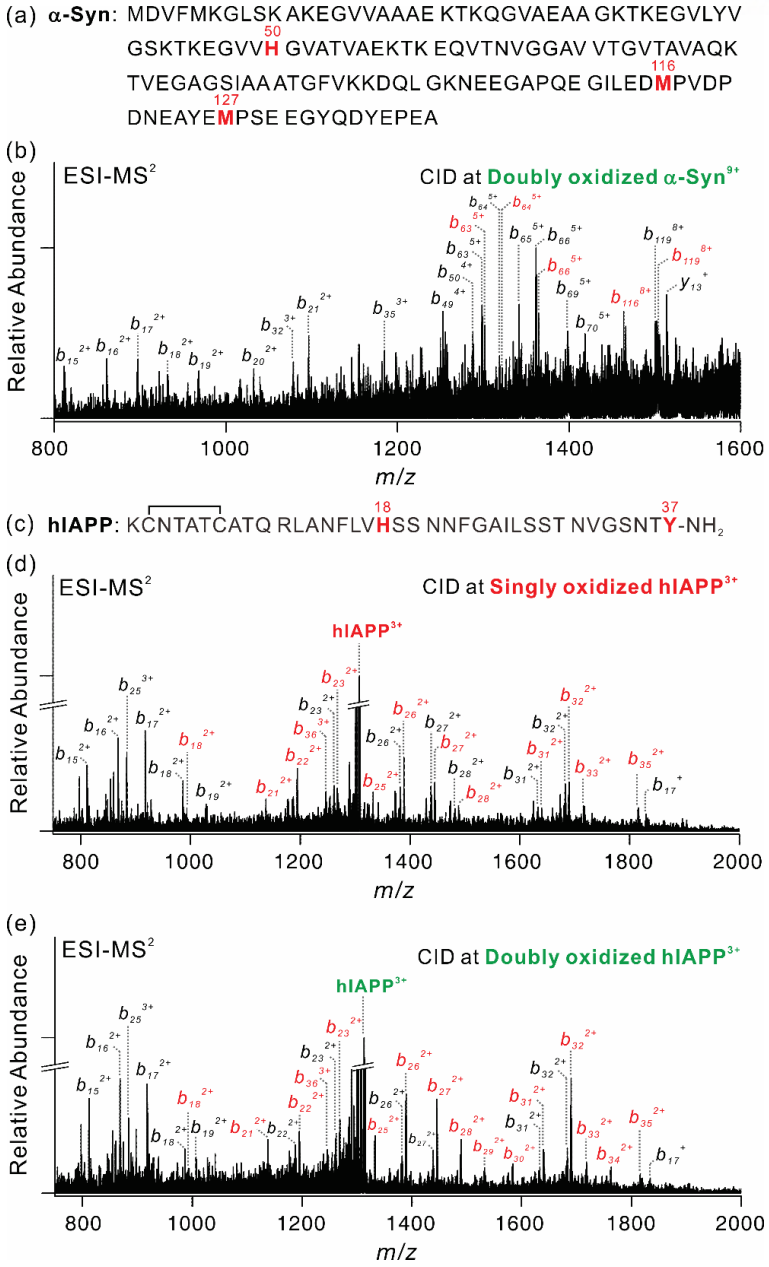

Figure 2.10. Identification of oxidation sites in α-Syn and hIAPP. Sequences of (a) α-Syn and (c) hIAPP. ESI-MS^2 spectra for (b) doubly oxidized α-Syn, and (d) singly and (e) doubly oxidized hIAPP. Nonoxidized, singly oxidized, and doubly oxidized fragments are indicated in black, red, and green, respectively.

M127. Based on our investigations for oxidation sites in Aβ_{40}, the histidine residue in α-Syn (i.e., H50) could be an oxidation site. Additionally, in the ESI-MS^2 spectra of singly and doubly oxidized hIAPP (Figure 2.10c–e), peptide oxidation was observed in fragments larger than b_{18}; this was indicative of H18 as a potential oxidation site. Fragments between b_{18} and b_{32}, however, appeared in both oxidized and nonoxidized forms, which suggested that there was another oxidation site apart from H18. In the spectrum of doubly oxidized hIAPP (Figure 2.10e), no doubly oxidized ion was displayed other than the whole peptide itself, which possibly revealed that Y37 might be the second oxidation site.

Previous studies proposed that methionine, histidine, and tyrosine residues in amyloidogenic peptides were susceptible to oxidative modification, which could affect their aggregation behavior.[17,20,22,60] Particularly, oxidative modifications of methionine residues have been reported to inhibit β-strand formation of amyloidogenic peptides.[20,22,60] Incorporation of oxygen atoms into methionine residues could provide partial negative charges and further enhance the polarity of peptides.[15,20,60] In the case of Aβ, the increased polarity of oxidized M35 could reduce hydrophobic contacts in the C-terminal region and destabilize a β-strand structure in which M35 proximately interacts with the aromatic ring of F19.[20,60] Along with a change in polarity, greater structural disorder and reduced helicity were also found in methionine-oxidized α-Syn.[15,61] Specifically, oxidation at M116 and M127 presumably disrupts α-Syn aggregation because these residues are suggested to mediate long-range interactions with the central hydrophobic regions.[62] Other important oxidation sites are histidine residues. Due to its structural features, such as an imidazole ring and two protonation states, histidine has versatile roles in multiple interactions (e.g., cationic–π interactions, π–π stacking, hydrogen–π interactions, coordination, and hydrogen bonding).[63] Depending on pH, histidine can present different protonation states that have effects on the molecular behavior of amyloidogenic peptides, including aggregation, through alteration of the strength of interactions.[63,64] In addition, histidine is known as a metal binding site in amyloidogenic peptides.[65–69] Binding of metal ions [e.g., Cu(II), Zn(II)] to peptides is shown to accelerate amyloidogenic peptide aggregation or induce the formation and stabilization of toxic oligomeric aggregates.[2,66,67,70] Upon the formation of 2-oxo-histidine, metal binding affinities were reported to be substantially decreased; thus, oxidative modifications of histidine residues might destabilize complexes of amyloidogenic peptides with metal ions.[69,71] Collectively, methionine, histidine, and/or tyrosine residues, the potential oxidation sites of Aβ, α-Syn, or hIAPP, which were suggested to be essential for the properties and aggregation of these amyloidogenic peptides, were indicated by our MS and NMR studies. Oxidative modifications are present at a few specific residues in amyloidogenic peptides, which might be able to modulate their aggregation pathways potentially through altering intra- or intermolecular interactions critical for β-strand formation (see below).

2.2.4. Aggregation Behavior Influenced upon Oxidation of Amyloidogenic Peptides by Light-Activated Ir-1

2.2.4.1. Change in the Size Distribution

To investigate whether peptide oxidation could transmute the aggregation of amyloidogenic peptides, two inhibition (Figures 2.11a and 2.12a) and disaggregation (Figure 2.13a) experiments[8–11] were carried out mainly with Aβ (two major isoforms, $A\beta_{40}$ and $A\beta_{42}$). Size distributions of the resultant $A\beta_{40}$ and

$A\beta_{42}$ species treated with **Ir-1** were evaluated by gel electrophoresis with Western blotting (gel/Western blot) by using an anti-Aβ antibody (6E10).

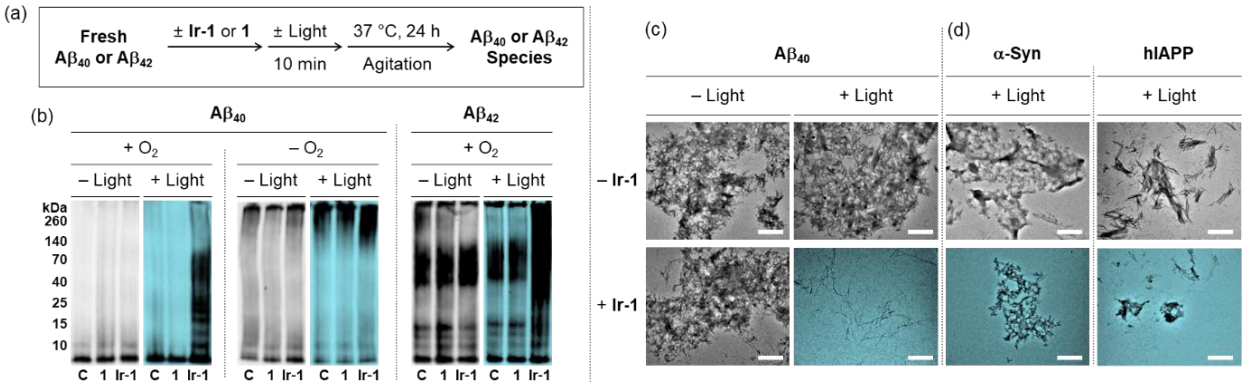

Figure 2.11. Effects of **Ir-1** and **1** on peptide aggregation pathways. (a) Scheme of the inhibition experiments. (b) Analyses of the resultant $A\beta_{40}$ and $A\beta_{42}$ species generated from various conditions [aerobic (left) and anaerobic (right) conditions] by gel/Western blot with an anti-Aβ antibody (6E10). Lanes: (C) $A\beta_{40}$ or $A\beta_{42}$; (1) $A\beta_{40}$ or $A\beta_{42}$ + **1**; (Ir-1) $A\beta_{40}$ or $A\beta_{42}$ + **Ir-1**. (c and d) TEM images of the samples from (b) and the light-treated samples containing α-Syn or hIAPP with and without **Ir-1** (scale bar = 1 μm). Conditions: [peptide] = 25 μM; [**Ir-1** or **1**] = 50 μM; pH 7.4; 37 °C; 24 h; constant agitation; 1 sun light for 10 min (for samples treated with light).

In the inhibition studies (Figure 2.11a), when fresh $A\beta_{40}$ was incubated with **Ir-1** in the presence of light under aerobic conditions, various molecular weights (MWs) of peptide species were visualized in the gel/Western blot (Figure 2.11b, left). Distinct from the result with light exposure, **Ir-1** could not generate diverse sizes of Aβ aggregates without light. In addition, when the ligands, **1** and 2-phenylquinoline (Figure 2.1b), were not coordinated to the Ir(III) center, they had no noticeable effect on Aβ aggregation, even with light under aerobic conditions (Figures 2.11b and 2.12). When **Ir-1** was incubated with fresh $A\beta_{42}$, similar reactivity trends were presented to those with $A\beta_{40}$ (Figure 2.11b, right). Diverse MW distributions of $A\beta_{42}$ species were shown with both **Ir-1** and light. Furthermore, the inhibition experiments were conducted in the absence of O_2 to verify if Aβ aggregation could be influenced upon oxidation of peptides by oxidants generated by O_2 with light-activated **Ir-1**. Aβ aggregation pathways were not indicated to be varied under anaerobic conditions, even in the presence of light (Figure 2.11b, middle).

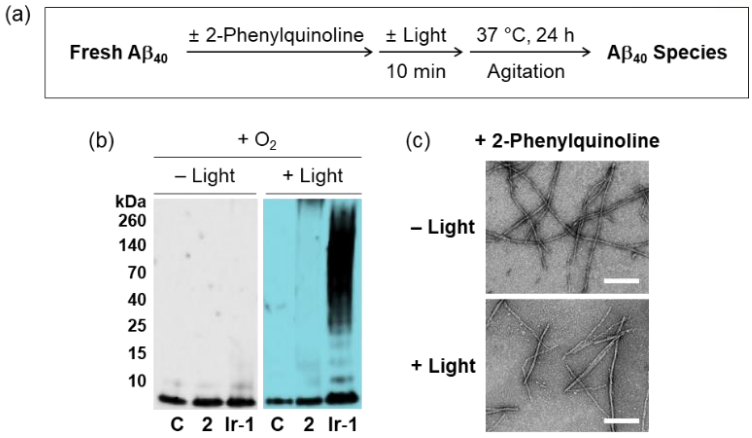

Figure 2.12. Effect of the ligand (2-phenylquinoline, Figure 2.1) on $A\beta_{40}$ aggregation. (a) Scheme of the inhibition experiment. (b) Analysis of the resultant $A\beta_{40}$ species visualized by gel/Western blot with an anti-Aβ antibody (6E10). Lanes: (C) $A\beta_{40}$; (2) $A\beta_{40}$ + 2-phenylquinoline; (Ir-1) $A\beta_{40}$ + **Ir-1**. (c) TEM images of the samples from (b) (scale bar = 200 nm). Conditions: [$A\beta_{40}$] = 25 μM; [2-phenylquinoline or **Ir-1**] = 50 μM; pH 7.4; 37 ℃; 24 h; constant agitation; 1 sun light for 10 min (for the samples treated with light).

Moreover, in order to disassemble preformed $A\beta_{40}$ aggregates or redirect their further aggregation upon oxidation with **Ir-1** in the presence of light and O_2, the disaggregation experiment was carried out (Figure 2.13). Similar to the inhibition studies, preformed $A\beta_{40}$ aggregates were observed with a wide range of sizes only after treatment with **Ir-1** upon light exposure in the presence of O_2. Overall, our gel/Western blot results from both inhibition and disaggregation experiments suggest that 1) **Ir-1** is able to transmute Aβ aggregation pathways only with light activation under aerobic conditions; and 2) the overall structure of **Ir-1** over individual structural components (e.g., ligand **1**) is essential to alter Aβ aggregation in the presence of both light and O_2. Combining the results with the control of light and O_2, it is demonstrated that Aβ oxidation, triggered by photoactivated **Ir-1** with O_2, could direct the modulation of peptide aggregation pathways.

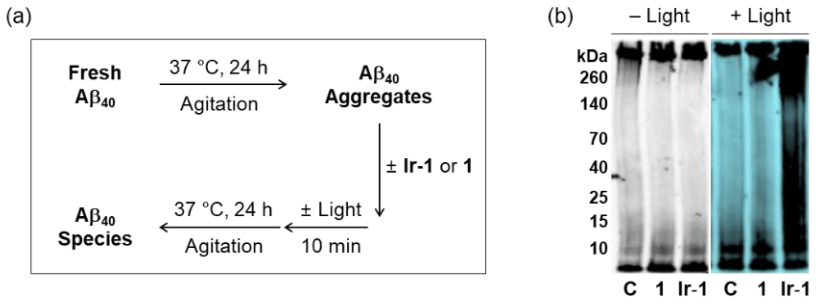

Figure 2.13. Effects of **Ir-1** and **1** on the disassembly of preformed $A\beta_{40}$ aggregates. (a) Scheme of the disaggregation experiment. (b) Analysis of the resultant $A\beta_{40}$ species was visualized by gel/Western blot with an anti-Aβ antibody (6E10). Conditions: [$A\beta_{40}$] = 25 μM; [**Ir-1** or **1**] = 50 μM; pH 7.4; 37 ℃; 24 h; constant agitation; 1 sun light for 10 min (for the samples treated with light); aerobic conditions. Lanes: (C) $A\beta_{40}$; (1) $A\beta_{40}$ + **1**; (Ir-1) $A\beta_{40}$ + **Ir-1**.

2.2.4.2. Morphological Changes of Amyloidogenic Peptides

The degree of regulating the aggregation pathways of amyloidogenic peptides was also monitored through morphological changes visualized by transmission electron microscopy (TEM) (Figure 2.11c and d). From the TEM analyses, the resultant peptides upon treatment with both **Ir-1** and light under aerobic conditions were observed to be smaller, while either structured fibrils or large aggregates were indicated without light. In the case of $A\beta_{40}$, the treatment of the peptide with **Ir-1** induced the formation of short and thin fibrils in the presence of both light and O_2 (Figure 2.11c). Additionally, the morphologies of α-Syn and hIAPP were also transformed to smaller amorphous aggregates when **Ir-1** was added with exposure of both light and O_2, instead of large aggregates or fibrils produced in the absence of **Ir-1** (Figure 2.11d). Therefore, along with the gel/Western blot data, our TEM studies imply that the aggregation of amyloidogenic peptides could be transfigured upon treatment with light-activated **Ir-1** under aerobic conditions.

2.3. Conclusions

Several strategies for understanding and suppressing the aggregation of amyloidogenic peptides, found in amyloid-related disorders and suggested to be linked to their pathogenesis, have been developed. One of the tactics would be related to oxidative modifications of the amino acid residues essential for properties and aggregation behaviors of peptides. For the oxidation of amyloidogenic peptides, an inorganic complex, **Ir-1**, was rationally designed to be a chemical tool that has a relatively stable framework and is capable of generating oxidants (e.g., $^1O_2$) from readily accessible O_2 simply upon photoactivation employing low-energy radiation.

On the basis of our biochemical and biophysical analyses, **Ir-1** is shown to significantly induce oxidative modifications of amyloidogenic peptides, such as Aβ, α-Syn, and hIAPP, followed by alteration of their aggregation pathways. Peptide oxidation by photoactivated **Ir-1** is more noticeable for amyloidogenic peptides over well-structured nonamyloidogenic peptides. By MS and NMR, the oxidation sites are indicated to be potentially located at methionine, histidine, and/or tyrosine residues in these amyloidogenic peptides. Through minor alterations at a few specific residues in peptides by photoactivated **Ir-1** under mild conditions, their aggregation pathways can be modulated. Overall, our rational design and fundamental investigations of **Ir-1** demonstrate the promise of an inorganic complex in being developed as a chemical tool for oxidative modifications of amyloidogenic peptides with the subsequent control of their aggregation. Such a tool will assist in advancing our fundamental understanding towards amyloidogenic peptides, as well as providing insight into developing effective approaches for amyloid management.

2.4. Experimental Section

2.4.1. Materials and Methods

All reagents were purchased from commercial suppliers and used as received, unless otherwise noted. Compound **1** (**1** = methyl 4-(dimethylamino)picolinate)[72] and the cyclometalated chloridebridged Ir(III) dimer ($[Ir(C^N)_2(\mu\text{-}Cl)_2]$)[73] were prepared by following previously reported procedures. The prepared **Ir-1** was characterized by NMR, FTIR, HRMS, and elemental analyzer on an Agilent 400-MR DD2 NMR spectrometer, Varian Cary 620/670 FTIR spectrometer (UNIST Central Research Facilities, Ulsan, Republic of Korea), Bruker maXisTM HD Ultra-high resolution Q-TOF LC MS/MS system (HRMS; The Cooperative Laboratory Center of Pukyong National University, Busan, Republic of Korea), and Thermo Flash 2000 (UNIST Central Research Facilities, Ulsan, Republic of Korea), respectively. $A\beta_{40}$ and $A\beta_{42}$ were purchased from Anygen ($A\beta_{40}$ = DAEFRHDSGYEVHHQKLVFFAEDVGSNKGAIIG-LMVGGVV, $A\beta_{42}$ = DAEFRHDSGYEVHHQKLVFFAEDVGSNKGAIIGLMVGGVVIA; Nammyun, Jangseong-gun, Republic of Korea). α-Syn and hIAPP were obtained from Anaspec and Peptron, respectively [α-Syn = MDVFMKGLSKAKEGVVAAAEKTKQGVAEAAGKTKEGVLYVGSKTKE-GVVHGVATVAEKTKEQVTNVGGAVVTGVTAVAQKTVEGAGSIAAATGFVKKDQLGKNEEGA PQEGILEDMPVDPDNEAYEMPSEEGYQDYEPEA (Fremont, CA, USA); hIAPP = KCNTATCATQRLANFLVHSSNNFGAILSSTNVGSNKCNTATCATQRLANFLVHSSNNFGAILSS TNVGSNTY-NH_2 (Daejeon, Republic of Korea)]. Ubiquitin was purchased from Sigma Aldrich (ubiquitin = MQIFVKTLTGKTITLEVEPSDTIENVKAKIQDKEGIPPDQQRLIFAGKQLEDGRTLS-DYNIQKESTLHLVLRLRGG; St. Louis, MO, USA). Double-distilled H_2O (ddH_2O) was obtained from a Milli-Q Direct 16 system (Merck KGaA, Darmstadt, Germany). Irradiation with 1 sun was obtained with a Newport IQE-200 solar simulator (Irvine, CA, USA). ESI-MS and IM-MS analyses were performed by using a Waters Synapt G2-Si quadrupole time-of-flight ion mobility mass spectrometer equipped with an ESI source (DGIST Center for Core Research Facilities, Daegu, Republic of Korea). NMR studies of Aβ with **Ir-1** were conducted on a Bruker Avance 600 MHz spectrometer equipped with a TCI triple-resonance inverse detection cryoprobe. The data was processed by using TOPSPIN 2.1 (Bruker) software and assignments were made by using SPARKY 3.1134 software. Anaerobic reactions were performed in a N_2-filled glove box (Korea Kiyon, Bucheon-si, Gyeonggi-do, Republic of Korea). TEM images were taken by using a JEOL JEM-1400 transmission electron microscope (UNIST Central Research Facilities, Ulsan, Republic of Korea). Photophysical properties were measured by using an Agilent Cary 100 UV/Vis spectrophotometer and a Varian Cary Eclipse fluorescence spectrophotometer (UNIST Central Research Facilities, Ulsan, Republic of Korea). Timecorrelated single-photon counting (TCSPC) was performed for lifetime measurements with a Ti:sapphire laser Mira900 (Coherent, Santa Clara, CA, USA), monochromator Acton series SP-2150i (Princeton Instruments, Acton, MA, USA), and TCSPC module PicoHarp 300 (PicoQuant, Berlin,

Germany) together with MCP-PMT R3809U-59 (Hamamatsu, Shizuika-ken, Japan) and fitted by PicoQuant FluoFit software (UNIST Central Research Facilities, Ulsan, Republic of Korea).

2.4.2. Synthesis of Ir-1

2-Phenylquinoline (680 mg, 3.3 mmol) was added to a solution of $IrCl_3 \cdot nH_2O$ (500 mg, 1.7 mmol) in a mixture of 2-methoxyethanol and H_2O (3:1). The solution was heated at reflux under N_2 (g) for 24 h. After cooling to room temperature, brown precipitates were obtained by treatment with additional H_2O. The crude product (cyclometalated chloride-bridged Ir(III) dimer, $[Ir(C\hat{}N)_2(\mu\text{-}Cl)_2]$) was washed with hexanes and cold diethyl ether several times, dried, and used without further purification.[73]

A mixture of the cyclometalated chloride-bridged Ir(III) dimer (353 mg, 0.28 mmol), **1** (150 mg, 0.83 mmol), and Na_2CO_3 (294 mg, 2.8 mmol) was dissolved in 2-ethoxyethanol. The mixture was heated at reflux under N_2 (g) for 12 h. After cooling to room temperature, the solution was concentrated, followed by the addition of H_2O. The organic phase was extracted with CH_2Cl_2 three times. The collected organic solution was dried with Na_2SO_4 and the solvent was removed under reduced pressure. The crude materials were purified by column chromatography (SiO_2, 50:1 CH_2Cl_2/CH_3OH, R_f = 0.6) to give the product as a red powder (340 mg, 80%). FTIR (neat): ν = 3057, 2021, 1608, 1516, 1437, 1381, 1338, 1163, 1028, 762 cm^{-1}; UV/Vis (H_2O): λ_{max} (ε) = 463 nm (5.78 (± 0.12) × 10^3 M^{-1} cm^{-1}). ^1H NMR (400 MHz, $CDCl_3$): δ = 8.79 (d, J = 8.0 Hz, 1H), 8.13 (t, J = 8.0 Hz, 1H), 8.07 (m, 3H), 7.92 (dd, J = 8.0 Hz, 1H), 7.80 (dd, J = 8.0 Hz, 1H), 7.70 (dd, J = 8.0 Hz, 1H), 7.67 (dd, J = 8.0 Hz, 1H), 7.51 (m, 2H), 7.42 (d, J = 8.0 Hz, 1H), 7.39 (ddd, 1H) 7.26 (ddd, 1H), 7.03 (m, 2H), 6.95 (m, 2H), 6.89 (dd, J = 8.0 Hz, 1H), 6.72 (m, 1H), 6.60 (dt, J = 6.8 Hz, 1H), 6.30 (m, 2H), 2.87 ppm (s, 6H); ^{13}C NMR (100 MHz, $CDCl_3$): δ = 173.0, 171.1, 169.2, 154.4, 151.8, 151.4, 148.7, 147.8, 147.0, 145.9, 145.1, 138.1, 136.3, 134.8, 129.4, 128.5, 126.0, 125.2, 121.5, 120.5, 116.1, 109.7, 108.8, 39.1 ppm; HRMS: *m/z* calcd for $C_{38}H_{29}IrN_4NaO_2$ $[M + Na]^+$: 789.1812; found: 789.1814; elemental analysis calcd (%) for $C_{38}H_{29}IrN_4O_2 \cdot 0.5CH_3OH$: C 59.14, H 4.00, N 7.17; found: C 59.00, H 4.01, N 7.19.

2.4.3. Photophysical Properties of Ir-1

Absorption and emission spectra were measured by UV-Vis and fluorescence spectrophotometers using a solution of **Ir-1** (20 μM in 20 mM HEPES, pH 7.4, 150 mM NaCl; final 1% v/v DMSO) at 298 K. Moreover, the quantum yield for phosphorescence (Φ_p) was calculated using [Ir(2-phenylquinoline)$_2$(2,2'-bipyridine)](PF_6) (Φ_{ref} = 0.31; 20 μM in 2-MeTHF solution) as a reference based on previously reported procedures.[74] The quantum yield of singlet oxygen ($^1O_2$) (Φ_s) was determined according to the method reported previously.[75] Solutions containing **Ir-1** (10 μM) and $^1O_2$ substrate [9,10-anthracenediyl-bi(methylene)dimalonic acid (ABDA, 100 μM)] were irradiated with 40% of 1 sun light. The absorbance of ABDA was obtained every 1 min up to 5 min. $[Ru(bpy)_3]^{2+}$ was

employed as a reference material ($\Phi_s = 0.18$).[76] Φ_s values were determined according to the following equation:

$$\Phi_{s(x)} = \Phi_{s(std)} \times \left(\frac{S_x}{S_{std}}\right) \times \left(\frac{F_{std}}{F_x}\right)$$

For measurement of the lifetime, time-correlated single photon counting (TCSPC) was performed. The second harmonic (SHG = 420 nm) of a tunable Ti:sapphire laser with ca. 150 fs pulse width and 76 MHz repetition rate was used as an excitation source. The emission was spectrally resolved by using some collection optics and a monochromator. The TCSPC module with a MCP-PMT was employed for ultrafast detection. The total instrument response function (IRF) for fluorescence decay was less than 150 ps, and the temporal time resolution was less than 10 ps. The deconvolution of the actual fluorescence decay and IRF was fitted by using the FluoFit software to deduce the time constant associated with an each exponential decay.

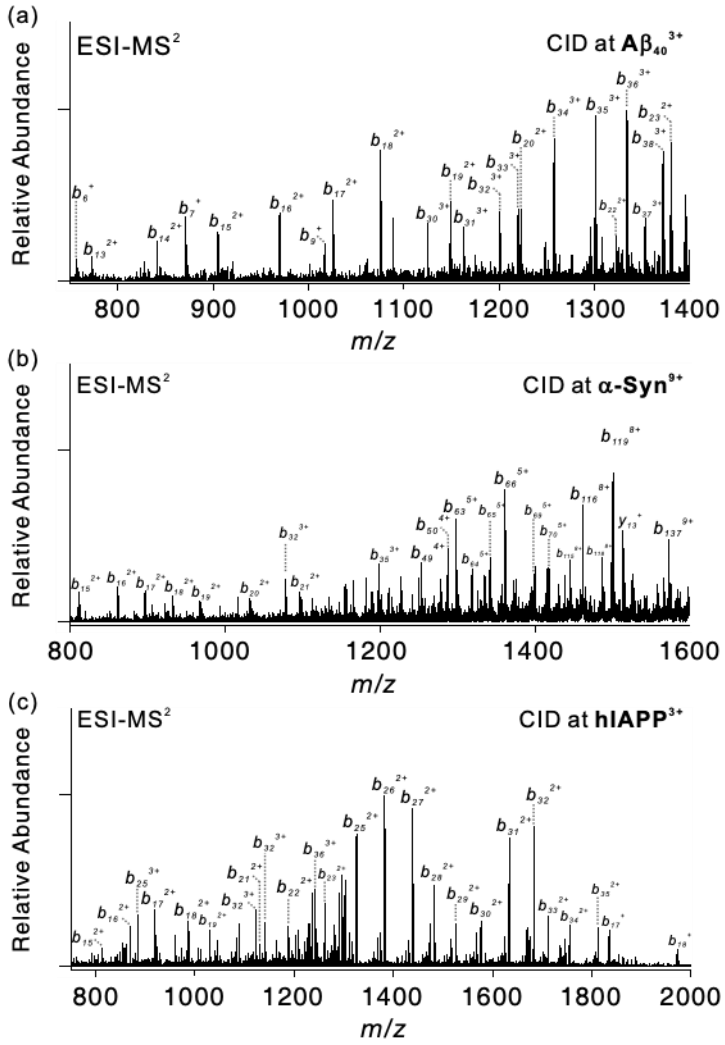

Figure 2.14. ESI-MS^2 of nonoxidized amyloidogenic peptides: (a) $A\beta_{40}$, (b) α-Syn, and (c) hIAPP.

2.4.4. Electrospray Ionization Ion Mobility Mass Spectrometry (ESI-IM-MS)

$A\beta_{40}$, α-Syn, hIAPP, and ubiquitin (100 mm) were incubated with **Ir-1** or **1** (500 μM) in 100 mM ammonium acetate (pH 7.5) at 37 °C without any agitation. Incubated peptides were diluted 10-fold and then injected into a mass spectrometer. The capillary voltage, sampling cone voltage, and source temperature were set to 2.8 kV, 70 V, and 40 °C, respectively. The backing pressure was adjusted to 3.2 mbar. Ion mobility wave height and velocity were adjusted to 10 V and 450 ms^{-1}, respectively, and gas flow for the helium cell and ion mobility cell was set to 120 and 30 $mLmin^{-1}$, respectively. Tandem MS (MS^2) analyses were additionally performed on the nonoxidized (Figure 2.14) and singly/doubly oxidized peptides. The ESI parameters and experimental conditions were same as those reported above. Collision-induced dissociation was conducted by applying the collision energy in the trap and adjusting LM resolution to 15. More than 200 spectra were obtained for each sample and averaged for analyses. To estimate collision cross-section values for obtained IM-MS data, calibration was also performed by following previously reported procedures (Figure 2.15).[77]

(a)

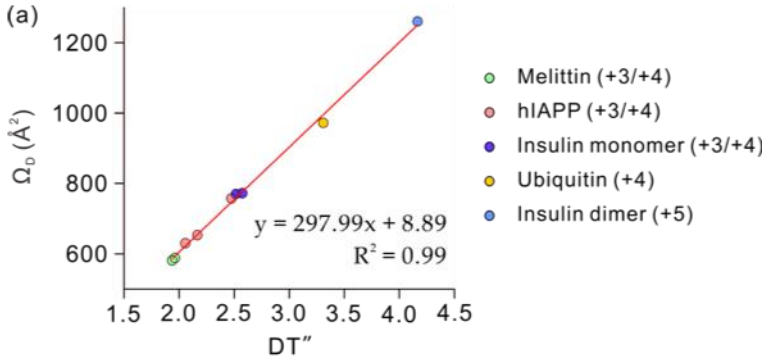

(b)

	Arrival Time (ms)	Ω_D (Å^2)
$[A\beta_{40} + 3H]^{3+}$	11.47	593.79
$[A\beta_{40} + 3H]^{3+}$	11.47	593.79
$[A\beta_{40} + O + 3H]^{3+}$	11.36	590.76
$[2A\beta_{40} + 5H]^{5+}$	10.80	950.99
	15.55	1154.52
$[2A\beta_{40} + 5H]^{5+}$	10.80	950.99
	15.66	1158.86
$[2A\beta_{40} + 4O + 5H]^{5+}$	10.58	940.61
	15.88	1167.47

Figure 2.15. Calibration for the estimation of collision cross section values (Ω_D). Calibration was performed following the previously described procedure.[77] (a) Fitting plot to present a linear correlation between published collision cross section values of calibrant proteins and corrected drift time (DT″). All IM-MS results of calibrants were obtained in the same experimental parameters with those of $A\beta_{40}$. Published collision cross section values of calibrants could be found in previous reports.[78–79] (b) Experimentally obtained cross section values for nonoxidized and oxidized $A\beta_{40}$. The IM-MS spectra for +5-charged dimers and +3-charged monomers are shown in Figures 2.4 and 2.6, respectively.

2.4.5. Mass Spectrometric Analyses

Oxidized $A\beta_{40}$, α-Syn, hIAPP, and ubiquitin were observed upon incubation with **Ir-1** under aerobic conditions in the presence of light by using a Waters Synapt G2-Si Q-ToF mass spectrometer equipped with an ESI source. Only major charge states of all peptides (+3 for $A\beta_{40}$ and hIAPP, +9 for α-Syn, and +5 for ubiquitin) were selected and shown in all mass spectra. Generally, exact mass should be calculated based on monoisotopic mass; however, in the present study, the oxidized peaks were assigned based on *m/z* values of the most abundant peaks because monoisotopic mass values of α-Syn could not be well resolved without a high-resolution mass spectrometer. For example, +3-charged $A\beta_{40}$ was most dominantly found in ESI-MS (Figure 2.2a). Upon treatment of **Ir-1** and light, the singly oxidized $A\beta_{40}$ ions were abundantly observed at 1449.6 *m/z*, corresponding to a 16 Da increase in mass from the nonoxidized $A\beta_{40}$ peak at 1444.2 *m/z* (Figure 2.2a, bottom; blue). In the case of +9-charged α-Syn at 1607.8 *m/z*, the singly oxidized peak was not well defined due to overlap with sodiated ions at 1610.2 *m/z*. With the treatment of **Ir-1** and light, doubly oxidized α-Syn was found at 1611.3 *m/z*, which indicated an approximate 32 Da increase in mass (Figure 2.2b, bottom; blue). The +3-charged hIAPP presented an oxidized peak at 1306.9 m/z, indicating a 14 Da difference in mass from nonoxidized ions with 1302.2 *m/z* upon treatment with **Ir-1** and light (Figure 2.2c, bottom; blue). Different from $A\beta_{40}$ and α-Syn, singly oxidized hIAPP indicated a 14 Da increase in mass. In the ESI-MS spectra of ubiquitin, the +5 charge state was most abundantly detected (Figure 2.7). Singly and doubly oxidized ubiquitin were found at 1717.2 and 1720.3 *m/z*, respectively, which were approximately 16 and 32 Da increases in mass from nonoxidized ubiquitin centered at 1713.9 *m/z* (Figure 2.7, bottom; blue).

2.4.6. Peptide Aggregation Experiments

Peptide aggregation experiments were conducted as previously published.[80] Amyloid-β (Aβ) or α-synuclein (α-Syn) was dissolved with ammonium hydroxide (NH_4OH, 1% v/v, aq), aliquoted, lyophilized, and stored at -80 °C. A stock solution (ca. 200 μM) was prepared by re-dissolving Aβ or α-Syn with NH_4OH (1% w/v, aq, 10 μL) followed by dilution with ddH_2O. In the case of hIAPP, the peptide was dissolved in 1,1,1,3,3,3-hexafluoro-2-propanol (HFIP, purchased from Tokyo Chemical Industries Inc., Ltd., Tokyo, Japan) at a concentration of 100 μM to remove preformed aggregates. After the treatment with HFIP for 2 h at the room temperature, hIAPP aliquots were prepared by evaporating the solvent. The peptide concentration in solution was determined by measuring the absorbance of the solution at 280 nm (ε = 1450 $M^{-1}cm^{-1}$ for $A\beta_{40}$; ε = 1490 $M^{-1}cm^{-1}$ for $A\beta_{42}$; ε = 5400 $M^{-1}cm^{-1}$ for α-Syn; ε = 1280 $M^{-1}cm^{-1}$ for hIAPP).

For inhibition experiments, the peptide (25 μM; 20 mM HEPES (4-(2-hydroxyethyl)-1-piperazineethanesulfonic acid), pH 7.4, 150 mM NaCl) was first treated with **Ir-1** or **1** (50 μM; 1% v/v final DMSO concentration) followed by exposure to 1 sun light for 10 min. The resulting samples were

incubated at 37 °C for 24 h with constant agitation. For disaggregation experiments, the peptide was initially incubated at 37 °C for 24 h with steady agitation. **Ir-1** or **1** was added afterward followed by an additional 24 h of incubation at 37 °C with constant agitation. For the experiments under anaerobic conditions, all samples were prepared following the same procedure described above for aerobic samples in a N_2-filled glovebox.

2.4.7. 2D NMR Spectroscopy

2D band-selective optimized flip-angle short transient heteronuclear multiple quantum coherence (SOFAST-HMQC) NMR was applied to the sample containing uniformly-^{15}N-labeled $A\beta_{40}$ and **Ir-1** at 10 °C.[81] Uniformly-^{15}N-labeled $A\beta_{40}$ (rPeptide, Bogart, GA, USA) was dissolved in 1% NH_4OH and lyophilized to ensure the absence of preformed aggregates. The peptide was re-dissolved in 3 mL of DMSO-d_6 (Cambridge Isotope, Tewksbury, MA, USA) and in buffer to a final peptide concentration of 80 μM (20 mM d_{11}-Tris, pH 7.4, 50 mM NaCl, 10% v/v D_2O). **Ir-1** was then titrated into the peptide solution from a 20 mM stock in DMSO-d_6. Following the completion of each titration (up to 2 equiv, 160 μM) the solution was exposed to ambient light within the NMR tube for 1 h and another spectrum was recorded. Each spectrum was obtained using 320 complex t_1 points and a 0.1 sec recycle delay on a Bruker Avance 600 MHz spectrometer. The data were processed using TOPSPIN 2.1 (Bruker) and assignment was performed using SPARKY 3.1134 using published assignments as a guide.[82–84] Chemical shift perturbation (CSP) was calculated using the following equation:

$$\Delta\delta_{NH} = \sqrt{\Delta\delta_H^2 + (\frac{\Delta\delta_N}{5})^2}$$

2.4.8. Gel Electrophoresis with Western Blotting (Gel/Western Blot)

The resultant Aβ species from both inhibition and disaggregation experiments were analyzed by gel electrophoresis followed by Western blotting (gel/Western blot) using an anti-Aβ antibody (6E10).[80] Each sample (10 μL; [$A\beta_{40}$ or $A\beta_{42}$] = 25 μM) was separated using a 10-20% gradient Tris-tricine gel (Invitrogen, Grand Island, NY, USA). The gel was transferred to a nitrocellulose membrane and blocked with a bovine serum albumin (BSA) solution (3% w/v; Sigma, St. Louis, MO, USA) in Tris-buffered saline (TBS; Fisher, Pittsburgh, PA, USA) containing 0.1% Tween-20 (TBS-T; Sigma-Aldrich) for 3 h at room temperature. The membrane was treated with the Aβ monoclonal antibody (6E10; Covance, Princeton, NJ, USA; 1:2,000; BSA, 2% w/v, in TBS-T) for overnight at 4 °C and then incubated with a horseradish peroxidase-conjugated goat anti-mouse secondary antibody (1:5,000; Cayman Chemical, Ann Arbor, MI, USA) in 2% BSA in TBS-T solution for 1 h at room temperature. Aβ species were visualized using the self-made ECL solution (2.5 mM luminol, 0.20 mM *p*-coumaric acid, and 0.018% H_2O_2 in 100 mM Tris, pH 8.6).

2.4.9. Transmission Electron Microscopy (TEM)

Peptide samples for TEM were prepared following the previously reported methods.[80] Glow discharged grids (Formvar/Carbon 300-mesh; Electron Microscopy Sciences, Hatfield, PA, USA) were treated with the resultant peptide (5 μL) for 2 min at room temperature. Excess sample was removed with filter paper, and the grids were washed with ddH_2O three times. Each grid was stained with uranyl acetate (1% w/v ddH_2O; 5 μL) for 1 min. Uranyl acetate was blotted off, and grids were dried for 20 min at room temperature. Images of samples were taken by a JEOL JEM-1400 transmission electron microscope (120 kV, 25,000× magnification).

2.5. Acknowledgments

This work was supported by the 2016 UNIST research fund (1.160001.01) (to M.H.L., T.-H.K. & H.-W.R.); the National Research Foundation of Korea (NRF) Grant funded by the Korean Government [NRF-2014S1A2A2028270 (to M.H.L and A.R.); NRF-2014R1A2A2A01004877 and NRF-2016R1A5A1009405 (to M.H.L.)]; the University of Michigan Protein Folding Disease Initiative (to M.H.L. and A.R.); the National Institutes of Health (NIH) (to A.R.); the Ministry of Science, ICT and Future Planning (KCRC 2014M1A8A1049320) (to J.C.). J.K. thanks the support from the Global Ph.D. fellowship program through the National Research Foundation of Korea (NRF) funded by the Ministry of Education (NRF-2015HIA2A1030823).

2.6. References

(1) Lambert, M. P.; Barlow, A. K.; Chromy, B. A.; Edwards, C.; Freed, R.; Liosatos, M.; Morgan, T. E.; Rozovsky, I.; Trommer, B.; Viola, K. L.; Wals, P.; Zhang, C.; Finch, C. E.; Krafft, G. A.; Klein, W. L. *Proc. Natl. Acad. Sci. USA* **1998**, *95*, 6448-6453.

(2) Savelieff, M. G.; DeToma, A. S.; Derrick, J. S.; Lim, M. H. *Acc. Chem. Res.* **2014**, *47*, 2475-2482.

(3) Baba, M.; Nakajo, S.; Tu, P.-H.; Tomita, T.; Nakaya, K.; Lee, V. M.-Y.; Trojanowski, J. Q.; Iwatsubo, T. *Am. J. Pathol.* **1998**, *152*, 879-884.

(4) Cooper, G. J. S.; Leighton, B.; Dimitriadis, G. D.; Parry-Billings, M.; Kowalchuk, J. M.; Howland, K.; Rothbard, J. B.; Willis, A. C.; Reid, K. B. *Proc. Natl. Acad. Sci. USA* **1988**, *85*, 7763-7766.

(5) Chiti, F.; Dobson, C. M. *Annu. Rev. Biochem.* **2006**, *75*, 333-366.

(6) Hartley, D. M.; Walsh, D. M.; Ye, C. P.; Diehl, T.; Vasquez, S.; Vassilev, P. M.; Teplow, D. B.; Selkoe, D. J. *J. Neurosci.* **1999**, *19*, 8876-8884.

(7) Cohen, S. I. A.; Arosio, P.; Presto, J.; Kurudenkandy, F. R.; Biverstål, H.; Dolfe, L.; Dunning, C.; Yang, X.; Frohm, B.; Vendruscolo, M.; Johansson, J.; Dobson, C. M.; Fisahn, A.; Knowles, T. P. J.; Linse, S. *Nat. Struct. Mol. Biol.* **2015**, *22*, 207-213.

(8) Hyung, S.-J.; DeToma, A. S.; Brender, J. R.; Lee, S.; Vivekanandan, S.; Kochi, A.; Choi, J.-S.; Ramamoorthy, A.; Ruotolo, B. T.; Lim, M. H. *Proc. Natl. Acad. Sci. USA* **2013**, *110*, 3743-3748.

(9) Lee, H. J.; Kerr, R. A.; Korshavn, K. J.; Lee, J.; Kang, J.; Ramamoorthy, A.; Ruotolo, B. T.; Lim, M. H. *Inorg. Chem. Front.* **2016**, *3*, 381-392.
(10) Derrick, J. S.; Kerr, R. A.; Nam, Y.; Oh, S. B.; Lee, H. J.; Earnest, K. G.; Suh, N.; Peck, K. L.; Ozbil, M.; Korshavn, K. J.; Ramamoorthy, A.; Prabhakar, R.; Merino, E. J.; Shearer, J.; Lee, J.-Y.; Ruotolo, B. T.; Lim, M. H. *J. Am. Chem. Soc.* **2015**, *137*, 14785-14797.
(11) Beck, M. W.; Derrick, J. S.; Kerr, R. A.; Oh, S. B.; Cho, W. J.; Lee, S. J. C.; Ji, Y.; Han, J.; Tehrani, Z. A.; Suh, N.; Kim, S.; Larsen, S. D.; Kim, K. S.; Lee, J.-Y.; Ruotolo, B. T.; Lim, M. H. *Nat. Commun.* **2016**, *7*, 13115.
(12) Yellol, G. S.; Yellol, J. G.; Kenche, V. B.; Liu, X. M.; Barnham, K. J.; Donaire, A.; Janiak, C.; Ruiz, J. *Inorg. Chem.* **2015**, *54*, 470-475.
(13) Taniguchi, A.; Sasaki, D.; Shiohara, A.; Iwatsubo, T.; Tomita, T.; Sohma, Y.; Kanai, M. *Angew. Chem. Int. Ed.* **2014**, *53*, 1382-1385.
(14) Friedemann, M.; Helk, E.; Tiiman, A.; Zovo, K.; Palumaa, P.; Tõugu, V. *Biochem. Biophys. Rep.* **2015**, *3*, 94-99.
(15) Glaser, C. B.; Yamin, G.; Uversky, V. N.; Fink, A. L. *Biochim. Biophys. Acta* **2005**, *1703*, 157-169.
(16) Zhou, W.; Long, C.; Reaney, S. H.; Di Monte, D. A.; Fink, A. L.; Uversky, V. N. *Biochim. Biophys. Acta* **2010**, *1802*, 322-330.
(17) Uversky, V. N.; Yamin, G.; Souillac, P. O.; Goers, J.; Glaser, C. B.; Fink, A. L. *FEBS Lett.* **2002**, *517*, 239-244.
(18) Palmblad, M.; Westlind-Danielsson, A.; Bergquist, J. *J. Biol. Chem.* **2002**, *277*, 19506-19510.
(19) He, L.; Wang, X.; Zhu, D.; Zhao, C.; Du, W. *Metallomics* **2015**, *7*, 1562-1572.
(20) Hou, L.; Shao, H.; Zhang, Y.; Li, H.; Menon, N. K.; Neuhaus, E. B.; Brewer, J. M.; Byeon, I.-J. L.; Ray, D. G.; Vitek, M. P.; Iwashita, T.; Makula, R. A.; Przybyla, A. B.; Zagorski, M. G. *J. Am. Chem. Soc.* **2004**, *126*, 1992-2005.
(21) Hou, L.; Kang, I.; Marchant, R. E.; Zagorski, M. G. *J. Biol. Chem.* **2002**, *277*, 40173-40176.
(22) Watson, A. A.; Fairlie, D. P.; Craik, D. J. *Biochemistry* **1998**, *37*, 12700-12706.
(23) Taniguchi, A.; Shimizu, Y.; Oisaki, K.; Sohma, Y.; Kanai, M. *Nat. Chem.* **2016**, *8*, 974-982.
(24) Paik, S. R.; Shin, H.-J.; Lee, J.-H. *Arch. Biochem. Biophys.* **2000**, *378*, 269-277.
(25) Guedes, S.; Vitorino, R.; Domingues, R.; Amado, F.; Domingues, P. *Rapid Commun. Mass Spectrom.* **2009**, *23*, 2307-2315.
(26) Inoue, K.; Garner, C.; Ackermann, B. L.; Oe, T.; Blair, I. A. *Rapid Commun. Mass Spectrom.* **2006**, *20*, 911-918.
(27) Pietruszka, M.; Jankowska, E.; Kowalik-Jankowska, T.; Szewczuk, Z.; Smużyńska, M. *Inorg. Chem.* **2011**, *50*, 7489-7499.
(28) DeRosa, M. C.; Crutchley, R. J. *Coord. Chem. Rev.* **2002**, *233–234*, 351-371.
(29) Tomita, M.; Irie, M.; Ukita, T. *Biochemistry* **1969**, *8*, 5149-5160.
(30) Shen, H.-R.; Spikes, J. D.; Smith, C. J.; Kopeček, J. *J. Photochem. Photobiol. A* **2000**, *130*, 1-6.
(31) Agon, V. V.; Bubb, W. A.; Wright, A.; Hawkins, C. L.; Davies, M. J. *Free Radic. Biol. Med.* **2006**, *40*, 698-710.
(32) Huvaere, K.; Skibsted, L. H. *J. Am. Chem. Soc.* **2009**, *131*, 8049-8060.
(33) Plowman, J. E.; Deb-Choudhury, S.; Grosvenor, A. J.; Dyer, J. M. *Photochem. Photobiol. Sci.* **2013**, *12*, 1960-1967.
(34) Castaño, C.; Oliveros, E.; Thomas, A. H.; Lorente, C. *J. Photochem. Photobiol. B* **2015**, *153*, 483-489.

(35) Lee, B. I.; Lee, S.; Suh, Y. S.; Lee, J. S.; Kim, A.-k.; Kwon, O.-Y.; Yu, K.; Park, C. B. *Angew. Chem. Int. Ed.* **2015**, *54*, 11472-11476.
(36) Takizawa, S.-y.; Aboshi, R.; Murata, S. *Photochem. Photobiol. Sci.* **2011**, *10*, 895-903.
(37) Kim, K.; Fancy, D. A.; Carney, D.; Kodadek, T. *J. Am. Chem. Soc.* **1999**, *121*, 11896-11897.
(38) Fancy, D. A.; Denison, C.; Kim, K.; Xie, Y.; Holdeman, T.; Amini, F.; Kodadek, T. *Chem. Biol.* **2000**, *7*, 697-708.
(39) Amini, F.; Denison, C.; Lin, H.-J.; Kuo, L.; Kodadek, T. *Chem. Biol.* **2003**, *10*, 1115-1127.
(40) Meunier, S.; Strable, E.; Finn, M. G. *Chem. Biol.* **2004**, *11*, 319-326.
(41) Alarcon, E.; Edwards, A. M.; Aspee, A.; Borsarelli, C. D.; Lissi, E. A. *Photochem. Photobiol. Sci.* **2009**, *8*, 933-943.
(42) Drössler, P.; Holzer, W.; Penzkofer, A.; Hegemann, P. *Chem. Phys.* **2003**, *286*, 409-420.
(43) Niu, E.; Ghiggino, K. P.; Mau, A. W.-H.; Sasse, W. H. F. *J. Lumin.* **1988**, *40–41*, 563-564.
(44) Ferreira, J. A.; Barral, R.; Baptista, J. D.; Ferreira, M. I. C. *J. Lumin.* **1991**, *48–49*, 385-390.
(45) Temenoff, J. S.; Shin, H.; Engel, P. S.; Mikos, A. G. in *Proceedings of the Second Joint EMBS/BMES Conference*, **2002**, 687-688.
(46) Yoshimura, M.; Ono, M.; Watanabe, H.; Kimura, H.; Saji, H. *Sci. Rep.* **2014**, *4*, 6155.
(47) Lee, C.-W.; Kung, M.-P.; Hou, C.; Kung, H. F. *Nucl. Med. Biol.* **2003**, *30*, 573-580.
(48) Liu, Z.; Sadler, P. J. *Acc. Chem. Res.* **2014**, *47*, 1174-1185.
(49) You, Y. *Curr. Opin. Chem. Biol.* **2013**, *17*, 699-707.
(50) Lowry, M. S.; Bernhard, S. *Chem. Eur. J.* **2006**, *12*, 7970-7977.
(51) Zhong, H.-J.; Lu, L.; Leung, K.-H.; Wong, C. C. L.; Peng, C.; Yan, S.-C.; Ma, D.-L.; Cai, Z.; Wang, H.-M. D.; Leung, C.-H. *Chem. Sci.* **2015**, *6*, 5400-5408.
(52) Kang, T.-S.; Mao, Z.; Ng, C.-T.; Wang, M.; Wang, W.; Wang, C.; Lee, S. M.-Y.; Wang, Y.; Leung, C.-H.; Ma, D.-L. *J. Med. Chem.* **2016**, *59*, 4026-4031.
(53) Onishi, N.; Xu, S.; Manaka, Y.; Suna, Y.; Wang, W.-H.; Muckerman, J. T.; Fujita, E.; Himeda, Y. *Inorg. Chem.* **2015**, *54*, 5114-5123.
(54) Shin, I.-S.; Kim, J. I.; Kwon, T.-H.; Hong, J.-I.; Lee, J.-K.; Kim, H. *J. Phys. Chem. C* **2007**, *111*, 2280-2286.
(55) Schey, K. L.; Finley, E. L. *Acc. Chem. Res.* **2000**, *33*, 299-306.
(56) Lanucara, F.; Holman, S. W.; Gray, C. J.; Eyers, C. E. *Nat. Chem.* **2014**, *6*, 281-294.
(57) Vijay-Kumar, S.; Bugg, C. E.; Cook, W. J. *J. Mol. Biol.* **1987**, *194*, 531-544.
(58) Wysocki, V. H.; Resing, K. A.; Zhang Q.; Cheng, G. *Methods* **2005**, *35*, 211-222.
(59) Schöneich, C.; Williams, T. D. *Chem. Res. Toxicol.* **2002**, *15*, 717-722.
(60) Brown, A. M.; Lemkul, J. A.; Schaum, N.; Bevan, D. R. *Arch. Biochem. Biophys.* **2014**, *545*, 44-52.
(61) Binolfi, A.; Limatola, A.; Verzini, S.; Kosten, J.; Theillet, F.-X.; Rose, H. M.; Bekei, B.; Stuiver, M.; van Rossum, M.; Selenko, P. *Nat. Commum.* **2016**, *7*, 10251.
(62) Bertoncini, C. W.; Jung, Y.-S.; Fernandez, C. O.; Hoyer, W.; Griesinger, C.; Jovin, T. M.; Zweckstetter, M. *Proc. Natl. Acad. Sci. USA* **2005**, *102*, 1430-1435.
(63) Liao, S.-M.; Du, Q.-S.; Meng, J.-Z.; Pang, Z.-W.; Huang, R.-B. *Chem. Cent. J.* **2013**, *7*, 44-55.
(64) Garai, K.; Frieden, C. *Proc. Natl. Acad. Sci. USA* **2013**, *110*, 3321-3326.
(65) Faller, P.; Hureau, C. *Dalton Trans.* **2009**, *7*, 1080-1094.
(66) Rasia, R. M.; Bertoncini, C. W.; Marsh, D.; Hoyer, W.; Cherny, D.; Zweckstetter, M.; Griesinger, C.; Jovin, T. M.; Fernández, C. O. *Proc. Natl. Acad. Sci. USA* **2005**, *102*, 4294-4299.

(67) Valiente-Gabioud, A. A.; Torres-Monserrat, V.; Molina-Rubino, L.; Binolfi, A.; Griesinger, C.; Fernández, C. O. *J. Inorg. Biochem.* **2012**, *117*, 334-341.
(68) Brender, J. R.; Hartman, K.; Nanga, R. P. R.; Popovych, N.; de la Salud Bea, R.; Vivekanandan, S.; Marsh, E. N. G.; Ramamoorthy, A. *J. Am. Chem. Soc.* **2010**, *132*, 8973-8983.
(69) Cheignon, C.; Faller, P.; Testemale, D.; Hureau, C.; Collin, F. *Metallomics* **2016**, *8*, 1081-1089.
(70) Yu, Y.-P.; Lei, P.; Hu, J.; Wu, W.-H.; Zhao, Y.-F.; Li, Y.-M. *Chem. Commun.* **2010**, *46*, 6909-6911.
(71) Traore, D. A. K.; Ghazouani, A. E.; Jacquamet, L.; Borel, F.; Ferrer, J.-L.; Lascoux, D.; Ravanat, J.-L.; Jaquinod, M.; Blondin, G.; Caux-Thang, C.; Duarte, V.; Latour, J.-M. *Nat. Chem. Biol.* **2009**, *5*, 53-59.
(72) Bolink, H. J.; Coronado, E.; Santamaria, S. G.; Sessolo, M.; Evans, N.; Klein, C.; Baranoff, E.; Kalyanasundaram, K.; Graetzel, M.; Nazeeruddin, M. K. *Chem. Commun.* **2007**, *31*, 3276-3278.
(73) Nonoyama, M. *Bull. Chem. Soc. Jpn.* **1974**, *47*, 767-768.
(74) Kwon, T.-H.; Oh, Y. H.; Shin, I.-S.; Hong, J.-I. *Adv. Funct. Mater.* **2009**, *19*, 711-717.
(75) Kuznetsova, N. A.; Gretsova, N. S.; Yuzhakova, O. A.; Negrimovskii, V. M.; Kaliya, O. L.; Luk'yanets, E. A. *Russ. J. Gen. Chem. 71*, 36-41.
(76) Wessels, J. M.; Foote, C. S.; Ford, W. E.; Rodgers, M. A. J. *J. Photochem. Photobiol.* **1997**, *65*, 96-102.
(77) Ruotolo, B. T.; Benesch, J. L. P.; Sandercock, A. M.; Hyung, S.-J.; Robinson, C. V. *Nat. Protoc.* **2008**, *3*, 1139-1152.
(78) Dupuis, N. F.; Wu, C.; Shea, J.-E.; Bowers, M. T. *J. Am. Chem. Soc.* **2009**, *131*, 18283-18292.
(79) Salbo, R.; Bush, M. F.; Naver, H.; Campuzano, I.; Robinson, C. V.; Pettersson, I.; Jørgensen, T. J. D.; Haselmann, K. F. *Rapid Commun. Mass Spectrom.* **2012**, *26*, 1181-1193.
(80) Derrick, J. S.; Kerr, R. A.; Korshavn, K. J.; McLane, M. J.; Kang, J.; Nam, E.; Ramamoorthy, A.; Ruotolo, B. T.; Lim, M. H. *Inorg. Chem.* **2016**, *55*, 5000-5013.
(81) Schanda, P.; Brutscher, B. *J. Am. Chem. Soc.* **2005**, *127*, 8014-8015.
(82) Vivekanandan, S.; Brender, J. R.; Lee, S. Y.; Ramamoorthy, A. *Biochem. Biophys. Res. Commun.* **2011**, *411*, 312-316.
(83) Yoo, S. I.; Yang, M.; Brender, J. R.; Subramanian, V.; Sun, K.; Joo, N. E.; Jeong, S.-H.; Ramamoorthy, A.; Kotov, N. A. *Angew. Chem. Int. Ed.* **2011**, *50*, 5110-5115.
(84) Fawzi, N. L.; Ying, J.; Torchia, D. A.; Clore, G. M. *J. Am. Chem. Soc.* **2010**, *132*, 9948-9951.

Chapter 3.

Chemical Strategies to Modify Amyloidogenic Peptides by Iridium(III) Complexes: Coordination and Photo-induced Oxidation

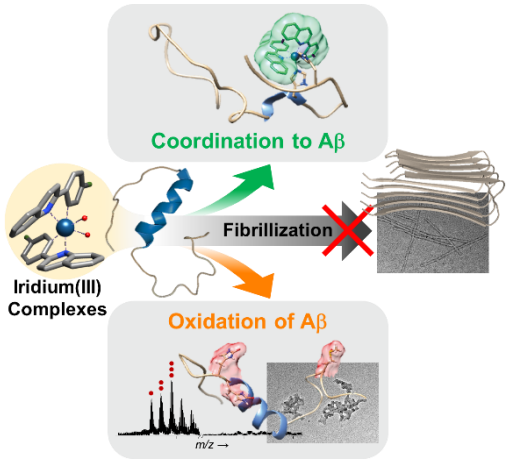

The results and discussion presented in this chapter were described in the submitted manuscript [Kang, J.;† Nam, J. S.;† Lee, H. J.; Nam, G.; Rhee, H.-W.; Kwon, T.-H.; Lim, M. H. *Submitted* (†equal contribution)]. Professor Tae-Hyuk Kwon and Jung Seung Nam prepared Ir(III) complexes and measured their photophysical properties with data analysis. Dr. Hyuck Jin Lee and I performed the mass spectrometric investigations with data analysis. I carried out gel/Western blot, TEM, and cell studies with data analysis. I and Geewoo Nam wrote the manuscript under the direction of Professor Mi Hee Lim.

3.1. Introduction

A substantial amount of research efforts has been dedicated towards identifying the association of amyloidogenic peptides with the pathologies of neurodegenerative diseases. Among these amyloidogenic peptides, amyloid-β (Aβ), a proteolytic product of the amyloid precursor protein found in the AD-affected brain with a self-aggregation propensity, has been implicated as a pathological factor in Alzheimer's disease (AD).[1–4] As the main component of senile plaques, Aβ accumulation is a major pathological feature of AD.[1–3,5] Recent development in Aβ research (e.g., clinical failures of Aβ-directed therapeutics) has led to the re-evaluation of the amyloid cascade hypothesis.[6] Aβ pathology, however, remains a pertinent facet of the disease with indication of Aβ oligomers as toxic species responsible for disrupting neuronal homeostasis.[1–3,7] Furthering our elucidation of Aβ pathology presents an investigative challenge arising from its heterogeneous nature and intrinsically disordered structure.[1,2] To overcome this obstacle and advance our understanding of Aβ-related contribution towards AD, in this study, we illustrate chemical approaches to modify Aβ peptides at the molecular level using transition metal complexes.

Transition metal complexes are capable of harnessing a wide range of chemical and biological functionality, including peptide modifications (e.g., hydrolytic cleavage and peptide oxidation).[8–37] In particular, the ability of transition metal complexes to alter peptides stems from their properties, such as capacity for peptide coordination.[17–29,36,37] Herein, we report effective chemical strategies for modifications of Aβ peptides using a single Ir(III) complex in a in a photo-dependent manner (Figure 3.1). Aβ modifications, achieved by our rationally engineered Ir(III) complexes, include two events: (i) complexation with Aβ in the absence of light; (ii) Aβ oxidation upon coordination and photoactivation, which can significantly regulate their aggregation and toxicity. Through our overall multidisciplinary studies, presented in this work, we demonstrate the feasibility of developing new chemical tactics for modifications of amyloidogenic peptides using transition metal complexes, useful for identifying their properties, such as aggregation, at the molecular level.

3.2. Results and Discussion

3.2.1. Rational Strategies for Peptide Modifications by Ir(III) Complexes

To chemically modify Aβ peptides in a photo-irradiation-dependent manner (Figure 3.1a), four Ir(III) complexes (**Ir-Me**, **Ir-H**, **Ir-F**, and **Ir-F2**; Figure 3.1b) were rationally designed and prepared. Iridium is a third row transition metal exhibiting strong spin-orbit coupling at the center of Ir(III) complexes with facile electronic transitions.[38,39] This spin-orbit coupling can be further strengthened by fine-tuning ancillary ligands of Ir(III) complexes. As a result, Ir(III) complexes confer notable photophysical properties upon excitation by relatively low energy irradiation in the visible range, including their ability

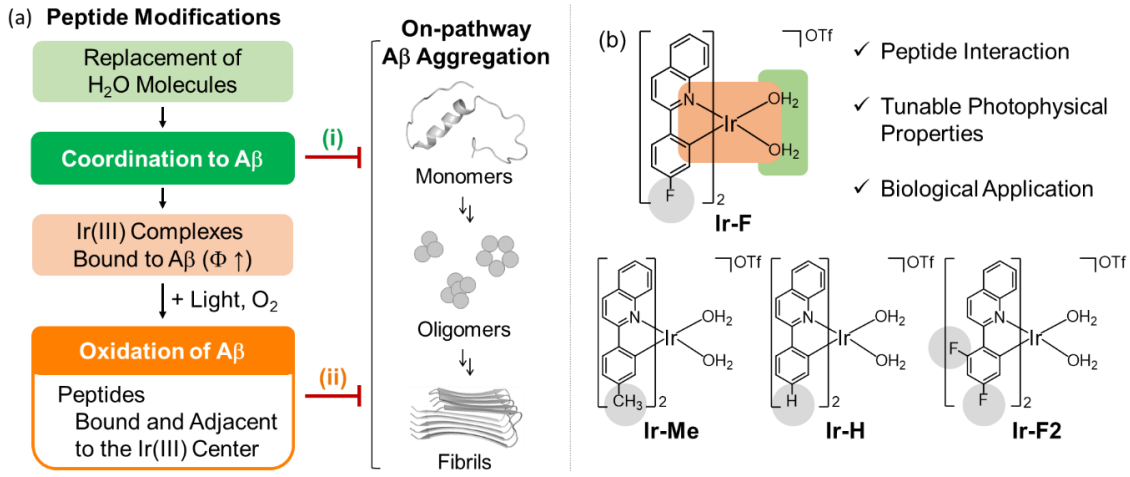

Figure 3.1. Chemical approaches to modify Aβ peptides using rationally designed Ir(III) complexes. (a) Two types of modifying Aβ peptides by Ir(III) complexes for control of Aβ aggregation: (i) coordination to Aβ peptides and (ii) oxidation of Aβ peptides mediated by coordination and photoactivation (Φ = emission quantum yield). (b) Design criteria and chemical structures of **Ir-F**, **Ir-Me**, **Ir-H**, and **Ir-F2**. Substituents are highlighted in gray.

Scheme 3.1. Synthetic routes to Ir(III) complexes.

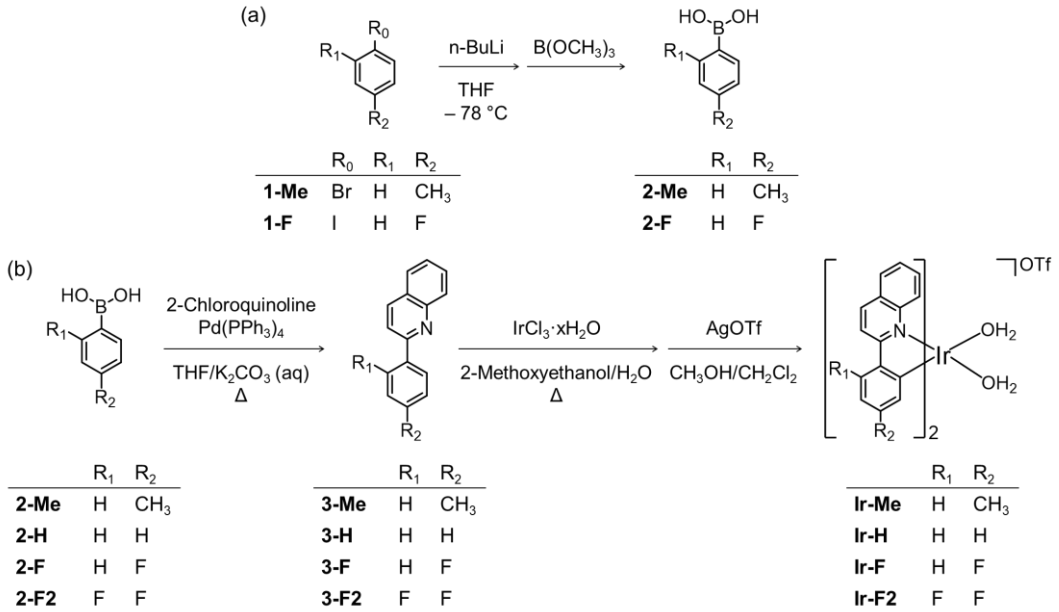

	R_0	R_1	R_2
1-Me	Br	H	CH_3
1-F	I	H	F

	R_1	R_2
2-Me	H	CH_3
2-F	H	F

	R_1	R_2
2-Me	H	CH_3
2-H	H	H
2-F	H	F
2-F2	F	F

	R_1	R_2
3-Me	H	CH_3
3-H	H	H
3-F	H	F
3-F2	F	F

	R_1	R_2
Ir-Me	H	CH_3
Ir-H	H	H
Ir-F	H	F
Ir-F2	F	F

to generate reactive oxygen species (ROS) via electron or energy transfer.[38,40–42] Incorporation of 2-phenylquinoline derivatives as ligands yielded high emission quantum yield (Φ) and robust ROS generation.[40] Thereby, the ancillary ligands of four complexes were constructed based on the 2-phenylquinoline backbone by applying simple structural variations to provide appropriate structural and electronic environments to promote the photochemical activity of the corresponding Ir(III) complexes.[40] Moreover, fluorine atoms were introduced to the ancillary ligand framework, affording **Ir-F** and **Ir-F2**, to chemically impart the ability to interact with Aβ through hydrogen bonding, alter photophysical properties of the complexes, and enhance the molecules' biocompatibility.[40,43–45] Two water (H_2O) molecules were incorporated as ligands to enable covalent coordination to Aβ via replacement with amino acid residues of the peptide, e.g., histidine (His).[20,46,47] The four Ir(III) complexes were synthesized following the previously reported procedures with modifications (Scheme 3.1).[20,48–50]

Table 3.1. Photophysical properties of Ir(III) complexes.

	Ir-Me		**Ir-H**		**Ir-F**		**Ir-F2**	
	– His	+ His	– His	+ His	– His	+ His	– His	+ His
$\lambda_{ex,\,max}$ (nm) (ε, x 10^3 $M^{-1}cm^{-1}$)	280 (± 27), 336 (± 14), 449 (± 3)	274 (± 29), 343 (± 16), 449 (± 3)	275 (± 29), 339 (± 15), 452 (± 3)	268 (± 32), 338 (± 15), 445 (± 3)	274 (± 34), 336 (± 17), 446 (± 4)	269 (± 33), 335 (± 16), 433 (± 4)	277 (± 36), 350 (± 21), 441 (± 7)	272 (± 37), 348 (± 19), 432 (± 6)
$\lambda_{em,\,max}$ (nm)	587	592	587	593	589	573	573	578
Φ	0.0038 (± 0.0007)	0.19 (± 0.01)	0.0037 (± 0.0006)	0.31 (± 0.03)	0.0071 (± 0.001)	0.26 (± 0.03)	0.0027 (± 0.0002)	0.081 (± 0.007)
τ (ns)	5.8 (± 1.8)	601 (± 20)	11 (± 1)	619 (± 61)	4.8 (± 1.9)	810 (± 23)	4.4 (± 0.4)	484 (± 41)
k_r (x 10^5 s^{-1})	6.5	3.2	3.3	5.0	15	3.3	6.1	1.7
k_{nr} (x 10^5 s^{-1})	1.7 x 10^3	13	883	11	2.6 x 10^3	9.1	2.3 x 10^3	19

3.2.2. Coordination-Dependent Photophysical Properties and Singlet Oxygen Production of Ir(III) Complexes

Photophysical properties of the prepared Ir(III) complexes were investigated by UV-Vis and fluorescence spectroscopy. Effects of His coordination to the Ir(III) center on Φ of Ir(III) complexes, a measure of the molecules' ability to produce singlet oxygen ($^1O_2$) with photoactivation, were comparatively evaluated. Upon addition of His, Φ of the Ir(III) complexes drastically increased (e.g., $\Phi_{\mathbf{Ir\text{-}F}} = 0.0071$ versus $\Phi_{\mathbf{Ir\text{-}F}\,+\,His} = 0.26$; Table 1), indicating His coordination of the complexes, which was further confirmed by electrospray ionization-mass spectrometry (ESI-MS) (Figure 3.2a). **Ir-F** showed the strongest binding affinity with His ($K_d = 2.7 \times 10^{-6}$ M; Figure 3.2b) and generated the largest amount of $^1O_2$ upon photoactivation among four Ir(III) complexes (Figure 3.3). Based on these

amount of $^1O_2$ upon photoactivation among four Ir(III) complexes (Figure 3.3). Based on these properties, we selected **Ir-F** as a representative candidate of our Ir(III) complexes and illustrated its ability to modify Aβ peptides in detail (vide infra).

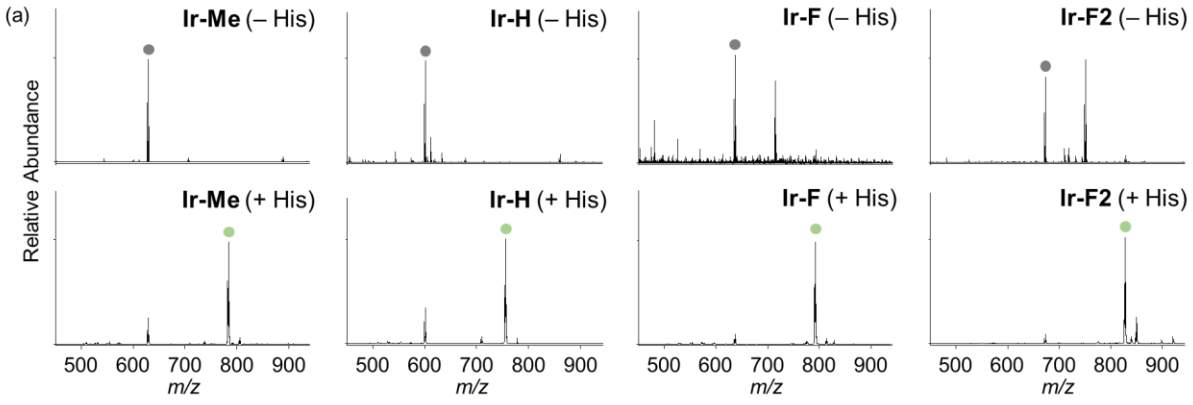

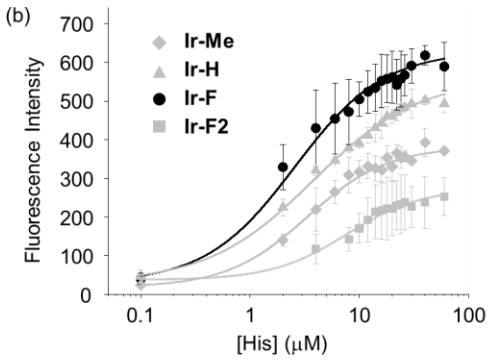

	Ir-Me	Ir-H	Ir-F	Ir-F2
K_d (x 10^{-6} M)	4.2	3.6	2.7	11

Figure 3.2. Histidine binding of Ir(III) complexes. (a) ESI-MS analysis of Ir(III) complexes (gray dots; top) with and without His. The complex formation between His and Ir(III) complexes that do not contain two H_2O molecules on the Ir(III) center [Ir(III) complexes - $2H_2O$] was observed (light green dots; bottom). Conditions: [Ir(III) complex] = 20 μM; [His] = 200 μM; room temperature; 2 h; no agitation. (b) His binding affinities of Ir(III) complexes. Dissociation constants (K_d) were determined through His titration experiments. Conditions: [Ir(III) complex] = 2 μM; [His] = 0-60 μM; room temperature; 2 h; no agitation.

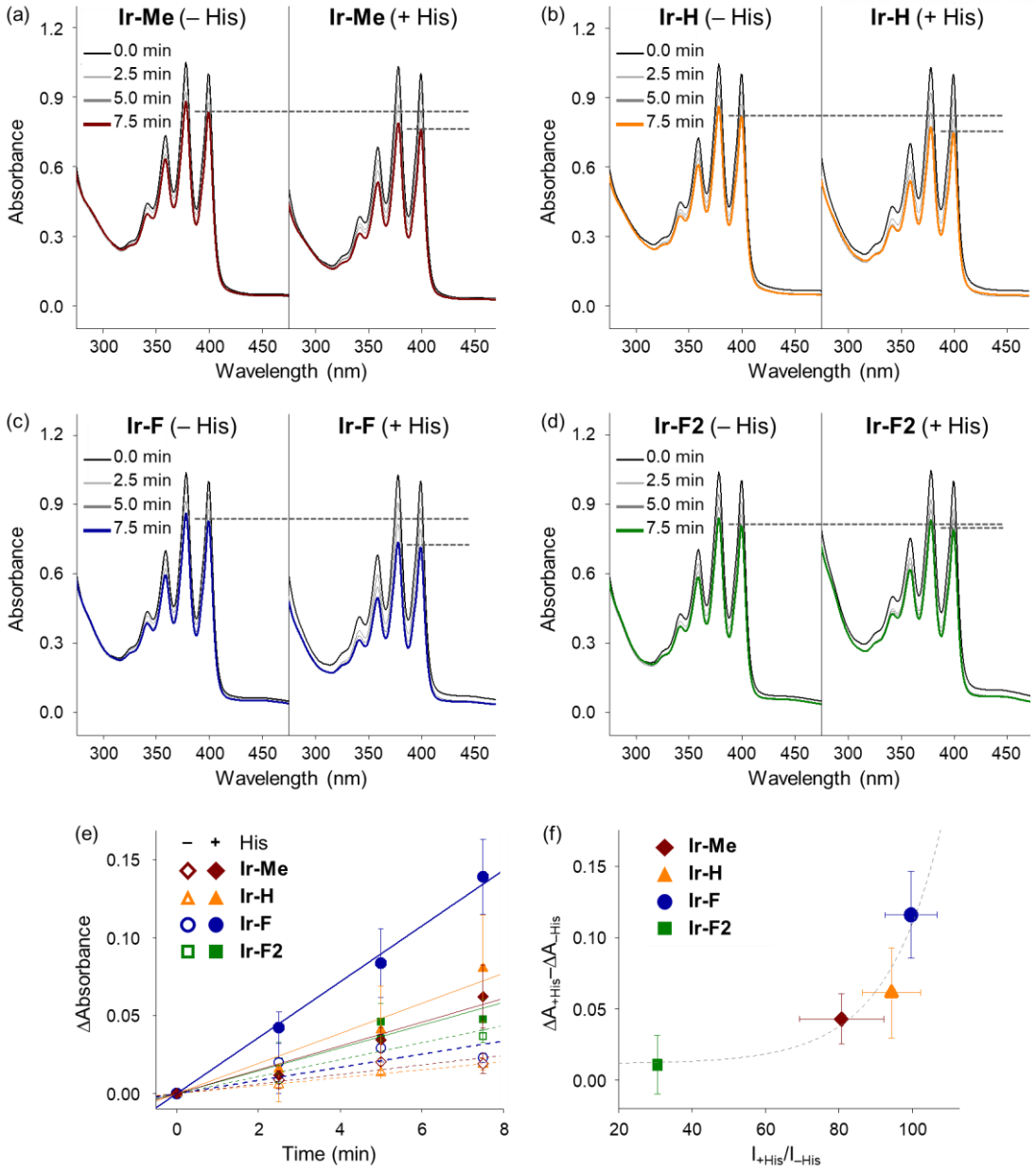

Figure 3.3. Analysis of the amount of singlet oxygen ($^1O_2$) generated by Ir(III) complexes in the absence and presence of histidine. (a-d) Time-dependent absorbance of 9,10-anthracenediyl-bis(methylene)dimalonic acid (ABDA) upon $^1O_2$ generation triggered by (a) **Ir-Me**, (b) **Ir-H**, (c) **Ir-F**, and (d) **Ir-F2**. (e) Absorbance attenuation of ABDA with photoactivated Ir(III) complexes. (f) Correlation between the ability to produce $^1O_2$ and the emission intensity of Ir(III) complexes upon His binding. Note that $^1O_2$ generation is closely related to the triplet-to-singlet electronic transition of the complexes. Since $^1O_2$ generation takes place through energy transfer, it is important that the energy donor (i.e., Ir(III) complex) can efficiently emit the photon (phosphorescence) by transferring its energy to the energy acceptor (ground state O_2). Conditions: [Ir(III) complex] = 10 μM; [His] = 0 or 10 μM; [ABDA] = 100 μM; room temperature; 40% of 1 sun light.

3.2.3. Photoirradiation-Dependent Peptide Modifications by Ir(III) Complexes

Modifications of Aβ peptides upon treatment with **Ir-F** were monitored via mass spectrometric techniques [i.e., ESI-MS, ESI-MS^2, and ion mobility-mass spectrometry (IM-MS)]. The ESI-MS analysis of **Ir-F**-treated Aβ samples revealed the complex formation between Aβ and **Ir-F'** (the **Ir-F** form that does not contain the two H_2O ligands; Figure 3.4b) in the absence of light as an indication at 1653 *m/z* (Figure 3.4a, middle; green). To identify the molecular species corresponding to 1653 *m/z*, the peak was further analyzed via ESI-MS^2 in conjunction with collision-induced dissociation (CID; Figure 3.4c). The detected ion fragments exhibited *m/z* values responsible for $A\beta_{40}$ and **Ir-F'**. Therefore, our MS results demonstrate the complexation between Aβ and **Ir-F** with loss of two H_2O molecules from the Ir(III) center (Figure 3.1b). Note that the *m/z* value of the **Ir-F'**–$A\beta_{40}$ complex is equal to that of [$A\beta_{40}$ + 4OTf + $2H_2O$]; thus, we cannot rule out the co-existence of the complex and an OTf adduct.

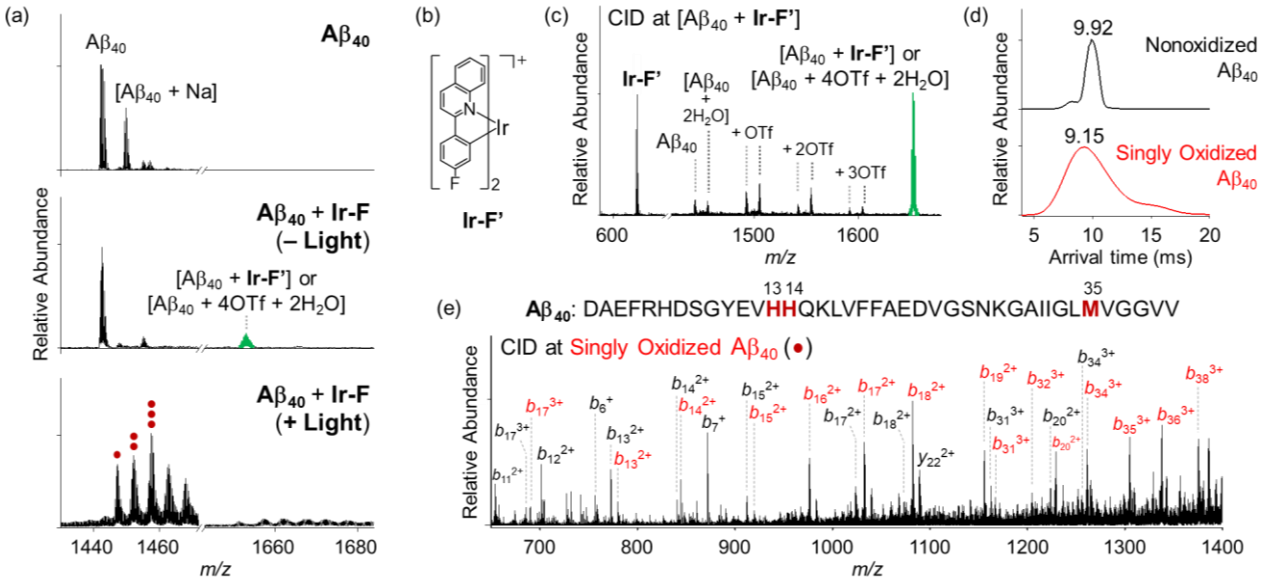

Figure 3.4. Analysis of the $A\beta_{40}$ species generated upon treatment with **Ir-F**. (a) ESI-MS spectra of **Ir-F**-incubated +3-charged $A\beta_{40}$ with and without light. The peak indicated in green corresponds to a complex of $A\beta_{40}$ and **Ir-F'** [structure shown in (b)]. The peaks corresponding to oxidized $A\beta_{40}$ species are indicated with red dots. The number of red dots presents the number of oxygen atoms incorporated into $A\beta_{40}$. (c) Collision-induced dissociation (CID) spectrum at 1653 *m/z* [green peak from (a)]. (d) Arrival time distributions (ATDs) between nonoxidized and singly oxidized $A\beta_{40}$ monomers. (e) Sequence of $A\beta_{40}$ and CID spectrum of the singly oxidized $A\beta_{40}$ found in (a). Monooxidized *b* fragments are notated in red. Charges are omitted in the MS spectra. Conditions: [$A\beta_{40}$] = 100 μM; [**Ir-F**] = 500 μM; 37 °C; 1 h; no agitation; 1 sun light for 10 min (for the samples treated with light); aerobic conditions.

Upon photoirradiation, the ESI-MS analysis of **Ir-F**-treated Aβ$_{40}$ samples led to the detection of oxidized Aβ$_{40}$ (Figure 3.4a, bottom). Aβ$_{40}$ oxidation manifested a conformational change as probed by IM-MS (Figure 3.4d). The most dominant arrival time distribution (ATD) of the singly oxidized Aβ$_{40}$ treated with **Ir-F** showed a broad peak at 9.15 ms, while that of native Aβ$_{40}$ indicated a peak at 9.92 ms. These results suggest that Aβ$_{40}$ oxidation induced by **Ir-F** can alter the structural distribution of Aβ$_{40}$. Similar observations were observed with **Ir-Me**, **Ir-H**, and **Ir-F2**, where the complexes were able to oxidize Aβ$_{40}$ and consequently vary its structural distribution (Figures 3.5 and 3.6). In order to determine the location of peptide oxidation, the Aβ fragment ions, generated by selectively applying collisional energy to singly oxidized Aβ, were analyzed by ESI-MS^2 (Figure 3.4e). All *b* fragments smaller than b_{13} were detected in their nonoxidized forms, while those larger than b_{34} were only

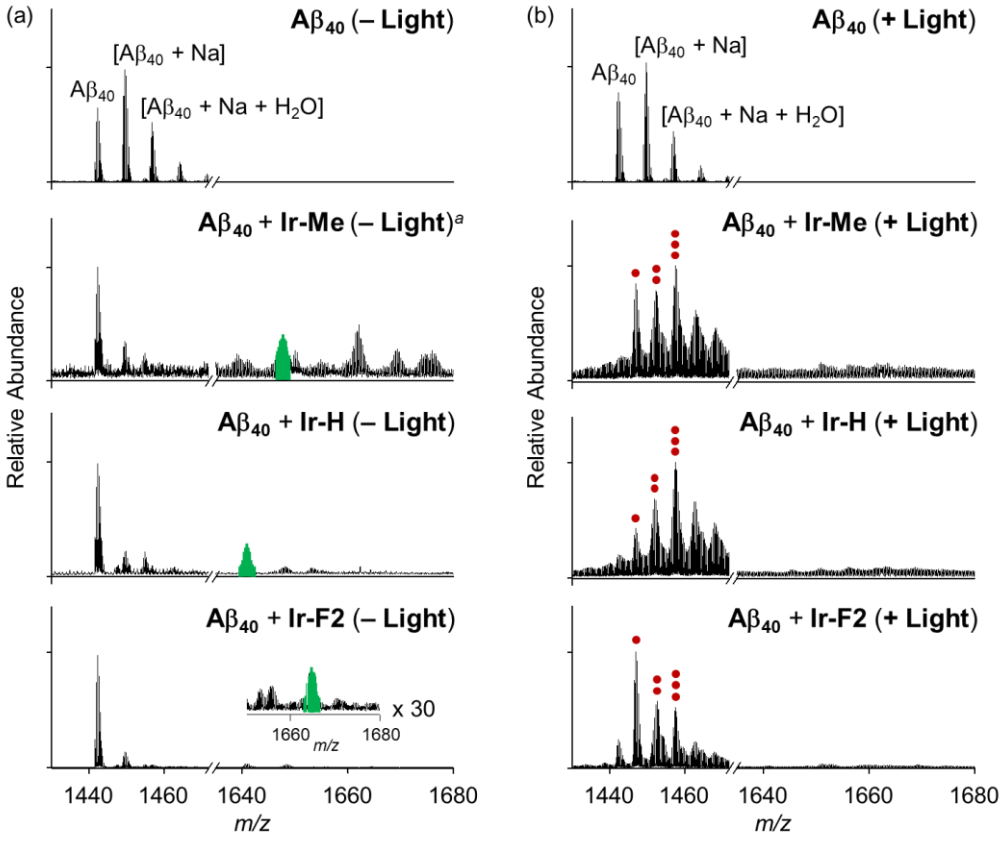

Figure 3.5. ESI-MS spectra of +3-charged Aβ$_{40}$ treated with **Ir-Me**, **Ir-H**, and **Ir-F2** in the (a) absence and (b) presence of light. The peaks [shown in (a)] corresponding to the complexes composed of Aβ$_{40}$ and Ir(III) complexes are indicated in green. The peaks [shown in (b)] corresponding to oxidized Aβ$_{40}$ species are highlighted with red dots. The number of red dots presents the number of oxygen atoms incorporated into Aβ$_{40}$. Conditions: [Aβ$_{40}$] = 100 μM; [Ir(III) complex] = 500 μM; 37 ℃; 1 h ([a]0.5 h for the sample of Aβ$_{40}$ with **Ir-Me** without light treatment); no agitation; 1 sun light for 10 min (for the samples treated with light); aerobic conditions.

monitored in their oxidized forms. The *b* fragments between b_{13} and b_{34} were indicated in both their oxidized and nonoxidized forms. Such observations, along with previous reports regarding Aβ oxidation,[19,51] suggest His13, His14, and Met35 of Aβ as plausible oxidation sites. Collectively, our studies demonstrate that Aβ peptides can be modified upon treatment with **Ir-F** [(i) coordination to Aβ by replacing two H_2O ligands with the peptide in the absence of light; (ii) coordination-mediated oxidation of Aβ at three possible amino acid residues (e.g., His13, His14, and Met35) upon photoactivation (Figure 3.1a)].

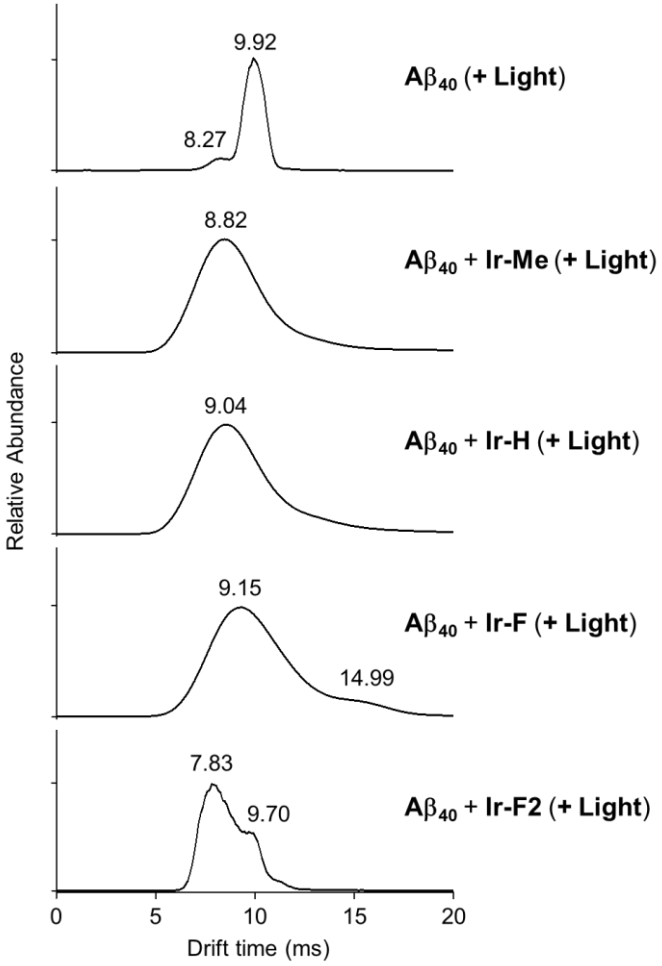

Figure 3.6. IM-MS spectra of +3-charged $Aβ_{40}$ incubated with and without Ir(III) complexes. Arrival time distributions (ATDs) for nonoxidized (top; the "$Aβ_{40}$ + Light" sample) and singly oxidized $Aβ_{40}$ generated upon treatment of light-activated Ir(III) complexes were detected.

3.2.4. Effects of Peptide Modifications Triggered by Ir(III) Complexes on Aβ Aggregation

Based on the photoirradiation-dependent Aβ modifications by Ir(III) complexes, the impact of such peptide variations on the aggregation pathways of Aβ was determined employing $Aβ_{40}$ and $Aβ_{42}$, two main Aβ isoforms found in the AD-affected brain.[1–4,52–56] For these experiments, freshly prepared Aβ solutions were treated with Ir(III) complexes with and without light under both aerobic and anaerobic conditions. The molecular weight (MW) distribution and the aggregate morphology of resultant Aβ species were analyzed by gel electrophoresis with Western blotting (gel/Western blot) using an anti-Aβ antibody (6E10) and transmission electron microscopy (TEM), respectively (Figure 3.7a).

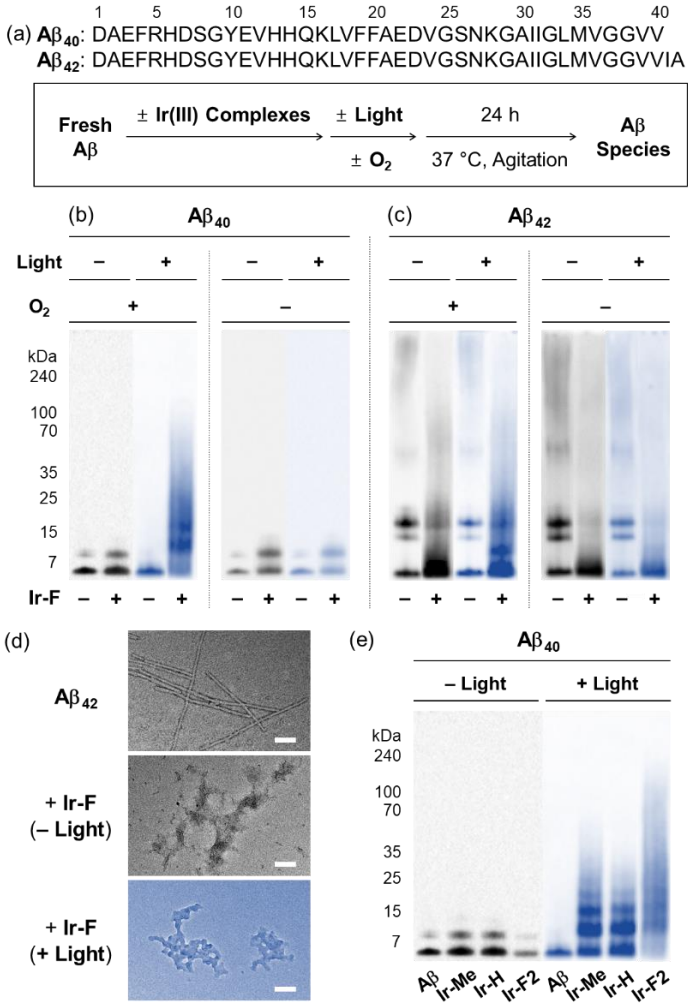

Figure 3.7. Change in the formation of Aβ aggregate with incubation of Ir(III) complexes. (a) Sequences of $Aβ_{40}$ and $Aβ_{42}$ and Scheme of the inhibition experiments. (b,c,e) Analysis of the resultant $Aβ_{40}$ and $Aβ_{42}$ species generated under various conditions by gel/Western blot with an anti-Aβ antibody (6E10). (d) TEM images of the Aβ aggregates formed from (c) (scale bar = 100 nm). Conditions: [Aβ] = 25 μM; [Ir(III) complexes] = 250 μM; 37 ℃; 24 h; constant agitation; 1 sun light for 10 min (for the samples treated with light).

Under aerobic conditions (Figure 3.7b, left), the aggregation of $A\beta_{40}$ was affected with treatment of **Ir-F** prompting a shift in the MW distributions in the absence of light. Photoactivation of the **Ir-F**-treated $A\beta_{40}$ sample resulted in a more diverse MW distribution compared to that of the corresponding sample without light (light, MW ≤ 100 kDa; no light, MW < 15 kDa). The distinct modulation of $A\beta_{40}$ aggregation upon addition of **Ir-F** with photoirradiation is likely a consequence of the complex's ability to generate $^1O_2$ and oxidize Aβ through photoactivation as observed in our spectrometric studies (vide supra; Figure 3.4). Therefore, the same experiments were performed under anaerobic conditions to

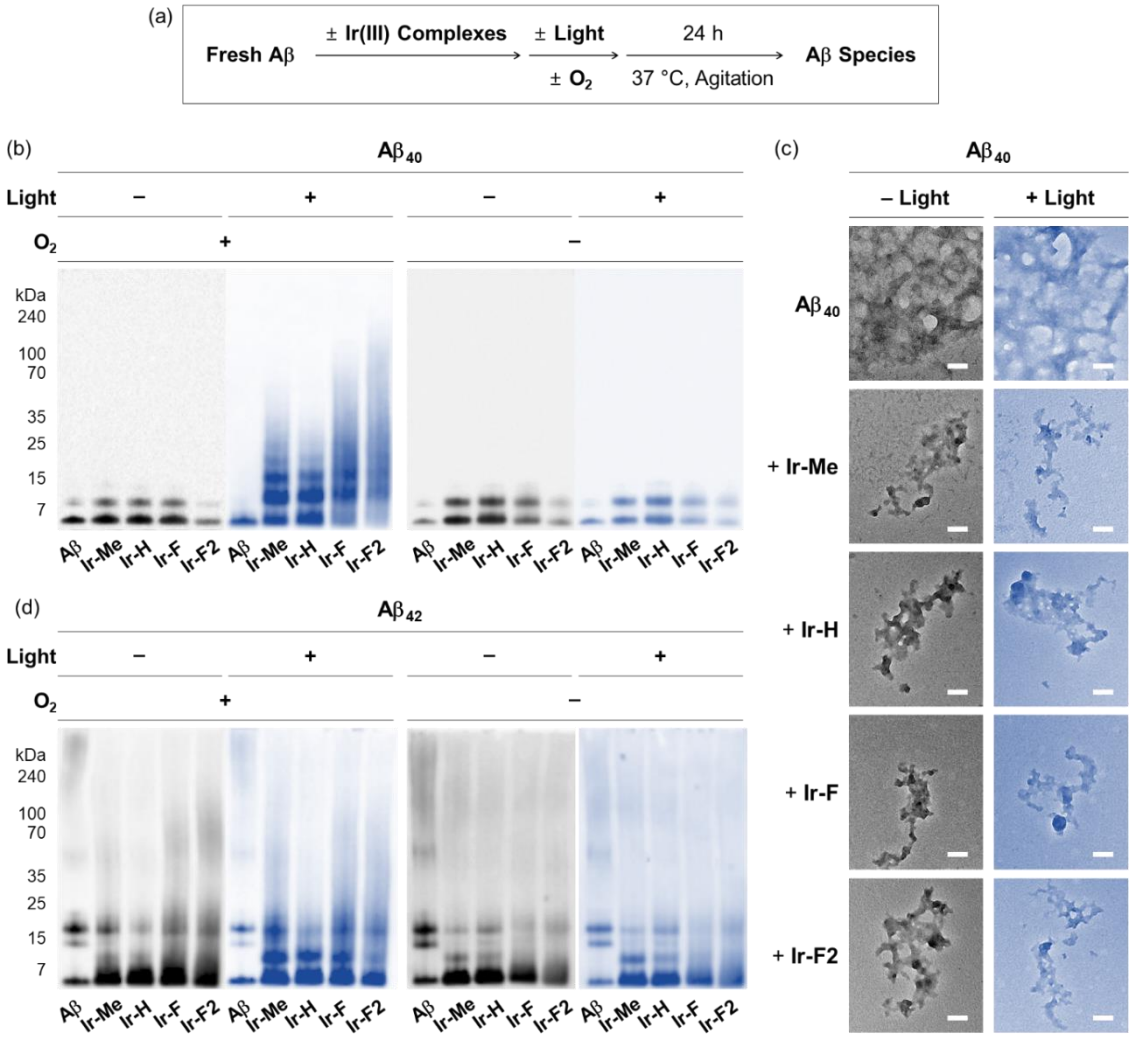

Figure 3.8. Influence of Ir(III) complexes on the formation of Aβ aggregates. (a) Scheme of the experiments. Analyses of the resultant (b) $A\beta_{40}$ and (d) $A\beta_{42}$ species produced from various experimental conditions by gel/Western blot with an anti-Aβ antibody (6E10). Conditions: [Aβ] = 25 μM; [Ir(III) complex] = 250 μM; 1 sun light for 10 min (for the samples treated with light). (c) TEM images of the $A\beta_{40}$ aggregates produced from (b) (scale bar = 100 nm).

directly monitor the role of O_2 in **Ir-F**'s modulative reactivity against $A\beta_{40}$ aggregation. In the absence of O_2 (Figure 3.7b, right), $A\beta_{40}$ aggregation was also altered by **Ir-F** regardless of light treatment. Our results suggest that both light and O_2 are important in the regulation of $A\beta_{40}$ aggregation through coordination-/photo-mediated peptide oxidation triggered by **Ir-F**. In addition, in the absence of light and O_2, $A\beta_{40}$ aggregation is directed by the covalent interactions between **Ir-F** and the peptide. Similar modulation of $A\beta_{42}$ aggregation was observed upon incubation with **Ir-F** exhibiting different MW distributions compared to the $A\beta_{42}$ samples without **Ir-F** in the absence and presence of light and O_2 (Figure 3.7c). Moreover, smaller amorphous aggregates of both $A\beta_{40}$ and $A\beta_{42}$, reported to be less toxic,[57,58] were visualized by TEM from the samples containing **Ir-F** regardless of irradiation (Figures 3.7d and 3.8c).

Furthermore, preformed Aβ aggregates, generated at various preincubation time points (i.e., 2, 4, and 24 h), were disassembled and their aggregation pathways were altered, when **Ir-F** was introduced (Figure 3.9). Such **Ir-F**-induced effects on preformed Aβ aggregates were observed to be dependent on photoirradiation. Moreover, the aggregation of both $A\beta_{40}$ and $A\beta_{42}$ was also changed with addition of the other Ir(III) complexes (i.e., **Ir-Me**, **Ir-H**, and **Ir-F2**) with and without light (Figures 3.7e, 3.8 and 3.9).

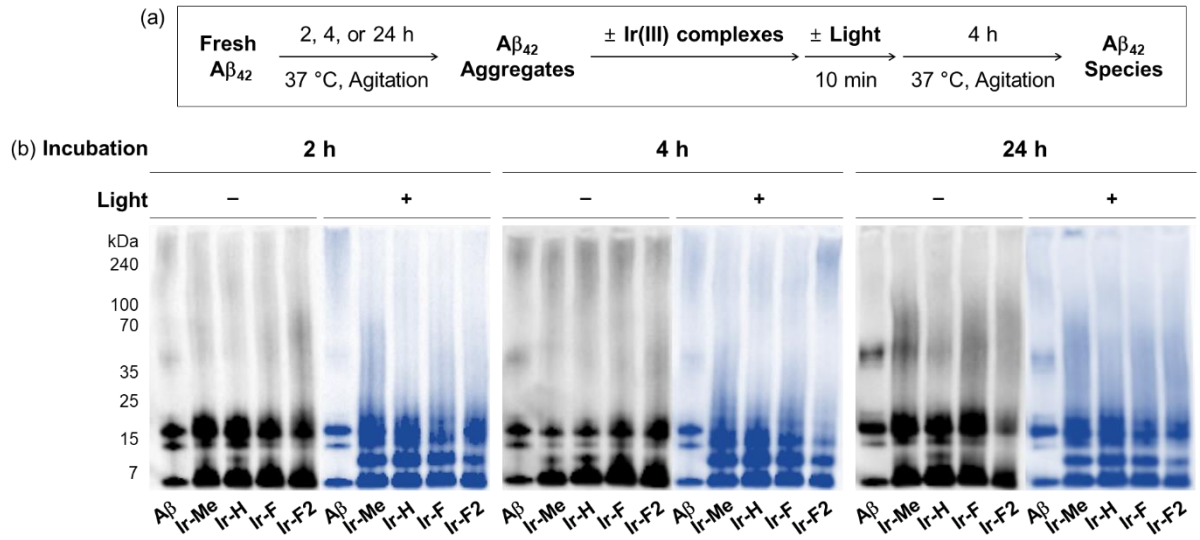

Figure 3.9. Impact of Ir(III) complexes on the disassembly of preformed $A\beta_{42}$ aggregates produced at various incubation time points (i.e., 2 h, 4 h, and 24 h). (a) Scheme of the experiments. (b) Analysis of the resultant $A\beta_{42}$ species by gel/Western blot with an anti-Aβ antibody (6E10). Conditions: [$A\beta_{42}$] = 25 μM; [Ir(III) complex] = 250 μM; 1 sun light for 10 min (for the samples treated with light).

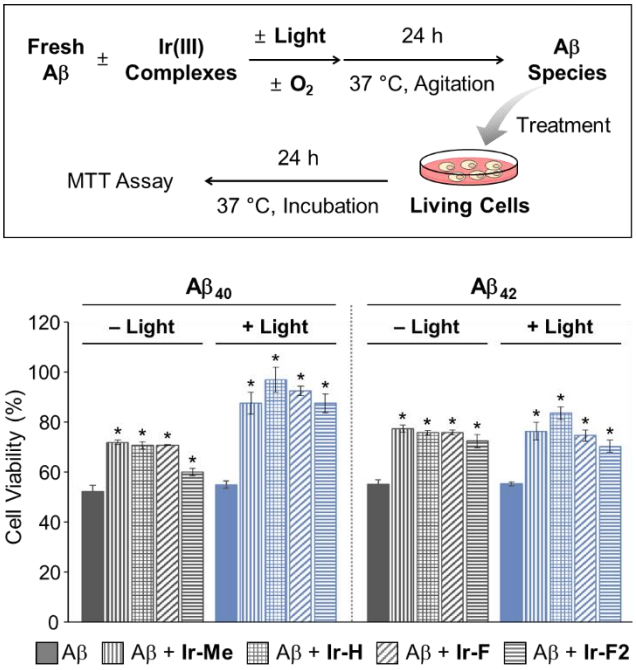

Figure 3.10. Viability of N2a cells upon 24 h treatment with Aβ species produced by incubation with Ir(III) complexes for 24 h with and without light activation. Cell viability (%), measured by the MTT assay, was calculated compared with that treated with an equivalent amount of DMSO only. Conditions (final concentration): [Aβ] = 20 μM; [Ir(III) complexes] = 5 μM. Error bars represent the standard error of the mean from three independent experiments. **P* < 0.05.

3.2.5. Cytotoxicity of Aβ Species Generated upon Incubation with Ir(III) Complexes

Moving forward, the toxicity of Aβ species produced with treatment of our Ir(III) complexes was determined in murine Neuro-2a (N2a) neuroblastoma cells by the MTT assay [MTT = 3-(4,5-dimethyl-2-thiazolyl)-2,5-diphenyl-2*H*-tetrazolium bromide] (Figure 3.10). The cytotoxicity of $A\beta_{40}$ species incubated with our Ir(III) complexes was noticeably reduced in a photoirradiation-dependent manner. In the absence of light, the $A\beta_{40}$ samples incubated with our Ir(III) complexes exhibited a decrease in cytotoxicity (ca. 20%) than the sample of the complex-free $A\beta_{40}$. As for the photoirradiated samples, $A\beta_{40}$-induced toxicity was lowered by ca. 35% when being treated with our Ir(III) complexes. Furthermore, the cytotoxicity of $A\beta_{42}$ species formed with Ir(III) complexes was also diminished by ca. 20% regardless of photoactivation. Note that the survival (≥ 80%) of cells added with our Ir(III) complexes under the concentration used for cell studies with Aβ peptides was observed with and without light exposure (Figure 3.11).

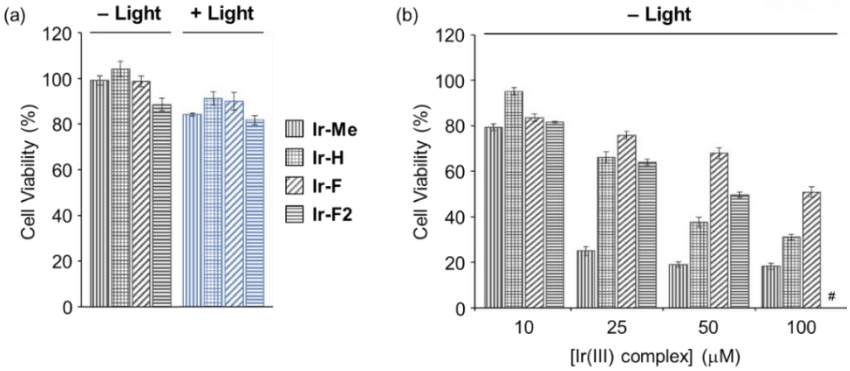

Figure 3.11. Viability of N2a cells with Ir(III) complexes. (a) Cell viability of Ir(III) complexes (5 μM) in the absence and presence of light. (b) Survival of the cells treated with different concentrations of Ir(III) complexes (10-100 μM; #the value was not obtained due to limited solubility) in the absence of light exposure. Cell viability (%), measured by the MTT assay, was calculated compared with cells obtained with an equivalent amount of DMSO only. Error bars represent S.E.M. from three independent experiments.

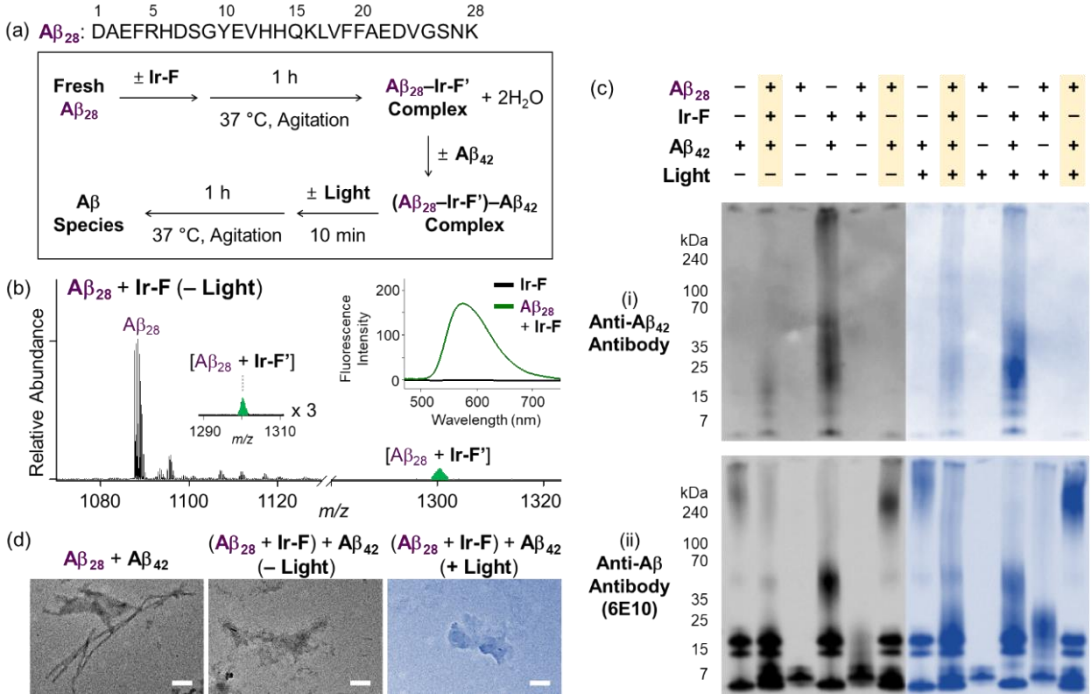

Figure 3.12. Impact of **Ir-F**-preincubated $A\beta_{28}$ on the aggregation of $A\beta_{42}$. (a) Sequence of $A\beta_{28}$ and scheme of the experiments. (b) ESI-MS spectrum of +3-charged $A\beta_{28}$ upon incubation with **Ir-F**. The complex peak is indicated in green. (Inset) Fluorescence response of **Ir-F** to $A\beta_{28}$ (λ_{ex} = 433 nm). Charges are omitted in the MS spectra. Conditions: [$A\beta_{28}$] = 100 μM; [**Ir-F**] = 100 μM; 37 ℃; 1 h; no agitation; 1 sun light for 10 min (for the samples treated with light); aerobic conditions. (c) Analysis of the resultant Aβ species, obtained by addition of $A\beta_{42}$ into **Ir-F** preincubated with $A\beta_{28}$, by gel/Western blot with (i) anti-$A\beta_{42}$ and (ii) anti-Aβ (6E10) antibodies. (d) TEM images of the Aβ aggregates produced from (c) (scale bar = 100 nm). Conditions: [$A\beta_{28}$] = 50 μM; [**Ir-F**] = 10 μM; [$A\beta_{42}$] = 20 μM; 37 °C; 2 h; constant agitation; 1 sun light for 10 min (for the samples treated with light); aerobic conditions.

3.2.6. Ternary Complexation with Aβ and Intramolecular and Intermolecular Aβ Oxidation

Premised on **Ir-F**'s covalent bond formation with Aβ and oxidation of Aβ (vide supra), additional studies regarding ternary complexation and promotion of intermolecular oxidation of Aβ were carried out employing **Ir-F** (Figure 3.12). $A\beta_{28}$, a fragment of Aβ equipped with the metal binding and self-recognition sites of $A\beta_{40}$ and $A\beta_{42}$ with a relatively less propensity to aggregate than the full-length peptide,[1,59–61] was used to form a complex with **Ir-F'** (Figure 3.4b) as evidenced by ESI- MS (1301 *m/z*; Figure 3.12b) and increased fluorescence (Figure 3.12b, inset). As shown in Figure 3.12a, following incubation, the sample of the $A\beta_{28}$–**Ir-F'** complex was treated to freshly prepared $A\beta_{42}$ to monitor its effect on $A\beta_{42}$ aggregation. Based on the gel/Western blot and TEM analyses, the aggregation of $A\beta_{42}$ was modulated by the $A\beta_{28}$–**Ir-F'** complex (Figure 3.12c and d). Our mass spectrometric studies confirmed that such control of $A\beta_{42}$ aggregation by the $A\beta_{28}$–**Ir-F'** complex was a result of the ternary complex formation with $A\beta_{42}$, i.e., ($A\beta_{28}$–**Ir-F'**)–$A\beta_{42}$, and (ii) oxidation of $A\beta_{42}$, both intramolecular and intermolecular, upon photoactivation (Figure 3.13). Based on previous reports detailing intermolecular interactions between Aβ peptides, hydrophobic interactions between the self-recognition site (LVFFA) of Aβ are likely responsible for ternary complexation,[1,2,62] consequentially altering the

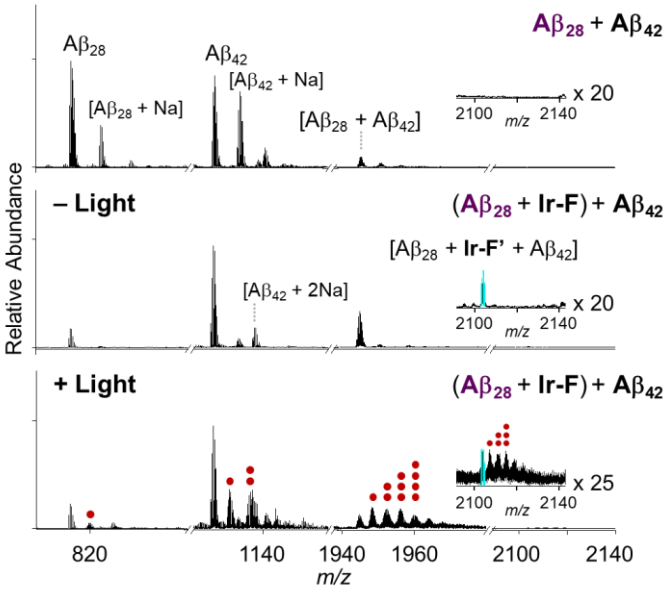

Figure 3.13. ESI-MS spectra of **Ir-F**-incubated +4-charged $A\beta_{28}$ and $A\beta_{42}$ with and without light. The peak indicated in cyan refers to a ternary complex of $A\beta_{28}$, **Ir-F'**, and $A\beta_{42}$. The peaks corresponding to oxidized peptides (i.e., $A\beta_{28}$, $A\beta_{42}$, and $A\beta_{28}$ with $A\beta_{42}$) are indicated with red dots. The number of red dots presents the number of oxygen atoms incorporated into each peptide. Charges are omitted in the MS spectra. Conditions: [$A\beta_{28}$] = 100 μM; [**Ir-F**] = 100 μM; [$A\beta_{42}$] = 100 μM; 37 ℃; 2 h; no agitation; 1 sun light for 10 min (for the samples treated with light); aerobic conditions.

aggregation pathways of Aβ in the absence of photoirradiation. Furthermore, these studies indicate that intermolecular oxidation of Aβ can be promoted by **Ir-F** upon photoactivation (Figures 3.13 and 3.14). This observation may explain the distinct difference between the modulation of Aβ aggregation with and without light as the intermolecular Aβ oxidation by Ir(III) complexes could modify Aβ at sub-stoichiometric levels.

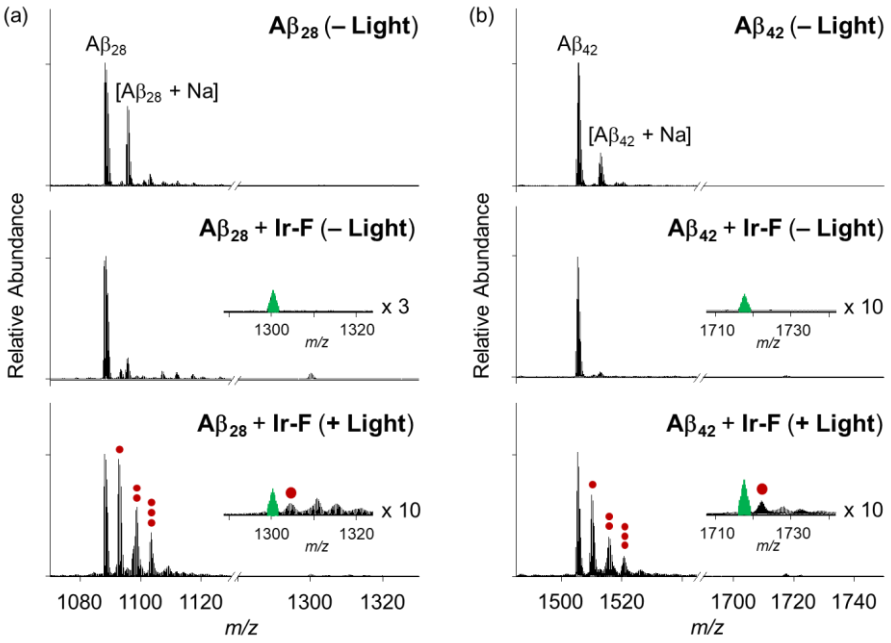

Figure 3.14. ESI-MS spectra of +3-charged (a) $A\beta_{28}$ or (b) $A\beta_{42}$ treated with **Ir-F** in the absence and presence of light. The peak indicated in green refers to the complex generation between Aβ and **Ir-F'** (the **Ir-F** form that does not contain two H_2O molecules). The peaks corresponding to oxidized Aβ species are indicated with red dots. The number of red dots presents the number of oxygen atoms incorporated into Aβ. Conditions: [Aβ] = 100 μM; [**Ir-F**] = 100 μM; 37 ℃; 1 h; no agitation; 1 sun light for 10 min (for the samples treated with light); aerobic conditions.

3.3. Conclusions

Effective chemical strategies (i.e., coordination to Aβ and coordination-/photo-mediated Aβ oxidation) for modifications of Aβ peptides using a single Ir(III) complex were rationally developed. Such changes in Aβ peptides are able to lead to the noticeable modulation of their aggregation and toxicity in living cells. Our Ir(III) complexes can covalently bind to Aβ by replacing two H_2O ligands with Aβ regardless of light and O_2 [coordination to Aβ; Figure 3.1a (i)]. In the presence of light and O_2, Ir(III) complexes bound to Aβ are capable of inducing the intramolecular and intermolecular oxidation of Aβ at His13, His14, and/or Met35 [oxidation of Aβ; Figure 3.1b (ii)]. Taken together, our multidisciplinary studies

demonstrate the feasibility of establishing new chemical approaches towards modifications of amyloidogenic peptides (e.g., Aβ) by transition metal complexes designed based on their coordination and photophysical properties. In general, chemical modifications in peptides of interest can assist in furthering our understanding of principles in their properties, such as peptide assembly.

3.4. Experimental Section

3.4.1. Materials and Methods

All reagents were purchased from commercial suppliers and used as received unless otherwise noted. Analyses of small molecules by nuclear magnetic resonance (NMR) spectroscopy, Fourier-transform infrared (FT-IR) spectroscopy, and mass spectrometry (MS) were conducted on a Bruker AVANCE III HD NMR spectrometer, Varian Cary 620/670 FT-IR spectrometer (UNIST Central Research Facilities, Ulsan, Republic of Korea), and a Thermo Scientific Q Exactive Hybrid Quadrupole-Orbitrap Mass Spectrometer, respectively. $A\beta_{40}$, $A\beta_{42}$, and $A\beta_{28}$ were purchased from Anygen ($A\beta_{40}$ = DAEFRHDSGYEVHHQKLVFFAEDVGSNKGAIIGLMVGGVV; $A\beta_{42}$ = DAEFRHDSGYEVHHQ-KLVFFAEDVGSNKGAIIGLMVGGVVIA; Nam-myun, Jangseong-gun, Republic of Korea) and AnaSpec ($A\beta_{28}$ = DAEFRHDSGYEVHHQKLVFFAEDVGSNK; Fremont, CA, USA), respectively. Double distilled H_2O was obtained from a Milli-Q Direct 16 system (Merck KGaA, Darmstadt, Germany). 1 sun light (100 $mWcm^{-2}$) was treated from a Newport IQE-200 solar simulator (Irvine, CA, USA). Anaerobic reactions were performed in a N_2-filled glovebox (Korea Kiyon, Bucheon-si, Gyeonggi-do, Republic of Korea). Transmission electron microscopical images were taken by a JEOL JEM-2100 transmission electron microscope (UNIST Central Research Facilities, Ulsan, Republic of Korea). Analysis by electrospray ionization-ion mobility-mass spectrometry (ESI-IM-MS) was carried out using a Waters Synapt G2-Si quadrupole time-of-flight ion mobility mass spectrometer (DGIST Center for Core Research Facilities, Daegu, Republic of Korea) equipped with an ESI source. Photophysical properties were measured by a Shimadzu UV-2600 UV-visible (UV-Vis) spectrophotometer and a Varian Cary Eclipse fluorescence spectrophotometer (UNIST Central Research Facilities, Ulsan, Republic of Korea). Time-correlated single photon counting (TCSPC) was conducted for lifetime measurements with Ti:sapphire laser Mira900 (Coherent, Santa Clara, CA, USA), monochromator Acton Series SP-2150i (Princeton Instruments, Acton, MA, USA), and TCSPC module PicoHarp 300 (PicoQuant, Berlin, Germany), with micro channel plate photomultiplier tube (MCP-PMT) R3809U-59 (Hamamatsu, Shizuika-ken, Japan) and fitted by PicoQuant FluoFit software (UNIST Central Research Facilities, Ulsan, Republic of Korea). A SpectraMax M5e microplate reader (Molecular Devices, Sunnyvale, CA, USA) was used to measure the absorbance for the MTT assay.

3.4.2. Synthesis of Ir(III) Complexes

3.4.2.1. Preparation of 2-Me

2-Me was synthesized by modifications of previously reported procedures.[63] $CH_3(CH_2)_3Li$ (*n*-BuLi; 2.5 M; 7.0 mL, 18 mmol) was slowly dropped to a solution of 4-bromotoluene (**1-Me**; 2.0 g, 12 mmol) in tetrahydrofuran (THF) under -78 °C, and the solution was vigorously stirred for 1 h. $B(OCH_3)_3$ (2.2 g, 21 mmol) was slowly added to the solution, and the reaction mixture was stirred for additional 4 h. The reaction mixture was quenched with H_2O. The product was extracted with CH_2Cl_2 three times. The collected organic solution was treated with $MgSO_4$ and removed under the reduced pressure to obtain a white powder product. (1.2 g, yield 64%). ^{1}H NMR [400 MHz, $CDCl_3$, δ (ppm)]: 8.13 (d, J = 7.9 Hz, 2H), 7.31 (d, J = 7.5 Hz, 2H), 2.45 (s, 3H).

3.4.2.2. Preparation of 2-F

2-F was synthesized by the same procedure as **2-Me** using 4-fluoroiodobenzene (**1-F**; 3.0 g, 14 mmol), *n*-BuLi (2.5 M; 8.1 mL, 20 mmol), and $B(OCH_3)_3$ (2.5 g, 24 mmol) (white powder; 820 mg, yield 43%).[63] ^{1}H NMR [400 MHz, $CDCl_3$, δ (ppm)]: 8.19-8.24 (m, 2H), 7.19 (t, J = 8.8 Hz, 2H).

3.4.2.3. Preparation of 3-H

3-H was synthesized by modifications of previously reported procedures.[64] 2-Chloroquinoline (400 mg, 2.4 mmol), phenylboronic acid (**2-H**; 358 mg, 2.9 mmol), and $Pd(PPh_3)_4$ (141 mg, 0.12 mmol) were added to a mixture of degassed THF and K_2CO_3 (2 M, aq) (1:1). The solution was refluxed under N_2 (g) overnight. After cooling down to room temperature, the solution was concentrated, and H_2O was added into the resulting solution. The organic phase was extracted with ethyl acetate (EtOAc) three times. The collected organic solution was treated with $MgSO_4$ and removed under the reduced pressure. The crude materials were purified by column chromatography (SiO_2, 10:1 hexanes:EtOAc, R_f = 0.6; white powder; 297 mg, yield 59%). ^{1}H NMR [400 MHz, DMSO-d_6, δ (ppm)]: 8.45 (d, J = 8.8 Hz, 1H), 8.26 (d, J = 7.2 Hz, 2H), 8.14 (d, J = 8.0 Hz, 1H), 8.06 (d, J = 8.0 Hz, 1H), 7.98 (d, J = 8.0 Hz, 1H), 7.77 (t, J = 7.2 Hz, 1H), 7.46-7.62 (m, 4H).

3.4.2.4. Preparation of 3-Me

3-Me was synthesized by the same procedure as **3-H** using 2-chloroquinoline (600 mg, 3.7 mmol), **2-Me** (600 mg, 4.4 mmol), and $Pd(PPh_3)_4$ (212 mg, 0.18 mmol) (10:1 hexanes:EtOAc, R_f = 0.6; white powder; 733 mg, yield 91%). ^{1}H NMR [400 MHz, DMSO-d_6, δ (ppm)]: 8.18 (t, J = 9.2 Hz, 2H), 8.08 (d, J = 8.0 Hz, 2H), 7.86 (d, J = 8.4 Hz, 1H), 7.82 (dd, J = 8.1, 1.5 Hz, 1H), 7.72 (ddd, J = 8.4, 6.9, 1.5 Hz, 1H), 7.52 (ddd, J = 8.1, 6.8, 1.2 Hz, 1H), 7.34 (d, J = 8.1 Hz, 2H), 2.44 (s, 3H). ^{13}C NMR [100 MHz, DMSO-d_6, δ (ppm)]: 157.3, 148.3, 139.4, 136.9, 136.7, 129.7, 129.6, 129.4, 127.5, 127.1, 126.8, 126.1, 118.9, 21.4. FT-IR (neat cm^{-1}): 3055, 3026, 2958, 2914, 2858, 1597, 1552, 1496, 1431, 1373, 1319, 1288, 1244, 1213, 1184, 1157, 1126, 1111, 1053, 1016, 974, 949, 814, 789, 746, 717. HRMS for $[C_{16}H_{13}N + H]^+$ Calcd, 220.1121; found, 220.1116.

3.4.2.5. Preparation of 3-F

3-F was synthesized by the same procedure as **3-H** using 2-chloroquinoline (500 mg, 3.1 mmol), **2-F** (500 mg, 3.6 mmol), and $Pd(PPh_3)_4$ (176 mg, 0.15 mmol) (10:1 hexanes:EtOAc, R_f = 0.7; white powder; 616 mg, yield 90%). ^{1}H NMR [400 MHz, DMSO-d_6, δ (ppm)]: 8.22 (d, J = 8.4 Hz, 1H), 8.17 (t, J = 8.0 Hz, 3H), 7.83 (dd, J = 8.8 Hz, 2H), 7.73 (ddd, J = 8.5, 7.0, 1.5 Hz, 1H), 7.53 (ddd, J = 8.1, 6.8, 1.2 Hz, 1H), 7.21 (t, J = 8.8 Hz, 2H). ^{13}C NMR [100 MHz, DMSO-d_6, δ (ppm)]: 168.8, 162.9, 160.4, 148.2, 143.8, 143.8, 143.3, 140.9, 131.7, 129.1, 129.0, 128.9, 127.7, 127.1, 125.9, 119.7, 119.6, 117.5, 109.5, 109.3. FT-IR (neat cm^{-1}): 3067, 1736, 1594, 1558, 1515, 1495, 1432, 1324, 1286, 1270, 1230, 1162, 1125, 1098, 1047, 1012, 977, 940, 852, 820, 789, 758, 710, 691, 673. HRMS for $[C_{15}H_{10}FN + H]^+$ Calcd, 224.0870; found, 224.0864.

3.4.2.6. Preparation of 3-F2

3-F2 was synthesized by the same procedure as **3-H** using 2-chloroquinoline (860 mg, 5.3 mmol), 2,4-difluorophenylboronic acid (**2-F2**; 996 mg, 6.3 mmol), and $Pd(PPh_3)_4$ (304 mg, 0.26 mmol) (10:1 hexanes:EtOAc, R_f = 0.7; white powder; 742 mg, yield 59%). ^{1}H NMR [400 MHz, DMSO-d_6, δ (ppm)]: 8.46 (d, J = 8.8 Hz, 1H), 8.07-8.14 (m, 2H), 8.02 (d, J = 8.0 Hz, 1H), 7.88 (dd, J = 8.4, 2.4 Hz, 1H), 7.80 (t, J = 7.6 Hz, 1H), 7.63 (t, J = 7.6 Hz, 1H), 7.43 (t, J = 9.2 Hz, 1H), 7.28 (t, J = 8.8 Hz, 1H). ^{13}C NMR [100 MHz, DMSO-d_6, δ (ppm)]: 164.5, 162.0, 159.5, 152.8, 148.0, 137.3, 133.2, 130.5, 129.5, 128.3, 127.3, 124.4, 122.3, 112.7, 105.1. FT-IR (neat cm^{-1}): 3057, 2954, 2923, 2853, 1676, 1613, 1596, 1497, 1456, 1430, 1418, 1318, 1294, 1264, 1134, 1096, 1053, 970, 942, 836, 808, 758. HRMS for $[C_{15}H_9F_2N + H]^+$ Calcd, 242.0776; found, 242.0772.

3.4.2.7. Preparation of Ir-H

Ir-H was synthesized by modifications of previously reported methods.[49,50] **3-H** (859 mg, 4.2 mmol) was added to a solution of $IrCl_3 \cdot nH_2O$ (500 mg, 1.7 mmol) in a mixture of 2-methoxyethanol and H_2O (3:1). The solution was refluxed under N_2 (g) for 24 h. After cooling down to room temperature, brown precipitates were obtained by addition of H_2O. The crude product (the cyclometalated chloride-bridged Ir(III) dimer, $[Ir(\mu\text{-}Cl)(\mathbf{3\text{-}H})_2]_2$) was washed with hexanes and cold diethyl ether (Et_2O) several times, dried, and used without further purification.[48]

A solution of $[Ir(\mu\text{-}Cl)(\mathbf{3\text{-}H})_2]_2$ (150 mg, 0.12 mmol) and AgOTf (91 mg, 0.35 mmol) was dissolved in a mixture of CH_2Cl_2 and CH_3OH (1:1). The solution was stirred under inert conditions for 6 h. The reaction mixture was filtered through Celite to remove precipitates. The filtrate was concentrated in vacuo, and the resultant residues were solidified with hexanes. The target product (orange powder; 41 mg, yield 22%) was collected by additional crystallization with $CHCl_3$ and hexanes. ^{1}H NMR [400

MHz, DMSO-d_6, δ (ppm)]: 9.12 (d, J = 8.8 Hz, 2H), 8.68 (d, J = 8.8 Hz, 2H), 8.46 (d, J = 8.8 Hz, 2H), 8.16 (d, J = 8.0 Hz, 2H), 7.96 (d, J = 7.6 Hz, 2H), 7.87 (t, J = 8.4 Hz, 2H), 7.73 (t, J = 7.2 Hz, 2H), 6.86 (t, J = 7.2 Hz, 2H), 6.55 (t, J = 7.2 Hz, 2H), 6.03 (d, J = 7.6 Hz, 2H).

3.4.2.8. Preparation of Ir-Me

Ir-Me was synthesized by the same procedure as **Ir-H** using **3-Me** (700 mg, 3.2 mmol), $IrCl_3 \cdot nH_2O$ (433 mg, 1.5 mmol), [Ir(μ-Cl)(**3-Me**)$_2$]$_2$ (132 mg, 0.10 mmol), and AgOTf (77 mg, 0.30 mmol) (red powder; 72 mg, yield 44%). ^{1}H NMR [400 MHz, DMSO-d_6, δ (ppm)]: 9.06 (d, J = 8.4 Hz, 2H), 8.66 (d, J = 8.8 Hz, 2H), 8.41 (d, J = 8.8 Hz, 2H), 8.16 (dd, J = 8.1, 1.5 Hz, 2H), 7.83-7.90 (m, 4H), 7.72 (ddd, J = 8.0, 6.8, 1.1 Hz, 2H), 6.72 (d, J = 8.8 Hz, 2H), 5.89 (s, 2H), 1.85 (s, 6H). ^{13}C NMR [100 MHz, DMSO-d_6, δ (ppm)]: 169.8, 148.4, 144.0, 141.5, 140.2, 139.1, 134.8, 131.2, 128.7, 127.5, 126.6, 126.5, 126.3, 123.0, 122.3, 119.1, 117.1, 21.2. FT-IR (neat cm^{-1}): 3361 (br), 3088, 2916, 1606, 1579, 1554, 1520, 1451, 1430, 1338, 1247, 1226, 1170, 1075, 1027, 988, 962, 876, 817, 785, 762, 734, 681, 662. HRMS for [M - 2H_2O - OTf]$^+$ Calcd, 629.1563; found, 629.1564.

3.4.2.9. Preparation of Ir-F

Ir-F was synthesized by the same procedure as **Ir-H** using **3-F** (616 mg, 2.8 mmol), $IrCl_3 \cdot nH_2O$ (358 mg, 1.2 mmol), [Ir(μ-Cl)(**3-F**)$_2$]$_2$ (134 mg, 0.10 mmol), and AgOTf (77 mg, 0.30 mmol) (orange powder; 67 mg, yield 41%). ^{1}H NMR [400 MHz, DMSO-d_6, δ (ppm)]: 9.08 (d, J = 8.8 Hz, 2H), 8.75 (d, J = 8.7 Hz, 2H), 8.50 (d, J = 8.8 Hz, 2H), 8.21 (dd, J = 8.1, 1.5 Hz, 2H), 8.12 (dd, J = 8.7, 5.9 Hz, 2H), 7.92 (ddd, J = 8.7, 6.8, 1.5 Hz, 2H), 7.78 (ddd, J = 8.0, 6.8, 1.1 Hz, 2H), 6.79 (td, J = 8.8, 2.6 Hz, 2H), 5.67 (dd, J = 9.9, 2.5 Hz, 2H). ^{13}C NMR [100 MHz, DMSO-d_6, δ (ppm)]: 168.8, 162.9, 160.4, 148.2, 143.8, 143.8, 143.3, 140.9, 131.7, 129.1, 129.0, 128.9, 127.7, 127.1, 125.9, 122.3, 119.7, 119.6, 119.1, 117.5, 109.5, 109.3. FT-IR (neat cm^{-1}): 3359 (br), 3088, 2933, 2860, 1595, 1571, 1550, 1516, 1469, 1451, 1432, 1395, 1341, 1297, 1232, 1194, 1182, 1149, 1070, 1025, 980, 962, 889, 864, 847, 834, 804, 782, 744, 709, 675, 662. HRMS for [M - 2H_2O - OTf]$^+$ Calcd, 637.1062; found, 637.1060.

3.4.2.10. Preparation of Ir-F2

Ir-F2 was synthesized by the same procedure as **Ir-H** using **3-F2** (927 mg, 3.8 mmol), $IrCl_3 \cdot nH_2O$ (459 mg, 1.5 mmol), [Ir(μ-Cl)(**3-F2**)$_2$]$_2$ (100 mg, 0.071 mmol), and AgOTf (54 mg, 0.21 mmol) (orange powder; 18 mg, yield 15%). ^{1}H NMR [400 MHz, DMSO-d_6, δ (ppm)]: 8.89 (d, J = 8.8 Hz, 2H), 8.80 (d, J = 9.2 Hz, 2H), 8.51 (d, J = 9.2 Hz, 2H), 8.22 (d, J = 8.4 Hz, 2H), 7.92 (t, J = 7.2 Hz, 2H), 7.79 (t, J = 7.2 Hz, 2H), 6.86 (t, J = 11 Hz, 2H), 5.63 (d, J = 8.8 Hz, 2H). ^{13}C NMR [100 MHz, DMSO-d_6, δ (ppm)]: 167.0, 166.9, 163.4, 162.4, 160.8, 160.7, 159.9, 159.8, 148.5, 145.3, 142.2, 137.6, 132.5, 132.0, 131.9, 131.2, 130.7, 129.4, 128.4, 128.0, 127.9, 127.5, 126.6, 122.8, 120.4, 120.2, 119.6, 117.3, 117.1, 99.7, 99.4, 99.1. FT-IR (neat cm^{-1}): 3319 (br), 3081, 2935, 1597, 1556, 1518, 1433, 1411, 1317, 1295,

1216, 1190, 1162, 1106, 1019, 992, 830, 756. HRMS for $[M - 2H_2O - OTf]^+$ Calcd, 673.0868; found, 673.0864.

3.4.3. Photophysical Properties of Ir(III) Complexes

Absorption and emission spectra of the solution of Ir(III) complexes (20 μM in H_2O; final 1% v/v DMSO) with or without histidine (His) or $A\beta_{28}$ (200 μM in H_2O) were recorded at 298 K by UV-Vis and fluorescence spectroscopy, respectively. Quantum yield (Φ) was calculated following previously reported procedures. [Ir(2-phenylquinoline)$_2$(2,2'-bipyridine)]Cl (Φ_{ref} = 0.53 in H_2O, 1% v/v DMSO) was used as a reference.[40] For lifetime measurements, time-correlated single photon counting (TCSPC) was performed. The second harmonic generation (SHG = 420 nm) of a tunable Ti:sapphire laser with ca. 150 fs pulse width and 76 MHz repetition rate was used as an excitation source. The emission was spectrally resolved by using some collection optics and a monochromator. The TCSPC module with an MCP-PMT was used for ultrafast detection. The total instrument response function (IRF) for measuring the fluorescence decay was less than 150 ps, and the temporal time resolution was less than 10 ps. The deconvolution of the actual fluorescence decay and IRF was fitted by using the FluoFit software to deduce the time constant associated with each exponential decay. Radiative decay constant (k_r) and nonradiative decay constant (k_{nr}) were calculated on the basis of previously reported equations.[65]

3.4.4. Histidine Binding Affinities of Ir(III) Complexes

The solution of **Ir-Me**, **Ir-H**, **Ir-F**, or **Ir-F2** (20 μM in H_2O, 1% v/v DMSO) with or without His (200 μM) was measured by ESI-MS (Agilent 1200 and Bruker HCT). Dissociation constants (K_d) were determined through His titration experiments. Fluorescence intensity of the solution of **Ir-Me**, **Ir-H**, **Ir-F**, or **Ir-F2** (2 μM in H_2O; 1% v/v DMSO) with His (0-60 μM) was measured after 2 h incubation without agitation at room temperature. The resultant titration points were fitted to the Hill's equation [$y = V_{max} \{x^n / (x^n + k^n)\}$] [$V_{max}$, emission intensity of complete saturation; n, cooperativity; k, half maximal effective concentration (EC_{50})] in non-linear curve fit (OriginPro 2015, OriginLab Corporation, Northampton, MA, USA) and the K_d values were calculated by the obtained constant [$K_d = k^n$].

3.4.5. Singlet Oxygen ($^1O_2$) Generation by Ir(III) Complexes

The amounts of singlet oxygen ($^1O_2$) generated upon treatment with **Ir-Me**, **Ir-H**, **Ir-F**, and **Ir-F2** were determined according to the method reported previously.[40] Solutions containing Ir(III) complexes (10 μM in H_2O, 1% v/v DMSO) and 9,10-anthracenediyl-bis(methylene)dimalonic acid (ABDA as a $^1O_2$ substrate, 100 μM) with or without His (10 μM) were irradiated with 40% of 1 sun light (40 $mWcm^{-2}$; optimized intensity for ABDA not to be degraded). The absorbance of ABDA was measured for 7.5 min with a 2.5 min interval.

3.4.6. Electrospray Ionization-Ion Mobility-Mass Spectrometry (ESI-IM-MS)

(i) [$A\beta_{40}$ (100 μM) with **Ir-Me**, **Ir-H**, **Ir-F**, or **Ir-F2** (500 μM)] and (ii) [$A\beta_{28}$ and/or $A\beta_{42}$ (100 μM) with **Ir-F** (100 μM)] upon 10 min exposure to 1 sun light were incubated in H_2O at 37 °C for 1 h without agitation. The incubated samples were diluted by 10 fold and then injected into a mass spectrometer. The capillary voltage, sampling cone voltage, and source temperature were set to 2.8 kV, 70 V, and 60 °C, respectively. The backing pressure was adjusted to 3.2 mbar. Ion mobility wave height and velocity were adjusted to 10 V and 450 ms^{-1}, respectively, and gas flow for the helium cell and ion mobility cell was set to 120 and 30 $mLmin^{-1}$, respectively. Tandem MS (MS^2) analysis was additionally performed on the +3-charged [$A\beta_{40}$ + **Ir-F'**] (*m/z* = 1656) and singly oxidized $A\beta_{40}$ (*m/z* = 1449). The ESI parameters and experimental conditions were same as above. Collision-induced dissociation was conducted by applying the collision energy in the trap. More than 200 spectra were obtained for each sample and averaged for analysis.

3.4.7. Aβ Aggregation Experiments

Aβ experiments were conducted as previously published.[19] Aβ peptides were dissolved with ammonium hydroxide (NH_4OH, 1% v/v, aq), aliquoted, lyophilized, and stored at -80 °C. A stock solution (ca. 200 μM) was prepared by re-dissolving Aβ with NH_4OH (1% w/v, aq, 10 μL) followed by dilution with H_2O. The peptide concentration in solution was determined by measuring the absorbance of the solution at 280 nm (ε = 1450 $M^{-1}cm^{-1}$ for $A\beta_{40}$; ε = 1490 $M^{-1}cm^{-1}$ for $A\beta_{42}$ and $A\beta_{28}$). (i) For the inhibition experiments, Aβ (25 μM; H_2O) was first treated with Ir(III) complexes (i.e., **Ir-Me**, **Ir-H**, **Ir-F**, or **Ir-F2**; 250 μM; 5% v/v final DMSO concentration) followed by exposure to 1 sun light for 10 min. The resulting samples were incubated at 37 °C for 24 h with constant agitation. (ii) For the disaggregation experiments, Aβ (25 μM; H_2O) was initially incubated at 37 °C for 2, 4, or 24 h with steady agitation. Ir(III) complexes (250 μM; 5% v/v final DMSO concentration) were added to the preincubated Aβ samples with or without 1 sun light for 10 min followed by an additional 4 h of incubation at 37 °C with constant agitation. (iii) For $A\beta_{28}$ experiments, $A\beta_{28}$ (50 μM; H_2O) was treated with **Ir-F** (10 μM; 1% v/v final DMSO concentration) and incubated at 37 °C for 1 h with steady agitation. $A\beta_{42}$ (20 μM; H_2O) was treated to the $A\beta_{28}$–**Ir-F'** sample followed by exposure to 1 sun light for 10 min. The resulting samples were incubated at 37 °C for 1 h with constant agitation. For the experiments under anaerobic conditions, all samples were prepared following the same procedure described above for the aerobic samples in a N_2-filled glovebox.

3.4.8. Gel Electrophoresis with Western Blotting (Gel/Western Blot)

The resultant Aβ species from both inhibition and disaggregation experiments were analyzed by gel electrophoresis followed by Western blotting (gel/Western blot) using an anti-Aβ antibody (6E10;

Covance, Princeton, NJ, USA) or anti-$A\beta_{42}$ antibody (Merck KGaA).[19] Each sample (10 μL) was separated using a 10–20% gradient Tris-tricine gel (Invitrogen, Grand Island, NY, USA). The gel was transferred to a nitrocellulose membrane and blocked with a bovine serum albumin (BSA) solution (3% w/v; Sigma, St. Louis, MO, USA) in Tris-buffered saline (TBS; Fisher, Pittsburgh, PA, USA) containing 0.1% Tween-20 (TBS-T; Sigma-Aldrich) for 3 h at room temperature. The membrane was treated with either an anti-Aβ antibody [6E10; 1:2,000] or an anti-$A\beta_{42}$ antibody (1:2,000) in a solution of 2% BSA (w/v, in TBS-T) for 4 h at room temperature and then incubated with a horseradish peroxidase-conjugated goat anti-mouse secondary antibody (Cayman Chemical, Ann Arbor, MI, USA; 1:5,000) for 6E10-treated membranes or a horseradish peroxidase-conjugated anti-rabbit secondary antibody (Promega, Madison, WI, USA; 1:2,500) for anti-$A\beta_{42}$ antibody-treated membranes in 2% BSA in TBS-T solution (w/v) for 1 h at room temperature. A self-made ECL solution (2.5 mM luminol, 0.20 mM *p*-coumaric acid, and 0.018% H_2O_2 in 100 mM Tris, pH 8.6) was used to visualize the results on a ChemiDoc MP Imaging System (BioRad, Hercules, CA, USA).

3.4.9. Transmission Electron Microscopy (TEM)

Aβ samples for TEM were prepared following the previously reported methods.[19] Glow discharged grids (Formvar/Carbon 300-mesh; Electron Microscopy Sciences, Hatfield, PA, USA) were treated with the resultant Aβ (5 μL) for 2 min at room temperature. Excess sample was removed with filter paper and the grids were washed with H_2O three times. Each grid was stained with uranyl acetate (1% w/v H_2O; 5 μL) for 1 min. Uranyl acetate was blotted off and grids were dried for 20 min at room temperature. Images of samples were taken by a JEOL JEM-2100 transmission electron microscope (200 kV, 25000× magnification).

3.4.10. Cytotoxicity Studies

Mouse Neuro-2a (N2a) neuroblastoma cells were purchased from the American Type Cell Collection (ATCC, Manassas, VA, USA). Cells were maintained in the media containing 50% DMEM (GIBCO, Grand Island, NY, USA) and 50% opti-MEM (GIBCO), supplemented with 5% (v/v) fetal bovine serum (FBS; GIBCO), 1% (v/v) L-glutamine (GIBCO), 100 U/mL penicillin, and 100 mg/mL streptomycin (GIBCO). The cells were grown in a humidified atmosphere with 5% CO_2 at 37 °C. Cell viability was determined by the MTT assay [MTT = 3-(4,5-dimethyl-2-thiazolyl)-2,5-diphenyl-2*H*-tetrazolium bromide, Sigma-Aldrich]. The cells were seeded in a 96 well plate (15,000 cells in 100 μL per well). (i) To identify the cytotoxicity of Ir(III) complexes, the cells were treated with their various concentrations (5, 10, 25, 50, or 100 μM; 1% v/v final DMSO concentration) and incubated for 24 h. (ii) For the experiments with Aβ, Aβ ($A\beta_{40}$ or $A\beta_{42}$; final concentration, 20 μM) was added with the Ir(III) complexes (final concentration, 5 μM) exposed to 1 sun light for 10 min, and incubated for 24 h at

37 °C. The resultant Aβ species were treated with cells. After 24 h incubation, MTT [25 μM; 5 mgmL^{-1} in PBS (pH 7.4, GIBCO)] was incubated to each well and the plate was incubated for 3 h at 37 °C. Formazan produced by the cells was solubilized by addition of an acidic solution of *N*,*N*-dimethylformamide (DMF, 50% v/v, aq, pH 4.5) and sodium dodecyl sulfate (SDS, 20% w/v) overnight at room temperature in the dark. The absorbance was measured at 600 nm using a microplate reader. Cell viability was calculated relative to cells containing an equivalent amount of DMSO. Error bars were calculated as standard errors of mean (S.E.M.) from three independent experiments. For comparisons between two groups, Student's two-tailed unpaired *t* test was employed. Statistical difference was considered significant at $*P < 0.05$.

3.5. Acknowledgments

This work was supported by the National Research Foundation of Korea (NRF) grant funded by the Korean government [NRF-2017R1A2B3002585 and NRF-2016R1A5A1009405 (to M.H.L.); 2016R1A2B4009239 (to. T.-H.K.)]. J.K. acknowledges the Global Ph.D. fellowship program through the NRF funded by the Ministry of Education (NRF-2015HIA2A1030823). J.S.N. is grateful for the support from the ASAN Foundation biomedical science scholarship. We also thank Dr. Shin Jung C. Lee and Yonghwan Ji for the assistance with initial MS measurements with data analysis.

3.6. References

(1) Savelieff, M. G.; Nam, G.; Kang, J.; Lee, H. J.; Lee, M.; Lim, M. H. *Chem. Rev.* **2019**, *119*,1221–1322.
(2) Hamley, I. W. *Chem. Rev.* **2012**, *112*, 5147–5192.
(3) Kepp, K. P. *Coord. Chem. Rev.* **2017**, *351*, 127–159.
(4) Jakob-Roetne, R.; Jacobsen, H. *Angew. Chem. Int. Ed.* **2009**, *48*, 3030–3059.
(5) Hardy, J. A.; Higgins, G. A. *Science* **1992**, *256*, 184–185.
(6) Morris, G. P.; Clark, I. A.; Vissel, B. *Acta Neuropathol.* **2018**, *136*, 663–689.
(7) Lee, S. J. C.; Nam, E.; Lee, H. J.; Savelieff, M. G.; Lim, M. H. *Chem. Soc. Rev.* **2017**, *46*, 310–323.
(8) Zamora, A.; Vigueras, G.; Rodríguez, V.; Santana, M. D.; Ruiz, J. *Coord. Chem. Rev.* **2018**, *360*, 34–76.
(9) Haas, K. L.; Franz, K. J. *Chem. Rev.* **2009**, *109*, 4921–4960.
(10) Wai-Yin Sun, R.; Ma, D.-L.; Wong, E. L.-M.; Che, C.-M. *Dalton Trans.* **2007**, 0, 4884–4892.
(11) Leung, C.-H.; Zhong, H.-J.; Chan, D. S.-H.; Ma, D.-L. *Coord. Chem. Rev.* **2013**, *257*, 1764–1776.
(12) Leung, C.-H.; Lin, S.; Zhong, H.-J.; Ma, D.-L. *Chem. Sci.* **2015**, *6*, 871–884.
(13) Fancy, D. A.; Kodadek, T. *Proc. Natl. Acad. Sci. U.S.A.* **1999**, *96*, 6020–6024.
(14) Kenche, V. B.; Hung, L. W.; Perez, K.; Volitakes, I.; Ciccotosto, G.; Kwok, J.; Critch, N.; Sherratt, N.; Cortes, M.; Lal, V.; Masters, C. L.; Murakami, K.; Cappai, R.; Adlard, P. A.; Barnham, K. J. *Angew. Chem. Int. Ed.* **2013**, *52*, 3374–3378.
(15) Zhen, W.; Han, H.; Anguiano, M.; Lemere, C. A.; Cho, C.-G.P.; Lansbury, T. *J. Med. Chem.* **1999**, *42*, 2805–2815.

(16) Yellol, G. S.; Yellol, J. G.; Kenche, V. B.; Liu, X. M.; Barnham, K. J.; Donaire, A.; Janiak, C.; Ruiz, J. *Inorg. Chem.* **2015**, *54*, 470–475.
(17) Son, G.; Lee, B. I.; Chung, Y. J.; Park, C. B. *Acta Biomater.* **2018**, *67*, 147–155.
(18) He, L.; Wang, X.; Zhu, D.; Zhao, C.; Du, W. *Metallomics* **2015**, *7*, 1562–1572.
(19) Kang, J.; Lee, S. J. C.; Nam, J. S.; Lee, H. J.; Kang, M.-G.; Korshavn, K. J.; Kim, H.-T.; Cho, J.; Ramamoorthy, A.; Rhee, H.-W.; Kwon, T.-H.; Lim, M. H. *Chem. Eur. J.* **2017**, *23*, 1645–1653.
(20) Man, B. Y.-W.; Chan, H.-M.; Leung, C.-H.; Chan, D. S.-H.; Bai, L.-P.; Jiang, Z.-H.; Li, H.-W.; Ma, D.-L. *Chem. Sci.* **2011**, *2*, 917–921.
(21) Hayne, D. J.; Lim, S.; Donnelly, P. S. *Chem. Soc. Rev.* **2014**, *43*, 6701–6715.
(22) Liu, H.; Qu, Y.; Wang, X. *Future Med. Chem.* **2018**, *10*, 679–701.
(23) Barnham, K. J.; Kenche, V. B.; Ciccotosto, G. D.; Smith, D. P.; Tew, D. J.; Liu, X.; Perez, K.; Cranston, G. A.; Johanssen, T. J.; Volitakis, I.; Bush, A. I.; Masters, C. L.; White, A. R.; Smith, J. P.; Cherny, R. A.; Cappai, R. *Proc. Natl. Acad. Sci. U.S.A.* **2008**, *105*, 6813–6818.
(24) Lee, B. I.; Lee, S.; Suh, Y. S.; Lee, J. S.; Kim, A.-k.; Kwon, O-Y.; Yu, K.; Park, C. B. *Angew. Chem. Int. Ed.* **2015**, *54*, 11472–11476.
(25) Aliyan, A.; Paul, T. J.; Jiang, B.; Pennington, C.; Sharma, G.; Prabhakar, R.; Martí, A. A. *Chem* **2017**, *3*, 898–912.
(26) Messori, L.; Camarri, M.; Ferraro, T.; Gabbiani, C.; Franceschini, D. *ACS Med. Chem. Lett.* **2013**, *4*, 329–332.
(27) Wang, X.; Wang, X.; Zhang, C.; Jiao, Y.; Guo, Z. *Chem. Sci.* **2012**, *3*, 1304–1312.
(28) Kumar, A.; Moody, L.; Olaivar, J. F.; Lewis, N. A.; Khade, R. L.; Holder, A. A.; Zhang, Y.; Rangachari, V. *ACS Chem. Neurosci.* **2010**, *1*, 691–701.
(29) Suh, J.-M.; Kim, G.; Kang, J.; Lim, M. H. *Inorg. Chem.* **2019**, *58*, 8–17.
(30) Wong, C.-Y.; Chung, L.-H.; Lu, L.; Wang, M.; He, B.; Liu, L.-J.; Leung, C.-H.; Ma, D.-L. *Curr. Alzheimer Res.* **2015**, *12*, 439–444.
(31) Lu, L.; Zhong, H.-J.; Wang, M.; Ho, S.-L.; Li, H.-W.; Leung, C.-H.; Ma, D.-L. *Sci. Rep.* **2015**, *5*, 14619.
(32) Suh, J.; Yoo, S. H.; Kim, M. G.; Jeong, K.; Ahn, J. Y.; Kim, M.-s.; Chae, P. S.; Lee, T. Y.; Lee, J.; Lee, J.; Jang, Y. A.; Ko, E. H. *Angew. Chem. Int. Ed.* **2007**, *46*, 7064–7067.
(33) Derrick, J. S.; Lee, J.; Lee, S. J. C.; Kim, Y.; Nam, E.; Tak, H.; Kang, J.; Lee, M.; Kim, S. H.; Park, K.; Cho, J.; Lim, M. H. *J. Am. Chem. Soc.* **2017**, *139*, 2234–2244.
(34) Wu, W.-h.; Lei, P.; Liu, Q.; Hu, J.; Gunn, A. P.; Chen, M.-s.; Rui, Y.-f.; Su, X.-y.; Xie, Z.-p.; Zhao, Y.-F.; Bush, A. I.; Li, Y.-m. *J. Biol. Chem.* **2008**, *283*, 31657–31664.
(35) Donnelly, P. S.; Caragounis, A.; Du, T.; Laughton, K. M.; Volitakis, I.; Cherny, R. A.; Sharples, R. A.; Hill, A. F.; Li, Q.-X.; Masters, C. L.; Barnham, K. J.; White, A. R. *J. Biol. Chem.* **2008**, *283*, 4568–4577.
(36) Sasaki, I.; Bijani, C.; Ladeira, S.; Bourdon, V.; Faller, P.; Hureau, C. *Dalton Trans.* **2012**, *41*, 6404–6407.
(37) Valensin, D.; Anzini, P.; Gaggelli, E.; Gaggelli, N.; Tamasi, G.; Cini, R.; Gabbiani, C.; Michelucci, E.; Messori, L.; Kozlowski, H.; Valensin, G. *Inorg. Chem.* **2010**, *49*, 4720–4722.
(38) You, Y. *Curr. Opin. Chem. Biol.* **2013**, *17*, 699–707.
(39) Lowry, M. S.; Bernhard, S. *Chem. Eur. J.* **2006**, *12*, 7970–7977.
(40) Nam, J. S.; Kang, M.-G.; Kang, J.; Park, S.-Y.; Lee, S. J. C.; Kim, H.-T.; Seo, J. K.; Kwon, O.-H.; Lim, M. H.; Rhee, H.-W.; Kwon, T.-H. *J. Am. Chem. Soc.* **2016**, *138*, 10968–10977.
(41) Gao, R.; Ho, D. G.; Hernandez, B.; Selke, M.; Murphy, D.; Djurovich, P. I.; Thompson, M. E. *J. Am. Chem. Soc.* **2002**, *124*, 14828–14829.

(42) Liu, Z.; Sadler, P. J. *Acc. Chem. Res.* **2014**, *47*, 1174–1185.
(43) Wragg, A.; Gill, M. R.; Turton, D.; Adams, H.; Roseveare, T. M.; Smythe, C.; Su, X.; Thomas, J. A. *Chem. Eur. J.* **2014**, *20*, 14004–14011.
(44) Zhao, J.; Yu, Y.; Yang, X.; Yan, X.; Zhang, H.; Xu, X.; Zhou, G.; Wu, Z.; Ren, Y.; Wong, W.-Y. *ACS Appl. Mater. Interfaces* **2015**, *7*, 24703–24714.
(45) Etheridge, F. S.; Fernando, R. J.; Pejić, S.; Zeller, M.; Sauvé, G. *Beilstein J. Org. Chem.* **2016**, *12*, 1925–1938.
(46) Ma, D.-L.; Wong, W.-L.; Chung, W.-H.; Chan, F.-Y.; So, P.-K.; Lai, T.-S.; Zhou, Z.-Y.; Leung, Y.-C.; Wong, K.-Y. *Angew. Chem. Int. Ed.* **2008**, *47*, 3735–3739.
(47) Ma, D.-L.; Zhong, H.-J.; Fu, W.-C.; Chan, D. S.-H.; Kwan, H.-Y.; Fong, W.-F.; Chung, L.-H.; Wong, C.-Y.; Leung, C.-H. *PLoS ONE* **2013**, *8*, e55751.
(48) Matsuo, N. *Bulletin. Chem. Soc. Japan.* **1974**, *47*, 767–768.
(49) Schmid, B.; Garces, F. O.; Watts, R. J. *Inorg. Chem.* **1994**, *33*, 9–14.
(50) McDaniel, N. D.; Coughlin, F. J.; Tinker, L. L.; Bernhard, S. *J. Am. Chem. Soc.* **2008**, *130*, 210–217.
(51) Han, J.; Lee, H. J.; Kim, K. Y.; Lee, S. J. C.; Suh, J.-M.; Cho, J.; Chae, J.; Lim, M. H. *ACS Chem. Neurosci.* **2018**, *9*, 800–808.
(52) Bitan, G.; Tarus, B.; Vollers, S. S.; Lashuel, H. A.; Condron, M. M.; Straub, J. E.; Teplow, D. B. *J. Am. Chem. Soc.* **2003**, *125*, 15359–15365.
(53) Hou, L.; Kang, I.; Marchant, R. E.; Zagorski, M. G. *J. Biol. Chem.* **2002**, *277*, 40173–40176.
(54) Liao, S.-M.; Du, Q.-S.; Meng, J.-Z.; Pang, Z.-W.; Huang, R.-B. *Chem. Cent. J.* **2013**, *7*, 44.
(55) Brännström, K.; Islam, T.; Sandblad, L.; Olofsson, A. *FEBS Lett.* **2017**, *591*, 1167–1175.
(56) Kadlcik, V.; Sicard-Roselli, C.; Houée-Levin, C.; Kodicek, M.; Ferreri, C.; Chatgilialoglu, C. *Angew. Chem. Int. Ed.* **2006**, *45*, 2595–2598.
(57) Bieschke, J.; Russ, J.; Friedrich, R. P.; Ehrnhoefer, D. E.; Wobst, H.; Neugebauer, K.; Wanker, E. E. *Proc. Natl. Acad. Sci. U.S.A.* **2010**, *107*, 7710–7715.
(58) Hyung, S.-J.; DeToma, A. S.; Brender, J. R.; Lee, S.; Vivekanandan, S.; Kochi, A.; Choi, J.-S.; Ramamoorthy, A.; Ruotolo, B. T.; Lim, M. H. *Proc. Natl. Acad. Sci. U.S.A.* **2013**, *110*, 3743–3748.
(59) Cheignon, C.; Tomas, M.; Bonnefont-Rousselot, D.; Faller, P.; Hureau, C.; Collin, F. *Redox Biol.* **2018**, *14*, 450–464.
(60) Telpoukhovskaia, M. A.; Orvig, C. *Chem. Soc. Rev.* **2013**, *42*, 1836–1846.
(61) Klajnert, B.; Wasiak, T.; Ionov, M.; Fernandez-Villamarin, M.; Sousa-Herves, A.; Correa, J.; Riguera, R.; Fernandez-Megia, E. *Nanomedicine* **2012**, *8*, 1372–1378.
(62) Savelieff, M. G.; Lee, S.; Liu, Y.; Lim, M. H. *ACS Chem. Biol.* **2013**, *8*, 856–865.
(63) Haddenham, D.; Bailey, C. L.; Vu, C.; Nepomuceno, G.; Eagon, S.; Pasumansky, L.; Singaram, B. *Tetrahedron* **2011**, *67*, 576–583.
(64) Yu, J.; He, K.; Li, Y.; Tan, H.; Zhu, M.; Wang, Y.; Liu, Y.; Zhu, W.; Wu, H. *Dyes and Pigm.* **2014**, *107*, 146–152.
(65) Kwon, T.-H.; Cho, H. S.; Kim, M. K.; Kim, J.-W.; Kim, J.-J.; Lee, K. H.; Park, S. J.; Shin, I.-S.; Kim, H.; Shin, D. M.; Chung, Y. K.; Hong, J.-I. *Organometallics* **2005**, *24*, 1578–1585.

Chapter 4.

Monitoring Metal–Amyloid-β Complexation by a FRET-based Probe: Design, Detection, and Inhibitor Screening

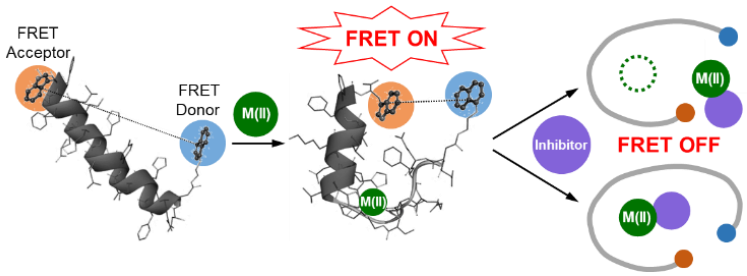

The results and results presented in this chapter were reported in the publication [Lee, H. J.;† Lee, Y. G.;† Kang, J.;† Yang, S. H.; Kim, J. H.; Ghisaidoobe, A. B. T.; Kang, H. J.; Lee, S.-R.; Lim, M. H.; Chung, S. J. *Chem. Sci.* **2019**, *10*, 1000–1007 (†equal contribution)]. Professor Sang J. Chung, Dr. Sang-Rae Lee, Professor Hyo Jin Kang, Young Geun Lee, Seung Hyun Yang, Ju Hwan Kim, and Amar B. T. Ghisaidoobe prepared **A-1**, measured its photophysical properties in the absence and presence of Zn(II) with data analysis, visualized possible binding modes between **A-1** and Zn(II) by modeling, and conducted inhibitor screening. Dr. Hyuck Jin Lee performed the FRET measurements and the mass spectrometric investigations with data analysis and TEM. I and Dr. Hyuck Jin Lee performed cell studies and analyzed the data. I and Dr. Hyuck Jin Lee wrote the manuscript with the guidance of Professor Mi Hee Lim.

4.1. Introduction

The number of aged people affected by neurodegenerative diseases has been increasing; however, the development of treatments for the diseases has not been successful due to the lack of understanding about their pathogenesis.[1,2] The proposed risk factors of neurodegenerative diseases include metal ions [e.g., Zn(II)] and amyloidogenic peptides [e.g., amyloid-β (Aβ) and tau for Alzheimer's disease, α-synuclein for Parkinson's disease, and huntingtin for Huntington's disease].[3–12] Toxic aggregates are formed upon aggregation of these amyloidogenic peptides, particularly in the presence of metal ions.[2,13–15] The aggregation and conformational changes of such amyloidogenic peptides have been previously studied by luminescence, including Förster resonance energy transfer (FRET).[16–21] In addition, the interactions between amyloidogenic peptides and metal ions (e.g., binding affinity and coordination geometry) have been investigated through multiple physical methods.[8,9,22–26] Such approaches, however, require high concentrations of peptides and metal ions (e.g., high μM) presenting significant challenge in performing the experiments due to the aggregation-prone properties of amyloidogenic peptides. Unfortunately, detecting the formation of metal-bound amyloidogenic peptides with a straightforward and efficient method (e.g., monitoring a turn-on signal) at a low concentration (ca. nM) has not been reported. Herein, we report a FRET-based probe (**A-1**; Figure 4.1 and Scheme 4.1), composed of $A\beta_{1-21}$ grafted with a pair of FRET donor and acceptor, for monitoring metal–Aβ complexation at a nanomolar range with a turn-on FRET signal. The FRET intensity of **A-1** was observed to increase upon binding to Zn(II) (green; Figure 4.2). Note that although other metal ions [particularly, Cu(II)] are reported to interact with Aβ,[10,24] the use of our probe, **A-1**, is limited for paramagnetic metal ions, such as Cu(II), because its fluorescence is quenched (Figure 4.2). Additionally, the FRET signal of **A-1** was changed when (i) Zn(II) binding of **A-1** was interfered by the metal chelator, **EDTA** (ethylenediamine

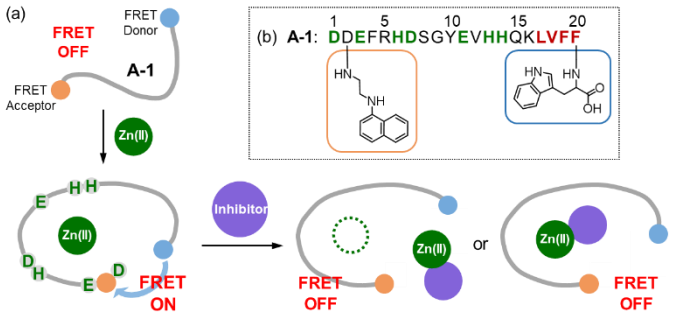

Figure 4.1. Design principle and sequence of the FRET-based probe, **A-1**. (a) FRET responses of **A-1** in the absence and presence of Zn(II) with and without inhibitors. (b) Amino acid sequence of **A-1**. **A-1** is composed of Trp (blue box) at the C-terminus as a FRET donor and 1-naphthylethylenediamine conjugated to the side chain of the Asp (orange box) at the N-terminus as a FRET acceptor. Proposed amino acid residues for metal binding and a portion of the self-recognition site are indicated in green and red, respectively.

Scheme 4.1. Synthetic routes to **A-1**.

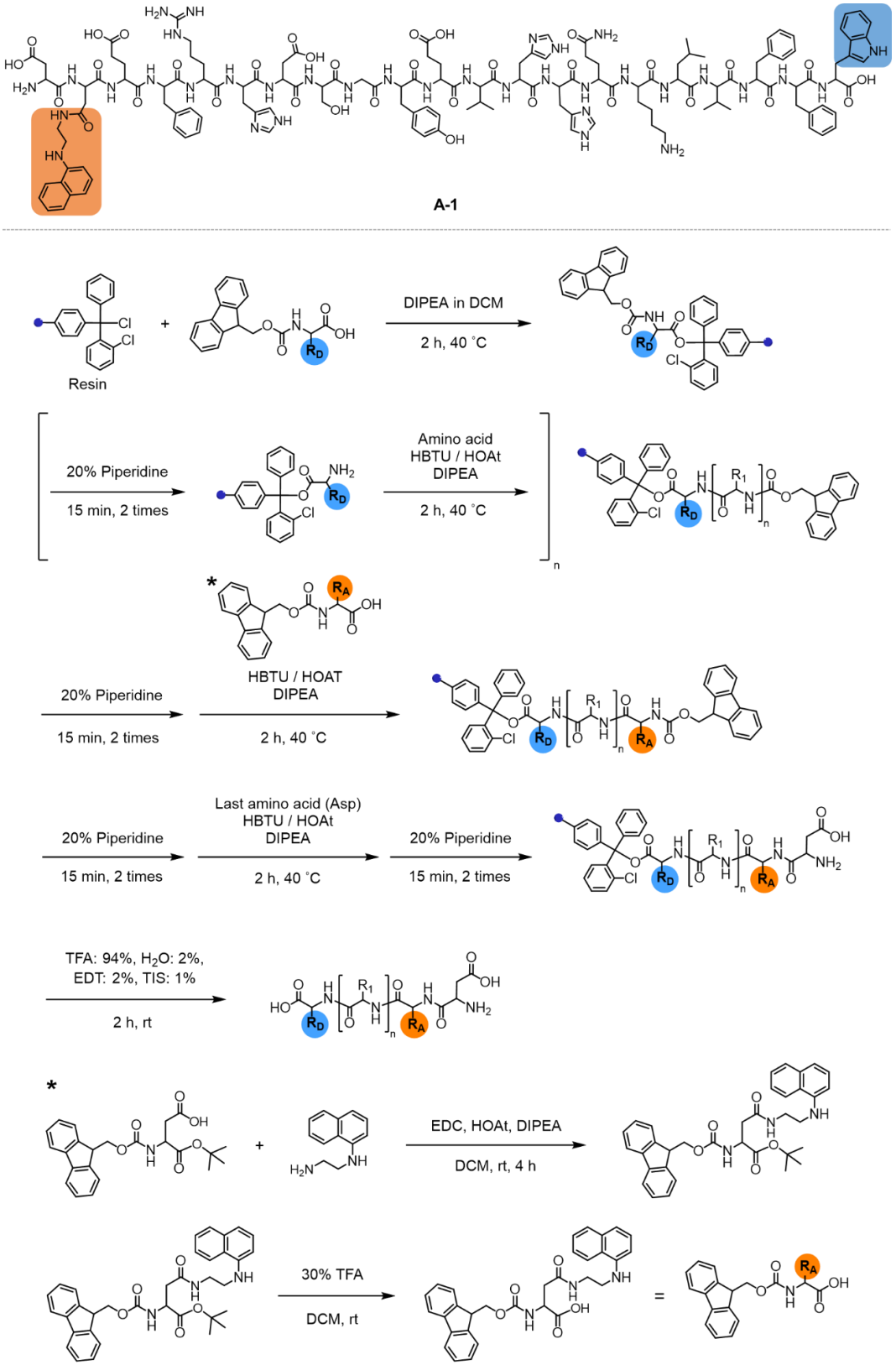

tetraacetic acid),[29] or the compound, **L2-b** [N^1N^1-dimethyl-N^4-(pyridin-2-ylmethyl)benzene-1,4-diamine],[30,31] capable of forming a ternary complex with Zn(II)–Aβ; (ii) the probe was aggregated. Moreover, a library of natural products as inhibitors against metal–Aβ interaction was screened based on the change in the FRET responses of Zn(II)-treated **A-1**. 8 out of 145 natural products were identified as effective inhibitors (> 80% inhibition) in vitro. Among the 8 molecules, 6 compounds were shown to lower the toxicity associated with Zn(II)–Aβ in living cells. Our studies demonstrate the feasibility of developing an efficient tactic to probe metal–amyloidogenic peptide complexation, along with its potential as a screening tool for drug discovery against neurodegenerative diseases.

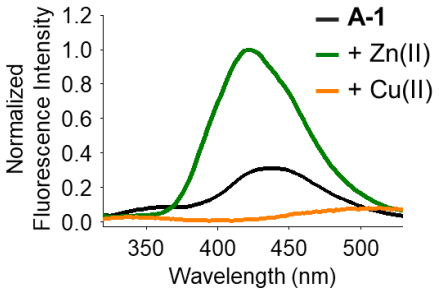

Figure 4.2. Fluorescent response of **A-1** (black) upon treatment with Zn(II) (green) or Cu(II) (orange). Conditions: [**A-1**] = 500 nM; [$ZnCl_2$] = 100 μM; [$CuCl_2$] = 500 μM; 10% DPBS; λ_{ex} = 280 nm; λ_{em} = 420 nm; room temperature.

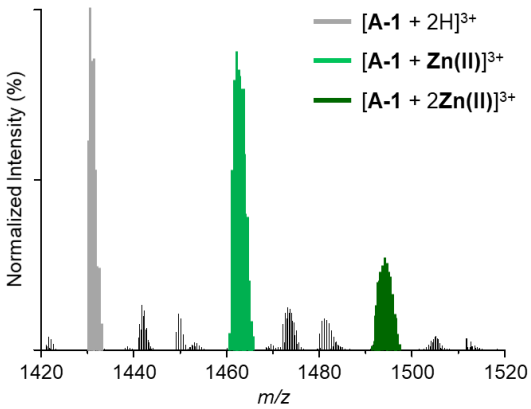

Figure 4.3. Zn(II) binding of **A-1**, monitored by MS. Conditions: [**A-1**] = 20 μM; [$ZnCl_2$] = 2.0 mM; incubation for 1 h; 20 mM ammonium acetate, pH 7.4; room temperature; no agitation.

4.2. Results and Discussion

4.2.1. Design and Preparation of A-1

Our probe, **A-1**, was designed to have a FRET donor (Trp; λ_{ex} = 280 nm, λ_{em} = 350 nm) and an acceptor (1-naphthylethylenediamine conjugated to the side chain of an Asp; λ_{ex} = 350 nm, λ_{em} = 420 nm) for FRET at the C- and N-termini of the $A\beta_{1–21}$ sequence, respectively (Figure 4.1). $A\beta_{1–21}$ was selected as the main framework of **A-1** to include the metal binding site of Aβ (Figure 4.1b; proposed metal binding residues highlighted in green, e.g., Asp1, Glu3, His6, Asp7, Glu11, His13, and His14).[10,26,32–35] Thus, **A-1** itself can interact with metal ions like Aβ. When **A-1** was treated with Zn(II), the Zn(II)–**A-1** complex was formed which was confirmed by mass spectrometry (MS) (Figure 4.3). Additionally, the binding affinity [K_d = 5.6 (± 0.9) μM] of **A-1** (5 μM) for Zn(II) was measured by a fluorescence measurement (Figure 4.4a), similar to the K_d values of Zn(II)–Aβ obtained using the same method from previous studies.[36–38] Moreover, the progression of peptide aggregation could be observed because **A-1** contains a portion of Aβ's self-recognition site (Figure 4.1b; red, Leu17–Phe20).[10,33,39] **A-1** was synthesized through solid phase peptide synthesis. The detailed synthetic routes are described in Scheme 4.1 and Experimental Section.

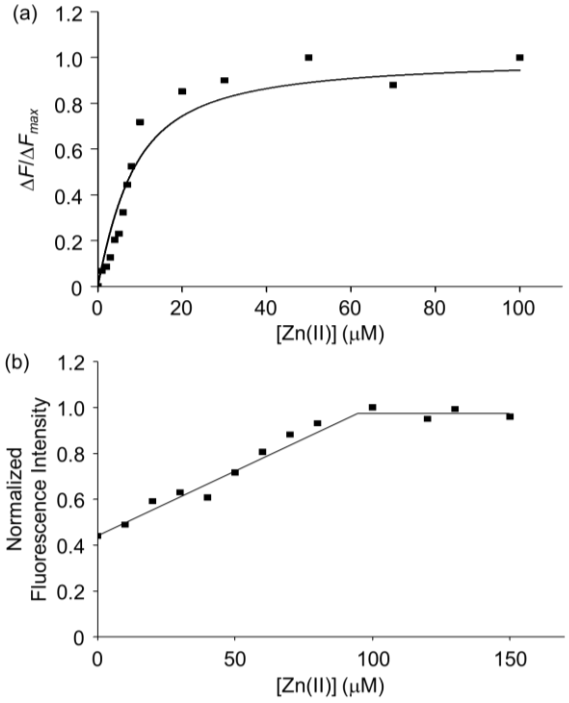

Figure 4.4. Variation of the FRET intensity of **A-1** (at 420 nm) upon titration with Zn(II). (a) Plot of $\Delta F/\Delta F_{max}$ of Zn(II)-bound **A-1** (5 μM) as a function of Zn(II) concentration. (b) Change in the fluorescence intensity of **A-1** (500 nM) upon treatment with various concentrations of Zn(II) at 420 nm. Conditions: [**A-1**] = 5 μM or 500 nM; [$ZnCl_2$] = 0–100 or 0–150 μM; 10% DPBS; λ_{ex} = 280 nm; λ_{em} = 420 nm; room temperature.

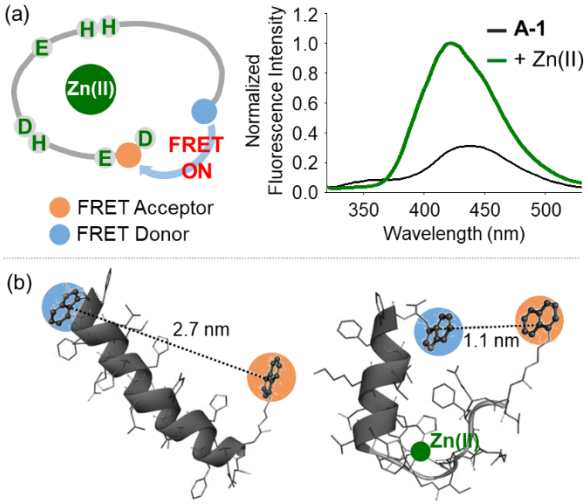

Figure 4.5. FRET response of **A-1** to Zn(II) and proposed structures of metal-free and Zn(II)-bound **A-1**. (a) Change in fluorescence upon incubation of **A-1** (black) with Zn(II) (green). Conditions: [**A-1**] = 0.5 μM; [$ZnCl_2$] = 100 μM; λ_{ex} = 280 nm. (b) Proposed structures of metal-free **A-1** (left) and Zn(II)-bound **A-1** (right). The structures were generated by modifications of the previously reported structures of metal-free Aβ (PDB: 1AMC)[27] and Zn(II)-bound Aβ (PDB:1ZE9).[28] The approximate distances between the FRET donor and acceptor were indicated with dashed lines.

4.2.2. FRET Signal of A-1 upon Zn(II) Binding

The presence of Zn(II) induced a significant turn-on FRET signal of **A-1** by > 2 fold compared to Zn(II)-free environment (Figure 4.5a). In order to minimize the aggregation of Zn(II)–**A-1** (vide infra; Figure 4.6), along with consideration of our probe's Zn(II) binding property, 250–500 nM of the probe and 100 μM of Zn(II) were used for this study. As shown in Figure 4.4b, the fluorescence intensity of **A-1** (500 nM) at 420 nm was enhanced upon titration and was saturated at ca. 100 μM of Zn(II). Since FRET occurs when a suitable donor and acceptor pair is in close proximity (1-10 nm) with the parallel orientation of the transition dipoles of the FRET donor and acceptor,[40,41] an increase in the FRET intensity is indicative of **A-1**'s folding upon Zn(II) binding (Figure 4.5a). The possible conformations of metal-free and Zn(II)-bound **A-1** were visualized by modeling with modifications of the previously reported structures of metal-free Aβ and Zn(II)-bound Aβ (PDB: 1AMC27 and 1ZE9,[28] respectively; Figure 4.5b). Without Zn(II), although the indole ring of the FRET donor and the naphthalene ring of the FRET acceptor are close enough for energy transfer (ca. 2.7 nm), they are not facing each other and shown to be unfavorable to have a dipole–dipole interaction for FRET (Figure 4.5b; left). Upon interacting with Zn(II), however, the indole and naphthalene rings become closer (ca. 1.1 nm) than those in metal-free **A-1** and are facing each other which could be favorable for the dipole–dipole interaction necessary for energy transfer, suggesting that an efficient FRET signal could be observed upon Zn(II) binding to the probe (Figure 4.5b; right). Additionally, the emission spectrum was blue shifted by ca. 25 nm possibly due to an environmental change of the FRET acceptor, naphthylamine, when **A-1** was

folded with Zn(II) treatment (Figure 4.5a; right). Note that we cannot rule out that intermolecular interactions resulted from **A-1**'s propensity to aggregate may induce the FRET.

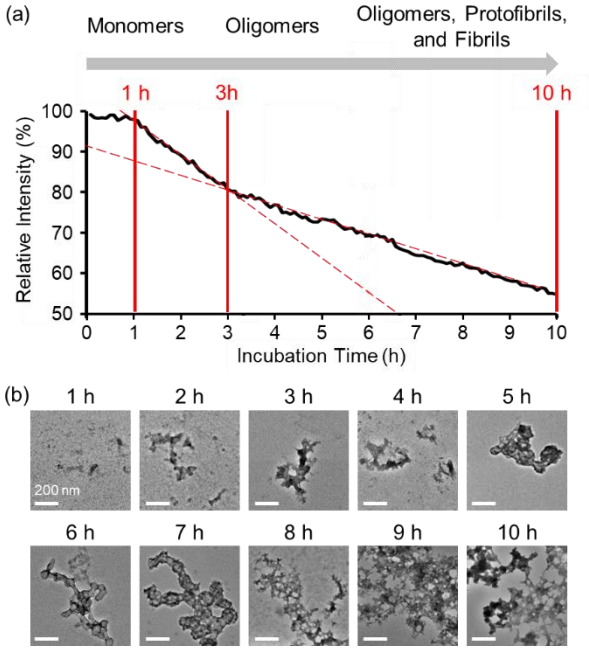

Figure 4.6. Time-dependent fluorescent response and aggregation progression of Zn(II)-treated **A-1**. (a) Change in the FRET signal of **A-1** with Zn(II) as a function of incubation time. (b) TEM images of Zn(II)-added **A-1** aggregates generated at various incubation time points (scale bar = 200 nm). Conditions: [**A-1**] = 0.25 μM (for FRET) and 2.5 μM (for TEM); [$ZnCl_2$] = 100 μM (for FRET) and 1 mM (for TEM); λ_{ex} = 280 mm; λ_{em} = 420 nm; incubation up to 10 h; room temperature.

4.2.3. Aggregation of Zn(II)-bound A-1

In the absence of Zn(II), the FRET signal of **A-1** reduced as a function of incubation time (ca. 70% and ca. 85% decrease after 1 and 3 h incubation, respectively; Figure 4.7). This lowered signal may be triggered by the aggregation of **A-1** since the probe contains a portion of the self-recognition region of Aβ.[10,33,39] In contrast, following incubation time, the FRET signal of Zn(II)-treated **A-1** decreased (ca. 2% and ca. 18% decrease after 1 and 3 h incubation, respectively; Figure 4.6a) at a slower rate compared to that of Zn(II)-free **A-1** (Figure 4.7). This indicates that the aggregation of **A-1** could be delayed by the presence of Zn(II), as observed with full-length $Aβ_{40}$ (Figure 4.8). This difference could stem from the disparate conformations of Aβ aggregates generated upon the aggregation of metal–Aβ, distinct from those of metal-free Aβ

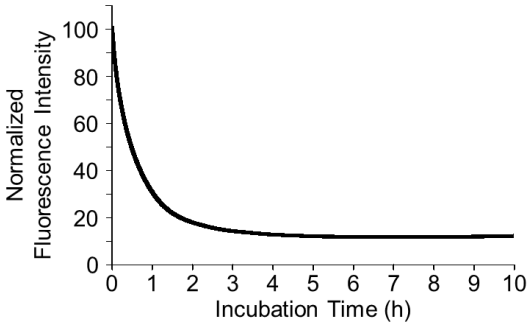

Figure 4.7. Change in the FRET signal of **A-1** following the incubation time without Zn(II). Conditions: [**A-1**] = 300 nM; λ_{ex} = 280 nm; λ_{em} = 420 nm; incubation for 10 h; room temperature.

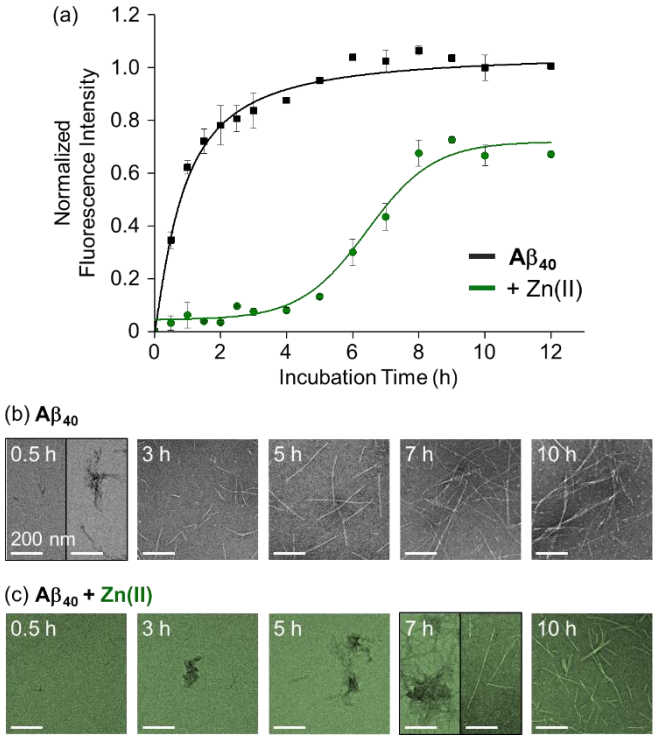

Figure 4.8. Time-dependent aggregation progression of $A\beta_{40}$ with and without Zn(II). (a) Aggregation kinetics of metal-free $A\beta_{40}$ and Zn(II)–$A\beta_{40}$, observed by the ThT assay. Conditions: [$A\beta_{40}$] = 20 μM; [$ZnCl_2$] = 20 μM; [ThT] = 20 μM; pH 7.4; 37 ℃; constant agitation. (b) Morphologies of $A\beta_{40}$ aggregates generated at various incubation time points, visualized by TEM (scale bar = 200 nm). Conditions: [$A\beta_{40}$] = 20 μM; [$ZnCl_2$] = 20 μM; pH 7.4; 37 ℃; constant agitation.

aggregates.[28,42] Thus, we analyzed the morphologies of Zn(II)–**A-1** aggregates upon incubation by transmission electron microscopy (TEM). As depicted in Figure 4.6b, small and amorphous aggregates were observed after 1 h incubation of Zn(II)-added **A-1** followed by the detection of larger and more structured aggregates with longer incubation. Based on the variation of the FRET intensity as the probe

aggregated, the aggregation process of Zn(II)–**A-1** could be divided into three stages: (i) 0–1 h; (ii) 1–3 h; (iii) 3–10 h (Figure 4.6a). Up to 1 h incubation, the FRET signal of Zn(II)–**A-1** did not significantly decrease from the initial measurement. From 1 to 3 h, the FRET intensity of Zn(II)–**A-1** dropped drastically and after 3 h incubation, the FRET responses of Zn(II)–**A-1** were shown to be distinguishably reduced slower than those during the 1–3 h incubation period. This could be because Zn(II)–**A-1** formed large-sized aggregates, including protofibrils and fibrils, which might restrict its rotation to limit the distance between the FRET donor and acceptor, along with its solubility in aqueous media. Thus, our FRET-based probe, **A-1**, could monitor the progression of Zn(II)–Aβ aggregation, distinct from metal-free Aβ aggregation.

4.2.4. Screening Inhibitors against Zn(II)–Aβ Interaction

To evaluate whether Zn(II)-bound **A-1** is an effective identification tool for inhibitors against Zn(II)–Aβ interaction, alteration of the FRET signal of Zn(II)–**A-1** was monitored upon addition of the metal chelator (i.e., **EDTA**) or the molecule capable of forming a ternary complex with Zn(II)–Aβ (i.e., **L2-b**) Table 4.1 and Figure 4.9a).[29–31] When **EDTA** was introduced to Zn(II)–**A-1**, the FRET intensity was reduced by 83%, compared to the FRET signal of Zn(II)–**A-1**, and the emission spectrum was red shifted back to that observed under Zn(II)-free conditions (Figure 4.9, i). This suggests that Zn(II) was chelated out from **A-1** by **EDTA**, causing the probe to be unfolded. Furthermore, the treatment of **L2-b** to Zn(II)–**A-1** exhibited a noticeably weaker FRET signal than Zn(II)–**A-1** by 82%, but did not present the same emission spectrum as that of Zn(II)-free **A-1** (Figure 4.9a, ii). The fluorescence behavior of **L2-b**-added Zn(II)–**A-1** implies that a ternary complex [e.g., **L2-b**–Zn(II)–**A-1**] could be formed and thus Zn(II) still interacts with **A-1**, but the distance between the FRET donor and acceptor may not be in close proximity. Note that the emission of Trp was not significantly changed at ca. 350 nm which was not absorbed by the FRET acceptor upon addition of **EDTA** and **L2-b** (Figure 4.9a), indicating that the compounds did not affect the absorption and emission of the FRET donor. Together, our probe, **A-1**, demonstrates the ability to identify molecules with inhibitory activity towards metal–Aβ interaction.

Table 4.1. Chemical structures of **EDTA**, **L2-b**, and the natural products in our chemical library and their inhibition values (%) of the interaction between Zn(II) and **A-1**. The inhibition values (%) are presented in parenthesis.

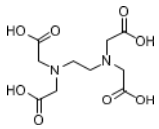		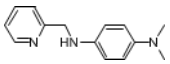	
EDTA (83%)		**L2-b** (82%)	
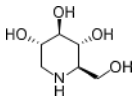	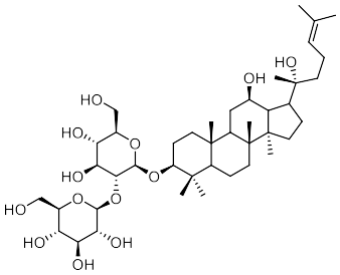	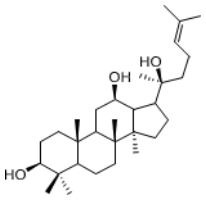	
1 (30%)	**2** (40%)	**3** (-24%)	
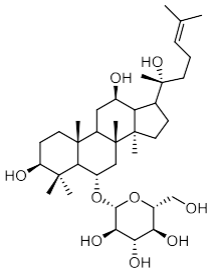	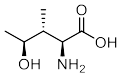	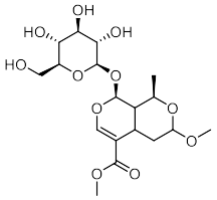	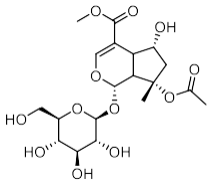
4 (23%)	**5** (-15%)	**6** (42%)	**7** (2.4%)
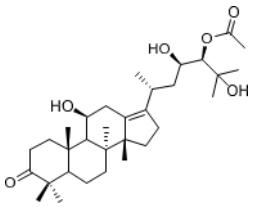	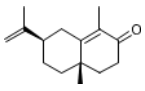	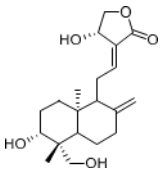	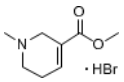
8 (53%)	**9** (96%)	**10** (57%)	**11** (31%)
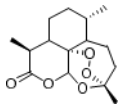	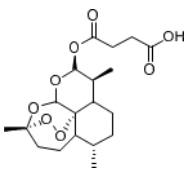	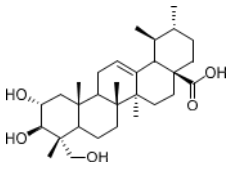	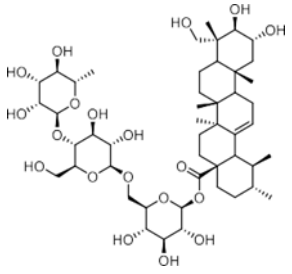
12 (48%)	**13** (69%)	**14** (28%)	**15** (24%)

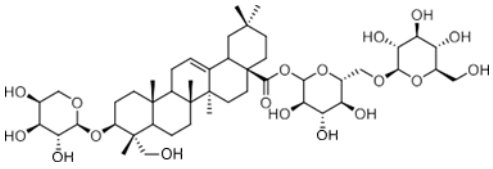	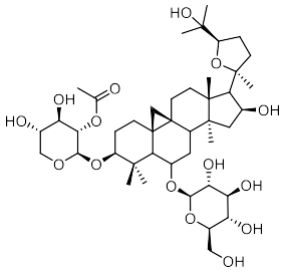
16 (17%)	**17** (37%)
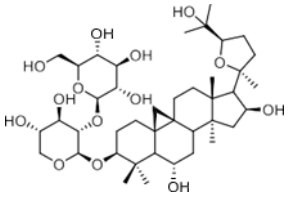	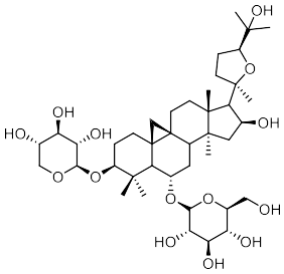
18 (-15%)	**19** (66%)

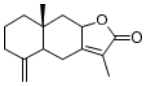	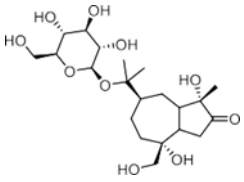	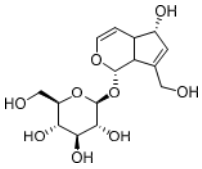	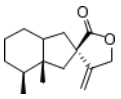
20 (76%)	**21** (54%)	**22** (40%)	**23** (33%)
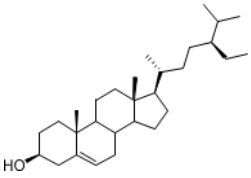	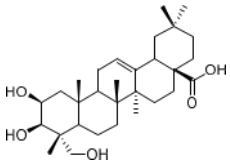	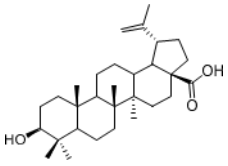	
24 (23%)	**25** (2.4%)	**26** (-1.1%)	
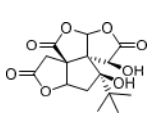	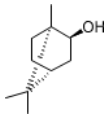	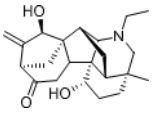	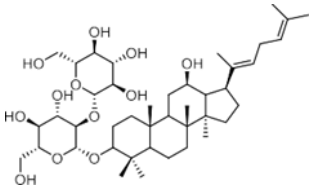
27 (37%)	**28** (31%)	**29** (44%)	**30** (68%)

	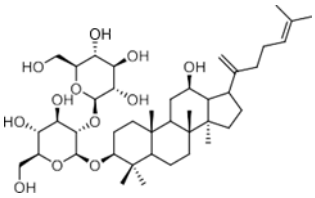	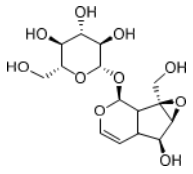	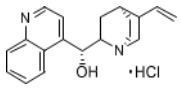
31 (49%)	**32** (-19%)	**33** (15%)	**34** (44%)
	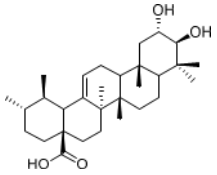	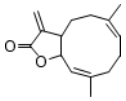	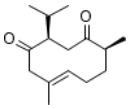
35 (46%)	**36** (-19%)	**37** (110%)	**38** (14%)
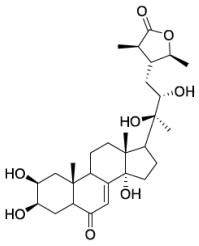	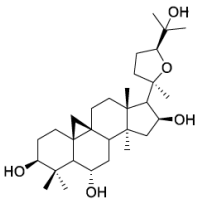	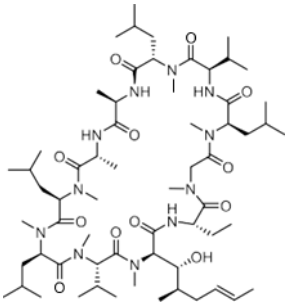	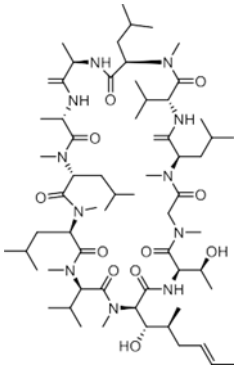
39 (19%)	**40** (-13%)	**41** (51%)	**42** (-16%)
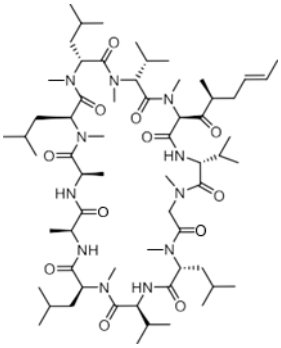	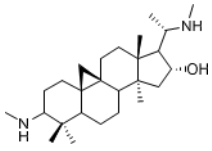	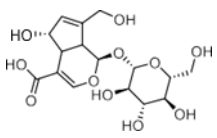	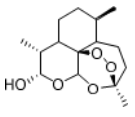
43 (52%)	**44** (19%)	**45** (53%)	**46** (37%)

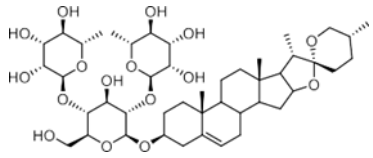	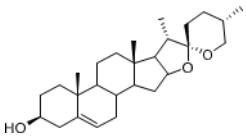
47 (-25%)	**48** (3.9%)
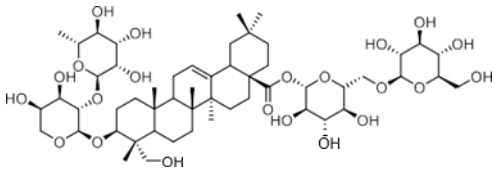	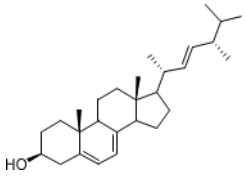
49 (2.8%)	**50** (46%)

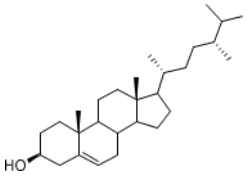	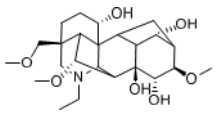	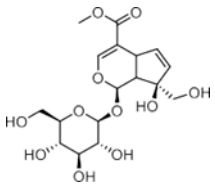	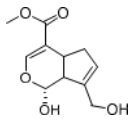
51 (17%)	**52** (27%)	**53** (25%)	**54** (67%)
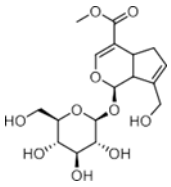	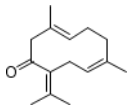	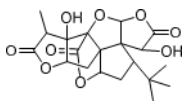	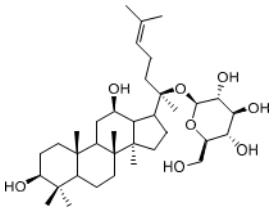
55 (28%)	**56** (54%)	**57** (23%)	**58** (36%)
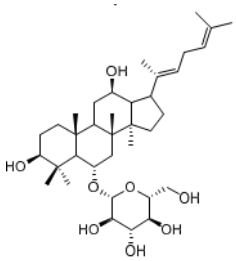	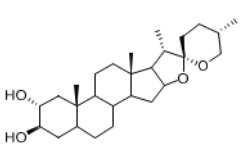	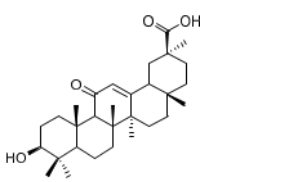	
59 (35%)	**60** (51%)	**61** (100%)	

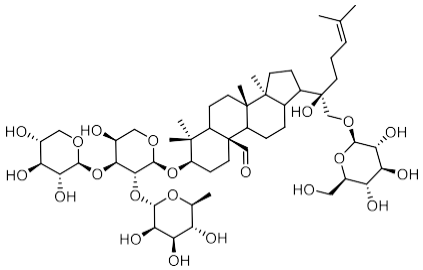	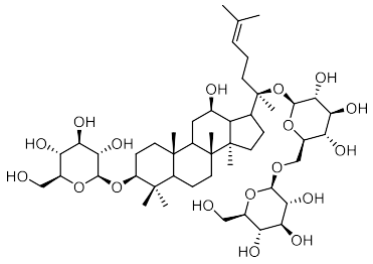
62 (39%)	**63** (22%)

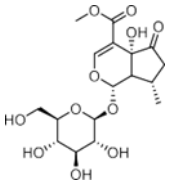	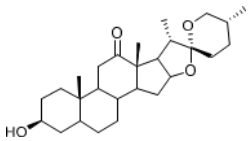	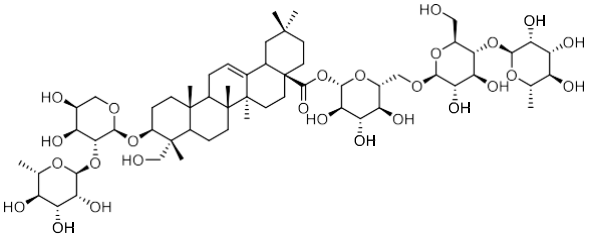
64 (22%)	**65** (50%)	**66** (-2.4%)

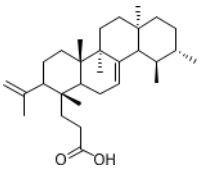	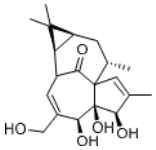	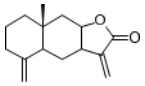	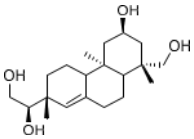
67 (6.8%)	**68** (16%)	**69** (54%)	**70** (30%)

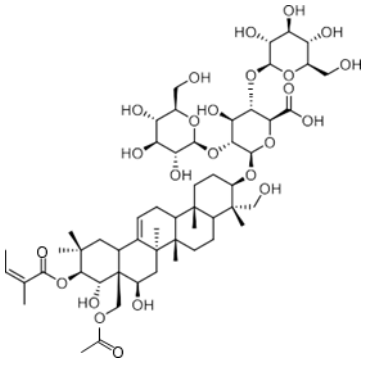	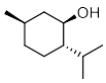	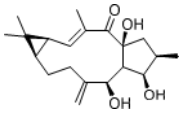	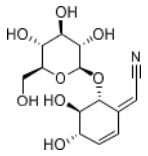
71 (86%)	**72** (11%)	**73** (100%)	**74** (32%)

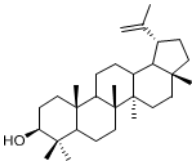	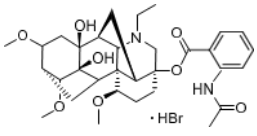	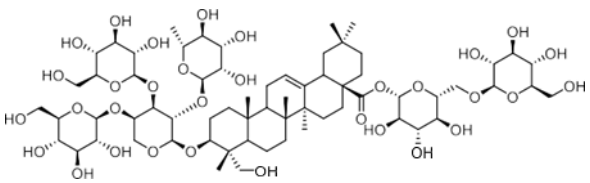
75 (-1.4%)	**76** (35%)	**77** (18%)

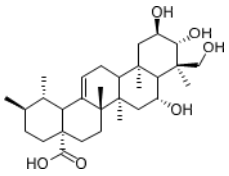	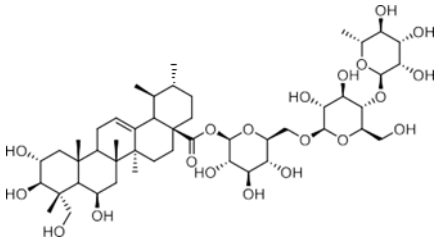	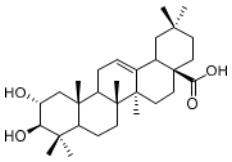
78 (24%)	**79** (9.6%)	**80** (27%)
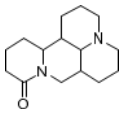	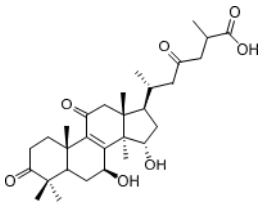	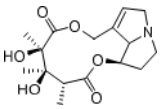
81 (22%)	**82** (50%)	**83** (21%)
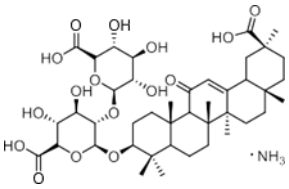	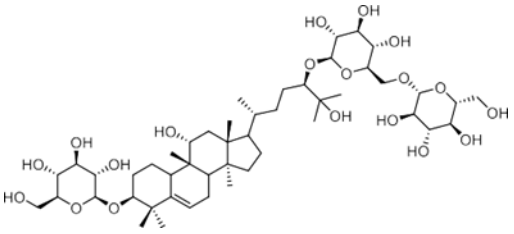	
84 (103%)	**85** (22%)	
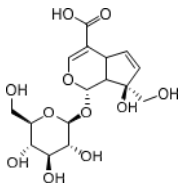	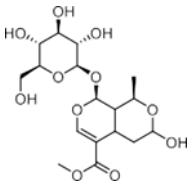	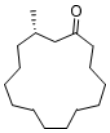	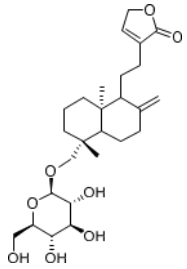
86 (71%)	**87** (32%)	**88** (18%)	**89** (37%)
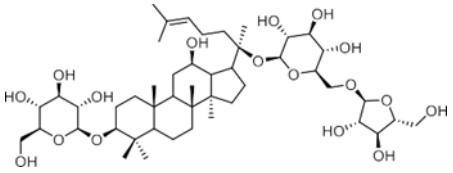	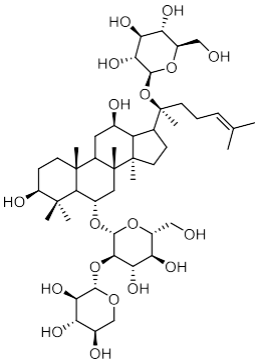	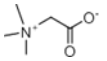
90 (32%)	**91** (13%)	**92** (18%)

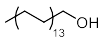	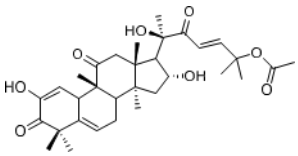	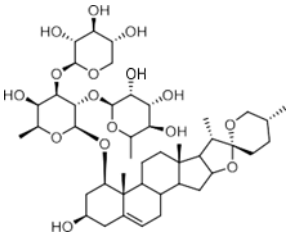	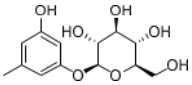
93 (21%)	**94** (68%)	**95** (-4.0%)	**96** (31%)
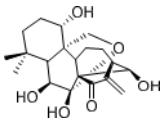	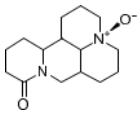	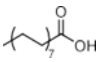	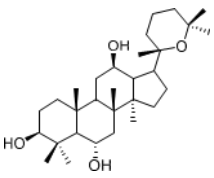
97 (35%)	**98** (18%)	**99** (31%)	**100** (0.30%)
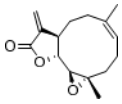	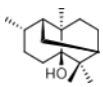	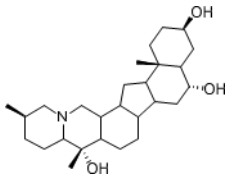	
101 (53%)	**102** (-3.2%)	**103** (12%)	
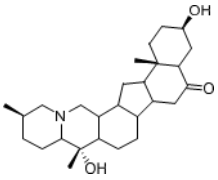	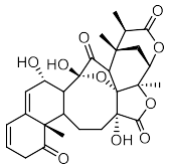	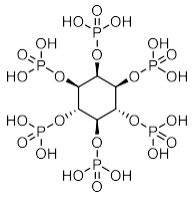	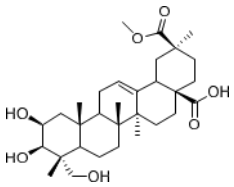
104 (33%)	**105** (49%)	**106** (99%)	**107** (34%)
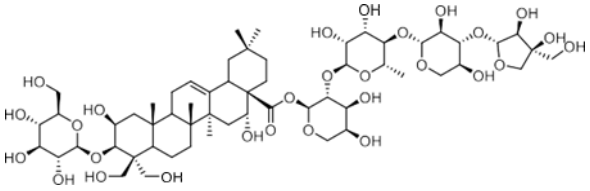		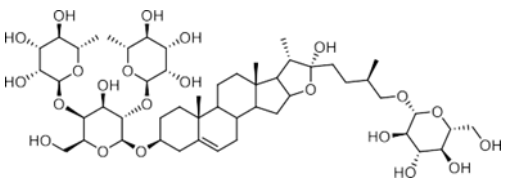	
108 (16%)		**109** (30%)	

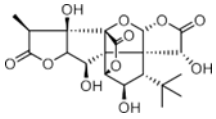	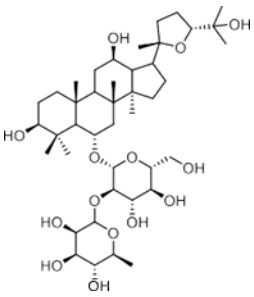	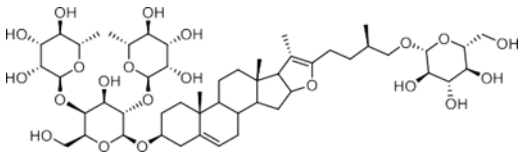
110 (14%)	**111** (32%)	**112** (25%)

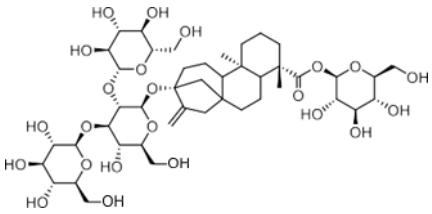	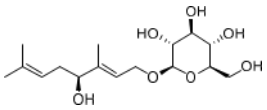	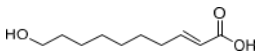
113 (17%)	**114** (32%)	**115** (21%)

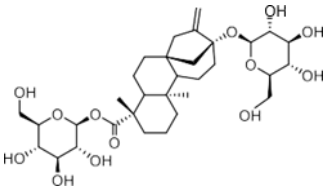	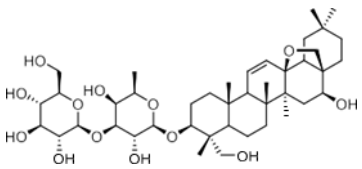
116 (13%)	**117** (16%)

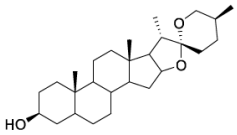	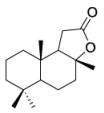	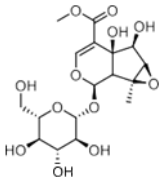	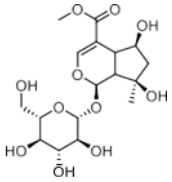
118 (14%)	**119** (10%)	**120** (32%)	**121** (16%)

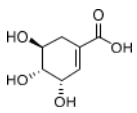	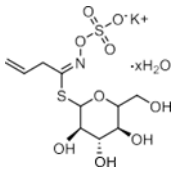	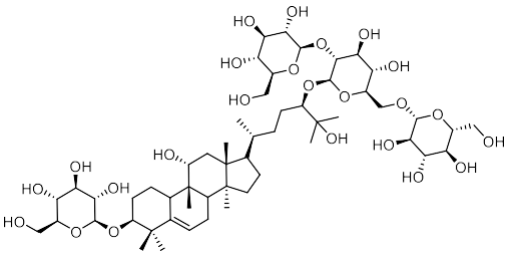
122 (27%)	**123** (26%)	**124** (37%)

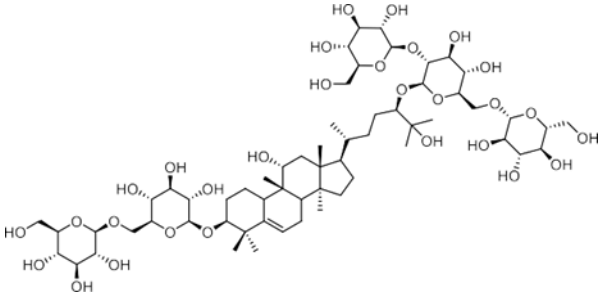	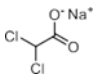
125 (12%)	**126** (18%)
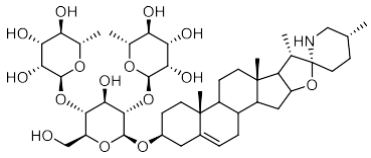	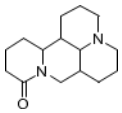
127 (-0.81%)	**128** (41%)
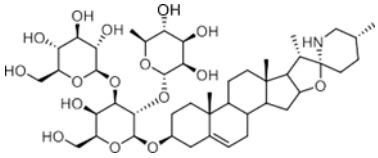	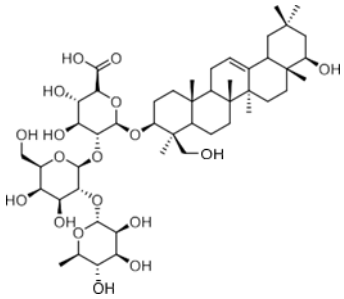
129 (24%)	**130** (-4.1%)
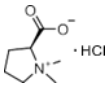	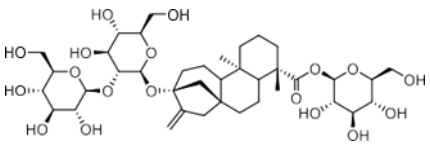
131 (33%)	**132** (33%)
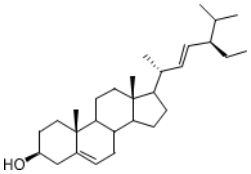	
133 (56%)	
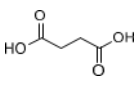	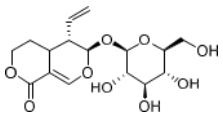
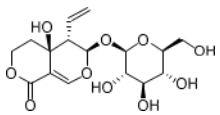	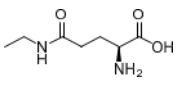
134 (51%)	**135** (31%)
136 (31%)	**137** (29%)

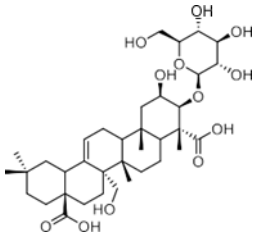	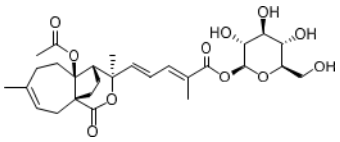	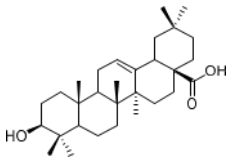
138 (19%)	**139** (104%)	**140** (9.9%)
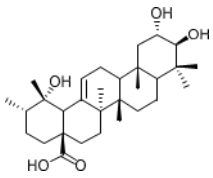	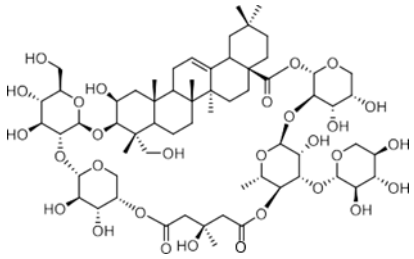	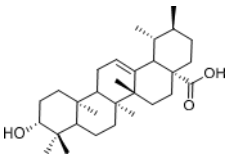
141 (23%)	**142** (33%)	**143** (3.6%)
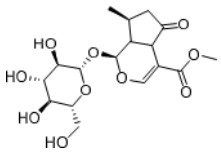	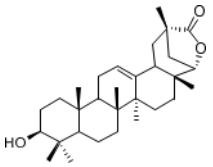	
144 (38%)	**145** (20%)	

Moving forward, to confirm the screening capability of our FRET-based method to verify molecules as potential inhibitors against metal–Aβ interaction, we built up a chemical library containing 145 natural products that do not absorb the FRET signal of Zn(II)–**A-1** at ca. 420 nm, similar to **EDTA** and **L2-b** (Figure 4.10 and Table 4.1). The FRET signal of Zn(II)–**A-1** upon addition of natural products was compared to that of Zn(II)–**A-1** to calculate % inhibition (Figures 4.9b, 4.11, and Table 4.1). In our library, (i) 15 molecules could not affect Zn(II) binding to **A-1**; (ii) 103 compounds showed 0 to 50% inhibition; (iii) 27 natural products induced a significant decrease in the fluorescence of Zn(II)–**A-1** by > ca. 50% (Figure 4.9b and Table 4.1). Furthermore, among the 27 natural products (> ca. 50% inhibition), 8 compounds (i.e., **9**, **37**, **61**, **71**, **73**, **84**, **106**, and **139**) demonstrated > 80% inhibitory activity against Zn(II)–**A-1** interaction. Three compounds (i.e., **61**, **71**, and **84** out of 8 potent inhibitors; Figure 4.9b and Table 4.1) contain both β-amyrin moiety and α,β-unsaturated carbonyl groups, previously reported for controlling metal–Aβ aggregation.[43] Note that the compounds containing an α,β-unsaturated carbonyl moiety could form a covalent adduct with Aβ possibly by reacting with Lys or His.[44,45] To verify the covalent bond formation between one of the effective inhibitors, **61**, and an Aβ

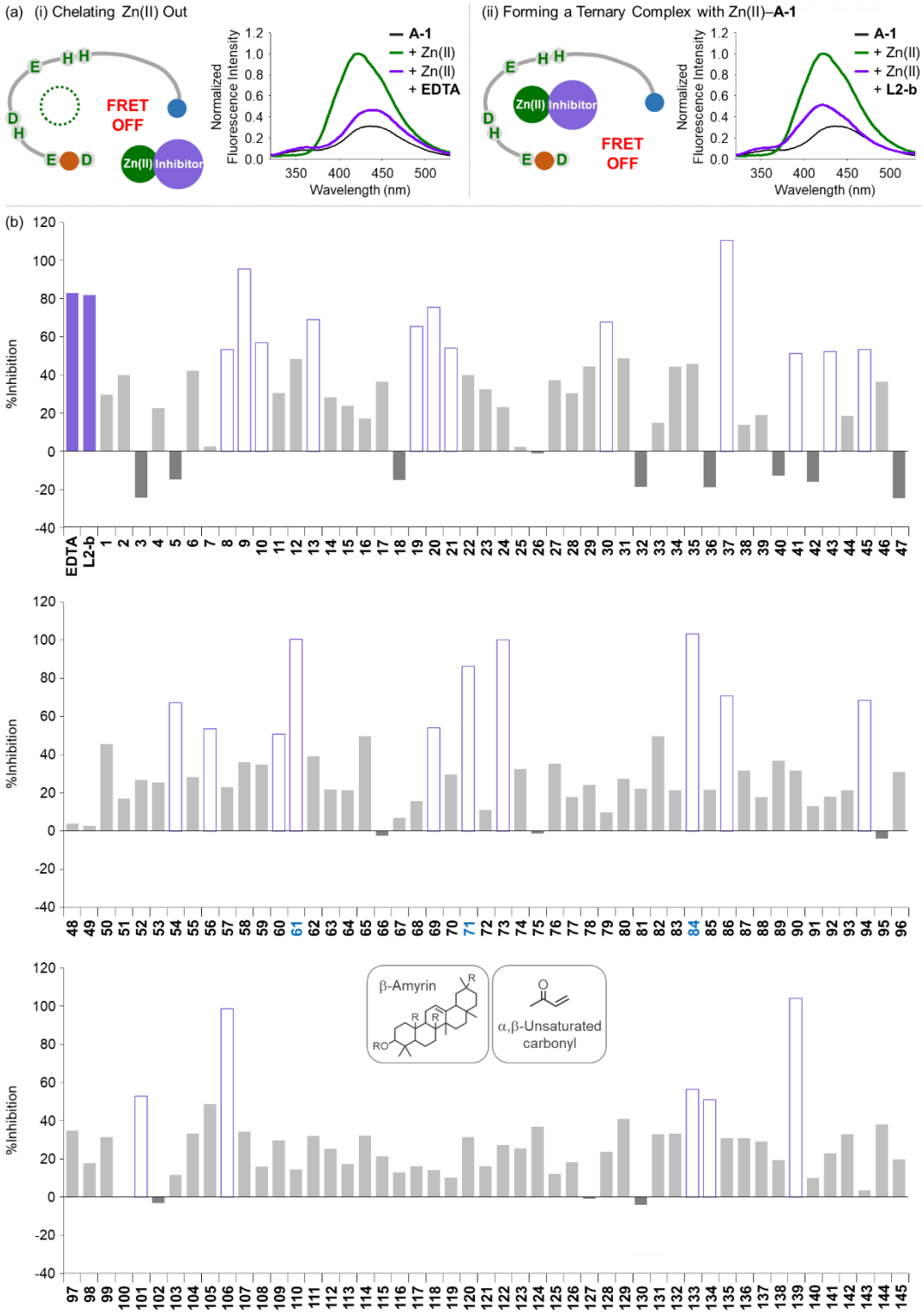

Figure 4.9. Change in the FRET signal of Zn(II)-bound **A-1** upon treatment with inhibitors against Zn(II)–Aβ interaction. (a) Fluorescent responses of **A-1** in the presence of both Zn(II) and compounds: [(i) **EDTA** and (ii) **L2-b**]. (b) Inhibition (%) of Zn(II)–**A-1** interaction by incubation with the natural products. Full data sets regarding the inhibition (%) of 145 natural products are summarized in Table 4.1. **61**, **71**, and **84** that contain both β-amyrin and α,β-unsaturated carbonyl groups and show > 80% inhibition against Zn(II)–**A-1** interaction are labeled in blue. Conditions: [**A-1**] = 0.3 μM; [$ZnCl_2$] = 100 μM; [inhibitor] = 100 μM; incubation for 10 min; room temperature; λ_{ex} = 280 nm; λ_{em} = 420 nm.

fragment ($A\beta_{28}$), the sample containing **61** and $A\beta_{28}$ was monitored by MS. The MS measurement presented a covalent $A\beta_{28}$–**61** adduct at 1244 *m/z* (blue peak; Figure 4.12a). In addition, the tandem MS analysis of the peak at 1244 *m/z* indicated $A\beta_{28}$ (at 1088 *m/z*) and **61** (at 471 *m/z*) confirming the formation of the covalent $A\beta_{28}$–**61** adduct (Figure 4.12b). Thus, our inhibitors containing an α,β-unsaturated carbonyl moiety have the potential to bind **A-1**. Overall, inhibitors against Zn(II)–Aβ interaction could be screened and identified by our probe, **A-1**, showing a variation in its FRET signal in the presence of Zn(II).

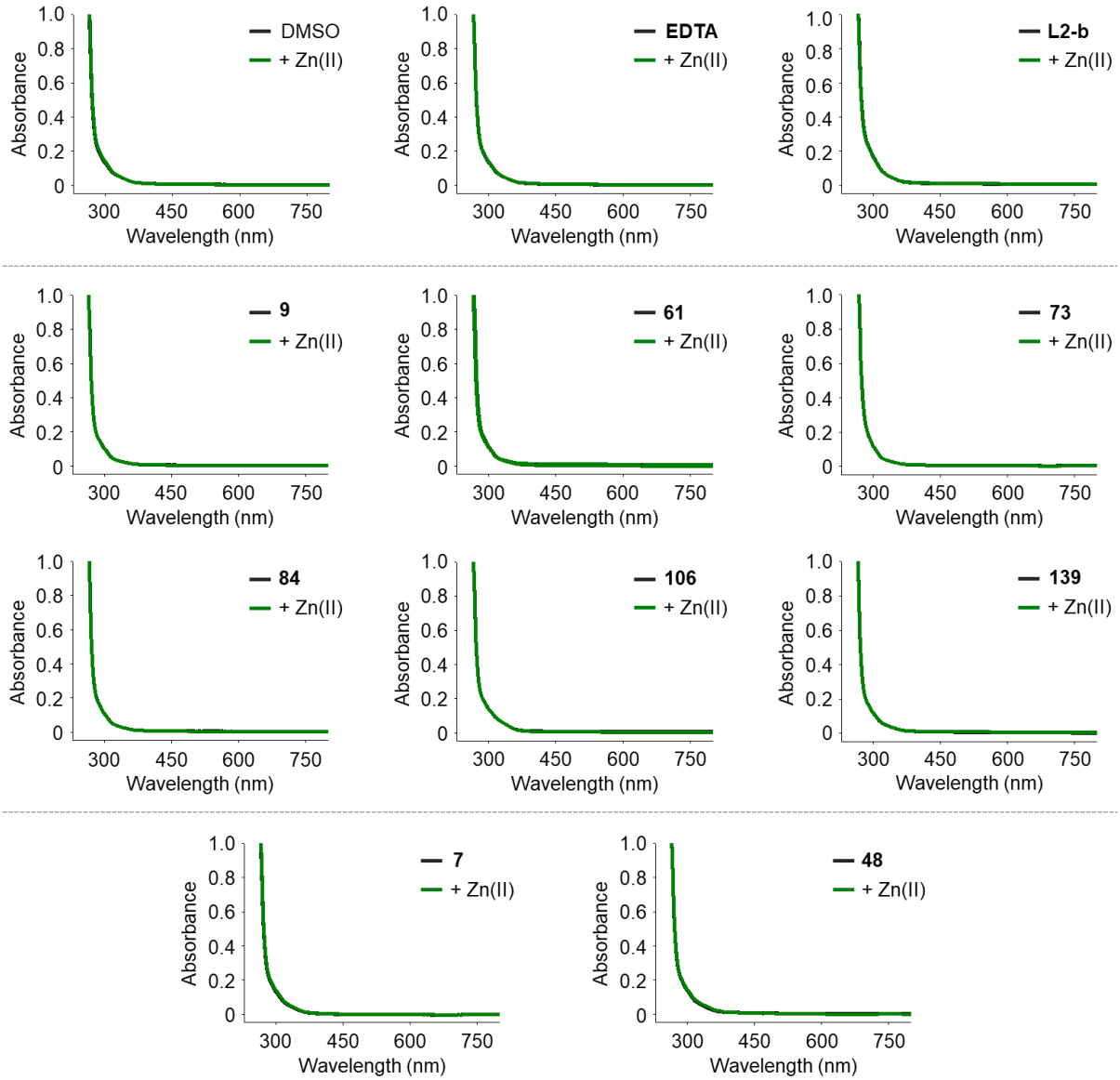

Figure 4.10. Absorption spectra of **EDTA**, **L2-b**, and the selected natural products in the absence (black) and presence (green) of Zn(II). Conditions: [compound] = 100 μM; [$ZnCl_2$] = 100 μM. Note that the absorption spectra were obtained by a microplate reader.

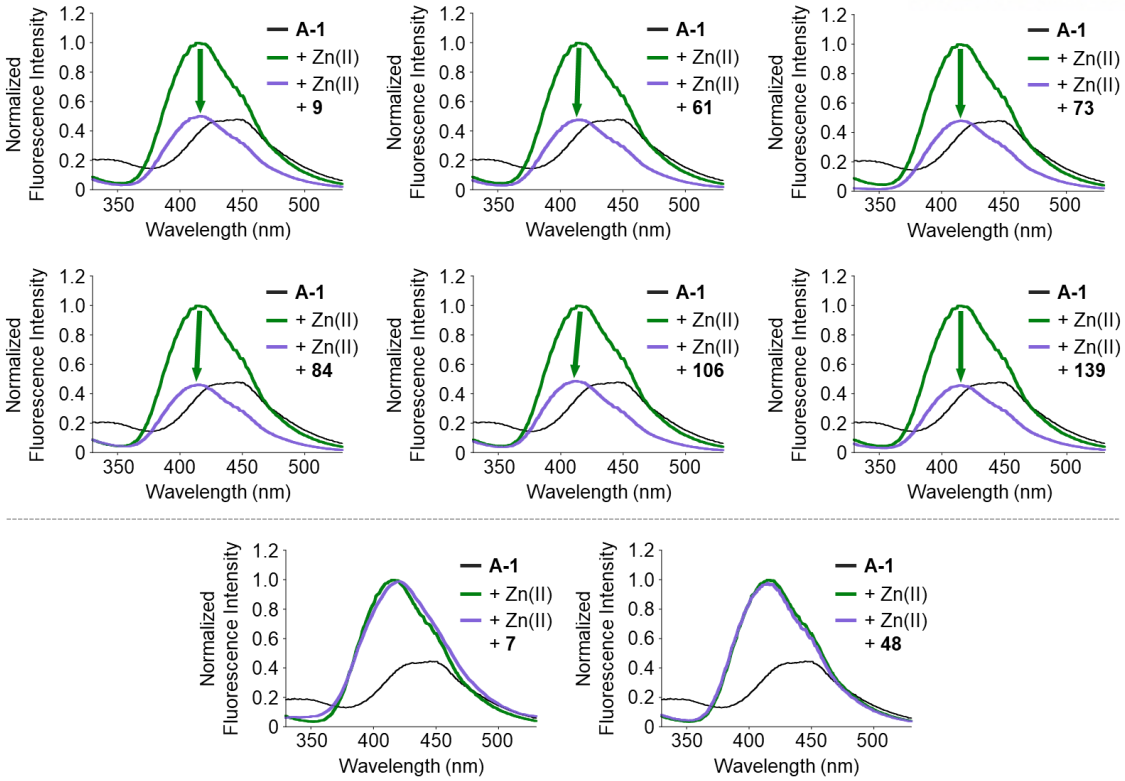

Figure 4.11. FRET responses of **A-1** (black) to Zn(II) without (green) and with (purple) the selected natural products. The FRET intensities of the selected natural products showing noticeable inhibition (**9**, **61**, **73**, **84**, **106**, and **139**) or no significant inhibition (**7** and **48**) against Zn(II)–Aβ interaction were monitored. Conditions: [**A-1**] = 300 nM; [$ZnCl_2$] = 100 μM; [compound] = 100 μM; λ_{ex} = 280 nm.

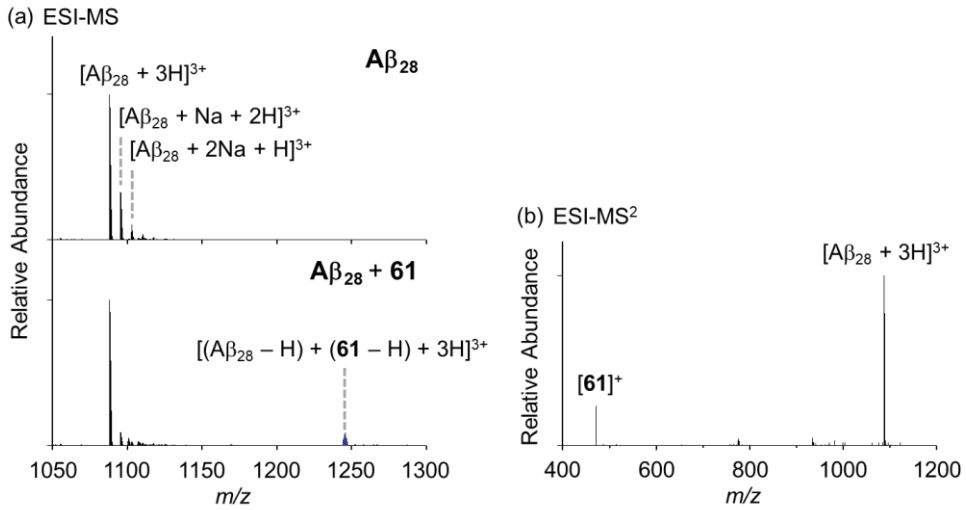

Figure 4.12. Mass spectrometric analysis of the sample containing $A\beta_{28}$ with the natural product, **61**. (a) ESI-MS spectra of $A\beta_{28}$ incubated without (top) and with (bottom) **61**. (b) Tandem MS (ESI-MS^2) spectrum of the +3-charged $A\beta_{28}$–**61** complex (blue, $[(A\beta_{28} - H) + (\mathbf{61} - H) + 3H]^{3+}$, 1244 *m/z*). The ESI-$MS^2$ results support the formation of a covalent complex composed of $A\beta_{28}$ and **61**. Conditions: [Aβ] = 5 μM; [**61**] = 25 μM; 20 mM ammonium acetate, pH 7.4; incubation for 2 h; room temperature; no agitation.

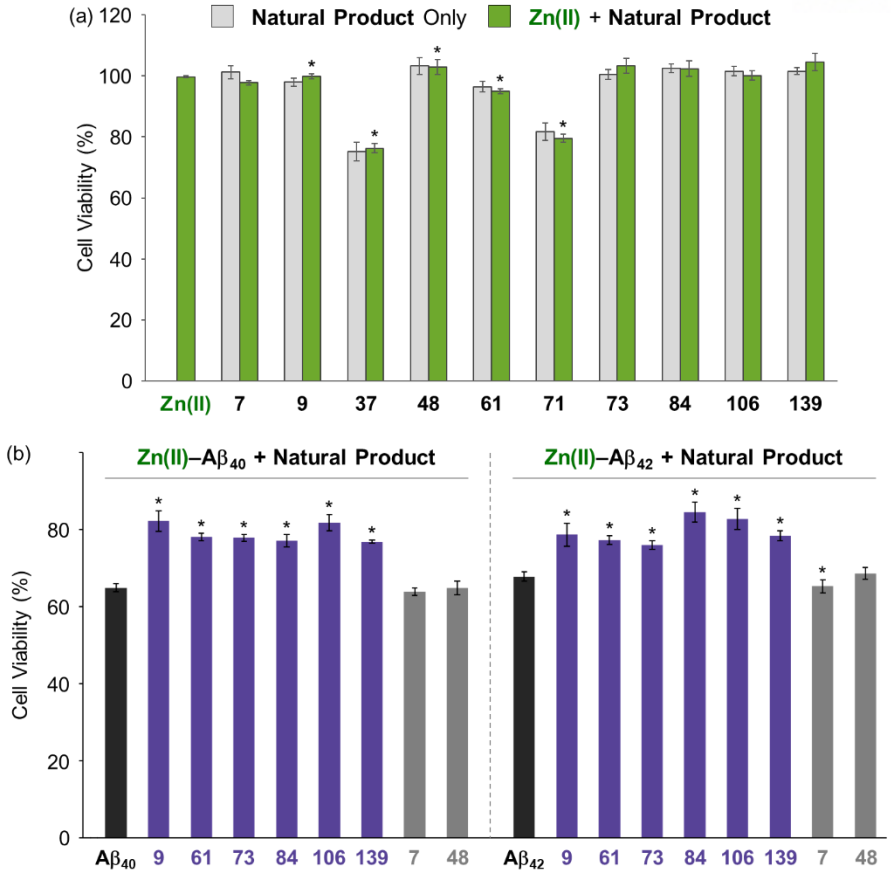

Figure 4.13. Effect of the selected natural products on the cytotoxicity triggered by Zn(II) and Zn(II)–Aβ. (a) Toxicity of the selected natural products with and without Zn(II) in 5Y cells. Cells were treated with compounds (10 μM) in the absence (light gray) and presence (light green) of Zn(II) (same equivalent to compounds; 10 μM) for 24 h at 37 °C. (b) $A\beta_{40}$ (left) or $A\beta_{42}$ (right; 10 μM) with Zn(II) (10 μM) was pre-incubated at room temperature for 1 h and then treated to 5Y cells with compounds (10 μM) for 24 h. Cell viability (%) was determined by the MTT assay compared to that obtained upon treatment with a volume of H_2O (1% v/v DMSO) equal to the samples added. Error bars represent the standard error of the mean from three independent experiments. $*P < 0.05$.

4.2.5. Influence of Inhibitors on Toxicity Associated with Zn(II) and Zn(II)–Aβ

The effect of the 8 natural products that showed > 80%inhibition against Zn(II)–**A-1** interaction on the toxicity triggered by metal-free and Zn(II)-treated $A\beta_{40}$ and $A\beta_{42}$ (two major isoforms of Aβ)[6,10] was determined in living cells. We first examined the toxicity of 10 natural products (i.e., 8 effective natural products: **9**, **37**, **61**, **71**, **73**, **84**, **106**, and **139**; 2 compounds which may not be able to disrupt Zn(II)–**A-1** interaction: **7** and **48**) in human neuroblastoma SH-SY5Y (5Y) cells. The tested compounds, except for **37** and **71**, were not relatively toxic (> ca. 80% of cell viability at more than 10 μM) in the absence and presence of Zn(II) (Figures 4.13a and 4.14). Employing the relatively less toxic natural products (i.e., **7**, **9**, **48**, **61**, **73**, **84**, **106**, and **139**) with and without Zn(II), their impact on the toxicity induced by pre-incubated $A\beta_{40}$ and $A\beta_{42}$ with and without Zn(II) for 1 h at room temperature was analyzed. The natural products could not ameliorate the toxicity induced by metal-free Aβ (Figure 4.15). On the other

hand, as depicted in Figure 4.13b (purple), cell survival was improved by 6 natural products, determined as effective inhibitors against metal–**A-1** interaction, even with the species of Zn(II)–Aβ. As expected, the compounds, **7** and **48**, shown to hinder Zn(II) binding to Aβ by less than ca. 5% (Figure 4.9b and Table 4.1), were not able to mitigate the toxicity induced by both metal-free and Zn(II)-associated Aβ (Figures 4.13b and 4.15; gray). Thus, our FRET-based method employing **A-1** demonstrates its practical utility to determine molecules that can affect metal–Aβ interaction and, as a result, alleviate metal–Aβ-linked cytotoxicity.

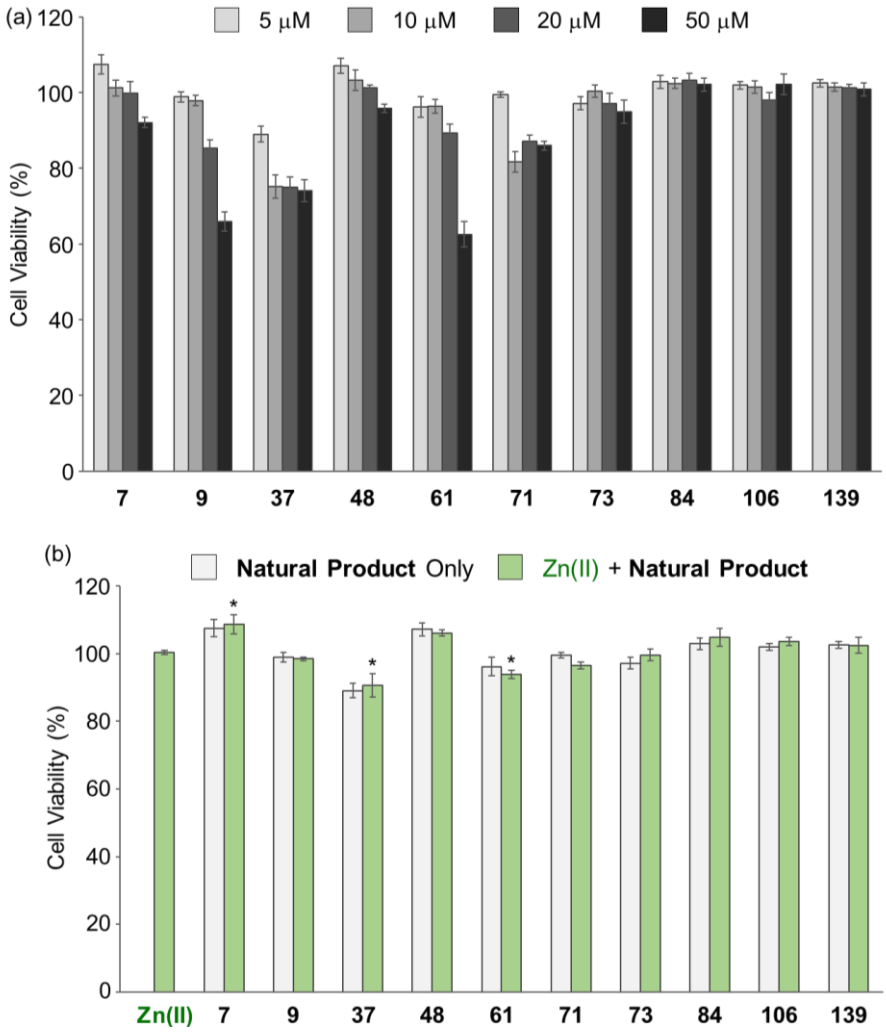

Figure 4.14. Toxicity of the selected natural products with and without Zn(II) in 5Y cells. (a) Cells were treated with various concentrations (5, 10, 20, and 50 μM) of compounds for 24 h at 37 ℃. (b) Compounds (5 μM) in the absence (gray) and presence (green) of Zn(II) (same equivalent to the compounds; 5 μM) were added to cells and incubated for 24 h at 37 ℃. Cell viability (%) was determined by the MTT assay. The viability value was calculated compared to that of the cells added with DMSO only (1%, v/v). Error bars represent S.E.M. from three independent experiments. *$P < 0.05$ [versus Zn(II) or natural products].

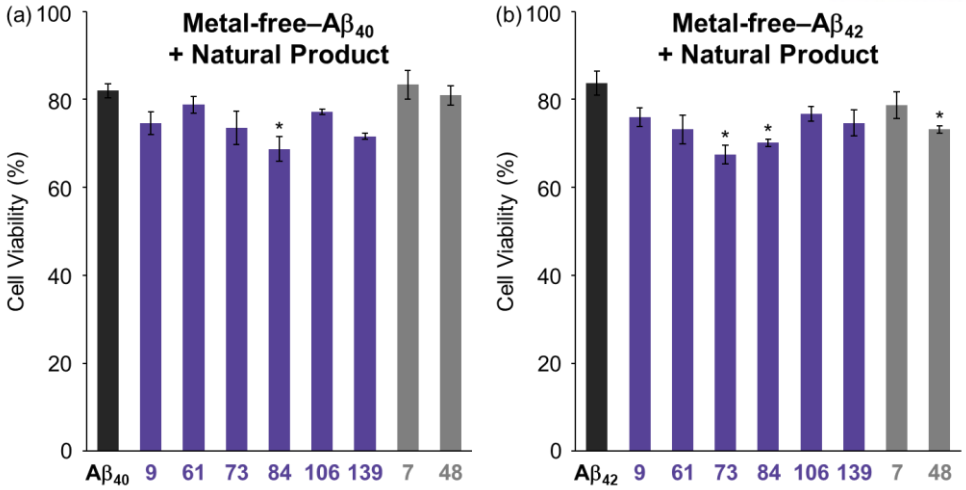

Figure 4.15. Effect of the selected natural products on the toxicity triggered by metal-free Aβ in 5Y cells. (a) $A\beta_{40}$ or (b) $A\beta_{42}$ (10 μM) was pre-incubated at room temperature for 1 h and then treated to 5Y cells with compounds (10 μM) for 24 h. Cell viability (%) was determined by the MTT assay compared to that of the cells treated with a volume of H_2O (1% v/v DMSO) equal to the samples added. Error bars represent S.E.M. from three independent experiments. $^*P < 0.05$.

4.3. Conclusions

Since metal ions and amyloidogenic peptides (e.g., Aβ) can interact with each other and induce neurotoxicity, our understanding of such complexation is important to reveal their effects in the pathogenesis of neurodegenerative diseases. In order to verify the feasibility of monitoring metal–amyloidogenic peptide interactions, we employed Aβ as an example of amyloidogenic peptides to develop a FRET-based probe, **A-1**, to detect the metal binding of Aβ and the progression of metal–Aβ aggregation effectively and efficiently. Upon addition of Zn(II), the FRET signal of **A-1** was significantly increased due to the folding of our probe. In addition, when the probe aggregated with Zn(II), its fluorescent response was altered in a distinct manner from that of metal-free case. Furthermore, by utilizing our FRET-based probe to screen a chemical library (total 145 compounds), we identified 6 natural products capable of significantly modulating metal–Aβ interaction (> 80% inhibition) in vitro and diminishing cytotoxicity associated with Zn(II)–Aβ in living cells. Our overall studies illustrate the development of a strategy to monitor metal–Aβ interaction and its applicability towards searching potent inhibitors against metal–Aβ interaction. In the near future, for biological applications, new and optimized probes will be developed to monitor the interaction between Aβ and Zn(II) or other metal ions, including Cu(II), showing more sensitive fluorescent responses with lower energy profiles for excitation and emission (e.g., near-infrared region). Applying our tactic to other amyloidogenic peptides, their interactions with metal ions could be, and the inhibitors against metal–amyloidogenic peptide interaction could be identified.

4.4. Experimental Section

4.4.1. Materials and Methods

All chemical reagents (reagent grade) were purchased from Sigma Aldrich or Tokyo Chemical Industry (Tokyo, Japan) and used as received. Fmoc-protected amino acids were purchased from Chemimpex (Wood Dale, IL, USA) and GL biochem (Shanghai, China). Full length Aβ (i.e., $A\beta_{40}$ and $A\beta_{42}$) peptides were purchased from Anaspec (Fremont, CA, USA) ($A\beta_{40}$ = DAEFRHDSGYEVHHQKLVFFAEDVG-SNKGAIIGLMVGGVV; $A\beta_{42}$ = DAEFRHDSGYEVHHQKLVFFAEDVGSNKGAIIGLMVGGVVI-A). Reaction products were analyzed using high performance liquid chromatography (HPLC), matrix associated laser desorption ionization time-of-flight mass spectrometry (MALDI-TOF MS), and nuclear magnetic resonance spectroscopy (NMR). HPLC analysis was performed using the Waters photodiode array detector 996, separation module 2695, and XBridgeTM C18 column (5 μm, 4.6 x 250 mm). Peptide purification was performed by the Waters XBridgeTM Prep C18 column (5 μm, 19 x 250 mm). Purified peptide samples and their Zn(II) binding studies were analyzed by a Bruker MALDI-TOF mass spectrometer (Sogang University, Seoul, Republic of Korea) and a Q Exactive Plus Orbitrap mass spectrometer (Thermo Fisher Scientific, Waltham, MA, USA), respectively. Fluorescence was recorded on a PerkinElmer LS55 fluorescence spectrometer (PerkinElmer, Waltham, MA, USA) and HORIBA PTI QuantaMaster 8000 fluorescence spectrometer (HORIBA, Kyoto, Japan). TEM images were taken by a JEOL JEM-2100 transmission electron microscope [UNIST Central Research Facilities (UCRF), Ulsan, Republic of Korea] and a Tecnai F30 (FEI) transmission electron microscope [KAIST Analysis Center for Research Advancement (KARA), Daejeon, Republic of Korea]. Absorbance values of compounds and the MTT assay and the fluorescence intensity of ThT were measured using a Molecular Devices SpectraMax M5e microplate reader (Sunnyvale, CA, USA). The complex formation between Aβ fragments and the natural product was analyzed by the MicrOTOF-QII Hybrid Quadrupole-Time of Flight mass spectrometer (Bruker, Billerica, MA, USA) equipped with an ESI source [KARA, KAIST, Republic of Korea].

4.4.2. Synthesis and Purification of A-1

A-1 was synthesized through solid phase peptide synthesis (SPPS) using the 2-chlorotritylchloride resin (loading = 1.2 mmol/1 g resin). The resin was swelled with dry dichloromethane (DCM) for 30 min at room temperature. Immobilization of the Fmoc-amino acid was carried out on 1 g resin using 2 equiv of the Fmoc amino acid (2.4 mmol) and 4 equiv of *N*,*N*-diisopropylethylenediamine (DIPEA) for 1 h at room temperature. Fmoc deblocking was achieved twice for 10 min at room temperature using 20% (v/v) piperidine in *N*,*N*-dimethylformamide (DMF) followed by washing with DMF. Peptide coupling reactions were executed according to a pre-activation (10 min) protocol using 4 equiv of the appropriate amino acid, 4 equiv of 2-(1*H*-benzotriazol-1-yl)-1,1,3,3-tetramethyluronium hexafluorophosphate (HBTU), 4 equiv of 1-hydroxy-benzotriazole (HOBt), and 8 equiv of DIPEA. Then, the preactivated

solution was added to the resin and allowed to shake for 2 h at 30 °C. Using the above protocol, the 21-mer peptide, **A-1** (DDnapEFRHDSGYEVHHQKLVFFW), composed of natural amino acids and/or a side chain-modified aspartic acid with 1-naphthylethylenediamine (Dnap) was synthesized. Cleavage of the final peptide from the resin and deprotection of the acid-labile protective groups were accomplished using a mixture of trifluoroacetic acid (TFA), thioanisole, ethanedithiol, and double-distilled water (ddH_2O) (94/1/2.5/2.5, v/v/v/v). The crude peptide was precipitated from the cleavage solution and thoroughly washed with ice-cold diethyl ether (Et_2O). After preparative HPLC purification using a gradient of acetonitrile (CH_3CN) with 0.075% TFA in ddH_2O containing 0.1% TFA, the product fractions were pooled and lyophilized to give a white powder. The identity of **A-1** was confirmed using MALDI-TOF MS (Calcd, 2860.342; found, 2860.206).

4.4.3. Side Chain-Functionalized Fmoc-Asp(Nap)-OH (Fmoc-Dnap)

Fmoc-Asp(Nap)-OtBu: Orthogonal protected Fmoc-Asp-OtBu (2.0 g, 4.9 mmol) was dissolved in DCM (0.2 M), and subsequently 1-hydroxy-7-azabenzotriazole (HOAt, 1 equiv, 0.65 g, 4.9 mmol), 1-ethyl-3-(3-dimethylaminopropyl)carbodiimide (EDC, 2 equiv, 1.9 g, 9.7 mmol), and DIPEA (3 equiv, 2.5 mL, 15 mmol) were added. The reaction mixture was stirred for 10 min at 0 °C followed by the addition of *N*-naphthylethylenediamine (Nap; 2 equiv, 2.5 g, 9.7 mmol) and DIPEA (2 equiv, 1.7 mL, 9.7 mmol). The reaction mixture was stirred for 20 min at 0 °C and stirring was continued at room temperature for additional 4 h. After complete disappearance of the starting material was confirmed by thin layer chromatography (TLC), the reaction mixture was diluted with DCM and subsequently washed with 1 M HCl (aq, 3x), saturated $NaHCO_3$ (aq, 3x), and brine (3x), dried Na_2SO_4, filtered, and concentrated in vacuo. The residue was purified using silica gel column chromatography [hexanes/ethyl acetate (EtOAc) = 2/1 → 1/1) to give the titled compound as a greenish solid (2.2 g; yield = 79%). ^{1}H NMR [500 MHz, $CDCl_3$, δ (ppm)]: 7.78 (s, 1H), 7.67 (d, J = 7.3 Hz, 3H), 7.46 (d, J = 7.4 Hz, 2H), 7.35 (s, 2H), 7.31 (t, J = 7.5 Hz, 2H), 7.23 (dd, J = 14.3, 7.2 Hz, 2H), 7.14 (d, J = 8.1 Hz, 1H), 6.47 (d, J = 7.5 Hz, 1H), 6.13 (s, 1H), 5.94 (d, J = 7.4 Hz, 1H), 5.22 (s, 1H), 4.41 (s, 1H), 4.22-4.31 (m, 1H), 4.21-4.14 (m, 1H), 4.06 (t, J = 7.0 Hz, 1H), 3.58 (d, J = 4.1 Hz, 2H), 3.33 (s, 2H), 2.74-2.85 (m, 1H), 2.70 (dd, J = 15.4, 2.5 Hz, 1H), 1.39 (s, 9H). ^{13}C NMR [125 MHz, $CDCl_3$, δ (ppm)]: 171.1, 170.0, 156.2, 143.8, 143.2, 141.3, 134.3, 128.6, 127.7, 127.1, 126.5, 125.9, 125.2, 124.9, 123.4, 120.3, 120.0, 117.5, 103.8, 82.7, 67.2, 51.5, 47.0, 44.8, 39.0, 38.4, 27.9. HRMS: Calcd, 524.2180; Found, 524.2181.

Fmoc-Asp(Nap)-OH: Fmoc-Asp(Nap)-OtBu (1, 1.5 g, 2.6 mmol) was co-evaporated with DCM and dissolved in a solution of 30% TFA in DCM at 0 °C. The reaction mixture was allowed to warm up to room temperature for 2 h, after which the volatiles were removed in vacuo. The residue was subjected to silica gel column chromatography (hexanes/EtOAc 1/5 → 1/15) to give the titled compound as a light greenish solid (1.3 g; 93%).^{1}H NMR [500 MHz, DMSO-d_6, δ (ppm)]: 12.73 (s, 7H), 8.18 (t, J =

5.7 Hz, 35H), 8.08 (d, *J* = 8.1 Hz, 34H), 7.88 (d, *J* = 7.5 Hz, 68H), 7.67-7.77 (m, 100H), 7.62 (d, *J* = 8.3 Hz, 30H), 7.35-7.47 (m, 136H), 7.23-7.35 (m, 103H), 7.10 (d, *J* = 8.1 Hz, 7H), 6.57 (t, *J* = 10.7 Hz, 34H), 6.21 (s, 33H), 4.43 (td, *J* = 8.1, 5.6 Hz, 6H), 4.26 (dd, *J* = 7.0, 2.6 Hz, 11H), 4.21 (dd, *J* = 14.3, 7.5 Hz, 8H), 3.32-3.46 (m, 37H), 3.27 (d, *J* = 3.8 Hz, 15H), 2.67 (d, *J* = 5.4 Hz, 3H), 2.64 (d, *J* = 5.3 Hz, 4H), 2.51-2.61 (m, 7H), 1.13-1.40 (m, 5H). ^{13}C NMR [125 MHz, DMSO-d_6, δ (ppm)]: 173.6, 170.2, 156.3, 144.3, 144.3, 144.3, 141.2, 134.5, 128.4, 128.1, 127.6, 127.3, 126.1, 125.7, 124.5, 123.4, 121.9, 120.6, 116.0, 103.2, 66.1, 51.2, 47.1, 43.4, 38.2, 37.6. HRMS: Calcd, 580.2806; Found, 580.2811.

4.4.4. Preparation of the Samples Containing A-1

A-1 was dissolved in hexafluoroisopropanol (HFIP, 1 mM) and allowed to stand for 1 h at room temperature. The resultant solution of **A-1** was aliquoted, lyophilized, and stored at -20 °C. The obtained powder was dissolved in a mixture of DMSO/ddH_2O (1:1, v/v) to give the final concentration of 1 mM. To aid the solvation of the peptide, the mixture was vortexed for 1 min followed by sonication for 10 min at room temperature. The resultant solution was allowed to be at room temperature for specified incubation time points. During fluorescence experiments, the solution of **A-1** was stored at 4 °C.

4.4.5. Zn(II) Binding Studies of A-1

The solution of **A-1** (20 μM) and $ZnCl_2$ (2.0 mM) was prepared in 20 mM ammonium acetate buffer (pH 7.4) and incubated for 1 h without agitation at room temperature. The MS analysis was performed using the Q Exactive Plus Orbitrap mass spectrometer (Thermo Fisher Scientific) with an electrospray ionization (ESI) source.

4.4.6. Modeling of A-1 with and without Zn(II)

The structures of metal-free **A-1** and Zn(II)-bound **A-1** were generated with modifications of the previously reported structures of metal-free Aβ (PDB: 1AMC)[27] and Zn(II)-bound Aβ (PDB: 1ZE9)[28] by Discovery Studio Visualizer.

4.4.7. Fluorescent Measurements

A-1 (250-500 nM) and $ZnCl_2$ (100 μM) with and without compounds (i.e., **L2-b**, **EDTA**, natural products; 100 μM) were mixed in 10% DPBS for 10 min without agitation. The mixture was excited at 280 nm. The FRET signal of Zn(II)-treated **A-1** was recorded from 300 to 600 nm. Particularly, the emission of **A-1** at 420 nm showed > ca. 2-fold increase in the presence of $ZnCl_2$, relative to that of **A-1** itself. The buffer for our measurements was selected based on (i) the solubility and (ii) aggregation rate of **A-1** as well as (iii) no presence of other divalent metal ions. In addition, based on Zn(II) titration experiments, the concentration of Zn(II) for fluorescence measurements was chosen. The fluorescence intensity of **A-1** (500 nM) at 420 nm was enhanced upon titration with Zn(II) and was saturated at ca.

100 μM of Zn(II). Thus, 500 nM of **A-1** and 100 μM of Zn(II) were used for fluorescence measurements. Moreover, Zn(II) titration to **A-1** (5 μM) was conducted in order to determine the dissociation constant (K_d) of Zn(II)–**A-1**. The K_d value was determined following previously reported methods.[36–38,46] Furthermore, the fluorescent response of **A-1** (500 nM) in the presence of Cu(II) (1 equiv to **A-1**) was monitored. Upon incubation with Cu(II), the fluorescent intensity of **A-1** was quenched.

4.4.8. Time-dependent Fluorescence Measurements

A-1 (250 nM) was dissolved in 10% DPBS and incubated with and without $ZnCl_2$ (100 μM) for 10 h. Fluorescence was recorded for 10 h with an interval of 5 min at room temperature.

4.4.9. Morphologies of the Aggregates of A-1 and Aβ$_{40}$ with and/or without Zn(II)

A-1 (2.5 μM) was incubated with $ZnCl_2$ (1.0 mM) in 10% DPBS at room temperature for 10 h without agitation. In addition, Aβ$_{40}$ (20 μM) was incubated with and without $ZnCl_2$ (20 μM) in a buffered solution (20 mM HEPES, pH 7.4, 150 mM NaCl) at 37 °C for 10 h with constant agitation. The samples for TEM were prepared according to previously reported methods.[30,31] Glow-discharged grids (Formvar/Carbon 300-mesh, Electron Microscopy Sciences, Hatfield, PA, USA) were treated with the samples from different incubation time points [1, 2, 3, 4, 5, 6, 7, 8, 9, and 10 h for Zn(II)-treated **A-1** (10 μL); 0.5, 3, 5, 7, and 10 h for metal-free Aβ$_{40}$ and Zn(II)-added Aβ$_{40}$ (5 μL)] for 2 min at room temperature. Excess sample was removed with filter paper and washed with ddH_2O. Each grid was treated with uranyl acetate (1% w/v ddH_2O; 5 μL) for 1 min. Excess stain was blotted off and the grids were air dried for at least 20 min at room temperature. Images from each sample were taken at 200 kV with 25,000x magnification [UCRF, Ulsan, Republic of Korea (for Zn(II)-treated **A-1** samples)] and 29,000x magnification [KARA, Daejeon Republic of Korea (for the samples of metal-free and Zn(II)-bound Aβ$_{40}$)].

4.4.10. Thioflavin-T (ThT) Assay

The kinetics of the formation of β-sheet-rich Aβ$_{40}$ aggregates were monitored by the ThT assay according to previous reported methods.[47,48] Each Aβ$_{40}$ sample (20 μM) was obtained after different incubation time points (up to 12 h) at 37 °C with constant agitation (in 20 mM HEPES, pH 7.4, 150 mM NaCl) followed by treatment with ThT (20 μM). After 20 min incubation, the fluorescence intensity of ThT (λ_{ex} = 440 nm; λ_{em} = 490 nm) was measured using a microplate reader, and normalized compared to that of 12 h incubated metal-free Aβ$_{40}$ samples.

4.4.11. Absorption Spectra of Inhibitors

The solutions of the inhibitors, i.e., **EDTA**, **L2-b**, **7**, **9**, **48**, **61**, **73**, **84**, **106**, and **139** (100 μM; 2% v/v DMSO), were prepared in 10% DPBS. Absorption spectra of the inhibitors with and without $ZnCl_2$ (100 μM) were obtained by a microplate reader at room temperature.

4.4.12. Analysis of the Covalent Bond Formation between $A\beta_{28}$ and the Inhibitor (61)

$A\beta_{28}$ (20 μM) was incubated with **61** (100 μM; 2% v/v DMSO; containing an α,β-unsaturated carbonyl group) in 20 mM ammonium acetate (pH 7.4) for 2 h at room temperature without agitation. The incubated samples were injected into the MicrOTOF-QII Hybrid Quadrupole-Time of Flight mass spectrometer (Bruker, Billerica, Massachusetts, USA) equipped with an ESI source (KARA, KAIST, Republic of Korea).

4.4.13. Cell Studies

The human neuroblastoma SH-SY5Y (5Y) cell line was purchased from the American Type Culture Collection (ATCC, Manassas, VA, USA). The cell line was maintained in media containing 50% minimum essential medium (MEM) and 50% F12 (GIBCO), and supplemented with 10% fetal bovine serum (Sigma-Aldrich) and 100 U/mL penicillin (GIBCO). Cells were grown and maintained at 37 °C in a humidified atmosphere with 5% CO_2. The cell culture used in this work did not indicate mycoplasma contamination. Cell viability upon treatment with compounds was determined by the MTT assay [MTT = 3-(4,5-dimethylthiazol-2-yl)-2,5-diphenyltetrazolium bromide]. Cells were seeded in a 96 well plate (15,000 cells in 100 μL per well). Cells were treated with pre-incubated samples containing Zn(II) and/or Aβ for 1 h at room temperature without agitation followed by addition of the selected natural products. After 24 h incubation, MTT [25 μL of 5 mg/mL in PBS (pH 7.4, GIBCO)] was added to each well and the plate was incubated for 4 h at 37 °C. Formazan produced by cells was solubilized using an acidic solution of *N*,*N*-dimethylformamide (DMF, pH 4.5, 50% v/v, aq) and sodium dodecyl sulfate (SDS, 20% w/v) overnight at room temperature in the dark. The absorbance was measured at 600 nm by a microplate reader. Cell viability was calculated relative to that of the cells containing a volume of ddH_2O (containing 1% DMSO) equal to the volume of protein sample added.

4.4.14. Statistical Analysis

All data present mean ± standard error of the mean (S.E.M.). For comparisons between two groups, Student's two-tailed unpaired *t* test was employed. Statistical difference was considered significant at $*P < 0.05$.

4.5. Acknowledgments

This work was supported by the Bio-Synergy Research Project (NRF-2012M3A9C4048775) (to S. J. C.); the National Research Foundation of Korea [NRF-2017M3A9C8031995 (to S. J. C.); NRF-2017R1A2B3002585 and NRF-2016R1A5A1009405 (to M. H. L.)]; KAIST (to M. H. L.). J. K. acknowledges the Global PhD fellowship program through the NRF funded by the Ministry of Education (NRF-2015HIA2A1030823). A. B. T. G. thanks the Korea Research Fellowship Program (NRF-2016H1D3A1938231) through NRF funded by the Ministry of Science and ICT. We thank Geewoo Nam for valuable help on preparation of the manuscript.

4.6. References

(1) Wyss-Coray, T. *Nature* **2016**, *539*, 180–186.
(2) Savelieff, M. G.; Nam, G.; Kang, J.; Lee, H. J.; Lee, M.; Lim, M. H. *Chem. Rev.* **2019**, *119*, 1221–1322.
(3) Li, S.-H.; Li, X.-J. *Trends Genet.* **2004**, *20*, 146–154.
(4) Rasia, R. M.; Bertoncini, C. W.; Marsh, D.; Hoyer, W.; Cherny, D.; Zweckstetter, M.; Griesinger, C.; Jovin T. M.; Fernández, C. O. *Proc. Natl. Acad. Sci. U. S. A.* **2005**, *102*, 4294–4299.
(5) Fox, J. H.; Kama, J. A.; Lieberman, G.; Chopra, R.; Dorsey, K.; Chopra, V.; Volitakis, I.; Cherny, R. A.; Bush A. I.; Hersch, S. *PLoS ONE* **2007**, *2*, e334.
(6) Jakob-Roetne, R.; Jacobsen, H. *Angew. Chem. Int. Ed.* **2009**, *48*, 3030–3059.
(7) Ross, C. A.; Shoulson, I. *Parkinsonism Relat. Disord.* **2009**, *15*, S135–S138.
(8) Valiente-Gabioud, A. A.; Torres-Monserrat, V.; Molina-Rubino, L.; Binolfi, A.; Griesinger, C.; Fernández, C. O. *J. Inorg. Biochem.* **2012**, *117*, 334–341.
(9) Binolfi, A.; Quintanar, L.; Bertoncini, C. W.; Griesinger, C.; Fernández, C. O. *Coord. Chem. Rev.* **2012**, *256*, 2188–2201.
(10) Savelieff, M. G.; Lee, S.; Liu, Y.; Lim, M. H. *ACS Chem. Biol.* **2013**, *8*, 856–865.
(11) Beck, M. W.; Pithadia, A. S.; DeToma, A. S.; Korshavn, K. J.; Lim, M. H. in *Ligand Design in Medicinal Inorganic Chemistry*, ed. Storr, T. Wiley, Chichester, **2014**, ch. 10, pp. 257–286.
(12) Kalia, L. V.; Lang, A. E. *Lancet* **2015**, *386*, 896–912.
(13) Bartzokis, G.; Lu, P. H.; Tishler, T. A.; Perlman, S. in *Neurodegenerative Diseases and Metal Ions*, ed. Sigel, A.; Sigel, H.; Sigel, R. K. O. Wiley, Chichester, **2006**, ch. 7, pp. 151–177.
(14) Bolognin, S.; Messori, L. Zatta, P. *NeuroMol. Med.* **2009**, *11*, 223–238.
(15) Breydo, L.; Uversky, V. N. *Metallomics* **2011**, *3*, 1163–1180.
(16) Elbaum-Garfinkle, S.; Rhoades, E. *J. Am. Chem. Soc.* **2012**, *134*, 16607–16613.
(17) Hayne, D. J.; Lim, S.; Donnelly, P. S. *Chem. Soc. Rev.* **2014**, *43*, 6701–6715.
(18) Tong, H.; Lou, K.; Wang, W. *Acta Pharm. Sin. B* **2015**, *5*, 25–33.
(19) Xu, M.-m.; Ren, W.-m.; Tang, X.-c.; Hu, Y.-h.; Zhang, H.-y. *Acta Pharmacol. Sin.* **2016**, *37*, 719–730.
(20) Warner IV, J. B.; Ruff, K. M.; Tan, P. S.; Lemke, E. A.; Pappu, R. V.; Lashuel, H. A. *J. Am. Chem. Soc.* **2017**, *139*, 14456–14469.
(21) Ferrie, J. J.; Haney, C. M.; Yoon, J.; Pan, B.; Lin, Y.-C.; Fakhraai, Z.; Rhoades, E.; Nath, A.; Petersson, E. J. *Biophys. J.* **2018**, *114*, 53–64.
(22) Danielsson, J.; Pierattelli, R.; Banci, L.; Gräslund, A. *FEBS J.* **2007**, *274*, 46–59.
(23) Talmard, C.; Bouzan, A.; Faller, P. *Biochemistry* **2007**, *46*, 13658–13666.
(24) Dorlet, P.; Gambarelli, S.; Faller, P.; Hureau, C. *Angew. Chem. Int. Ed.* **2009**, *48*, 9273–9276.

(25) Branch, T.; Girvan, P.; Barahona, M.; Ying, L. *Angew. Chem. Int. Ed.* **2015**, *54*, 1227–1230.
(26) Alies, B.; Conte-Daban, A.; Sayen, S.; Collin, F.; Kieffer, I.; Guillon, E.; Faller, P.; Hureau, C. *Inorg. Chem.* **2016**, *55*, 10499–10509.
(27) Talafous, J.; Marcinowski, K. J.; Klopman, G.; Zagorski, M. G. *Biochemistry* **1994**, *33*, 7788–7796.
(28) Zirah, S.; Kozin, S. A.; Mazur, A. K.; Blond, A.; Cheminant, M.; Ségalas-Milazzo, I.; Debey, P.; Rebuffat, S. *J. Biol. Chem.* **2006**, *281*, 2151–2161.
(29) Takeda, A.; Tamano, H.; Tempaku, M.; Sasaki, M.; Uematsu, C.; Sato, S.; Kanazawa, H.; Datki, Z. L.; Adlard, P. A.; Bush, A. I. *J. Neurosci.* **2017**, *37*, 7253–7262.
(30) Choi, J.-S.; Braymer, J. J.; Nanga, R. P. R.; Ramamoorthy, A.; Lim, M. H. *Proc. Natl. Acad. Sci. U. S. A.* **2010**, *107*, 21990–21995.
(31) Beck, M. W.; Oh, S. B.; Kerr, R. A.; Lee, H. J.; Kim, S. H.; Kim, S.; Jang, M.; Ruotolo, B. T.; Lee, J.-Y.; Lim, M. H. *Chem. Sci.* **2015**, *6*, 1879–1886.
(32) Zatta, P.; Drago, D.; Bolognin, S.; Sensi, S. L. *Trends Pharmacol. Sci.* **2009**, *30*, 346–355.
(33) Kepp, K. P. *Chem. Rev.* **2012**, *112*, 5193–5239.
(34) Barnham, K. J.; Bush, A. I. *Chem. Soc. Rev.* **2014**, *43*, 6727–6749.
(35) Faller, P.; Hureau, C.; La Penna, G. *Acc. Chem. Res.* **2014**, *47*, 2252–2259.
(36) Garzon-Rodriguez, W.; Yatsimirsky, A. K.; Glabe, C. G. *Bioorg. Med. Chem. Lett.* **1999**, *9*, 2243–2248.
(37) Tõugu, V.; Karafin, A.; Palumaa, P. *J. Neurochem.* **2008**, *104*, 1249–1259.
(38) Leong, S. L.; Young, T. R.; Barnham, K. J.; Wedd, A. G.; Hinds, M. G.; Xiao, Z.; Cappai, R. *Metallomics* **2014**, *6*, 105–116.
(39) Lee, S. J. C.; Nam, E.; Lee, H. J.; Savelieff, M. G.; Lim, M. H. *Chem. Soc. Rev.* **2017**, *46*, 310–323.
(40) Lakowicz, J. *Principles of Fluorescence Spectroscopy*, Springer, New York, **1999**.
(41) Jares-Erijman, E. A.; Jovin, T. M. *Nat. Biotechnol.* **2003**, *21*, 1387–1395.
(42) Pedersen, J. T.; Østergaard, J.; Rozlosnik, N.; Gammelgaard, B.; Heegaard, N. H. H. *J. Biol. Chem.* **2011**, *286*, 26952–26963.
(43) Liu, Y.; Kochi, A.; Pithadia, A. S.; Lee, S.; Nam, Y.; Beck, M. W.; He, X.; Lee, D.; Lim, M. H. *Inorg. Chem.* **2013**, *52*, 8121–8130.
(44) Uchida, K.; Stadtman, E. R. *Proc. Natl. Acad. Sci. U. S. A.* **1992**, *89*, 4544–4548.
(45) Resch, V.; Seidler, C.; Chen, B.-S.; Degeling, I.; Hanefeld, U. *Eur. J. Org. Chem.* **2013**, *2013*, 7697–7704.
(46) Tran, V.; Park, M. C. H.; Stricker, C. *Cell Calcium* **2018**, *71*, 86–94.
(47) Choi, T. S.; Lee, H. J.; Han, J. Y.; Lim, M. H.; Kim, H. I. *J. Am. Chem. Soc.* **2017**, *139*, 15437–15445.
(48) Lee, H. J.; Savelieff, M. G.; Kang, J.; Brophy, M. B.; Nakashige, T. G.; Lee, S. J. C.; Nolan, E. M.; Lim, M. H. *Metallomics* **2018**, *10*, 1116–1127.

Acknowledgments

I do not belive that I am about to complete the PhD program. I want to thank the following people. Without help from these people I may not finish the PhD program.

Professor Mi Hee Lim, thank you for being my advisor. I appreciate your kind attention, guidance, and support. I do not think I continue to study as a PhD student without your suggestion when I work as a researcher in the groups of you and Professor Gabrielle Rudenko. I hope you do not regret that decision. In addition, I would love to thank you for respecting me. You have always treated me as your student with respect. I have been trying and will try to deal with other people with respect as you have showed me. As your student, I will make efforts on acting and speaking properly at all times. Please find me anytime when you need me. I will be right there as a supporter.

Professor Tae-Hyuk Kwon, thank you for providing opportunities to study Ir(III) complexes. Now I have realized that Ir(III) complexes are amazing inorganic materials. Furthermore, thank you for being my advisor (suddenly). You have always treated me as one of your students from the beginning of our collaboration. I really appreciate it.

Professor Hyun-Woo Rhee, as my collaborator and my committee member, I have had an opportunity to learn from you how to design projects and think/see the studies differently. This has been great experience to me. Thank you for working with me, being my committee, and providing your kind efforts to our projects.

Professor Jung-Min Kee, I clearly remembered our discussion in your previous office (in Bldg. 103). I was impressed that you were thinking and worrying about my experiments and advised me in a right direction. Thank you for your guidance at that time and being my committee member.

Professor Young S. Park, thank you for being my thesis examining committee.

Previous and current group members, thank all of you for your support and help. Especially, thanks for listening the complaints from me. As you guys know, I am a chronic complainer. When I complain, you guys always listen to me even if my logic is missing at that moment! That helps me a lot to move forward. I wished I performed the same role for you guys. When you feel struggle, please let me know. I will try to help you as much as I can. I am proud of being a labmate of you. Thank you so much for being my labmate!

Lab manager: Mi Sook Lim, thank you for your kind effort to the lab. I still think Professor Lim cannot hire a sincere person in the lab than you even she pays a lot of money. Thanks to your sincere attitude in the lab, I could take more care of lab things without hesitation. If you think I am the person who cares about the lab, that would be influenced by you. I appreciate it.

Collaborators/friends: Myeong-Gyun Kang and Jung Seung Nam, it is great for me to be your collaborator and/or friend. Thank you for spending time and efforts for our projects. I hope you guys have great results with your projects and future. Let us have Chinese food in somewhere (probably in Seoul?).

My collaborators and staff members [(collaborators) Professor Ayyalusamy Ramamoorthy, Professor Jaeheung Cho, Professor Sang J. Chung, Professor Jae-sung Bae, Professor Hee Kyung Jin, Professor Su Wol Chung, Professor Joo-Yong Lee, Professor Young-Ho Lee, Professor So Youn Kim, Professor Oh-Hoon Kwon; Hyun-Tak Kim, Seunghee Lee, Na Kyung Kwon, Dr. Yuxi Lin, Dr. Sun-Young Park; (UCRF/UOBC staff) Eun-jung Han, Gyeong-ae Lee, Suhyun Park, Jin-hoe Hur, Mi-sun Cho, Seonhye Son, Sun-pil Han; (administrative staff) Yukyeong Park, Sihyung Park, Won Hyang Kang; (Vendor, JBIOTECH Co.) Jae-Mun Han], thank you all for your help. Without your assistance, I could not finish the projects and my PhD program properly. I appreciate your kind efforts.

My family (my parents, my sister, and my brother-in-law), thank you for your support. I could be confident when I think you are standing behind me. Thank you for trusting me. I will keep trying to be an independent person. Believe or not, I am about to be a doctor!

If I could not list your name, that does not mean I forget your help. I apologize in advance … This is the reason we need to keep fighting against Alzheimer's disease. I appreciate all people who study degenerative diseases. You are going to save the world!

Juhye Kang

Department of Chemistry
Ulsan National Institute of Science and Technology (UNIST)
UNIST-gil 50, Ulsan 44919, Republic of Korea.
Office Phone: +82-42-350-2866, Cell Phone: +82-11-772-6387
Email: juhye@unist.ac.kr

Education

Sep. 2014 – Present	**Ph.D. Candidate, Chemistry, Ulsan National Institute of Science and Technology (UNIST), Ulsan, Korea** Thesis Title: Development of Chemical Tactics to Study Fundamental Aspects of Pathogenic Factors Found in Neurodegenerative Diseases Advisors: Professors Mi Hee Lim and Tae-Hyuk Kwon
Mar. 2011 – Aug. 2014	**M.Sc., Fine Chemistry, Seoul National University of Science and Technology, Seoul, Korea** Thesis Title: Magnesium & Zinc Selective Chemosensors Based on Dipicolylamine Advisor: Professor Cheal Kim
Mar. 2007 – Feb. 2011	**B.S., Fine Chemistry, Seoul National University of Science and Technology, Seoul, Korea**

Honors, Awards, and Scholarships

July 2017	Grand Prize for Poster Award The 2017 Bioinorganic Chemistry Symposium
Apr. 2016	Best Poster Award The 117th National Meeting of the Korean Chemical Society
Mar. 2015 – Feb. 2018	Global Ph.D. Fellowship (GPF) National Research Foundation of Korea (NRF), Korea
Sep. 2014 – Feb. 2015	Research Assistant Fellowship Ulsan National Institute of Science and Technology (UNIST), Korea

Research Experience

Feb. 2014 – Aug. 2014	Researcher Ulsan National Institute of Science and Technology (UNIST), Korea

Research Topic: Synthesis of Compounds to Inhibit Binding of ΔFosB to DNA
Advisor: Professor Mi Hee Lim

Jan. 2013 – Dec.2013 — Vising Scholar
University of Michigan, USA
Research Topic: Synthesis of Compounds to Inhibit Binding of ΔFosB to DNA
Advisors: Professors Mi Hee Lim and Gabrielle Rudenko

Jan. 2010 – Feb.2011 — Undergraduate Researcher
Seoul National University of Science and Technology, Korea
Research Topic: Magnesium & Zinc Selective Chemosensors Based on Dipicolylamine
Advisor: Professor Cheal Kim

Teaching Experience

Mar. 2019 – Present — Bioinorganic Chemistry, Teaching Assistant
Korea Advanced Institute of Science and Technology (KAIST), Korea

Mar. 2016 – June 2016 — Inorganic Chemistry Laboratory, Teaching Assistant (Chief)
Ulsan National Institute of Science and Technology (UNIST), Korea

Mar. 2015 – Dec. 2015 — Inorganic Chemistry, Teaching Assistant
Ulsan National Institute of Science and Technology (UNIST), Korea

Mar. 2015 – June 2015 — Inorganic Chemistry Laboratory, Teaching Assistant
Ulsan National Institute of Science and Technology (UNIST), Korea

Sep. 2014 – Dec. 2015 — General Chemistry Laboratory, Teaching Assistant
Ulsan National Institute of Science and Technology (UNIST), Korea

Sep. 2011 – June 2012 — Inorganic Chemistry Laboratory, Teaching Assistant
Seoul National University of Science and Technology, Korea

Mar. 2011 – June 2011 — General Chemistry, Laboratory Teaching Assistant
Seoul National University of Science and Technology, Korea

Publications

1. **Juhye Kang**,† Jung Seung Nam,† Hyuck Jin Lee, Geewoo Nam, Hyun-Woo Rhee, Tae-Hyuk Kwon, and Mi Hee Lim. "Chemical Strategies to Modify Amyloidogenic Peptides by Iridium(III) Complexes: Coordination and Photo-induced Oxidation" *In Revision* (†Co-first authorship).

2. Geewoo Nam, Yonghwan Ji, HyuckJin Lee, **Juhye Kang**, Yelim Yi, Mingeun Kim, and Mi Hee Lim. "Orobol: An Isoflavone with Regulatory Multifunctionality against Four Pathological Factors of Alzheimer's Disease" *Submitted*.

3. Yuxi Lin, Bikash Sahoo, Daisaku Ozawa, Misaki Kinoshita, **Juhye Kang**, Mi Hee Lim, Masaki Okumura, Sihyun Ham, Hyung-Sik Won, Kyoung-Seok Ryu, Toshihiko Sugiki, Toshimichi Fujiwara, Ayyalusamy Ramamoorthy, Young-Ho Lee. "Diverse Structural Conversion and Aggregation Pathways of Alzheimer's Amyloid-β (1-40)" *In Revision*.

4. Misun Lee, Min Hee Park, Ju Youn Lee, Min Seock Jeong, Kang Ho Park, Seung Hoon Han, Geewoo Nam, Mingeun Kim, **Juhye Kang**, Eunyoung Tak, Min Sun Kim, Joo-Yong Lee, Hee Kyung Jin, Jae-Sung Bae, Mi Hee Lim. "A Compact Molecular Entity Improving Cognitive Functionby Restoring the Phagocytic Aptitude of Microglia" *Submitted*.

5. Mingeun Kim,† **JuhyeKang**,† Misun Lee,† JiyeonHan, Geewoo Nam, Eunyoung Tak, Min Sun Kim, Doin Kim, Hyuck Jin Lee, Eunju Nam, Joo-Yong Lee, and Mi Hee Lim. "Minimalistic Design Approach for Multi-reactivity against Free Radicals and Metal-free and Metal-bound Amyloid-β Peptides: Redox-based Substitutions of Benzene" *Manuscript in Preparation* (†Co-first authorship).

6. Hyuck Jin Lee,† Young Geun Lee,† **Juhye Kang**,† Seung Hyun Yang, Ju Hwan Kim, Amar B.T. Ghisaidoobe, Hyo Jin Kang, Sang-Rae Lee, Mi Hee Lim, and Sang J. Chung. "Monitoring Metal–Amyloid-β Complexation by a FRET-based Probe: Design, Detection, and Inhibitor Screening" *Chemical Science*, **2019**, *10*, 1000-1007 (†Co-first authorship).

   *Selected as "2018 Chemical Science HOT Article Collection" and featured as the "Back cover".

7. Jong-Min Suh, Gunhee Kim, **Juhye Kang**, Mi Hee Lim. "Strategies Employing Transition Metal Complexes to Modulate Amyloid-β Aggregation" *Inorganic Chemistry*, **2019**, *58*, 8-17.

8. Masha G. Savelieff,† Geewoo Nam,† **Juhye Kang**,† Hyuck Jin Lee, Misun Lee, and Mi Hee Lim. "Development of Multifunctional Molecules as Potential Therapeutic Candidates for Alzheimer's Disease, Parkinson's Disease, and Amyotrophic Lateral Sclerosis in the Last Decade" *Chemical Reviews*, **2019**, *119*, 1221-1322 (†Co-first authorship).

9. Hyuck Jin Lee, Masha G. Savelieff, **Juhye Kang**, Megan Brunjes Brophy, Toshiki G. Nakashige, Shin Jung C. Lee, Elizabeth M. Nolan, and Mi Hee Lim. "Calprotectin Influences the Aggregation of Metal-free and Metal-bound Amyloid-β by Direct Interaction" *Metallomics*, **2018**, *10*, 1116-1127.

10. Eunju Nam, Jeffrey S. Derrick, Seunghee Lee, **Juhye Kang**, Jiyeon Han, Shin Jung C. Lee, Su Wol Chung, and Mi Hee Lim. "Regulatory Activities of Dopamine and Its Derivatives toward Metal-free and Metal-induced Amyloid-β Aggregation, Oxidative Stress, and Inflammation in Alzheimer's Disease" *ACS Chemical Neuroscience*, **2018**, *9*, 2655-2666.

11. **Juhye Kang**, Yelim Yi, and Mi Hee Lim. "Design and Development of Small Molecule to Target Metal–Amyloid-β in Alzheimer's Disease" *Chemworld*, **2017**, *8*, 13-20.

12. Jeffrey S. Derrick, Jiwan Lee, Shin Jung C. Lee, Yujeong Kim, Eunju Nam, Hyeonwoo Tak, **Juhye Kang**, Misun Lee, Sun Hee Kim, Kiyoung Park, Jaeheung Cho, and Mi Hee Lim. "Mechanistic Insights into Tunable Metal-mediated Hydrolysis of Amyloid-β Peptides" *Journal of the American Chemical Society*, **2017**, *139*, 2234-2244.

    *Featured as the "Front Cover" & "JACS Spotlights".

13. Hyuck Jin Lee, Kyle J. Korshavn, Younwoo Nam, **Juhye Kang**, Thomas J. Paul, Richard A. Kerr, Il Seung Youn, Mehmet Ozbil, Kwang S. Kim, Brandon T. Ruotolo, Rajeev Prabhakar, Ayyalusamy Ramamoorthy, and Mi Hee Lim. "Structural and Mechanistic Insights into Development of Chemical Tools to Control Individual and Inter-related Pathological Features in Alzheimer's Disease" *Chemistry - A European Journal*, **2017**, *23*, 2706-2715.

14. **Juhye Kang**,† Shin Jung C. Lee,† Jung Seung Nam,† Hyuck Jin Lee, Myeong-Gyun Kang, Kyle J. Korshavn, Hyun-Tak Kim, Jaeheung Cho, Ayyalusamy Ramamoorthy, Hyun-Woo Rhee, Tae-Hyuk Kwon, and Mi Hee Lim. "An Iridium(III) Complex as a Photoactivatable Tool for Oxidation of Amyloidogenic Peptides with Subsequent Modulation of Peptide Aggregation" *Chemistry - A European Journal*, **2017**, 23, 1645-1653 (†Co-first authorship).

    *Selected as "Hot paper".

15. Jung Seung Nam,† Myeong-Gyun Kang,† **Juhye Kang**,† Sun-Young Park,† Shin Jung C. Lee, Hyun-Tak Kim, Jeong Kon Seo, Oh-Hoon Kwon, Mi Hee Lim, Hyun-Woo Rhee, and Tae-Hyuk Kwon. "Endoplasmic Reticulum-Localized Iridium(III) Complexes as Efficient Photodynamic Therapy Agents via Protein Modifications" *Journal of the American Chemical Society*, **2016**, *138*, 10968-10977 (†Co-first authorship).

16. Jeffrey S. Derrick, Richard A. Kerr, Kyle J. Torshavn, Michael J. McLane, **Juhye Kang**, Eunju Nam, Ayyalusamy Ramamoorthy, Brandon T. Ruotolo, and Mi Hee Lim. "Importance of the Dimethylamino Functionality on a Multifunctional Framework for Regulating Metals, Amyloid-β, and Oxidative Stress in Alzheimer's Disease" *Inorganic Chemistry*, **2016**, *55*, 5000-5013.

17. Hyuck Jin Lee, Richard A. Kerr, Kyle J. Korshavn, Jiyeon Lee, **Juhye Kang**, Ayyalusamy Ramamoorthy, Brandon T. Ruotolo, and Mi Hee Lim. "Effects of Hydroxyl Group Variations on a Flavonoid Backbone toward Modulation of Metal-free and Metal-induced Amyloid-β Aggregation" *Inorganic Chemistry Frontiers*, **2016**, *3*, 381-392.

18. Hyun Kim, **Juhye Kang**, Kyung Beom Kim, Eun Joo Song, and Cheal Kim. "A Highly Selective Quinoline-based Fluorescent Sensor for Zn(II)" *Spectrochimica Acta Part A: Molecular and Biomolecular Spectroscopy*, **2014**, *118*, 883-887.

19. Eun Joo Song, **Juhye Kang**, Ga Rim You, Gyeong Jin Park, Youngmee Kim, Sung-Jin Kim, Cheal Kim, and Roger G. Harrison. "A Single Molecule that Acts as a Fluorescence Sensor for Zinc and Cadmium and a Colorimetric Sensor for Cobalt" *Dalton Transactions*, **2013**, *42*, 15514-15520.

20. Jin Young Noh, Soojin Kim, In Hong Hwang, Ga Ye Lee, **Juhye Kang**, So Hyun Kim, Jisook Min, Sungsu Park, Cheal Kim, and Jinheung Kim. "Solvent-dependent Selective Fluorescence Assay of Aluminum and Gallium Ions Using Julolidine-based Probe" *Dye and Pigments*, **2013**, *99*, 1016-1021.

21. Jin Hoon Kim, Jin Young Noh, In Hong Hwang, **Juhye Kang**, Jinheung Kim, and Cheal Kim. "An Anthracene-based Fluorescent Chemosensor for Zn^{2+}" *Tetrahedron Letters*, **2013**, *54*, 2415-2418.

22. Jin Hoon Kim, In Hong Hwang, Seung Pyo Jang, **Juhye Kang**, Sumi Kim, Insup Noh, Youngmee Kim, Cheal Kim, and Roger G. Harrison. "Zinc Sensors with Lower Binding Affinities for Cellular Imaging" *Dalton Transactions*, **2013**, *42*, 5500-5507.

23. **Juhye Kang**, Hee Kyung Kang, Hyun Kim, Jungha Lee, Eun Joo Song, Kwang-Duk Jeong, Cheal Kim, and Jinheung Kim. "Fluorescent Chemosensor Based on Bispicolylamine for Selective Detection of Magnesium Ions" *Supramolecular Chemistry*, **2013**, *25*, 65-68.

24. Min Young Hyun, Soo Hyun Kim, Young Joo Song, Hong Gyu Lee, Young Dan Jo, Jin Hoon Kim, In Hong Hwang, Jin Young Noh, **Juhye Kang**, and Cheal Kim. "Terminal and Internal Olefin Epoxidation with Cobalt(II) as the Catalyst: Evidence for an Active Oxidant Co^{II}-Acylperoxo Species" *Journal of Organic Chemistry*, **2012**, *77*, 7307-7312.

25. In Hong Hwang, Young Dan Jo, Ha-Yeong Kim, **Juhye Kang**, Jin Young Noh, Min Young Hyun, Cheal Kim, Youngmee Kim, and Sung-Jin Kim. "Novel Mn^{II} Coordination Compounds Constructed from Benzoate and Various Bipyridyl Ligands: Magnetic Property and Catalytic Activity" *Polyhedron*, **2012**, *42*, 282-290.

26. **Juhye Kang**, Jin Kie Yeo, Pan-Gi Kim, Cheal Kim, and Youngmee Kim. "Bis(methanol-κO)bis(quinoline-2-carboxylato-κ^2N,O)nickel(II)" *Acta Crystallographica E*, **2011**, *E67*, m1151.

Patents

1. Tae-Hyuk Kwon, Hyun-Woo Rhee, Mi Hee Lim, Jung Seung Nam, **Juhye Kang**, Myeong-Gyun Kang, and Hyun-Tak Kim. "Pharmaceutical Composition for Anticancer Containing Cyclometalated Transition Metal Complex" *Korean Pat. Appl. Publ.* **2017**, 10-1743594.

2. Cheal Kim, Eun Joo Song, **Juhye Kang**, Ga Rim You, and Myoung Mi Lee. "Quinoline Compounds, Agent Selecting Zinc Ion, Cadmium Ion and Copper Ion Using the Same, Detecting Method and Detecting Device Thereof" *Korean Pat. Appl. Publ.* **2016**, 10-1638682.

Presentations

1. **Juhye Kang**, Shin Jung C. Lee, Jung Seung Nam, Hyuck Jin Lee, Kyle J. Korshavn, Hyun-Tak Kim, Jaeheung Cho, Ayyalusamy Ramamoorthy, Hyun-Woo Rhee, Tae-Hyuk Kwon, and Mi Hee Lim. Poster Slam & Presentation. "An Iridium(III) Complex as a Photoactivatable Tool for Oxidation of Amyloidogenic Peptides with Subsequent Modulation of Peptide Aggregation" *The 4th International Symposium for Molecular Neurodegenerative Disease Research*, **2018**.

2. **Juhye Kang**, Shin Jung C. Lee, Jung Seung Nam, Hyuck Jin Lee, Myeong-Gyun Kang, Kyle J. Korshavn, Hyun-Tak Kim, Jaeheung Cho, Ayyalusamy Ramamoorthy, Hyun-Woo Rhee, Tae-Hyuk Kwon, and Mi Hee Lim. "An Iridium(III) Complex as a Photoactivatable Tool for Oxidation of Amyloidogenic Peptides with Subsequent Modulation of Peptide Aggregation" *International Union of Materials Research Societies – International Conference on Electronic Materials 2018 (IUMRS-ICEM 2018)*, **2018**.

3. **Juhye Kang** and Mi Hee Lim. Oral Presentation. "Iridium(III) Complexes as Modulators for Amyloid-β Aggregation through Multiple Mechanisms" *Symposium on Chemistry and Life*, **2018**.

4. Hyuck Jin Lee, Young Geun Lee, **Juhye Kang**, Seung Hyun Yang, Ju Hwan Kim, Amar B.T. Ghisaidoobe, Hyo Jin Kang, Sang-Rae Lee, Mi Hee Lim, and Sang J. Chung. "FRET-based Method for the Real-time Identification of Metal–Amyloid-β Interaction: Rational Design, Detection, and Inhibitor Screening" *The Bioinorganic Chemistry Symposium*, **2018**.

5. **Juhye Kang** and Mi Hee Lim. Oral & Poster Presentations. "Iridium(III) Complexes as Modulators for Amyloid-β Aggregation through Multiple Mechanisms" *The Bioinorganic Chemistry Symposium*, **2017**.
   *Awarded as a "Grand Prize for Poster Award".

6. **Juhye Kang**, Shin Jung C. Lee, Jung Seung Nam, Hyuck Jin Lee, Myeong-Gyun Kang, Kyle J. Korshavn, Hyun-Tak Kim, Jaeheung Cho, Ayyalusamy Ramamoorthy, Hyun-Woo Rhee, Tae-Hyuk Kwon, and Mi Hee Lim. "An Iridium(III) Complex as a Photoactivatable Tool for Oxidation of Amyloidogenic Peptides with Subsequent Modulation of Peptide Aggregation" *The 8th Asian Biological Inorganic Chemistry Conference*, **2016**.

7. **Juhye Kang**, Shin Jung C. Lee, Jung Seung Nam, Hyuck Jin Lee, Kyle J. Korshavn, Hyun-Tak Kim, Jaeheung Cho, Ayyalusamy Ramamoorthy, Hyun-Woo Rhee, Tae-Hyuk Kwon, and Mi Hee Lim. "An Iridium(III) Complex as a Photoactivatable Tool for Oxidation of Amyloidogenic Peptides with Subsequent Modulation of Their Aggregation" *The 117th National Meeting of the Korean Chemical Society*, **2016**.
   *Awarded as a "Best Poster Award".

8. **Juhye Kang**, Jung Seung Nam, Shin Jung C. Lee, Hyuck Jin Lee, Hyuntak Kim, Hyun-Woo Rhee, Tae-Hyuk Kwon, and Mi Hee Lim. Poster Slam & Presentation. "Modulation of Amyloid-β Aggregation Pathways by Iridium(III) Complexes through Three Distinct

Mechanisms" *The 116th National Meeting of the Korean Chemical Society*, **2015**.

9. **Juhye Kang**, Hyuck Jin Lee, Shin Jung C. Lee, and Mi Hee Lim. "Modulation of Amyloid-β Aggregation Pathways by Iridium(III) Complexes" *The Bioinorganic Chemistry Symposium*, **2015**.

10. In Hong Hwang, **Juhye Kang**, Jin Young Noh, Eun Joo Song, Hyun Kim, Cheal Kim, Sung-Jin Kim, and Youngmee Kim. "Light- and Photo-induced [2 + 2] Cycloaddition of Metal-directed Assembly of Metal(II) Benzoates" *The 110th National Meeting of the Korean Chemical Society*, **2012**.

11. **Juhye Kang**, Jin Young Noh, Kyungbeom Kim, Hyun Kim, Myoung Mi Lee, Yu Jeong Na, and Cheal Kim. "Remarkable Solvent and Ligand Effects for Partition of the Multiple Active Oxidants in Manganese(III) Porphyrin-catalyzed Epoxidation with Peracids" *7th International Conference on Porphyrins and Phthalocyanines (ICPP-7)*, **2012**.

12. **Juhye Kang**, Jeong Mi Bae, Hyun Kim, Yu Jeong Na, and Cheal Kim. "Efficient Olefin Epoxidation of Robust Re_4 Cluster-supported Mn^{III} Complexes with Peracids" *The Bioinorganic Chemistry Symposium*, **2012**.

13. **Juhye Kang**, Young Dan Jo, Jin Young Noh, In Hong Hwang, Eun Joo Song, Kyeng Jin Park, Cheal Kim, Sung-Jin Kim, and Youngmee Kim. "Synthesis, Characterization, Photoluminescence, and Catalytic Activities of Cd(II) Complexes with a Bipyridyl Ligand" *The 109th National Meeting of the Korean Chemical Society*, **2012**.

14. **Juhye Kang**, Hyun Kim, Ji Hwan Park, and Cheal Kim. "Zinc Chemosensor Based on Pyridyl-Amide Receptor" *The 108th National Meeting of the Korean Chemical Society*, **2011**.

15. Hong Gyu Lee, **Juhye Kang**, Jin Young Noh, Hyun Kim, and Cheal Kim. "Zinc Selective Chemosensor Based on Pyridyl-Amide Fluorescence" *The Bioinorganic Chemistry Symposium*, **2011**.

16. Jin Hoon Kim, Young Dan Jo, **Juhye Kang**, Jin Young Noh, In Hong Hwang, Hyun Min Park, and Cheal Kim. "Efficient Hydrocarbon Oxidation Reactions by Amide-based Nonheme Manganese(III) catalysts" *241st American Chemical Society National Meeting & Exposition*, **2011**.